A new approach to understanding the origin of Fuerteventura, Canary Islands (Spain): A U-Pb, Hf and O isotope and minor- and trace-element detrital zircon study

by

Madisen Sagan

A thesis submitted in partial fulfillment of the requirements of the degree of

Master of Science

Department of Earth and Atmospheric Sciences

University of Alberta

ABSTRACT

The Canarian Archipelago contains seven islands proximal to the African continent and High Atlas Mountains. The origin and magmatic evolution of these islands has been a contentious issue for several decades. This particular archipelago is unique because three of the islands (Fuerteventura, La Palma, La Gomera) have been reported to contain uplifted portions of the intrusive complex, potentially exposing the earliest phases of the islands growth. There are numerous published K-Ar and Ar/Ar dates for this early magmatic activity on the oldest island, Fuerteventura, ranging from 68 to 25 Ma (Le Bas et al., 1986; Muñoz et al. 2005) but the veracity of these dates is uncertain due to a pervasive greenschist-facies metamorphic overprint.

In order to better understand Fuerteventura's early magmatic history, we have conducted a U-Pb, Hf and O isotope and minor- and trace-element detrital zircon study of sand samples from three locations proximal to the intrusive complex. A U-Pb and geochemical study of detrital zircons is an efficient method to evaluate the early growth history of the island since most of the uplifted complex consists of zircon-bearing rocks (granite, syenite, nepheline syenite, gabbro, anorthosite, carbonatite) and the U-Pb system is largely immune to low-grade metamorphism. The Hf and O isotope study helps to develop an understanding of the magma source of these intrusive rock units and evaluate the role of lithospheric contamination during the magmatic activity.

A total of 260 zircon grains were secured in an epoxy mount and analyzed using in-situ U-Pb Laser Ablation Inductively Coupled Plasma Mass Spectrometry (LA-MC-ICPMS). The U-Pb detrital zircon ages from this study range from the Early Oligocene to Early Pliocene (33.7-3.8 Ma), with mixture modelling results exhibiting four prominent

age peaks at 4.4, 16.8, 21.1, and 25.5 Ma. There is no evidence for the existence of Cretaceous magmatism on Fuerteventura in this study.

A total of 149 single detrital zircon grains were analyzed for their trace-element content using a New Wave UP-213 laser ablation workstation coupled with a Thermo Scientific iCAP-Q Quadrupole Inductively Coupled Plasma Mass Spectrometer (LA-ICPMS) to subdivide the zircons based on probable magma provenance (e.g., syenite, nepheline syenite, carbonatite, anorthosite, kimberlite, granite, and gabbro) to further develop our understanding of the islands magmatic evolution. The main distinguishing geochemical features of the detrital zircons are their Ti and Y concentrations, along with the magnitude of the Eu/Eu* anomaly. Using these geochemical criteria, the detrital zircons analyzed from this study indicate the following provenance: 51% syenite, 36% anorthosite/gabbro, 7% nepheline syenite, and 5% carbonatite. These rock proportions vary between sample populations, with the northern sector containing nepheline-syenite (39%), syenite (35%), carbonatite (26%) and the central sector containing syenite (54%), anorthosite/gabbro (42%), nepheline-syenite (2%), carbonatite (1%), and undefined (1%).

A subset of the mounted grains (n=133) were analyzed for their hafnium isotope composition using a Laser Ablation Split Stream (LASS) technique. The new zircon Hf isotopic data can be divided into three distinct groups: a predominant zircon suite with εHf_i values ranging from +7.5 to +10.4, a more 'depleted' population ranging from +10.6 to +15.2, and a more 'enriched' population ranging from -0.2 to +7.0. The zircon εHf values are relatively consistent (+7.5 to +10) in the early part of Fuerteventura's magmatic history from 34-20 Ma, but an abrupt change occurs at ~20 Ma, where these younger zircons display εHf variation reflecting both depleted and enriched isotopic

signatures. The depleted signature discontinues after an apparent hiatus from 14.5- 6.5 Ma, while the enriched signature is observed to persist into the Late-Miocene to Pliocene samples.

A total of 191 oxygen isotope ($^{18}O/^{16}O$) spot compositions were measured on 91 detrital zircon grains using a Cameca IMS 1280 multicollector ion microprobe. The oxygen isotope data exhibit two distinct populations. The first group, representing 12% of the sample population, resembles the mantle-like oxygen field (+5.3 ± 0.3‰) with $\delta^{18}O$ values ranging from 5.00-5.48‰ with an average of 5.14‰; the second group representing the remaining 88% of the population, records low $\delta^{18}O$ values (3.27-4.99‰, average of 4.31‰) that are below the zircon mantle field, representing 88% of the sample population. Low $\delta^{18}O$ values provide evidence for high temperature rock-water alteration in the source region of these magmas, suggesting an origin for some magmas by melting or assimilation of hydrothermally altered oceanic crust.

There are several new features of Fuerteventura's magmatic history revealed from this study: 1) there are four peaks of magmatic activity (25.7, 21.0, 16.7, 4.4 Ma), 2) Oligocene detrital zircons (33.7-24.4 Ma) dominate the northern part of the complex, 3) magmatic activity in general youngs from north to south, 4) a previously unrecognized period of Late Miocene and Early Pliocene intrusive rocks (6.5-3.8 Ma) must exist in the central part of the island, 5) zircon Hf isotope data require at least three mantle source endmembers to explain the generation of Fuerteventura's magmatic activity, including an enriched, depleted , and HIMU-plume component, and 6) low $\delta^{18}O$ values of some detrital zircons suggest the involvement of hydrothermally altered oceanic crust in the origin of many Fuerteventura magmas.

PREFACE

The research presented in this study investigates the origin and evolution of Fuerteventura, Canary Islands. Fieldwork was completed by Dr. Larry Heaman and myself with the assistance of previous published literature to guide selection of regions of interest.

U-Pb purification of zircon fractions from sample 2016MJ-14 and 2016MJ-34 was completed by Dr. Larry Heaman and James LeBlanc, with ID-TIMS analysis conducted by James LeBlanc.

The ideas presented here are my own, although they have been developed and refined by many discussions with my supervisor, Dr. Larry Heaman. All the writing and figures presented here are my own work.

ACKNOWLEDGEMENTS

First and most notably, I would like to thank Dr. Larry Heaman for providing such an incredible opportunity to pursue my passion of geology. His unwavering support and encouragement provided the grounds for large-scale thinking that was accompanied by high-quality science. He taught me to question the unknown, write with precision and clarity, and be transparent with all science that is reported. The understanding established in this thesis predominantly lends to Larry's influential teaching and mentorship. I could not have had a wiser, kinder, supervisor to study under and I feel forever thankful for the opportunity.

This study would not have been possible without all the support I received from several individuals at the University of Alberta. Dr. Graham Pearson and Dr. Chiranjeeb Sarkar are thanked for the U-Pb and Hf isotope laser split stream spectrometry maintenance and data. Dr. Andy DuFrane is thanked for the maintenance and prep of the LA-MC-ICPMS and Q-ICPMS data collection and review. Dr. Richard Stern is thanked for providing an opportunity to use the high-quality SIMS facility and the thought-provoking discussions. I would also like to thank the following people for various training, analysis, and logistics associated with this project: Andrew Locock, James LeBlanc, Nathan Gerein, Mark Labbe, Igor Jakab, and Marilyn Huff.

Any personal development that has taken place during this experience can be attributed to a variety of friends and colleagues. I would also like to thank the Heaman geochronology research group for training me on the various sample processing and preparation for U-Pb zircon studies. Ilona for providing such great morale and technical support. Alex Sheen for offering moments of clarity on multiple software programs. Alix

Osinchuk for providing great geological insight and for always offering a coffee break. Mike Belosevic for the great life discussions and added comical relief to my office days.

A huge thank you to my husband, Angus, who has always encouraged me to pursue my passion and for his unwavering support. Thank you to my family for always being there for me and to my dear friends outside of my academic world that have always been understanding and supportive.

TABLE OF CONTENTS

ABSTRACT II

PREFACE V

ACKNOWLEDGEMENTS VI

TABLE OF CONTENTS VIII

LIST OF TABLES X

LIST OF FIGURES XI

1. INTRODUCTION 1

2. BACKGROUND 4

2.1 Regional Geology 4
2.2 Fuerteventura Basal Complex 10
2.3 Subaerial Volcanic Series of the Neogene and Quaternary 12

3. METHODOLOGY 14

3.1 Zircon Mount Preparation 14
3.2 Zircon U-Pb Dating LA-ICP-MS 16
3.3 LA-Q-ICP-MS trace element analyses 20
3.4 Laser ablation split stream (LASS) 23
3.5 SIMS Oxygen 26

4. RESULTS 28

4.1 Zircon U-Pb Laser Ablation Inductively Coupled Plasma Mass Spectrometry (LA-MC-ICPMS) Analysis 28
4.1.1 Playa del Águila beach sand 2016MJ-04 30
4.1.2 Playa de Garcey beach sand 2016MJ-38 31
4.1.3 Barranco de la Solapa river sand 2016MJ-39 32
4.2 Zircon Trace-Element Geochemistry 34
4.2.1 Ti 35
4.2.2 Eu/Eu* 37
4.2.3 Ce/Ce* 39
4.2.4 Y 42
4.2.5 Th and U 44
4.2.6 Nb/Ta and Nb 48
4.3 Hf isotope analysis 50
4.4 Oxygen Isotope Compositions of Zircon 54

5. DISCUSSION 60

5.1 Duration and main periods of zircon-bearing alkaline magmatism 60
5.2 Age progression of magmatism on Fuerteventura 65
5.3 Defining the magma provenance of zircon using minor and trace elements 69
5.4 Magma sources and the role of lithosphere contamination in the magma evolution 76
5.5 Zircon Hafnium Isotope Signatures 79
5.6 Hf-O 82

CONCLUSIONS 87

FUTURE RESEARCH 90

REFERENCES 91

APPENDIX A: FUERTEVENTURA GEOCHRONOLOGY SUMMARY 100

APPENDIX B1: LA-ICPMS U-PB SUMMARY (SESSION 1-9435)..... 106
APPENDIX B2: LA-ICPMS U-PB SUMMARY (SESSION 2-9435)..... 107
APPENDIX B3: LA-ICPMS U-PB SUMMARY (SESSION 3-9435)..... 108
APPENDIX C1: LA-ICPMS U-PB SUMMARY (SAMPLE 2016MJ-04)..... 109
APPENDIX C2: LA-ICPMS U-PB SUMMARY (SAMPLE 2016MJ-38)..... 110
APPENDIX C3: LA-ICPMS U-PB SUMMARY (SAMPLE 2016MJ-39)..... 113
APPENDIX D1: CATHODOLUMINSCENCE IMAGES (2016MJ-04) 116
APPENDIX D2: CATHODOLUMINSCENCE IMAGES (2016MJ-38) 117
APPENDIX D3A: CATHODOLUMINSCENCE IMAGES (2016MJ-39) 118
APPENDIX D3B: CATHODOLUMINSCENCE IMAGES (2016MJ-39) 119
APPENDIX E: GEOCHEMISTRY SUMMARY..... 120
APPENDIX F: SUPPLEMENTARY DATA FROM HF LASS ANALYSIS..... 130
APPENDIX G1: δ^{18}O SIMS ANALYSIS (2016MJ-04) 135
APPENDIX G2: δ^{18}O SIMS ANALYSIS (2016MJ-38) 136
APPENDIX G3: δ^{18}O SIMS ANALYSIS (2016MJ-39) 137
APPENDIX H: SUMMARY OF U-PB, HF, AND O ISOTOPIC DATA, FUERTEVENTURA, DETRITAL ZIRCONS139

LIST OF TABLES

TABLE 3.2. REFERENCE MATERIAL 94-35 18

TABLE 3.3. NIST612 AND 91500 RESULTS AND ACCEPTED VALUES 22

APPENDIX A: FUERTEVENTURA GEOCHRONOLOGY SUMMARY 100

APPENDIX B1: LA-ICPMS U-PB SUMMARY (SESSION 1-9435) 106

APPENDIX B2: LA-ICPMS U-PB SUMMARY (SESSION 2-9435) 107

APPENDIX B3: LA-ICPMS U-PB SUMMARY (SESSION 3-9435) 108

APPENDIX C1: LA-ICPMS U-PB SUMMARY (SAMPLE 2016MJ-04) 109

APPENDIX C2: LA-ICPMS U-PB SUMMARY (SAMPLE 2016MJ-38) 110

APPENDIX C3: LA-ICPMS U-PB SUMMARY (SAMPLE 2016MJ-39) 113

APPENDIX E: GEOCHEMISTRY SUMMARY 120

APPENDIX F: SUPPLEMENTARY DATA FROM HF LASS ANALYSIS 130

APPENDIX G1: $\delta^{18}O$ SIMS ANALYSIS (2016MJ-04) 135

APPENDIX G2: $\delta^{18}O$ SIMS ANALYSIS (2016MJ-38) 136

APPENDIX G3: $\delta^{18}O$ SIMS ANALYSIS (2016MJ-39) 137

APPENDIX H: SUMMARY OF U-PB, HF, AND O ISOTOPIC DATA, FUERTEVENTURA, DETRITAL ZIRCONS 139

LIST OF FIGURES

FIGURE. 2.1A. MAP OF THE EASTERN NORTH ATLANTIC SHOWING THE CANARY ISLANDS 6

FIGURE. 2.1B. GEOLOGICAL MAP OF FUERTEVENTURA, MODIFIED FROM GUTIERREZ ET AL. (2006). 7

FIGURE. 2.1C. AN OUTCROP ON PLAYA ÁGULIA BEACH DEMONSTRATING THE UNCONFORMITY BETWEEN THE BASAL COMPLEX (BOTTOM) AND THE MIOCENE VOLCANICS (TOP). 8

FIGURE. 2.1D. CRETACEOUS SEDIMENTS IN A CAVE AT AJUI BEACH. 9

FIGURE. 2.1E. AN OUTCROP DEMONSTRATING MULTIPLE DYKE SWARMS AND INTRUSIONS 9

FIGURE. 2.2A. A SUMMARY OF PREVIOUSLY REPORTED AGES ON FUERTEVENTURA. 11

FIGURE. 2.2B. PROBABILITY DENSITY PLOT OF THE PREVIOUSLY REPORTED AGES FROM FUERTEVENTURA (K-AR, AR/AR, U-PB). 12

FIGURE. 3.2A. REFERENCE MATERIAL 94-35 SESSION 1 18

FIGURE. 3.2B. REFERENCE MATERIAL 94-35 SESSION 2 19

FIGURE. 3.2C. REFERENCE MATERIAL 94-35 SESSION 3 19

FIGURE. 3.4A. MUN-1 HF RESULTS WITH THE ACCEPTED MC-ICPMS SOLUTION VALUE (BLUE FIELD) 25

FIGURE. 3.4B. MUN-4 HF RESULTS WITH THE ACCEPTED MC-ICPMS SOLUTION VALUE (BLUE FIELD) 25

FIGURE. 4.1A. SAMPLE 2016MJ-04 CL IMAGES 29

FIGURE. 4.1B. SAMPLE 2016MJ-38 CL IMAGES 29

FIGURE. 4.1C. SAMPLE 2016MJ-39 CL IMAGES 29

FIGURE. 4.1.1A. 2016MJ-04 U-PB HISTOGRAM 30

FIGURE. 4.1.2A. 2016MJ-38 U-PB HISTOGRAM 32

FIGURE. 4.1.3A. 2016MJ-39 U-PB HISTOGRAM 33

FIGURE. 4.2.1A. AGE (MA) VERSUS TI CONCENTRATIONS 36

FIGURE. 4.2.2A. AGE (MA) VERSUS EU/EU* 38

FIGURE. 4.2.3A. EU/EU* VERSUS CE/CE* FOR FUERTEVENTURA DETRITAL ZIRCONS 40

FIGURE. 4.2.3B. AGE (MA) VERSUS CE/CE* FOR FUERTEVENTURA DETRITAL ZIRCONS 41

FIGURE. 4.2.4A. AGE (MA) VERSUS Y CONCENTRATIONS FOR FUERTEVENTURA DETRITAL ZIRCONS. 43

FIGURE. 4.2.5A. AGE (MA) VERSUS TH CONCENTRATIONS FOR FUERTEVENTURA DETRITAL ZIRCONS. 45

FIGURE. 4.2.5B. AGE (MA) VERSUS U CONCENTRATION IN CANARY DETRITAL ZIRCONS. 45

FIGURE. 4.2.5C. AGE (MA) VERSUS TH/U FOR FUERTEVENTURA DETRITAL ZIRCONS 47

FIGURE. 4.2.6A. NB CONCENTRATION VERSUS NB/TA IN FUERTEVENTURA DETRITAL ZIRCONS. ZIRCON ISOLATED FROM TWO FUERTEVENTURA SYENITES ARE ALSO SHOWN FOR COMPARISON. 49

FIGURE. 4.3A. PLAYA DEL ÁGUILA (2016MJ-04) DETRITAL ZIRCON EHFI VALUES 51

FIGURE. 4.3B. PLAYA DE GARCEY (2016MJ-38) EHFI VALUES 52

FIGURE. 4.3C. PLAYA DE GARCEY (2016MJ-38) EHFI HISTOGRAM DISTRIBUTION 52

FIGURE. 4.3D. BARRANCO DE LA SOLAPA (2016MJ-39) EHFI VALUES 53

FIGURE. 4.3E. EHFI VALUES OF DATED MIOCENE AND PLIOCENE ZIRCONS FROM BARRANCO DE LA SOLAPA (2016MJ-39). NOTE THE RELATIVELY ENRICHED VALUES COMPARED TO THE OTHER GRAINS FROM THIS SAMPLE. 53

FIGURE. 4.3F. HF ISOTOPE DATA FOR FUERTEVENTURA DETRITAL ZIRCONS 54

FIGURE. 4.4A. DETRITAL ZIRCON FROM THE PLAYA DE GARCEY BEACH SAMPLE..... 56

FIGURE. 4.4B. AGE (MA) VERSUS $\Delta^{18}O$ VALUES FOR DETRITAL ZIRCONS FROM PLAYA DEL ÁGUILA BEACH 58

FIGURE. 4.4C. AGE (MA) VERSUS $\Delta^{18}O$ VALUES FOR DETRITAL ZIRCON FROM PLAYA DE GARCEY BEACH58

FIGURE. 4.4D. AGE (MA) VERSUS $\Delta^{18}O$ VALUES FOR DETRITAL ZIRCON FROM BARRANCO DE LA SOLAPA 58

FIGURE. 5.1A. LA-MC-ICPMS PROBABILITY DENSITY PLOT FOR DETRITAL ZIRCON U-PB DATES FROM PLAYA DEL ÁGUILA BEACH (2016MJ-04), PLAYA DE GARCEY BEACH (2016MJ-38), AND BARRANCO DE LA SOLAPA RIVER (2016MJ-39). 63

FIGURE. 5.2A. (TOP) AND FIGURE. 5.2B. (BOTTOM) DEMONSTRATES THE U-PB DETRITAL ZIRCON AGE VARIATIONS BETWEEN FUERTEVENTURA'S NORTHERN AND CENTRAL SECTORS..... 67

FIGURE. 5.2C. DISTANCE VERSUS AGE PLOT FOR THE CANARY ARCHIPELAGO 68

FIGURE. 5.3A-G. PROVENANCE CLASSIFICATION OF DETRITAL ZIRCONS FROM SAMPLES 2016MJ-04, 2016MJ-38, AND 2016MJ-39 BASED ON MINOR AND TRACE ELEMENT GEOCHEMISTRY..... 73

FIGURE. 5.3H. AGE VERSUS EU/EU* IN FUERTEVENTURA DETRITAL ZIRCONS 74

FIGURE. 5.3I. YTTRIUM (PPM) VERSUS EU/EU* IN FUERTEVENTURA DETRITAL ZIRCONS..... 74

FIGURE. 5.3J. FUERTEVENTURA MAGMA PROVENANCE AGE VERSUS TI (PPM) IN FUERTEVENTURA DETRITAL ZIRCONS..... 75

FIGURE. 5.5A. EPSILON HF VERSUS AGE OF DETRITAL ZIRCONS FROM FUERTEVENTURA..... 80

FIGURE. 5.6A. FUERTEVENTURA DETRITAL ZIRCON EHFI VERSUS $\delta^{18}O$ PLOT 84

FIGURE. 5.6B. FUERTEVENTURA DETRITAL ZIRCON EHFI VERSUS $\delta^{18}O$ PLOT CORRELATED TO THE ROCK TYPE..... 84

FIGURE. 5.6C. SCHEMATIC REPRESENTATION OF THE VARIOUS MANTLE RESERVOIRS INVOLVED IN GENERATING FUERTEVENTURA'S MAGMATIC ACTIVITY BASED ON DETRITAL ZIRCON HF-O ISOTOPIC COMPOSITIONS 86

APPENDIX D1: CATHODOLUMINSCENCE IMAGES (2016MJ-04) 116

APPENDIX D2: CATHODOLUMINSCENCE IMAGES (2016MJ-38) 117

APPENDIX D3A: CATHODOLUMINSCENCE IMAGES (2016MJ-39) 118

APPENDIX D3B: CATHODOLUMINSCENCE IMAGES (2016MJ-39) 119

1. INTRODUCTION

The Canarian Archipelago is considered to be a peculiar island chain due to its long-lived alkaline-rich magmatism (Stillman & Robertson, 1979; Coello et al., 1992; Ancochea et al., 1996; Cantagrel et al., 1993; Muñoz et al., 2005; Allibon et al., 2011). Of these seven islands, Fuerteventura records the oldest, most complex geological history, which is mainly associated with the exposure of the uplifted seamount building stage in the western portion of the island. The geological units of Fuerteventura incorporate Mesozoic sediments, submarine volcanic rocks, dike swarms, alkaline plutons, subaerial Miocene basaltic volcanics, and Pliocene- Recent volcanics and sediments (Coello et al., 1992; Cantagrel et al., 1993; Ancochea et al., 1996; Demény et al., 1998; Muñoz et al., 2003; Muñoz et al., 2005; Gutiérrez et al., 2006; Meco et al., 2007; Allibon et al., 2011). The oldest plutonic rock bodies are commonly referred to as the Basal Complex, and contain alkaline rocks such as: syenites, nepheline syenites, gabbros, clinopyroxenites, ijolites, anorthosites, and carbonatites (Cantagrel et al., 1993; Muñoz et al., 2003; Muñoz et al., 2005; Gutiérrez et al., 2006; Allibon et al., 2011). One of the most controversial issues of Fuerteventura's geology is understanding when the onset of the magmatic activity began and the duration of magmatism. According to some authors, the magmatism began in the late Cretaceous-early Paleocene (Le Bas et al., 1986; Balogh et al., 1999), and continued until with the magmatic duration lasting around 65 Ma. These results are, however, based on conventional K-Ar dating methods, which may yield suspicious dates because of problems associated with excess argon and thermal resetting (Rona & Nalwalk, 1970; Abdel-Monen et al., 1971; Le Bas et al., 1986; Cantagrel et al., 1993). More recently, authors (Canagrel et al., 1993; Muñoz et al. 2005; Allibon et al.,

2011) have published U-Pb dates from zircon and baddeleyite using Laser Ablation Inductively Coupled Plasma Mass Spectrometry (LA-ICPMS) and Isotope Dilution Thermal Ionization Mass Spectrometry (ID-TIMS) methods. These studies suggest that the intrusive magmatic activity would have started around the Oligocene with plutons forming around 25 Ma.

Another point of contention is the magma source of this long-lived island chain. The island of Fuerteventura lies on old Jurassic oceanic crust, in close proximity to the coast of Morocco (100 km) and the Atlas Mountains (Araña & Ortiz, 1991; Carracedo et al., 1998). Due to this complex structural geology, several models have been proposed to explain the volcanic island origin: a propagating fracture, local rifting events, uplifting, or plume activity (Anguita & Herman, 1975; Stillman et al. 1975; Araña & Ortiz, 1991; Carracedo et al., 1998). In recent literature, the favoured hypothesis is the plume model; however, the source of the magmatic activity is still poorly understood. Hafnium isotope ratios are a powerful tool for investigating intraplate volcanism, particularly in plume models to identify mantle mixing signatures such as enriched-mantle (EM), depleted mantle (DM), and asthenosphere sources (Geldmacher et al., 2011). A hafnium study was completed by Geldmacher et al. (2011) on recent Fuerteventura basalt volcanics (<0.1 Ma) and demonstrated εHf_i values ranging from +8.4 to +10.4. This Hf range could potentially represent mixing trends with an older oceanic lithosphere (>1 Ga), depleted mantle peridotite, and enriched mantle sources, drawing a close parallel to the geochemistry observed in Satiago Island, Cape Verde (Martins et al., 2009; Geldmacher et al., 2011). An assessment of other magmatic episodes on Fuerteventura would be extremely valuable to understanding the magmatic evolution of the island, allowing us to

define any potential magma mixing throughout the duration of island formation. The Hf results can be paired with oxygen isotope data to look at the magmatic source and assess any crustal contamination (Demény et al., 1998; Demény et al., 2004). From previous studies (Demény et al., 1998; Demény et al., 2004), zircons from carbonatites associated with the initial magmatic activity have been interpreted to contain largely unaltered and uncontaminated primary compositions, demonstrating mantle-derived magmas (Demény et al., 1998). No further oxygen isotope studies have been completed to encompass other magmatic episodes on the island.

In order to evaluate the magmatic history of the intrusive alkaline bodies, we conducted a detrital zircon study to analyze the zircon-bearing plutonic provenance associated with: syenites, nepheline-syenites, gabbros, anorthosites, and carbonatites using LA-ICPMS U-Pb method. The obtained ages contribute to clarifying the previous age discrepancies and address the timing of the initial zircon-bearing plutonic activity, the duration of magmatism, and the main peaks in the magmatic activity. A detrital zircon study also provides a unique opportunity to assess the source and mixing trends of these uncharacteristic ocean island rocks by utilizing Hf and O isotope geochemistry. These new findings are combined to address the evolution of the island and promote new methods for analyzing Fuerteventura's geology.

2. BACKGROUND

Supplementary information of published ages can be found in Appendix. A.

2.1 Regional Geology

The Canary Islands are a volcanic island chain ~100 km off the west coast of Morocco in the east-central Atlantic Ocean, proximal to the African continent and the High Atlas Mountains (Figure. 2.1a). An east to west age progression in volcanism exists within the archipelago, with the oldest Canarian island, Fuerteventura, located in the eastern end of the island chain (Figure 2.1b; Coello et al., 1992; Ancochea et al., 1996; Muñoz et al., 2005; Allibon et al., 2011). The island group is situated on a slow-moving oceanic plate and was constructed on old (Jurassic) oceanic crust (195-154 Ma: Roest et al., 1992; Carracedeo et al. 1998). This archipelago is unique because three of the islands (Fuerteventura, La Palma, La Gomera) have been reported to contain uplifted portions of the earliest phases of the islands growth. This portion of the island has been referred to as the 'Basal Complex' by several authors (Stillman et al., 1975; Le Bas et al., 1986; Cantagrel et al., 1993; Muñoz et al., 2005, Allibon et al., 2011).

Fuerteventura's geology is generally divided into two major formations: the basal complex (BC) and the younger subaerial volcanic series (Stillman et al., 1975; Le Bas et al. 1986; Robertson & Stillman, 1989; Coello et al., 1992); separated by a widespread unconformity that is well-exposed on the west side of the island (Figure. 2.1c). The BC is exposed in the western central portion of the island and consists of Cretaceous sediments, alkaline plutons, dyke swarms, volcanic breccias, and pillow basalts (Figure. 2.1d) (Muñoz et al., 2003, 2005). The abundance of dykes are extreme throughout the basal complex, with dykes in some regions comprising >90% of the bed rock (Figure. 2.1e). The alkaline intrusive portion of the BC is composed of silica-undersaturated alkaline

rocks such as: clinopyroxenites, ijolites, nepheline syenites, syenites, and carbonatites (Coello et al., 1992; Ancochea et al., 1996; Muñoz et al., 2005; Allibon et al., 2011). Both the host rocks and dykes in the BC assemblage show pervasive greenschist-facies metamorphism but typically do not have a deformational fabric (Stillman et al., 1975).

The subaerial volcanics are comprised of Miocene, Pliocene, and recent volcanics (Fuster et al., 1968a; Coello et al., 1992; Cantagrel et al., 1993). The oldest volcanics in the sequence are considered to be the shield-building stage of development, lying unconformably on the BC (Fuster et al., 1968a; Coello et al., 1992). The age for this magmatic activity in published literature ranges from ~20-12 Ma (Ancochea et al., 1990). This rock series is dominated by basalts with ankaramite and trachybasaltic rock assemblages (Coello et al., 1992). After a period of magmatic quiescence, Pliocene and recent volcanics were erupted in much smaller volumes. This suite consists of basalts and associated lava flows (Meco and Stearns, 1981; Coello et al., 1992; Meco et al., 2007).

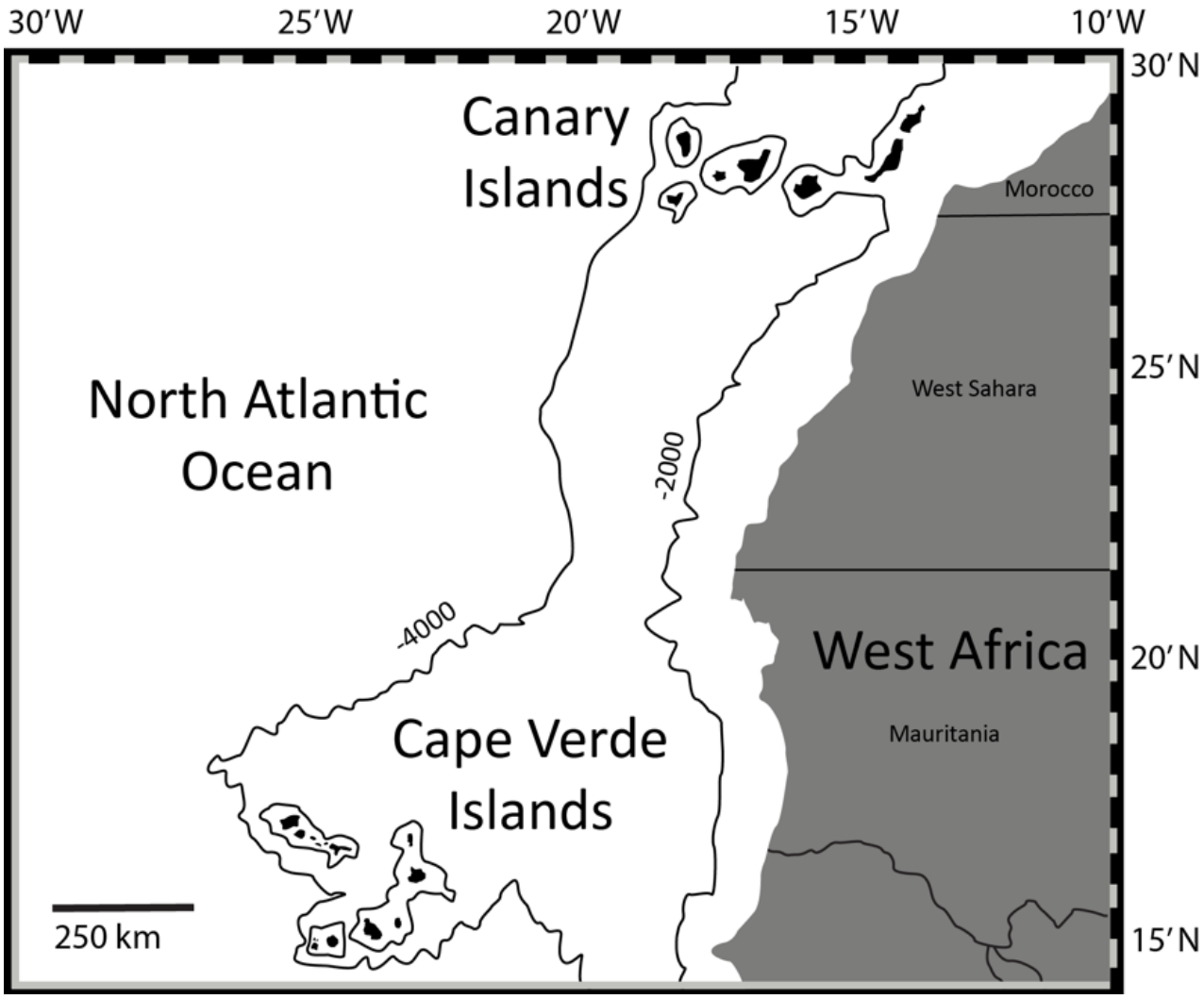

Figure. 2.1a. Map of the eastern North Atlantic showing the Canary Islands, Cape Verde Islands, and the west coast of Africa, modified from Hoernle et al. (2002).

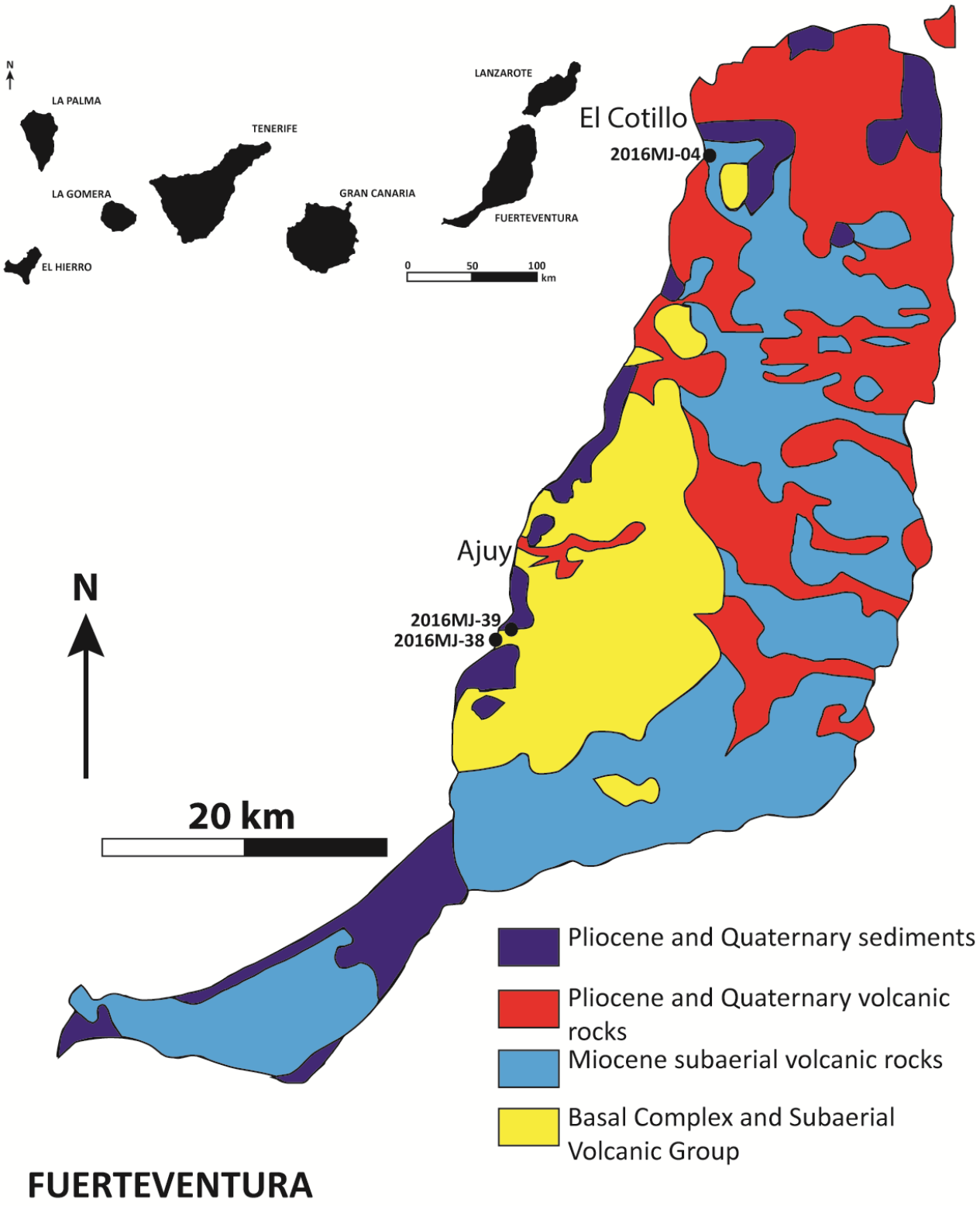

Figure. 2.1b. Geological map of Fuerteventura, modified from Gutierrez et al. (2006).

Figure. 2.1c. An outcrop on Playa Águlia beach demonstrating the unconformity between the basal complex (bottom) and the Miocene volcanics (top).

Figure. 2.1d. Cretaceous sediments in a cave at Ajui Beach.

Figure. 2.1e. An outcrop demonstrating multiple dyke swarms and intrusions covering >90% of the country rock in the region.

2.2 Fuerteventura Basal Complex

The basal complex (BC) consists of Mesozoic deep-water sediments (Upper Jurassic to Lower-Middle Cretaceous), followed by emplacement of basaltic volcanic breccias, hyaloclastites, and pillow-lavas (Fúster et al., 1980; Balogh et al., 1999). The earliest known plutonic rocks are exposed in the western portion of the island. An extensive archive of K-Ar dates have been reported for samples from the BC (>18 Ma) over the span of 4 decades (see summary in Appendix. A; Figure. 2.2a; Figure. 2.2b). From these previous geochronological studies, the BC has been subdivided into three successive magmatic events: EM1, PX1 and/or EM2, and EM3 (Muñoz et al., 2005; Allibon et al., 2011). The oldest intrusive event, EM1, is associated with an alkaline-carbonatite intrusive complex. The age of the initial complex emplacement has been a point of contention for several years. Le Bas et al. (1986) presented the oldest K-Ar dates for this unit, ranging from 48-20 Ma (Appendix. A; Figure. 2.2a); however, these dates have not been replicated in subsequent studies and are considered to be erroneous (Balogh et al., 1999; Muñoz et al., 2005). Another study by Balogh et al. (1999) demonstrated large scatter in the K-Ar and Ar/Ar ages from associated syenite intrusions, and also a clear effect of excess argon in some BC rock units. Balogh et al.'s (1999) study contains syenite ages ranging from 22-71 Ma but attributes the scatter of the ages to excess argon and hydrothermal resetting. In more recent literature, the BC has been dated by the U-Pb zircon and baddeleyite method using both Laser Ablation Inductively Coupled Plasma Mass Spectrometry (LA-ICP-MS) and Isotope Dilution Thermal Ionization Mass Spectrometry (ID-TIMS), as well as Ar/Ar method (Appendix. A). The ICP-MS data from Muñoz et al. (2005) gives a robust zircon U-Pb age on an EM1 syenite

at 25.4 ± 0.4 Ma, placing the complex crystallization in the late Oligocene. Cantagrel et al. (1993) dated a carbonatite dyke from the EM1 alkaline complex using the U-Pb ID-TIMS method and obtained a slightly younger age of 23.2 ± 0.2 Ma. The subsequent intrusive complex, PX1/EM2, was dated using the ID-TIMS method. The obtained age suggests the initial magma crystallization took place at 22.10 ± 0.07 Ma and lasted for 0.52 Ma (Allibon et al., 2011). The Vega de Rio Palma gabbro-syenite subvolcanic ring complex (EM3) is considered the youngest intrusive suite in the BC with K-Ar ages ranging from 22-18 Ma (Abdel-Monem et al., 1971; Cantagrel et al., 1993). This intrusive suite has not been dated using U-Pb systematics.

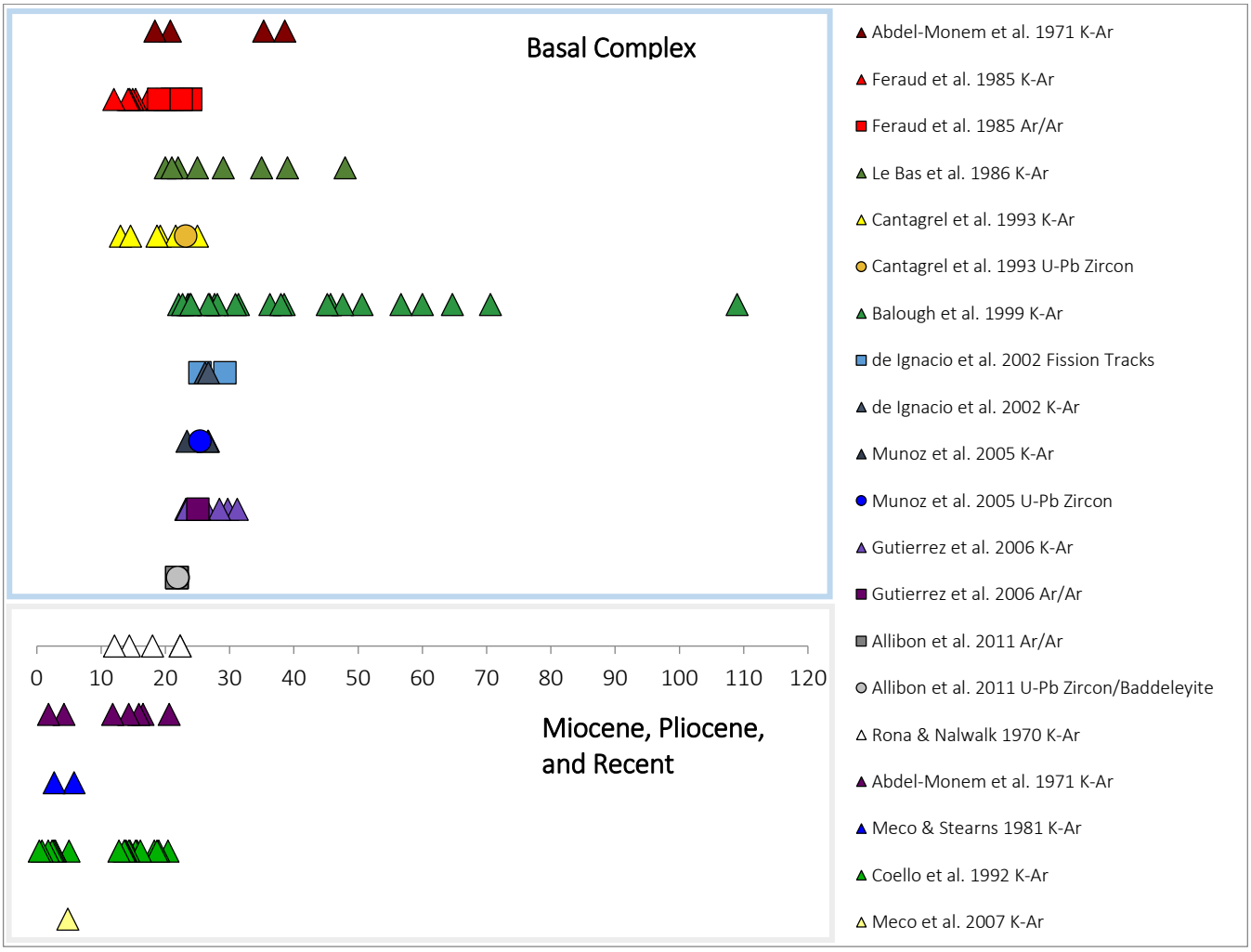

Figure. 2.2a. A summary of previously reported ages on Fuerteventura.

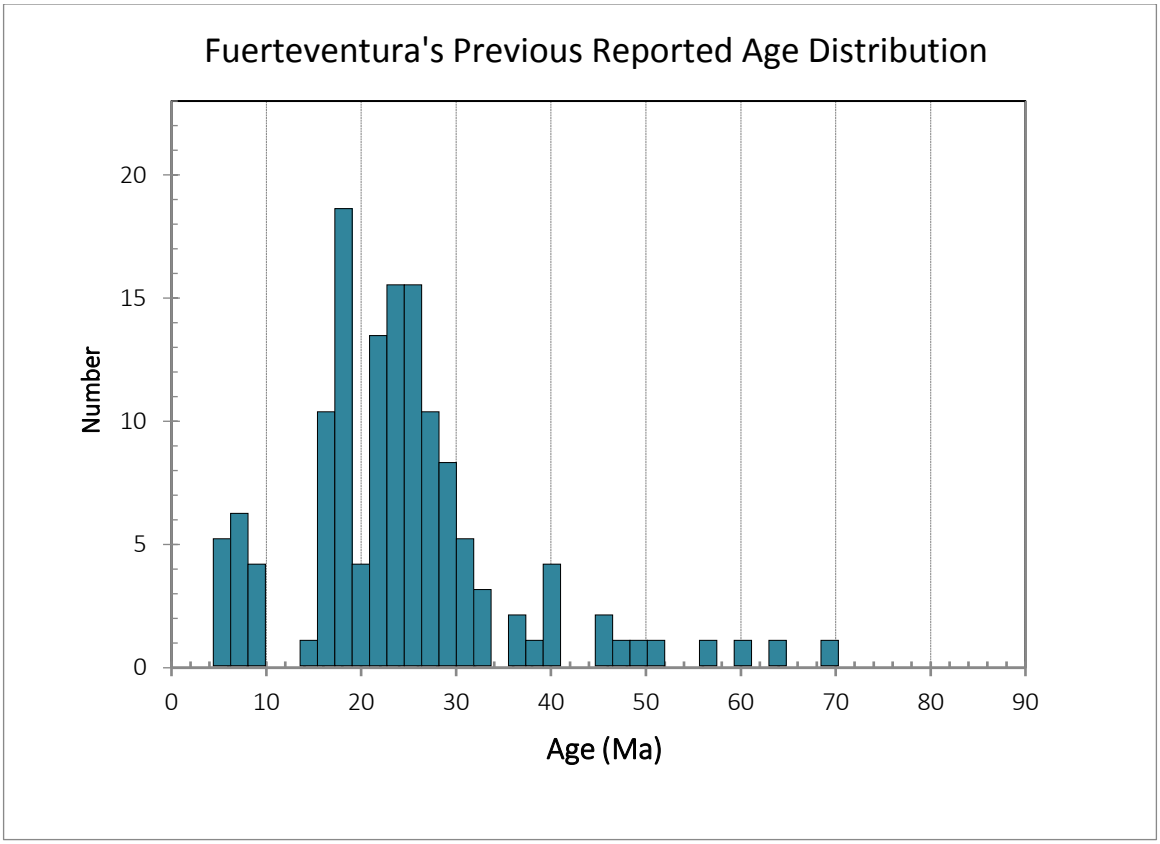

Figure. 2.2b. Probability density plot of the previously reported ages from Fuerteventura (K-Ar, Ar/Ar, U-Pb).

2.3 Subaerial Volcanic Series of the Neogene and Quaternary

The Miocene volcanics (20-12 Ma) represent the subaerial phase on Fuerteventura (see K-Ar whole rock dates reported by Coello et al. 1992; Ancochea et al., 1996; Appendix. A). Originally, Fuster et al. (1968a) identified the earliest Miocene volcanics unconformably overlying the BC, referring to this assemblage as the Old Basaltic Series. In the more recent literature, the earliest volcanics have been referred to as Series I, and have been subdivided into three volcanic complexes: northern, central, and southern (Coello et al., 1992; Ancochea et al. 1996). The definition of each edifice is based on the stratigraphy, morphology, radial dyke swarms and duration (Coello et al., 1992;

Ancochea et al., 1996). The rock assemblages includes: olivine basalts, trachytes, ankaramites, picritic and tholeiitic basalts (Coello et al., 1992; Appendix. A). After the initial subaerial magmatic activity, there was an eruptive gap during the Middle-Lower Miocene for approximately 7 Mya (Coello et al., 1992; Ancochea et al., 1996; Carracedo et al., 1998). This has been considered to represent the transformation from shield-building stage to post-erosional or rejuvenated-stage volcanism (Carreacedo et al., 1998). The subsequent magmatic sequences (Series II, III, IV) emplaced predominantly during the Pliocene were smaller volume eruptions compared to the initial subaerial magmatic activity (Ancochea et al., 1996). The rock assemblage associated with the later volcanics consists of pillow basalts, olivine basalts, basanites, and olivine nephelinites (Appendix. A) (Meco and Stearns, 1981; Coello et al., 1992; Meco et al., 2007). The eruption dates from these particular units are strictly based on the K-Ar whole rock method. Carracedo et al. (1998) does not use stratigraphic distinction with Series I, II, III, IV and strictly divides the Miocene and Pliocene/recent volcanics into 'shield-building' and 'post-erosional' stratigraphy. This is a parallel subdivision approach to previous Hawaiian shield volcano studies (MacDonald and Abbott, 1970).

3. METHODOLOGY

3.1 Zircon Mount Preparation

The sand samples collected for U-Pb zircon geochronology were between 2-3 kilograms. Zircon separation was completed at the University of Alberta, where the samples were initially sieved at <0.707 μm size to remove larger pebbles and granules. The samples were then separated into light, medium, and heavy mineral components using a Wilfey Table. The heavy concentrates were further separated based on magnetic susceptibility using a Frantz Isodynamic Separator in a free-fall and conventional mode. The non-magnetic and magnetic mineral fractions were separated using the conventional Frantz methods at current strengths of 0.1, 0.2, 0.4, 0.6, 1.0, 1.2, and 1.6 amperes. The non-magnetic minerals were then further separated based on density properties using the heavy liquid Methylene Iodide (d=3.3 g/cc^3). The grains were then examined under a high-magnification stereomicroscope, hand-picked, and secured into an epoxy mount for analysis.

The selected zircon grains were initially positioned with a small pipette onto a double-sided glass plate, which were then repositioned using fine-tipped tweezers into the mounting stage. Once 2.5 grams of epoxy resin was warmed, 0.5 grams of EpoxiCure hardener was added to a plastic vial. The epoxy mixture was then stirred with a wooden stir stick until a homogeneous solution formed and slowly poured into a grain mount casing to cover the zircon grains. The mount was then left to set overnight. After the epoxy dried, the bottom on the grain mount was polished with Carborundum wet silicon carbide waterproof paper 400 grit sand paper to level the outer edges of the mount. The top of the grain mount was polished with Carborundum wet silicon carbide waterproof

paper 1200 grit sand paper. The polishing process continued until both the core and outer edges of the zircon grains were exposed. Once the appropriate exposure was achieved, the mount was then polished with Buehler deagglomerated alpha alumina micropolish at both 1.0 and 0.3 micron to ensure the grains lost a majority of scratches/imperfections. Throughout the polishing process, the grains were checked under a reflected light microscope to monitor the polishing process.

3.2 Zircon U-Pb Dating LA-ICP-MS

U-Pb zircon dating was conducted on a polished epoxy grain mount using a New Wave 213 nm laser workstation coupled to a Nu Plasma I Multi-Collector Inductively Coupled Plasma Mass Spectrometer (LA-MC-ICP-MS) at the University of Alberta Radiogenic Isotope Facility. This MC-ICP-MS instrument has been customized to include 12 Faraday collectors and 3 ion-counting detectors (Simonetti et al., 2005). The ion counter detectors were configured to measure $^{204}Pb + {}^{204}Hg$, ^{206}Pb, and ^{207}Pb signals, and the Faraday collectors count U and Tl isotopes (Simonetti et al., 2005). The laser ablation spot diameter used in this study was 40 μm.

The LA-MC-ICP-MS method was preferred for this study due to the high spatial resolution, lower cost, and time efficiency, all benefits for a reconnaissance detrital zircon study. The zircon grains from the Canary Islands exhibit tremendous grain complexities associated with igneous oscillatory zoning, irregular zoning, regions of alteration, or fractures (see Results section, Figure 4.1a-c). Prior to analysis, the grains were characterized with cathodoluminescence (CL) imaging using a Zeiss Sigma 300 VP-FESEM microscope in the Scanning Electron Microscope Laboratory at the University of Alberta. These images were used as a reference to assist in spot selection during the analytical sessions. Due to the large size of the grains, the laser spot size of 40 μm diameter provided enough flexibility to analyze specific pristine areas of the grains yet capture enough material to ensure sufficient U and Pb signals (typically mass 206 signals were >1000 cps).

A disadvantage of the Nu Plasma ICP-MS method used in this study is the ion collectors are unable to distinguish between ^{204}Pb and ^{204}Hg ions due to isobaric

interference and there are insufficient ion counters to simultaneously measure ^{202}Hg. The majority of zircons had 204Pb cps values <100 so any common Pb correction in this study was negligible.

To ensure the accuracy of the analyses, zircon standards that had been previously accurately dated were analysed periodically throughout the laser session. During the analysis session, two zircon standards were analyzed after every 10 laser analyses of unknowns. One standard (GJ1-32) was used to test the accuracy of the method and instrument performance, while the other (94-35) was used to determine the U/Pb and Pb/Pb fractionation (Simonetti et al., 2005). The GJ1-32 standard has been described by Simonetti et al. (2008) using the ID-TIMS method, yielding a ^{207}Pb/^{206}Pb weighted mean age of 606.7±2.3 (2σ) Ma. This age was then tested on a LA-MC-ICP-MS, which was in agreement with the obtained age. The primary standard 94-35 has been described by Klepeisa et al. (1998) and is accurately dated by ID-TIMS and yielded a weighted mean ^{207}Pb/^{206}Pb age of 55.5 ± 1.5 Ma (2σ). The LA-MC-ICP-MS reference material ages can be found in Table. 3.2. All analyses are reported in Appendix. B1-3.

During the three analytical sessions, zircon 94-35 was measured repeatedly throughout (after ~10 unknown analyses). Due to the young age of the grains and their extremely low ^{207}Pb contents, the ^{206}Pb/^{238}U weighted mean age is reported. The first analytical session was with sample 2016MJ-04 with a ^{206}Pb/^{238}U weighted mean age is 55.62± 0.81 Ma (MSWD= 1.02; n= 10/10) (Figure. 3.2a). The second session was completed on sample 2016MJ-38 with a ^{206}Pb/^{238}U weighted mean age is 57.23± 0.55 Ma (MSWD= 0.29; n= 10/12) (Figure. 3.2b). The third analytical session was completed on 2016MJ-39 with a ^{206}Pb/^{238}U weighted mean age of 56.27± 0.97 Ma (MSWD= 2.5; n=

11/13) (Figure. 3.c). Each session was in analytical agreement within uncertainty of the published date.

Sample	Session	Date Analyzed	$^{206}Pb/^{238}U$ Weighted Mean	Number of Samples
2016MJ-04	1	May. 17th, 2017	55.6± 0.8 Ma	10 out of 10
2016MJ-38/39*	2	May. 18th, 2017	57.2± 0.6 Ma	10 out of 12
2016MJ-39	3	May. 19th, 2017	56.3± 1.0 Ma	11 out of 13

*2016MJ-39, zircons 1-12

Table 3.2. Reference Material 94-35

Once filtered and evaluated, the data were plotted using an Excel add-in, Isoplot (Ludwig 2008). All age errors are reported with 2 sigma level of uncertainty or at the 95% confidence level. The uranium decay constant, $^{238}U=1.55125\times10^{-10}$ year^{-1}, as determined by Jaffey et al. (1971) was used in the age calculations.

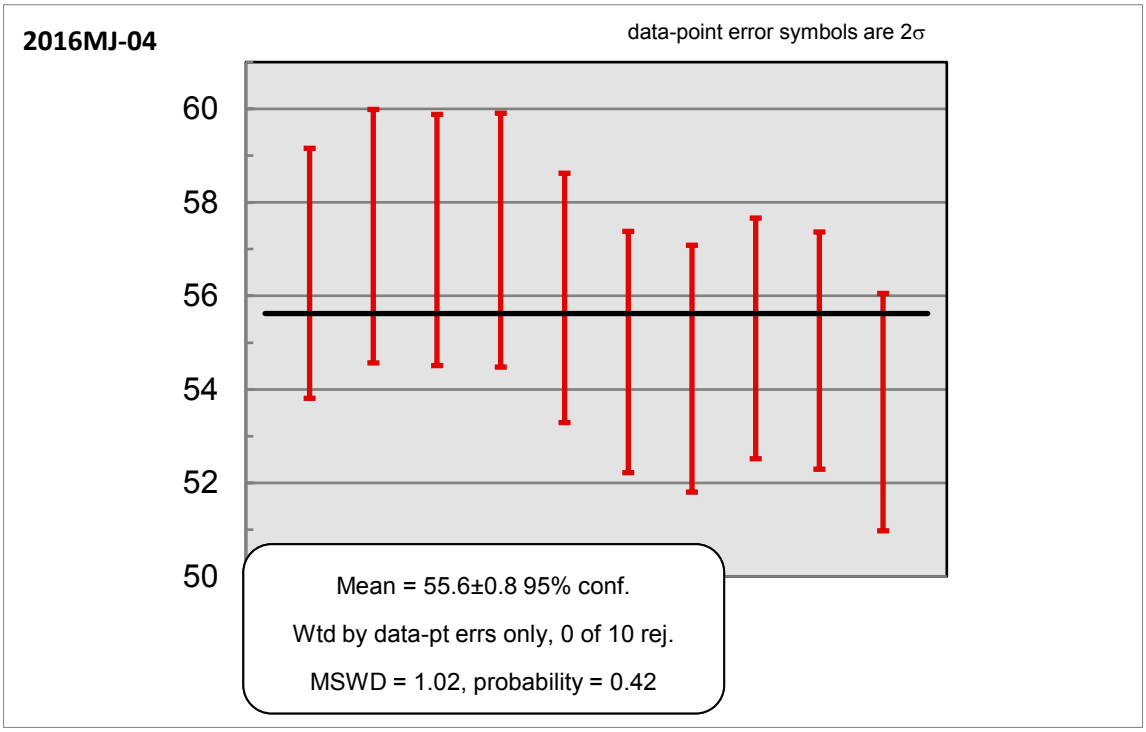

Figure. 3.2a. Reference material 94-35 session 1

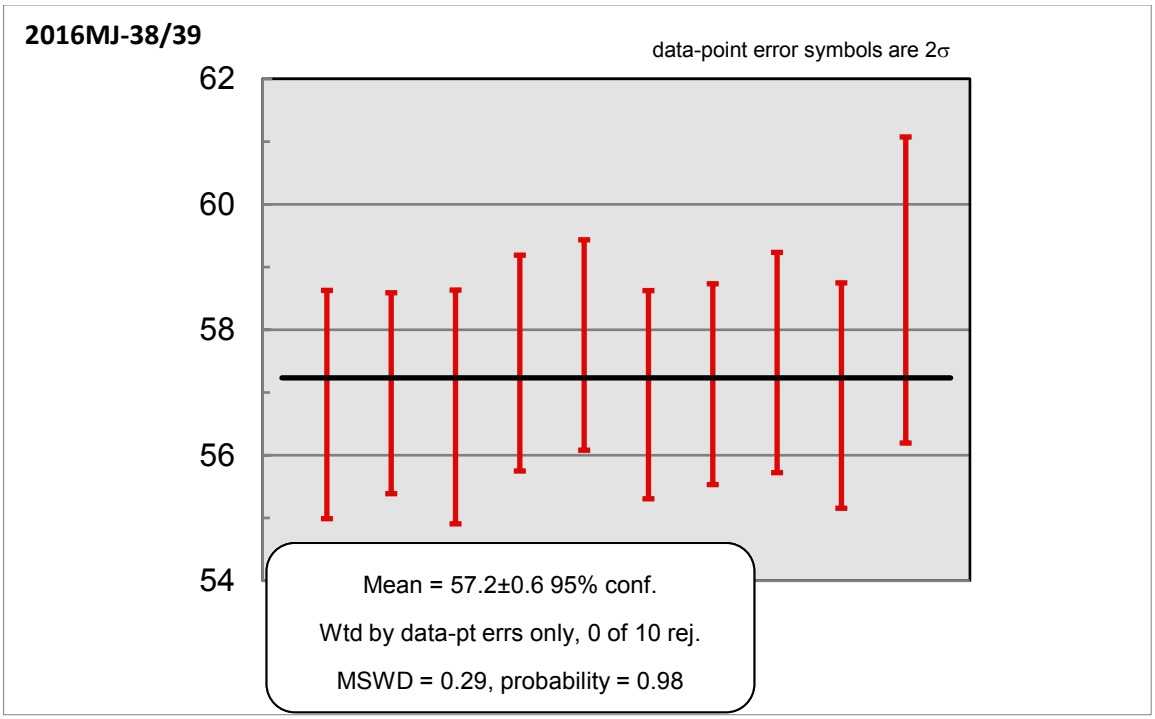

Figure. 3.2b. Reference material 94-35 session 2

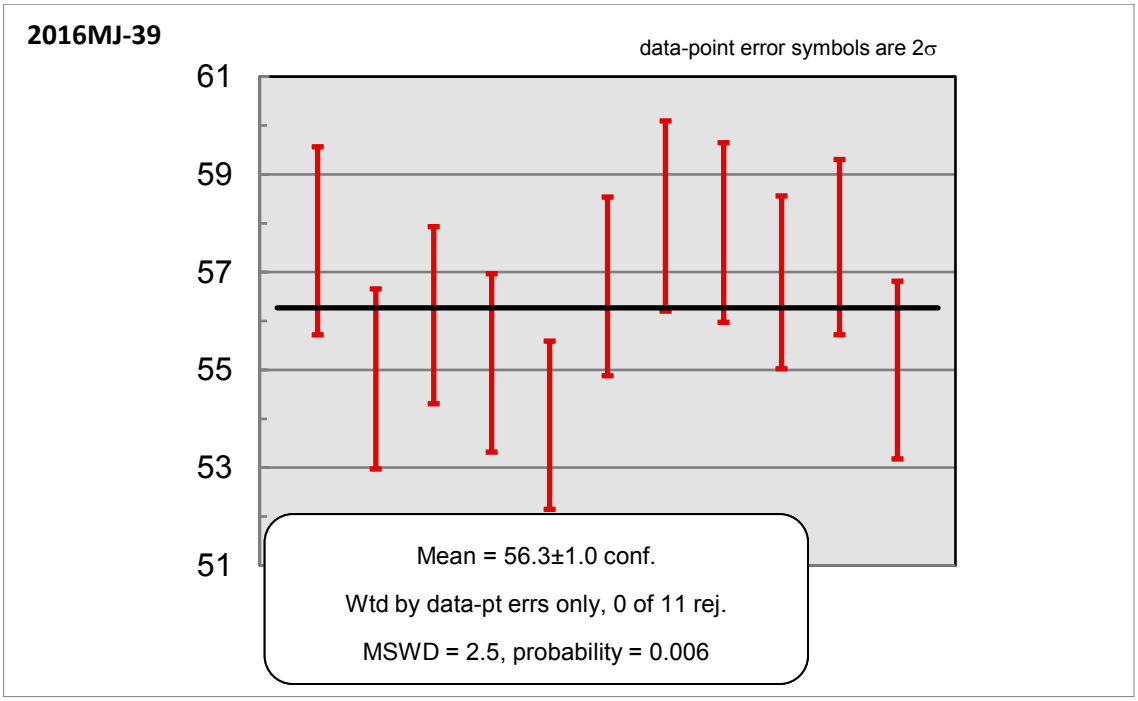

Figure. 3.2c. Reference material 94-35 session 3

3.3 LA-Q-ICP-MS trace element analyses

Zircon trace-element data were acquired using a New Wave 213 nm laser-ablation system coupled with a Thermo Scientific iCAP-Q Quadrupole Inductively Coupled Plasma Mass Spectrometer at the University of Alberta Radiogenic Isotope Facility. Concentrations for twenty-three elements were acquired: ^{31}P, ^{45}Sc, ^{49}Ti, ^{89}Y, ^{93}Nb, ^{139}La, ^{140}Ce, ^{141}Pr, ^{146}Nd, ^{147}Sm, ^{153}Eu, ^{157}Gd, ^{159}Tb, ^{163}Dy, ^{165}Ho, ^{166}Er, ^{169}Tm, ^{172}Yb, ^{175}Lu, ^{177}Hf, ^{181}Ta, ^{232}Th, and, ^{238}U using a 5 Hz laser pulse rate, fluence of 3-4 J/cm^2, and a Helium flow rate of 0.5L per minute. The repetition rate was set to yield wider, shallower pit diameter/depth ratios to ensure the fractionation of select trace elements was minimized. Each analysis comprised 25 seconds for baseline measurement, 30 seconds for an integrated measurement, followed by 70 seconds of ablation time. The laser spot diameter was 30 μm.

NIST 612 standard glass and 91500 were used to tune the ICPMS after every 10 unknowns were analyzed to ensure the production rates are within the correct range. An average of the session analyses and accepted values from the GeoReM standards can be found in Table. 3.3.

The concentrations in the NIST612 standard glass from this study all reside within the accepted values from GeoReM 5211, within the 2 standard error range (Jochum et al., 2011). The zirconium value is substantially higher than the accepted GeoReM value but falls within a large range of uncertainty. The 91500 standard results obtained in this study are in excellent agreement with published data (Wiedenbeck et al. 2004; Yuan et al. 2004) for the majority of elements. Exceptions include higher than expected phosphorus with 42.8 ± 8.58 ppm obtained in this study compared to the value of 24.0 ± 1.0 ppm

recommended for GeoReM 293 (Yuan et al., 2004) and slightly lower ytterbium values (65.8 ± 2.68 ppm) compared to the accepted value of 74.0 ± 4.0 ppm (Wiedenbeck et. al., 2004). The measured zirconium value was ~160,000 ppm lower than the accepted value of 497,700 ppm. Other issues included an undetermined scandium value and titanium, lanthanum, and promethium concentrations below detection limit.

Table 3.3. NIST612 and 91500 Results and Accepted Values

Element	P	Sc	Ti	Ti	Y	Zr	Nb	La	Ce	Pr	Nd	Sm	Eu	Gd	Tb	Dy	Ho	Er	Tm	Yb	Lu	Hf	Ta	Th	U
	31	**45**	**49**	**50**	**89**	**91**	**93**	**139**	**140**	**141**	**146**	**147**	**153**	**157**	**159**	**163**	**165**	**166**	**169**	**172**	**175**	**177**	**181**	**232**	**238**
NIST612																									
This study	53	41.1	44.1	49	37.9	75.1	39.6	35.4	38.8	36.8	35.9	39.1	34.9	36.6	35.9	35.9	37.8	38.1	37.9	38.6	36.7	35.1	39.9	37.8	37.5
2 SE	16.4	2.6	8.3	25.3	2.6	29.5	2.7	2.5	2.8	2.4	3.1	3.3	2.5	3.1	2.4	2.9	2.5	3.0	2.5	3.1	2.4	4.3	2.5	2.7	2.9
GeoReM 5211	46.6	39.9	44	N/A	38.3	37.9	38.9	36	38.4	37.9	35.5	37.7	35.6	37.3	37.6	35.5	38.3	38	36.8	39.2	37	36.7	37.6	37.8	37.4
2 SE	6.9	2.5	2.3	N/A	1.4	1.2	2.1	0.7	0.7	1	0.7	0.8	0.8	0.9	1.1	0.7	0.8	0.9	0.6	0.9	0.9	1.2	1.9	0.1	0.1
91500																									
This study	42.8	343.1	BDL	BDL	140.8	3.3E+05	1.1	BDL	2.4	BDL	0.2	0.4	0.2	2.2	0.8	11.5	4.7	26.2	6.6	65.8	14.2	5891.0	0.5	28.7	73.4
2 SE	8.58	8.82	BDL	BDL	4.01	1.0E+04	0.10	BDL	0.15	BDL	0.09	0.14	0.06	0.36	0.08	0.73	0.24	1.07	0.30	2.68	0.57	188.00	0.07	1.04	2.54
GeoRem*	24	N/A	6	N/A	140	4.9E+05	0.79	0.006	2.6	0.024	0.24	0.5	0.24	2.2	0.86	12	4.8	25	6.9	74	13	5900	0.5	30	80
2 SE	1	N/A	1	N/A	14	2.2E+03	0.07	0.003	0.3	0.015	0.04	0.08	0.03	0.3	0.07	1	0.4	3	0.4	4	1	300	0.1	3	8
*GeoReM 293 (P, Ti), GeoReM 104 all other elements																									

All concentrations are reported in ppm.

3.4 Laser ablation split stream (LASS)

The laser Ablation Split Stream (LASS) technique described by Yuan et al. (2008), Xie et al. (2008) and Fisher et al. (2011, 2014) was used to analyze 134 detrital zircon grains. The simultaneous U-Pb and Hf measurements were obtained at the University of Alberta Artic Resources Laboratory. The U-Pb isotope measurements were acquired on a single-collector Thermo Element XR mass spectrometer using single secondary electron multiplier (SEM). Hf isotope measurements were obtained simultaneously on a multi-collector Thermo Neptune Plus mass spectrometer using multiple Faraday detectors with 10^{11} Ω amplifiers operating in static collection mode. The samples were ablated using a Resolution Excimer 193 nm laser operating with a 40 μm diameter spot size**.** The duration of each analysis was approximately 105 seconds, consisting of 30 seconds of background measurements; 45 seconds of ablation time, and 30 seconds wash out time. Both U-Pb and Hf were processed using the Iolite v3.32 software. Analytical errors are reported as 2 standard errors (SE), representing confidence limits of 95%.

The advantage of the LASS method is that is provides an opportunity to analyze both U-Pb and Hf isotope ratio simultaneously from the same ablated area in a grain. The Iolite data reduction process permits each data point to be adapted to ensure each grain analysis is collecting a uniform age and Hf isotope composition. Once the analytical data were reduced, the Hf was converted into εHf_t using the present-day chondritic uniform reservoir (CHUR): $^{176}Hf/^{177}Hf$=0.282785 and $^{176}Lu/^{177}Hf$=0.0336 (Bouvier et al., 2008). The ^{176}Lu decay constant used for the calculation is 1.867 x 10^{11} yr-1 (Söderlund et al., 2004). The U-Pb data were then filtered based on the quantity of common lead counts per second (Appendix. F). Samples did not contain large portions of ^{204}Pb (<100 cps), eliminating concerns regarding the isobaric interference from ^{204}Hg and ^{204}Pb. This filtering process is essential because the $^{206}Pb/^{238}U$ is not

corrected for common lead. Since ^{204}Pb ions cannot be quantified, a common lead correction runs the risk of incorrectly estimating the absolute amount of ^{204}Pb (Simonetti et al., 2005). The filtered data were plotted using Isoplot software (refer to the MC-ICP-MS section for method). The uranium decay constant Jaffey et al. (1971) was used in the age calculations.

The disadvantage of the LASS method on young zircon samples with low uranium is the spot size had to be increased to 40 μm in order to reach the required signals of U, Pb, and Hf. This decreases the spatial resolution; however, the Canary Island zircons this is not problematic because the large grains size provided adequate area in each region.

Another disadvantage with this method is the isobaric interference observed in ^{176}Yb and ^{176}Lu on the ^{176}Hf ions. In order to overcome this interference, each analytical run included two synthetic zircon standards (MUN1 and MUN4) that contain the same $^{176}Hf/^{177}Hf$ ratios, however, contain different of HREE concentrations (varied Yb/Hf ratios) to determine the interference correction (Fisher et al., 2011) (analytical results in Figures. 3.4a. and 3.4b.). MUN1 and MUN4 were chosen because they provide a wide-scale linear trend, creating a large window to interpolate $^{176}Hf/^{177}Hf$ ratios in the unknowns. The measured $^{176}Yb/^{173}Yb$ ratio was obtained during a standard sequence run to optimize the Yb interference correction throughout the entire session. The mean $^{176}Hf/^{177}Hf$ for MUN1 and MUN4 ($0.282130 \pm 2.64952 \times 10^{-5}$ (2SD), n=21; $0.282160 \pm 4.10476 \times 10^{-5}$ (2SD), n=21), compared to the MC-ICPMS solution values of 0.282140 ±6 (2SD) and 0.282141 ± 6 (2SD) (Fisher et al., 2011). The MUN1 results are in close agreement to the solution value, whereas MUN4 yields a significantly higher value than the solution, but within error. Due to the high Yb/Hf ratio, higher errors are typically seen in MUN4.

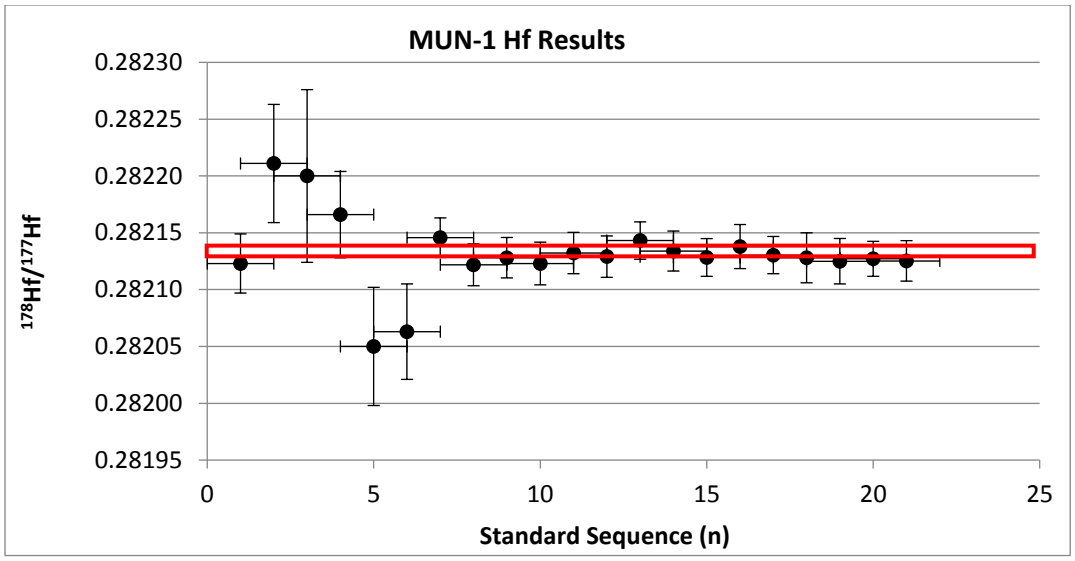

Figure. 3.4a. MUN-1 Hf Results with the accepted MC-ICPMS solution value (red field)

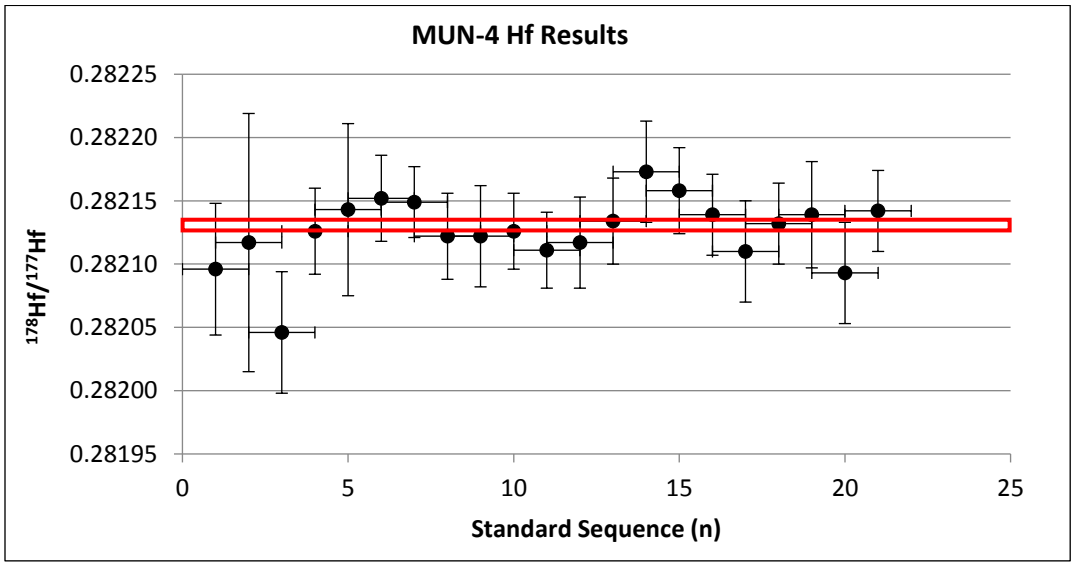

Figure. 3.4b. MUN-4 Hf Results with the accepted MC-ICPMS solution value (red field)

3.5 SIMS Oxygen

Mount preparation was completed in the Canadian Centre for Isotopic Microanalysis (CCIM) at the University of Alberta. The epoxy grain mount (CCIM ID: M1479) contains zircon from samples 2016MJ-04, 38, and 39 and reference materials (RM) prepared for SIMS analysis. The RM used in the mount were TEM2 and UAMT1 zircon (CCIM ID: S0022 and S0081). During mount preparation, previously analyzed grains (U-Pb, Hf, trace elements) were carefully removed from mounts used in U-Pb and Hf isotope analysis and remounted onto a mount stage using a fine-tipped needle probe and tweezers. These grains were then covered in the epoxy and left to set. Once the mount was set, the unknowns and RM's were polished with one 25mm diameter epoxy mount using diamond grit and cleaned with lab soap and de-ionized H_2O. The mount was then coated with 10nm of high-purity Au prior to the scanning electron prior to scanning electron microscopy (SEM) utilizing a Zeiss EVO MA15 instrument equipped with a high-sensitivity cathodoluminescence (CL) and backscattered electron detectors. Beam conditions were 15kV and 3 – 5 nA sample current. A further 40 nm of Au was subsequently deposited on the mount prior to SIMS analysis.

Oxygen isotope ($^{18}O/^{16}O$) compositions were measured on 191 spots on 91 detrital zircon grains using a Cameca IMS 1280 multicollector ion microprobe. A $^{133}Cs^+$ primary beam was operated with impact energy of 20 keV and beam current of 1.5 – 2.0 nA. The ~10 μm diameter ion beam was rastered (20 x 20 μm) for 45 s prior to acquisition, and then 5 x 5 μm during acquisition, forming analyzed areas ~15 μm across and ~2 μm deep. The normal incidence electron gun was utilized for charge compensation. Negative secondary ions were extracted through 10 kV into the secondary (transfer) column. Transfer conditions included a 122 μm entrance slit, a 5 x 5 mm pre-ESA (field) aperture, and 100x sample magnification at the field

aperture, transmitting all regions of the sputtered area. No energy filtering was employed. The mass/charge separated oxygen ions were detected simultaneously in Faraday cups L'2 ($^{16}O^-$) and H'2 ($^{18}O^-$) at mass resolutions (m/Δm at 10%) of 1950 and 2250, respectively. Secondary ion count rates for $^{16}O^-$ and $^{18}O^-$ were typically ~2 x 10^9 and 4 x 10^6 counts/s utilizing 10^{10} Ω and 10^{11} Ω amplifier circuits, respectively. Faraday cup baselines were measured at the start of the analytical session. A single analysis took 280 s, including pre-analysis rastering, automated secondary ion tuning, and 75 s of continuous peak counting.

Instrumental mass fractionation (IMF) was monitored by repeated analysis of zircon primary (TEM2, $\delta^{18}O_{VSMOW}$ = +8.2 ‰; Black et al., 2004) and secondary (S0081 = UAMT1, $\delta^{18}O_{VSMOW}$ = +4.87; R. Stern, unpublished laser fluorination data, University of Oregon) reference materials. The $^{18}O^-/^{16}O^-$ data set for the primary RM S0022 was processed collectively for two sessions (N = 23, 17), yielding standard deviations of 0.08‰ and 0.10‰, following correction for systematic within-session drift of ≤0.2‰; overall IMF was +1.1 ‰. The individual spot uncertainties for the unknowns at 95% confidence for $\delta^{18}O_{VSMOW}$ include errors relating to within-spot counting statistics, between-spot (geometric) effects, and correction for instrumental mass fractionation, and average ±0.23‰. Results for multiple spots on multiple grains of the secondary RM (S0081) gave mean session values for $\delta^{18}O_{VSMOW}$ = +4.81 ±0.05‰ and + 4.78 ±0.06‰.

$\delta^{18}O_{VSMOW}$ was calculated as follows:

$\delta^{18}O_{VSMOW} = ((^{18}O / ^{16}O_{SAMPLE}) / (^{18}O / ^{16}O_{VSMOW})^{1})$ where $^{18}O / ^{16}O_{VSMOW}$ = 0.0020052, and reported in ‰.

4. RESULTS

4.1 Zircon U-Pb Laser Ablation Inductively Coupled Plasma Mass Spectrometry (LA-MC-ICPMS) Analysis

Supplementary U-Pb data can be found in Appendix C1-3.

In-situ U-Pb Laser Ablation Inductively Couple Plasma Mass Spectrometry (LA-MC-ICPMS) analyses were completed on 260 zircon grains from three locations on Fuerteventura (see Geological Map; Figure. 2.1b.). The zircon yield varied significantly with 2016MJ-04 producing zircon in the several tens of grains, in contrast to samples 2016MJ-38 and 2016MJ-39 containing several thousand grains. Prior to analysis, each sample was analyzed in a mount using cathodoluminescence (CL) microscope (see Methodology 3.2 for details). Supplementary zircon images are provided in Appendix. D1-D3B. The CL imaging provided an understanding of the zircon characteristics and morphologies. The laser spot location was determined from the CL images, systematically avoiding fractures, irregularities, and inclusions. The most notable CL variation was observed in sample 2016MJ-04, exhibiting irregular zoning and sponge-like textures (Figure. 4.1a). Samples 2016MJ-38 and 2016MJ-39 contain less CL variation, exhibiting oscillatory zoning or no apparent zoning (Figure. 4.1b; Figure. 4.1c).

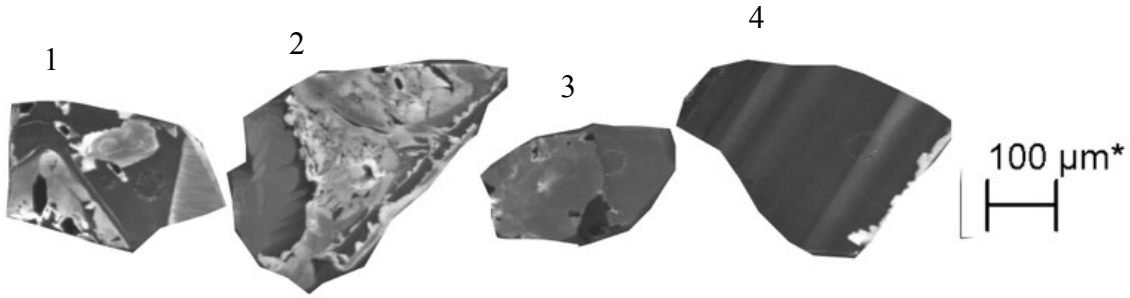

Figure. 4.1a. Sample 2016MJ-04 CL images demonstrating irregular, blocky zoning and sponge-like textures (1, 2), exhibiting no zoning (3), and oscillatory zoning (4).

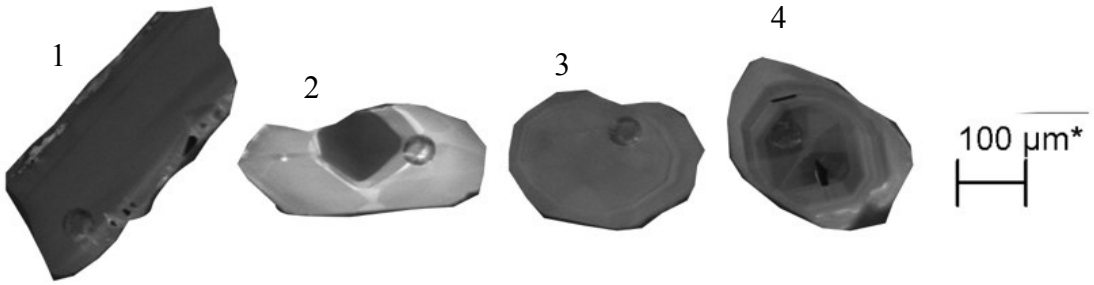

Figure. 4.1b. Sample 2016MJ-38 CL images demonstrating absence of zoning in grains (1) and oscillatory zoning in grains (2, 3, 4).

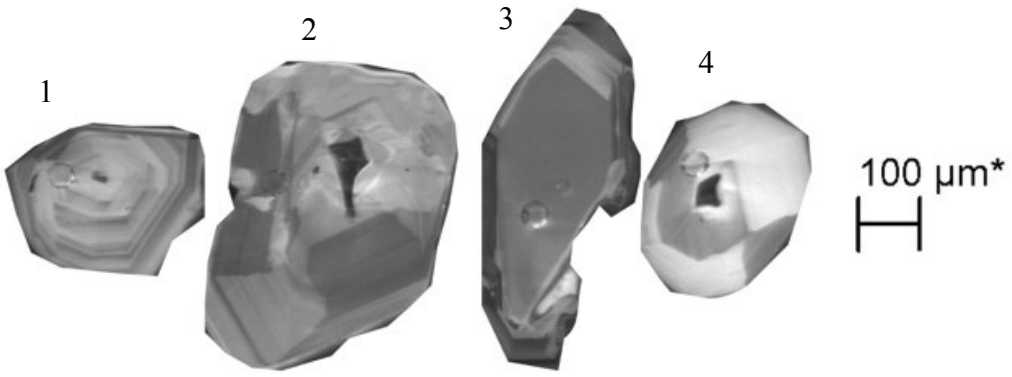

Figure. 4.1c. Sample 2016MJ-39 CL images demonstrating oscillatory zoning (1, 2, 3, 4).

4.1.1 Playa del Águila beach sand 2016MJ-04

U-Pb LA-MC-ICPMS detrital zircon ages were determined for sample 2016MJ-04, collected from Playa del Águila beach. A total of 36 zircon grains were analyzed, with ages ranging from 16.1 ± 0.8 to 33.7 ± 2.9 Ma. The peaks of the main age populations are at 16.9 ± 0.6 and 26.4 ± 0.2 Ma (Figure. 4.1.1a.). All reported age peaks were determined using Isoplot Unmixed Ages software (Ludwig, 2008). These ages are mostly in agreement with the geochronology literature from Fuerteventura (Coello et al., 1992; Muñoz et al. 2005; Gutiérrez et al., 2006; Allibon et al., 2011); however, the previously reported lower Miocene population (14.3-12.8 Ma) is missing from the present study. Another significant difference in the age population is the relatively large population of ages >27 Ma, an age group identified in a few previous studies (Gutiérrez et al., 2006).

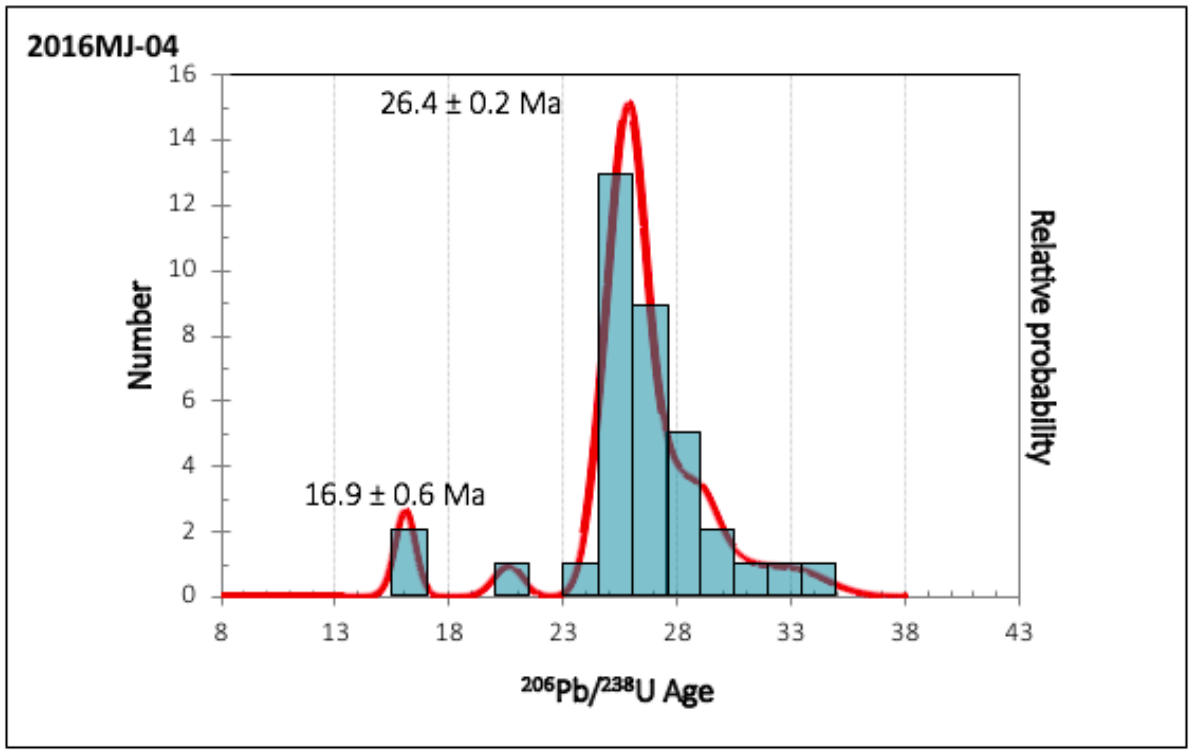

Figure. 4.1.1a. 2016MJ-04 U-Pb histogram

4.1.2 Playa de Garcey beach sand 2016MJ-38

U-Pb LA-MC-ICPMS detrital zircon ages were determined on sample 2016MJ-38, located on Playa de Garcey beach. A total of 105 zircon grains were analyzed, ranging from 3.8 to 30.8 Ma. There are 4 populations observed in 2016MJ-38, one dominant population at 16.7 ± 0.1 Ma, one subordinate population at 20.9 ± 0.3 Ma, and two very minor populations at 4.1 ± 0.1 Ma and 25.8 ± 0.4 Ma (Figure. 4.1.2a.). The 25.8 ± 0.4 Ma peak overlaps the U-Pb zircon age of the alkaline-carbonatite complex syenite at 25.4 ± 0.04 Ma (Muñoz et al. 2005). This dated syenite is considered to be part of the uplifted basal complex, incorporating the initial magmatic activity of the island (Muñoz et al. 2005) (Figure. 4.14a). The 20.8 ± 0.3 Ma is in close agreement to the central volcanic event and EM2 intrusions (also referred to as the Pájara pluton, PX1) described by Allibon et al. (2011) or the EM3 intrusions related to the emplacement of alkaline gabbros and syenites of the Vega de Río Palmas Complex (21.4-18.7 Ma) (Allibon et al. 2011, Muñoz et al., 2005). The 16.7 ± 0.1 Ma peak could possibly be linked to the EM4 event ranging from 17.5-14.5 Ma, incorporating the subvolcanic Betancuria trachytic-syenitic complex (Ancochea et al., 1996; Muñoz et al., 2005). There are 5 young grains observed in this population at: 3.8 ± 0.3 Ma, 3.9 ± 0.1 Ma, 4.1 ± 0.4 Ma, 4.4 ± 0.3 Ma, 4.4 ± 0.1 Ma, and 5.0 ± 0.5 Ma.

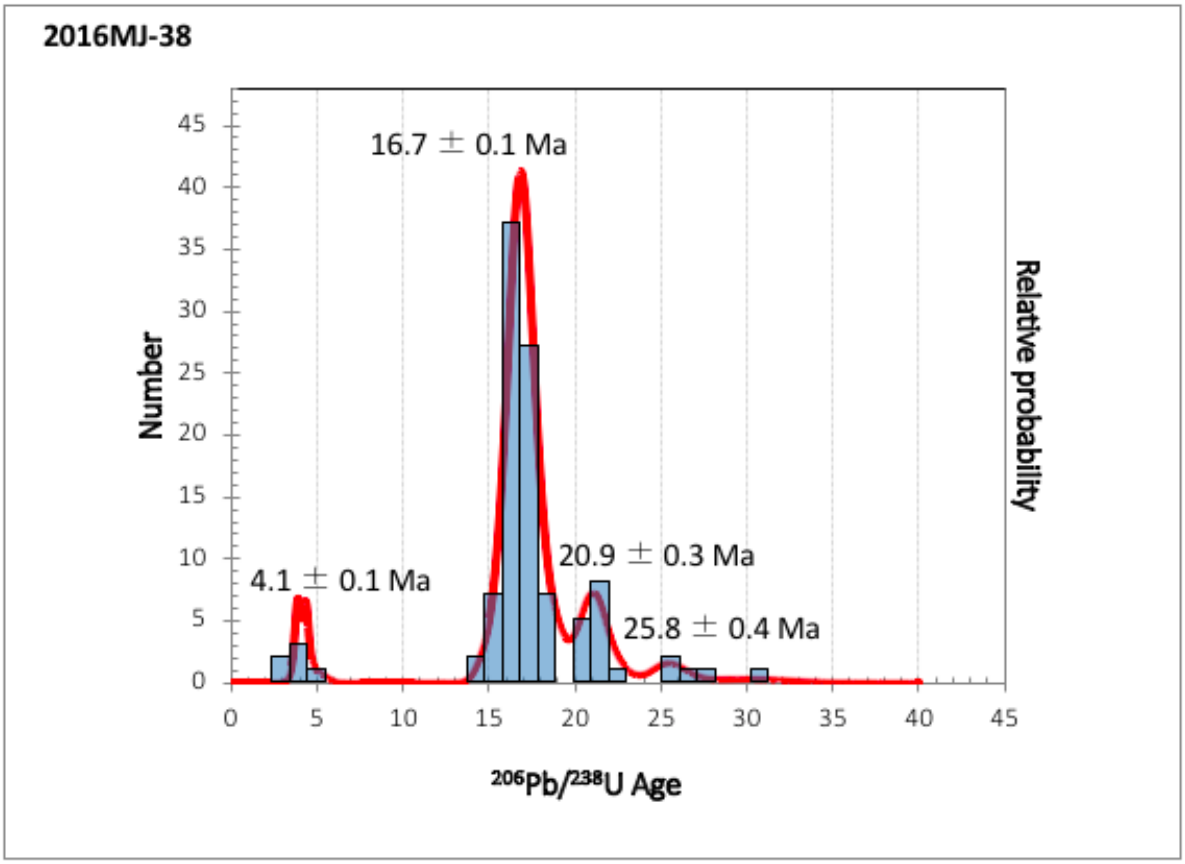

Figure. 4.1.2a. 2016MJ-38 U-Pb histogram

4.1.3 Barranco de la Solapa river sand 2016MJ-39

U-Pb LA-MC-ICPMS detrital zircon ages were determined on sample 2016MJ-39, located in Barranco de la Solapa. A total of 107 zircon grains were analyzed, ranging from 4.6 to 27.9 Ma. There were 3 observed peaks at 5.2 ± 0.1 Ma, 17.1 ± 0.1 Ma, and 21.6 ± 0.9 Ma (Figure. 4.1.3a.). In comparison to sample 2016MJ-38, this population has similar age groupings around 17.1 Ma and 21.6 Ma. There is also a unique age population around 23 Ma that is not observed in the 2016MJ-38 beach sample, representing 20% of the analyzed grains. This population overlaps the younger portion of the alkaline-carbonatite intrusions described by Muñoz et al. (2005). The Pliocene zircon peak observed at 5.2 ± 0.1 Ma is from 3 Pliocene

grains at 4.6 ± 0.2 Ma, 5.6 ± 0.2 Ma, and 6.5 ± 0.3 Ma. There is another prominent hiatus in analysis observed around 15.4-6.5 Ma, in close agreement with sample 2016MJ-38.

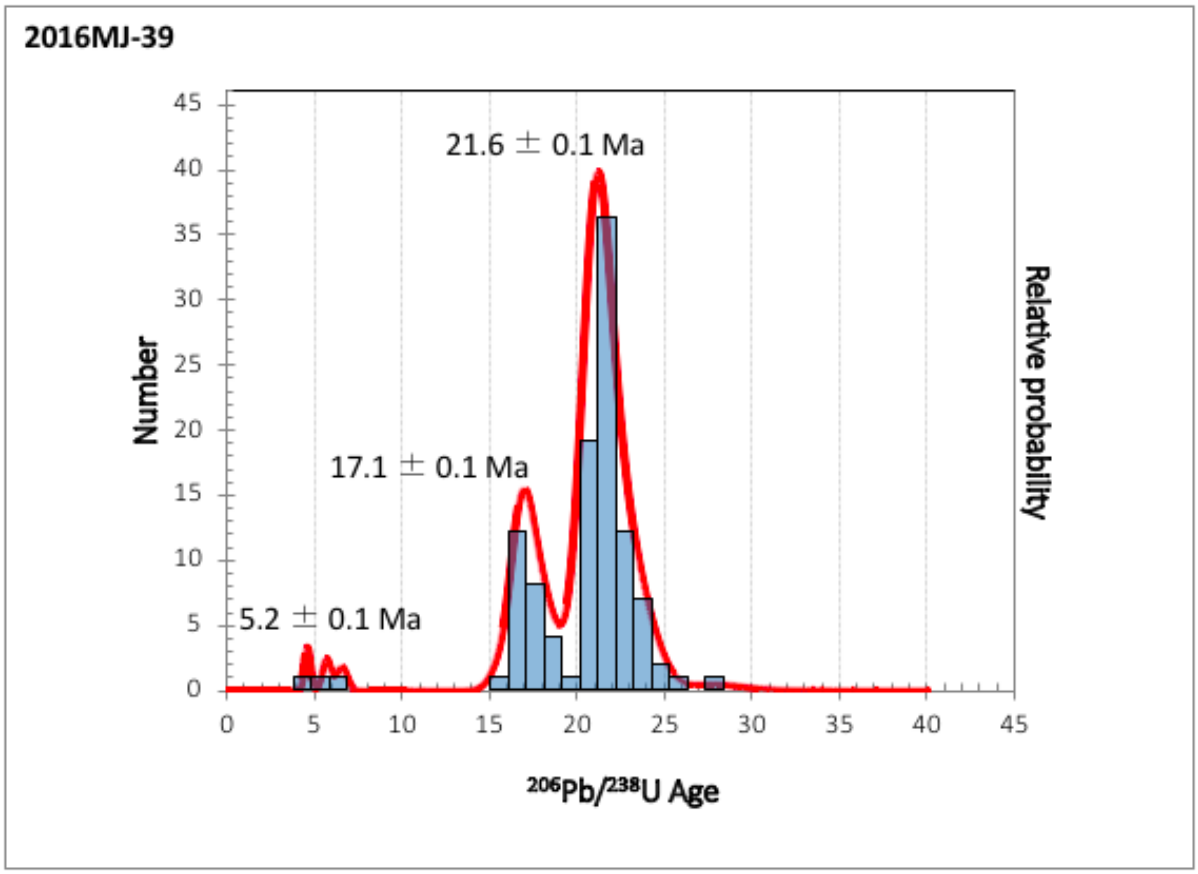

Figure. 4.1.3a. 2016MJ-39 U-Pb histogram

4.2 Zircon Trace-Element Geochemistry

Zircon is an accessory mineral that occurs in a wide variety of igneous rocks (granite, syenite, nepheline syenite, gabbro, anorthosite, kimberlite, and carbonatite). In addition to the widespread application of U-Pb zircon geochronology, zircon can be used to trace rock provenance because it incorporates a number of trace elements (e.g., REE, P, Y, Ti, Th, and U) during magma crystallization. There are numerous studies now that demonstrate the minor and trace element concentrations in zircon are generally controlled by original magma compositions (Murali et al., 1983; Heaman et al. 1990; Belousova et al., 2002; Hoskin, 2005 and references therein) and magma crystallization variables, such as temperature (Watson et al., 2006) and oxygen fugacity (Smythe and Brenan, 2016). The combination of precise U-Pb dating of single detrital zircons and their trace-element characteristics is a powerful provenance tool with the potential to help unravel a more detailed and complete record of Fuerteventura's early magmatic evolution.

In-situ minor and trace-element data were obtained using a New Wave UP-213 with a Thermo Scientific iCAP-Q Quadrupole Inductively Coupled Plasma Mass Spectrometer (LA-ICPMS) on 149 single detrital zircon grains from three different sand samples located along the west coast of Fuerteventura (see Geological Map. 2.1b.). Each 30-µm spot was selected using CL images to avoid any fractures, impurities, and rims (see Methodology 3.2. for detailed technique). A summary of all minor- and trace-element abundances are reported in Appendix. E.

4.2.1 Ti

A previous study by Fu et al. (2008) found that a majority of zircon grains from different tectonic settings and from both felsic and mafic magma types contain < 20 ppm Ti. They demonstrated that zircon Ti concentrations decrease from mafic to felsic lithologies and by inference with decreasing magma crystallization temperatures. This zircon Ti content and magma temperature correlation has provided an opportunity to utilize the Ti concentrations in zircon as a Ti-in-zircon thermometer (Watson et al., 2006; Fu et al., 2008). The highest Ti concentrations from their study (17-48 ppm) were from Mid-Atlantic Ridge gabbro and gabbro serpentinites and mantle zircon megacrysts from kimberlites (20-53 ppm).

Ti concentrations from the Fuerteventura zircon analyses range from 1-490 ppm, with 82% of the data points plotting between 10-100 ppm. (Figure. 4.2.1a). The analyses from sample 2016MJ-04 contain low Ti concentrations (<25 ppm), with a large portion of the sample population (65%) plotting below detection limit (~7-11 ppm). The zircon grains that fall below the detection limit are assigned a value of 1 ppm for plotting purposes to capture the existence of this low- Ti population. Sample 2016MJ-38 contains a wider Ti variation, with 55% of the analyses containing <20 ppm Ti concentrations. The remaining population comprises samples containing 20-48 ppm of Ti, with three outliers exceeding 60 ppm (63.6, 122, 490 ppm) between 16.8 to 20.8 Ma. Sample 2016MJ-39 also has a large portion of analyses with elevated Ti contents, with only 15% of the zircon grains containing <20 ppm Ti. A majority of the population ranges from ≥20 -78.2 ppm, with two outliers at 87 and 246 ppm. The grains with this range of Ti contents yield ages between 5.6 and 26.1 Ma. Fu et al. (2008) suggests that anomalously high Ti in zircon grains can be typically linked to impurities in the zircon grain.

Zircon trace-element data (unpublished, Heaman) from two syenites on Fuerteventura indictae two distinct Ti concentrations: (1) one sample 2016MJ-14 contains low Ti contents ranging from 6-14 ppm; (2) a second sample 2016MJ-34 contains elevated Ti concentrations ranging 140 -194 ppm (grey field; Figure. 4.2.1). The syenite sample 2016MJ-14 overlaps the detrital analyses observed in 2016MJ-04 and 2016MJ-38, while 2016MJ-34 lies in the upper Ti population associated with a small portion of 2016MJ-38 and 2016MJ-39.

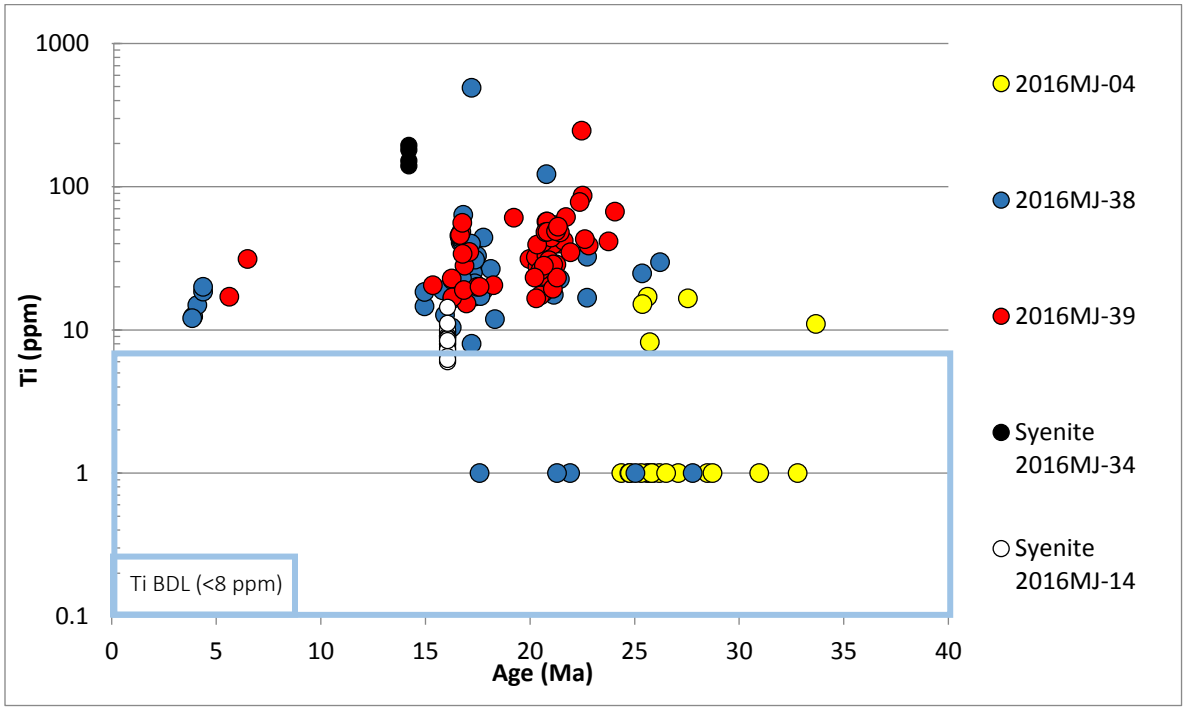

Figure. 4.2.1a. Age (Ma) versus Ti concentrations. The Ti below detection limit reference field covers the possible concentration range of the samples denoted as 1 ppm for display purposes only.

4.2.2 Eu/Eu*

The Eu anomaly (Eu/Eu*) is calculated as Eu*/SQRT(Sm*x Gd*), where the normalization (*) is calculated from the measured concentration/chondrite (values from Sun & McDonough, 1989). The Eu anomaly is important for zircon trace-element studies because it indicates if the magma was enriched or depleted in Eu during zircon crystallization (Sun & McDonough, 1989). The results from the three sand samples can be subdivided into two groups: those zircons with a negligible Eu anomaly (Eu/Eu*~1) and those with a strong to moderate negative Eu anomaly (0.18-0.80; Figure. 4.2.2a). Liebsch's (1996) study of the Laacher See Complex (LSC) contrasts phonolites with prominent negative Eu/Eu* anomalies to carbonatites from the Eifel volcanics that exhibit a lack of significant negative Eu/Eu* anomalies (Schmitt et al., 2010). In another study from Murali et al. (1983), negative Eu/Eu* anomalies (0.35-0.61) were also observed in nepheline syenites and syenites, in contrast to negligible Eu/Eu* anomalies observed in carbonatite (see grey field in Figure. 4.2.2a). This is a sensitive tool to monitor plagioclase crystallization from carbonatite magmas.

Sample 2016MJ-04 zircons exhibit the most consistent Eu/Eu* signature, ranging from 0.90-1.10, exhibiting a weak positive or negative Eu anomaly or no Eu anomaly at all. It is important to note that a majority of the 2016MJ-04 samples represents the oldest zircons measured in this study, with ages ranging from 24.4 to 33.7 Ma (Figure. 4.2.2a). The zircon in samples 2016MJ-38 and 2016MJ-39 zircons have a greater range of Eu/Eu* values, with a majority of the analyses (73%) having Eu/Eu* between 0.30-0.60 for grains with ages of 24.1 to 15.0 Ma (Figure. 4.2.2a). Sample 2016MJ-38 contains a small proportion of older grains (>25 Ma) that exhibits a more fractionated Eu/Eu* signature (0.47-0.56) than observed in 2016MJ-04 older grains (Figure. 4.2.2a). There is also a notable population of grains exhibiting negligible

Eu/Eu* anomalies from 0.83-1.00 in ages ranging from 4.4 to 25.0 Ma. A majority of the younger grains ranging from 3.84-6.49 Ma exhibit negative Eu/Eu* anomalies from 0.45-0.80.

Both of the Canary Island syenite zircons have negative Eu/Eu* anomalies, forming two clusters at 0.09-0.24 and ~0.45. Both of these populations overlap the detrital samples analyzed from this study. The anorthosite analyzed from Allibon et al. (2011) also demonstrates an overlapping relationship with the Eu/Eu* samples from 2016MJ-39 in the range of ~0.55 (Figure. 4.2.2a).

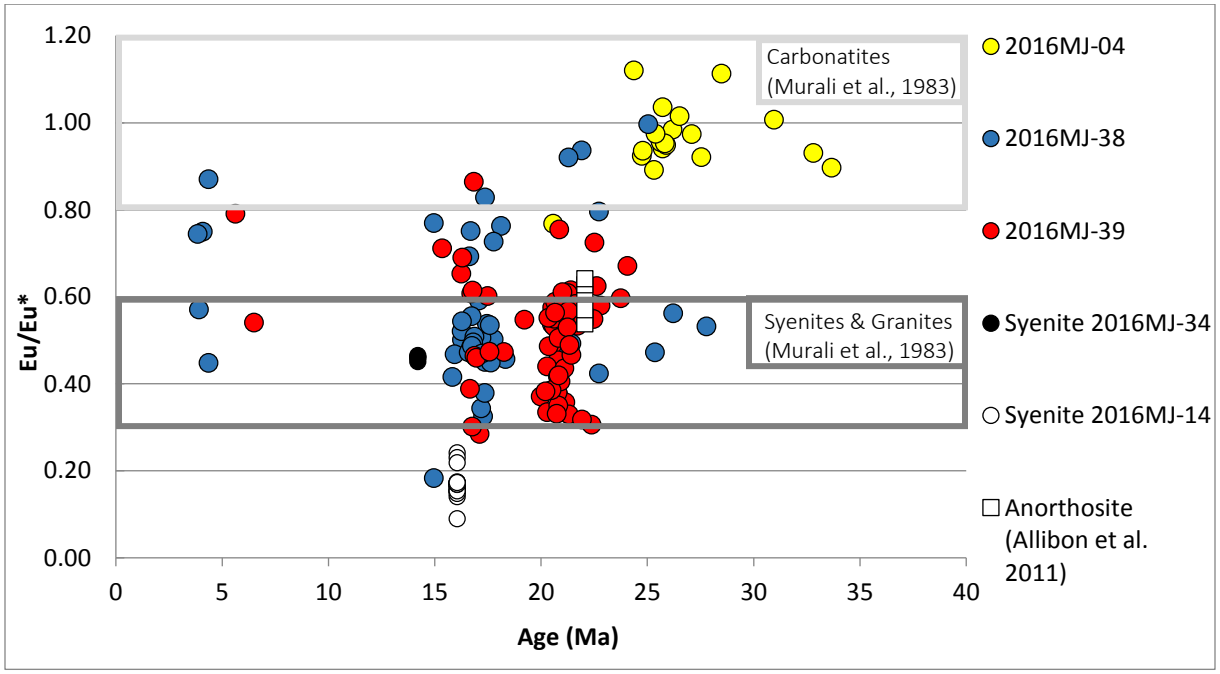

Figure. 4.2.2a. Age (Ma) versus Eu/Eu* with reference fields of carbonatite, syenite, and granite based on trace element data reported in Murali et al. (1983). Eu/Eu* values were normalized to chondrite using values reported in Sun and McDonough (1989).

4.2.3 Ce/Ce*

The Ce anomaly (Ce/Ce*) is calculated as Ce*/SQRT(La*x Pr*), where the normalization (*) is calculated from the measured concentration/chondrite (values from Sun & McDonough, 1989). The Ce anomaly can be used in conjunction with Eu anomaly to differentiate nepheline syenites, syenites, carbonatites, migmatites, and pegmatites (Murali et al., 1983; Belousova et al., 2002; Schmitt et al., 2010). The samples containing positive Ce/Ce* anomalies (1.7-9.6) with negative Eu/Eu* anomalies were typically associated with nepheline syenites and syenites, while samples with no apparent Ce/Ce* or Eu/Eu* anomaly were typically associated with carbonatites or pegmatites (Murali et al., 1983). Belousova et al. (2002) found a similar Ce/Ce* relationship, with the most pronounced Ce anomalies (Ce/Ce* from 2->300) observed in syenite pegmatites and weak Ce anomalies (Ce/Ce* from 1-10) found in zircon from kimberlites, carbonatites, and granitoids. Hoskin (2005) investigated hydrothermal vs. magmatic zircon and showed both have distinctive Ce anomalies; the hydrothermal zircon containing low Ce anomalies of 1.8-3.5, while the magmatic zircon had Ce anomalies ranging from 32-49 (Hoskin, 2005).

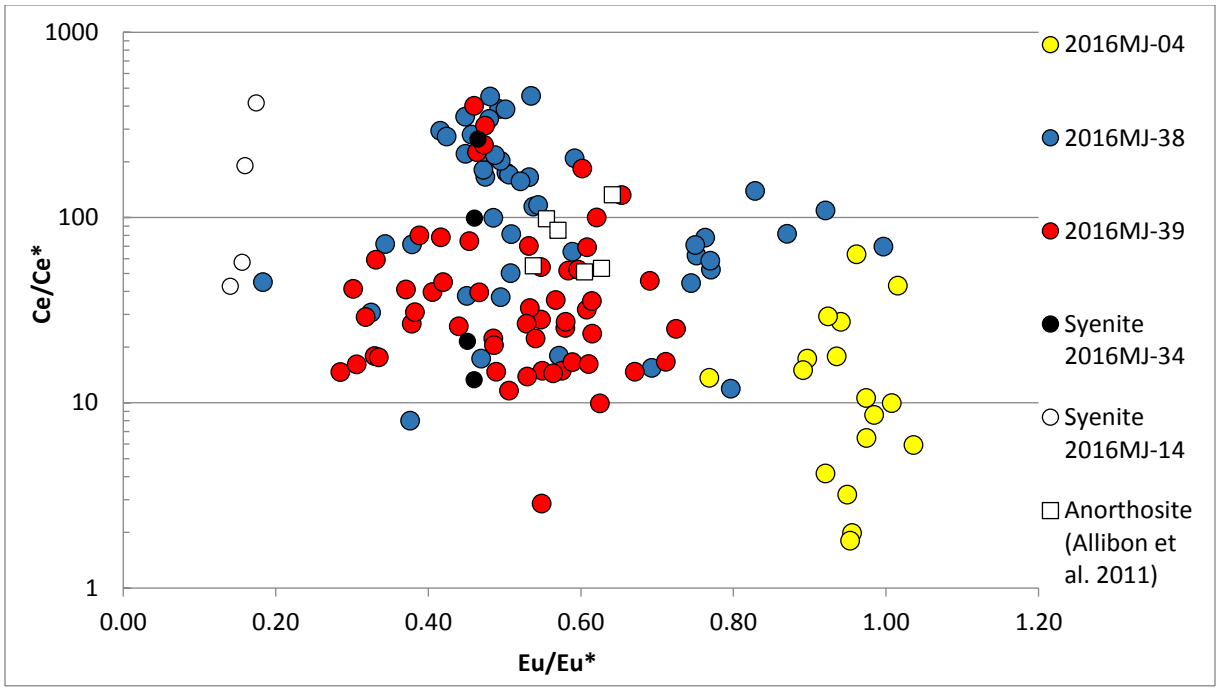

Figure. 4.2.3a. Eu/Eu* versus Ce/Ce* for Fuerteventura detrital zircons. All values were normalized to chondrite using values reported in Sun and McDonough (1989). Zircon from two syenite samples and an anorthosite sample (open squares) from Fuerteventura are shown for comparison.

In sample 2016MJ-04, the analyses with Ce/Ce* <10, with a negligible Eu/Eu* represent 47% of the sample population, with dates ranging from 25.7 to 31.0 Ma (Figure. 4.2.3a). These samples also typically fall within or close to the hydrothermal zircon field defined by Hoskin (2005) (Figure. 4.2.3b). The remaining portion of sample 2016MJ-04 contains analyses with positive Ce anomalies ranging from 10.6-63.4 and negligible Eu anomalies (~1). A majority of these analyses lie in or close to the magmatic zircon field identification in Hoskin (2005) study (Figure. 4.2.3b).

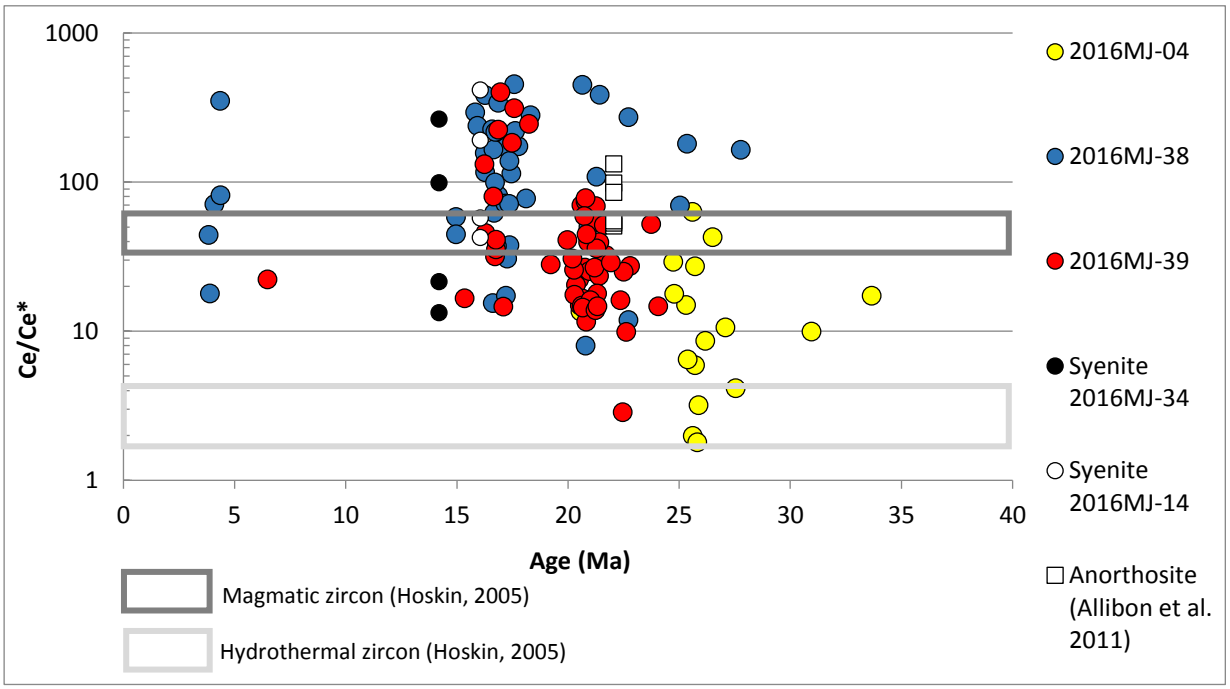

Figure. 4.2.3b. Age (Ma) versus Ce/Ce* for Fuerteventura detrital zircons with reference fields highlighting the magmatic zircon (dark grey) and hydrothermal zircon (light grey) fields from Hoskin (2005).

Sample 2016MJ-38 contains a large Ce/Ce* variation, ranging from 8.0-454.3. The majority of the analyses (53%) cluster between 114.7-454.3, with Eu anomalies ranging from 0.42-0.54 (Figure. 4.2.3a). Most of the analyses from this sample do not fall into either the magmatic or hydrothermal classification defined by Hoskin (2005), demonstrating much higher positive Ce anomalies. The analyses that do reside in or close to the fields defined by Hoskin (2005) fall into the magmatic field (Figure. 4.2.3b). The younger zircon population lies close to the magmatic zircon field with an Eu/Eu* ranging from 0.57-0.87.

Sample 2016MJ-39 exhibits a similar Ce/Ce* trend as sample 2016MJ-38, ranging from 2.9-401.1. A majority of the sample population (78%) groups from Ce/Ce* ranging from 11.6-70.2 and exhibits negative Eu anomalies ranging from 0.28-0.72 (Figure. 4.2.3a). The sample generally lies close to magmatic zircon field, with one analyses falling towards the hydrothermal

field (Figure. 4.2.3b.; Hoskin, 2005). Similar to sample 2016MJ-39, there is a substantial population that contains high positive Ce/Ce* anomalies (up to~400).

The syenites from Canary Islands exhibit elevated Ce/Ce* with 2016MJ-14 ranging from 42.5-415.8 and 2016MJ-34 ranging from 13.3-265.4. The Eu/Eu* vs. Ce/Ce* demonstrates that sample 2016MJ-34 closely parallels analyses observed in both 2016MJ-38 and 2016MJ-39 (Figure. 4.2.3a). Sample 2016MJ-14 is isolated from the main population, with extremely low Eu/Eu* values. The closest sample that matches this chemical composition is from 2016MJ-38 at 14.96 Ma. The anorthosite analyzed from Allibon et al. (2011) also overlaps portions of the 2016MJ-38 and 2016MJ-39 populations. Neither of the syenite samples or the anorthosite sample contain Ce/Ce* values <10.

4.2.4 Y

Belousova et al. (2002) also determined the Y contents of zircon and showed that the higher Y concentrations (>1000 ppm) are commonly observed in syenite, nepheline-syenite pegmatites, granitoids, larvikites, and some dolerites. Carbonatites typically have lower Y concentrations between 300-1000 ppm.

Sample 2016MJ-04 has Y concentrations ranging from 87-7780 ppm, exhibiting large variability in the oldest analyzed zircons (>25 Ma). The zircons in this sample can be subdivided into two groups: (1) those with higher Y concentrations (6360-7780 ppm) and (2) those with low Y concentrations (87.2-4870). Sample 2016MJ-38 zircon has Y contents ranging from 246-8560 ppm and sample 2016MJ-39 zircon has Y contents ranging from 168-7630 ppm. The youngest analyzed grains generally have Y concentrations <1000 ppm, with a few grains ranging from 1375-4090 ppm.

The two Canary Island syenites analyzed in the present study have different concentrations: 2016MJ-14 has Y content from 1540-5320 ppm; whereas 2016MJ-34 has higher concentrations ranging from 4800-5796 ppm (Figure. 4.2.4a). The syenite 2016MJ-14 closely parallels the Y concentrations observed in the 2016MJ-38 and 2016MJ-39 populations containing higher Y concentrations (>1500 ppm).

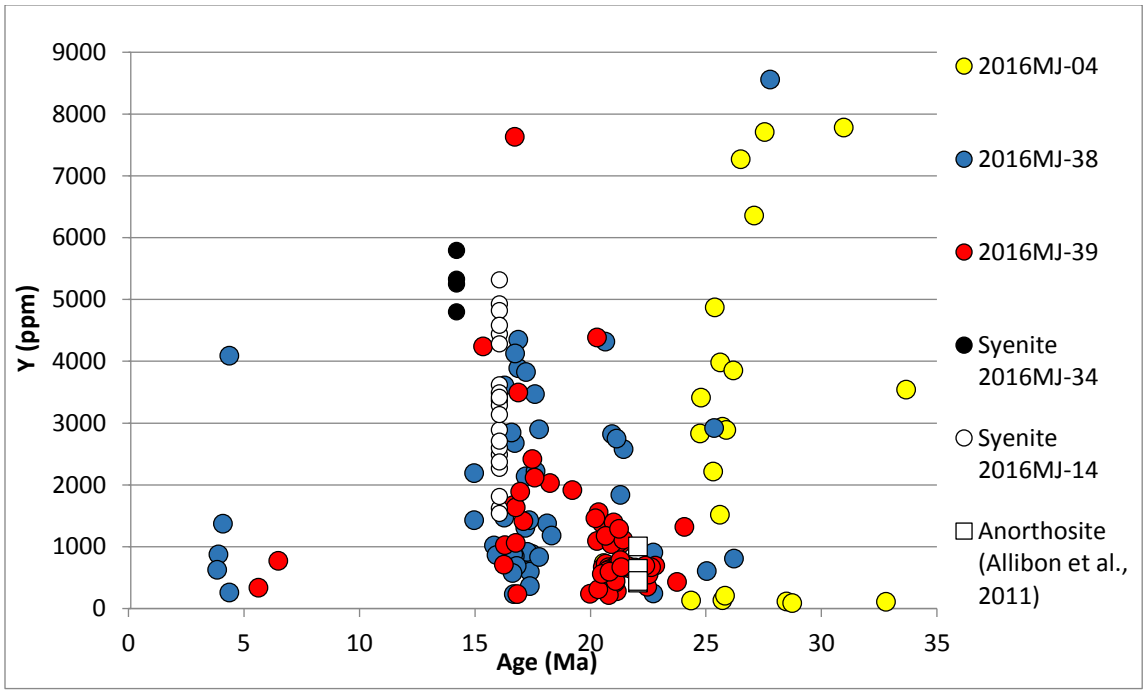

Figure. 4.2.4a. Age (Ma) versus Y concentrations for Fuerteventura detrital zircons. Zircon from two syenite samples and an anorthosite sample (open squares) from Fuerteventura are shown for comparison.

4.2.5 Th and U

Zircons from samples 2016MJ-38 and 2016MJ-39 have a wide and continuous range of Th concentrations from 19.4-2800 ppm (Figure. 4.2.5a). Zircons from sample 2016MJ-04 have a bi-modal distribution of Th concentrations; one group has Th concentrations similar to or higher than those of zircons in samples 2016MJ-38 and 2016MJ-39 (>3000 ppm), whereas the second group has Th less than 100 ppm.

Zircons from the two analyzed Canary Island syenite show a significant variation in Th concentrations ranging from 94-2390 ppm, overlapping a majority of the detrital samples. The Th variation from sample 2016MJ-14 ranges from 94-673 ppm, whereas sample 2016MJ-34 exhibits higher Th concentration ranging from 1970-2390 ppm. The Th contents of zircons from Canary Island anorthosite (Allibon et al., 2011) range from 113-225 ppm, overlapping with a portion of 2016MJ-38 and 2016MJ-39.

As was the case with Th , zircons from samples 2016MJ-38 and 2016MJ-39 have a wide and continuous range of U concentrations, with a bulk of the concentrations (96%) ranging from 30-1365 ppm, consistent over the duration of all the zircon ages (27.8-3.8 Ma) (Figure. 4.2.5b). The U concentration range of zircons in 2016MJ-04 is similar to that of zircons in the other two samples (38, 39). There are a select group of outliers observed in samples 2016MJ-04 and 2016MJ-38 that contain <30 ppm of U or >1365 ppm.

The U concentrations of zircons from the Canary Island syenite 2016MJ-14 ranges from 110-443 ppm, whereas 2016MJ-34 has a narrower range of U contents from 111-178 ppm. Anorthosite zircons from the Canary Islands (Allibon et al., 2011) have U contents from 88-155 ppm, similar to a small portion of analyses observed in 2016MJ-38 and 2016MJ-39.

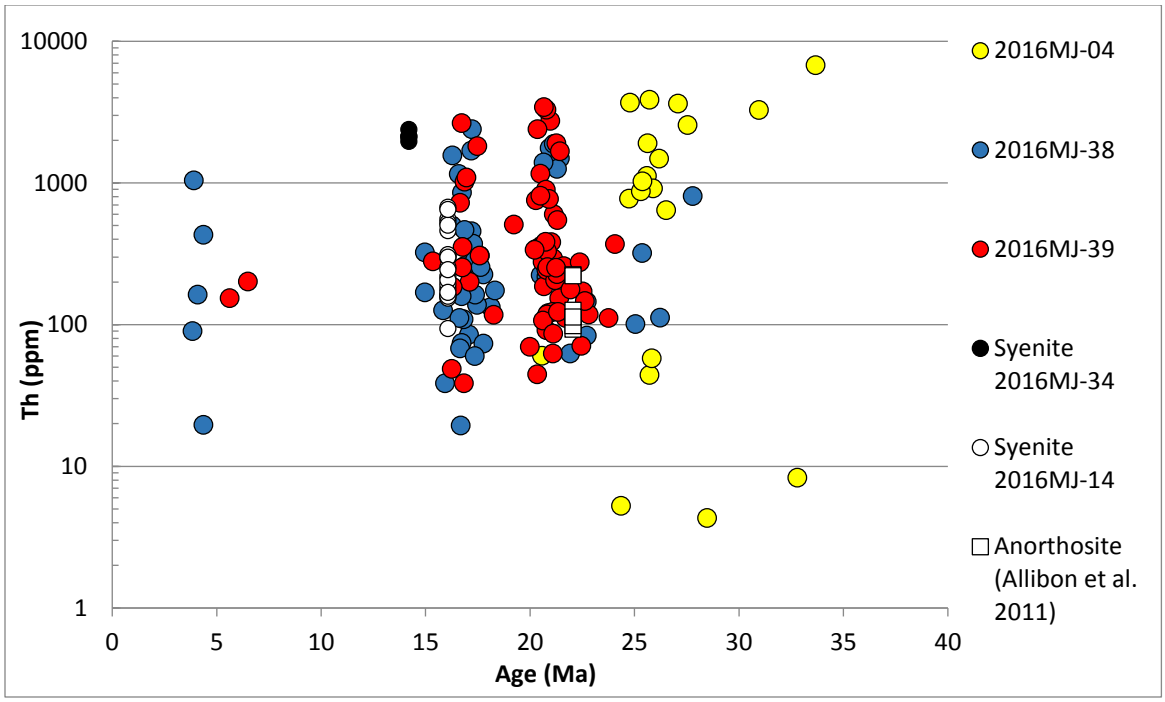

Figure. 4.2.5a. Age (Ma) versus Th concentrations for Fuerteventura detrital zircons. Zircon from two syenite samples and an anorthosite sample (open squares) from Fuerteventura are shown for comparison.

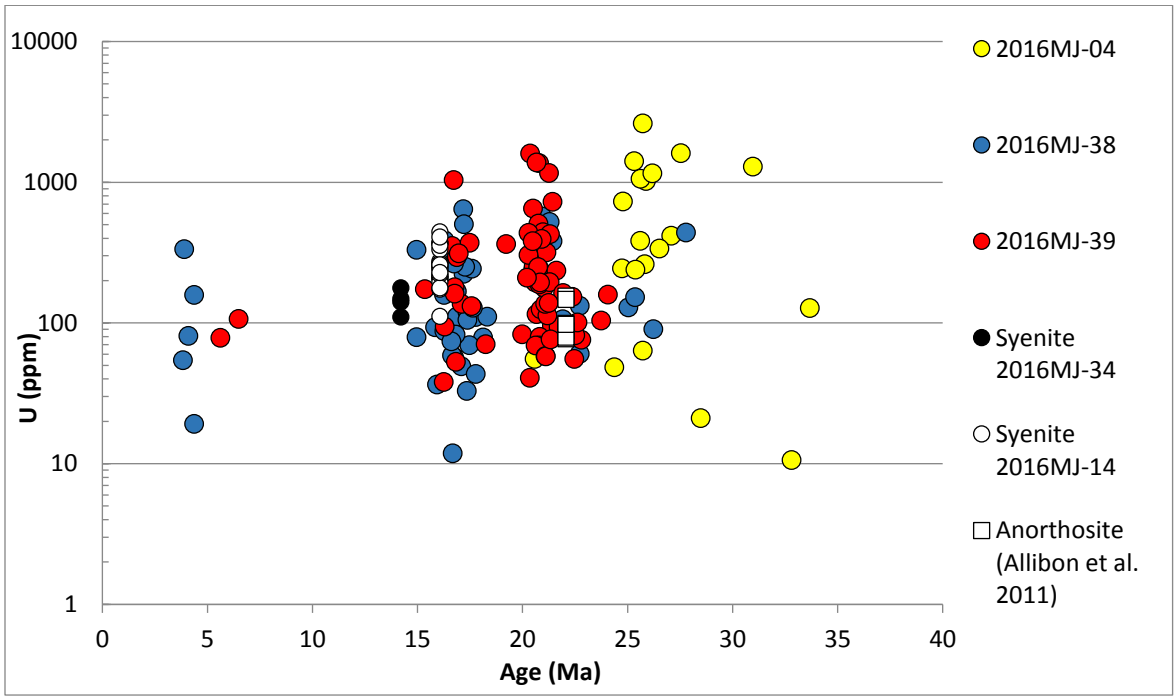

Figure. 4.2.5b. Age (Ma) versus U concentration in Canary detrital zircons. Zircon from two syenite samples and an anorthosite sample (open squares) from Fuerteventura are shown for comparison.

The Th and U content in zircon grains can vary substantially. The Th/U ratio tends to be less variable and has been used to distinguish crystallization environments (Amelin & Zaitsev, 2002; Hoskin & Schaltegger, 2003; Kirkland et al., 2015). Typically, magmatic zircon is characterized by Th/U ratio of 0.3- 0.6, while Th/U from carbonatites tend to be higher, with some reported from Kola Peninsula Russia up to 9000 (Amelin & Zaitsev, 2002; Kirkland et al., 2015).

Samples 2016MJ-38 and 2016MJ-39 fall into a relatively uniform Th/U pattern, ranging from 1.0-6.3, with select analyses having values <1.0 (Figure. 4.2.5c). The samples that deviate below the main cluster in 2016MJ-38 and 2016MJ-39 are observed in samples with ages 16.8 Ma, 21.9 Ma, and 25.0 Ma. A portion of sample 2016MJ-04 falls within a same range as 2016MJ-38 and 2016MJ-39; however, there are two distinct populations observed above and below this range. The higher Th/U ratios (8.7-53.5) are observed in samples recording 27.1 and 33.7 Ma ages, whereas the lower Th/U ratios (0.1-0.9) are observed in samples yielding ages between 24.4-32.8 Ma.

Despite the similar ranges in U and Th contents, the Th/U ratios of zircons in the two Canary Island syenites are distinct. Sample 2016MJ-14 contains low Th/U ratios ranging from 0.8-1.4, overlapping a large portion of samples 2016MJ-38-and 2016MJ-39. Zircons in sample 2016MJ-34 have much higher Th/U ratios ranging from 13.5-15.0 and does not directly overlap with any detrital zircon analysis; however, it does coincide with one outlier from 2016MJ-04 (Figure. 4.2.5c). The anorthosite described by Allibon et al. (2011) is within the same range as 2016MJ-14, with average Th/U ratios ranging from 1.3-1.5.

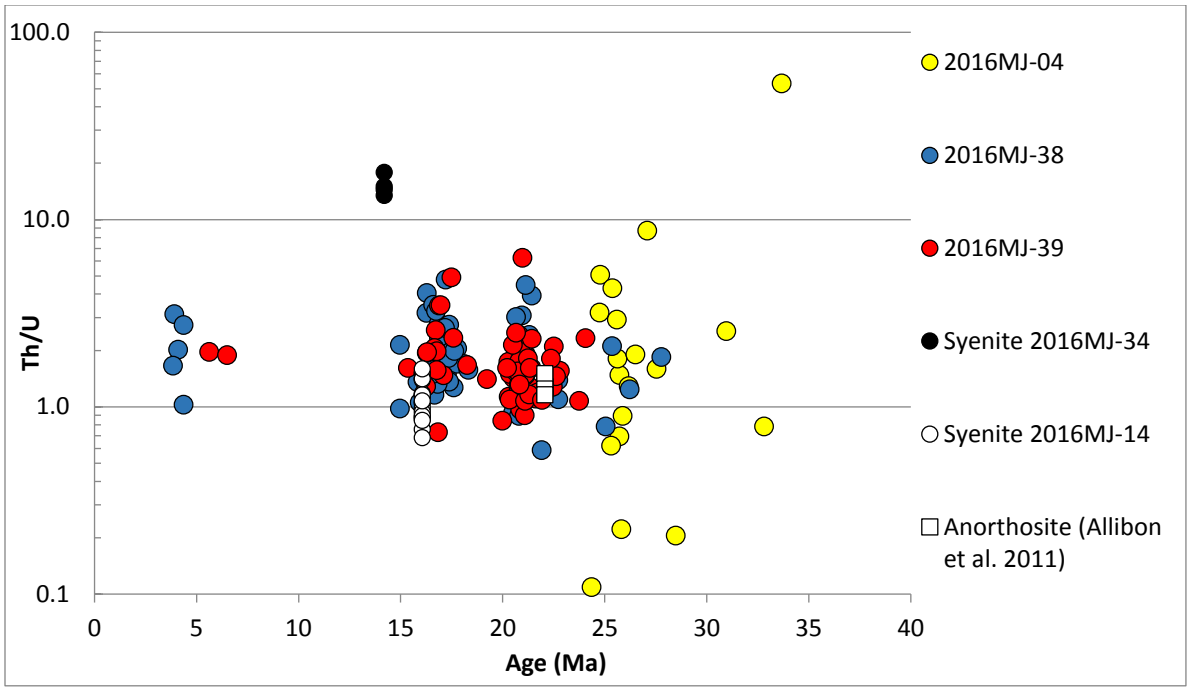

Figure. 4.2.5c. Age (Ma) versus Th/U for Fuerteventura detrital zircons. Zircon from two syenite samples and an anorthosite sample (open squares) from Fuerteventura are shown for comparison.

4.2.6 Nb/Ta and Nb

The Canary Island zircons have a very wide range of Nb/Ta ratios (1.1-30.0) (Figure. 4.2.6a). Belousova et al. (2002) found similar Nb/Ta ratios in carbonatites, syenites, nepheline syenites, and granitoids, which varied from 0.3 to 48 with an average of 3. The highest ratios reported in the Belousova et al. (2002) study were typically observed in syenites, nepheline-syenite pegmatites, and granitoids, while the lower values were associated with kimberlitic zircons.

Sample 2016MJ-04 has the highest Nb/Ta ratios ranging from 2.3-247.5 with an average of 37.3. The Nb/Ta ratios are fairly continuous from ~9- 200 ppm, with one outlier at 247 ppm. The main break is observed in the Nb concentration with a distinctly different lower group (<3 ppm) and a higher group (>9 ppm). Sample 2016MJ-38 Nb/Ta ratio ranges from 1.3-13.4 with an average of 4.7. Sample 2016MJ-39 ranges from 1.0-9.4 with an average of 2.5. This population contains the least amount of Nb/Ta variation, with the majority of the zircon population (75%) exhibiting Nb/Ta ratios <2.2. None of the samples analyzed have Nb/Ta ratios <1. The higher Nb/Ta ratios (>10) are observed in a majority of 2016MJ-04 grains (74%), with a minor of grains from 2016MJ-38.

The Nb/Ta ratios of zircons isolated from the two Canary Island syenites exhibit significant variability: (1) lower ratios ranging from 1.62-4.15; (2) elevated ratios ranging from 15.10-18.85 (Figure. 4.2.6a). The 2016MJ-34 syenite zircon contains comparable Nb/Ta values to a portion of the 2016MJ-04 detrital grains, with elevated Nb concentrations. The syenite 2016MJ-14 zircon closely parallels the Nb/Ta ratios and Nb concentrations observed in the 2016MJ-38 and 2016MJ-39 detrital populations.

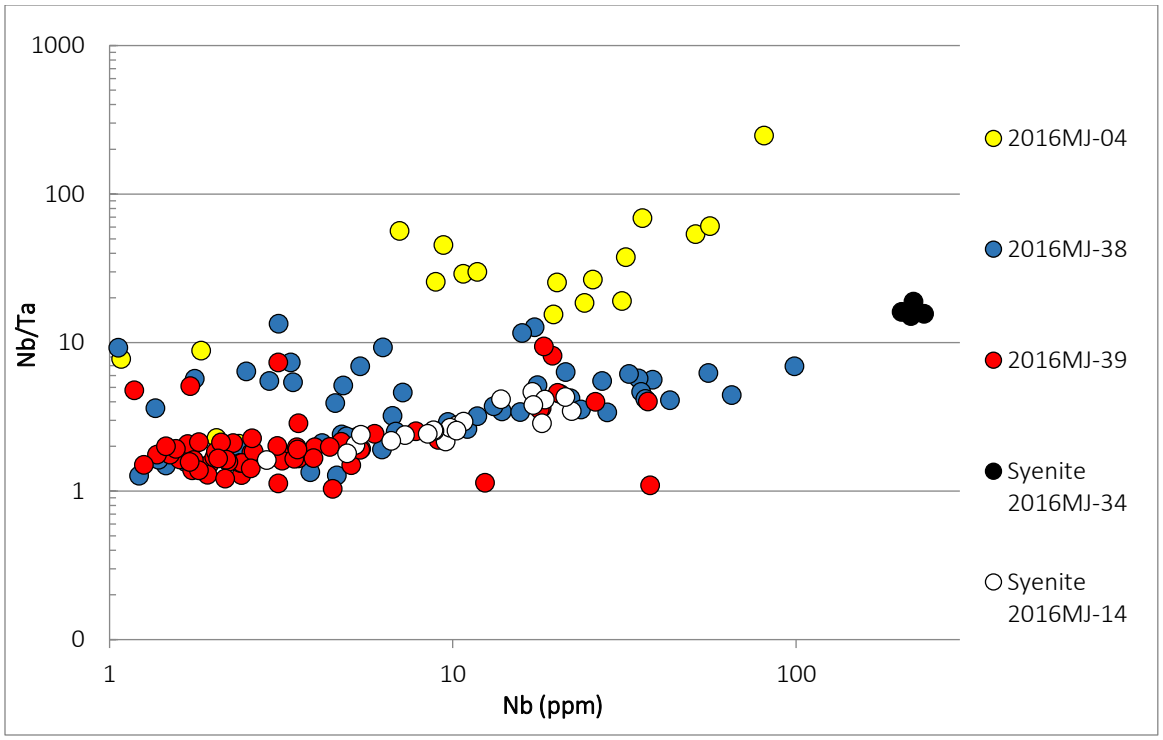

Figure. 4.2.6a. Nb concentration versus Nb/Ta in Fuerteventura detrital zircons. Zircon isolated from two Fuerteventura syenites are also shown for comparison.

4.3 Hf isotope analysis

The Hf isotope composition of detrital zircon allows us to evaluate the magma source throughout an island's formation. This is a strong analytical tool when used in conjunction with U-Pb geochronology and oxygen isotope signatures, allowing us to directly assess the temporal evolution and nature of the magma source and evaluate the effects of crustal contamination, metasomatism, or mixing events. Furthermore, a detrital zircon study provides a unique opportunity to analyze the provenance of zircon-bearing rocks (granite, syenite, nepheline-syenite, gabbro, carbonatite) throughout the magmatic history of Fuerteventura.

In this study, we performed 133 Hf isotope analyses from 133 detrital zircon grains from three sand samples collected in Fuerteventura. The errors are reported at the level 2σ (absolute). A summary of the hafnium isotope data can be found in Appendix. F.

The data from the northern portion of the island by Playa del Águila (2016MJ-04) represents the Hf isotope signatures of the oldest components of the analyzed zircon population ranging from 25.3-29.9 Ma (Refer to U-Pb results, Appendix. C1-3). The εHf_i values range from +6.8 to +9.7, with a weighted mean of εHf_i= +8.67 ± 0.36 (2 SE) (MSWD= 0.97, n=22) (Figure. 4.3a). A majority of the analyses lie within a similar εHf_i range (+8.4 to +10.4) as the young (<0.1 Ma) Fuerteventura basalts reported by Geldmacher et al. (2011) (Figure. 4.3a). The 6 analyses that do not fall within this young basalt range contain lower εHf_i values than previously reported, ranging from +6.8 to +8.2.

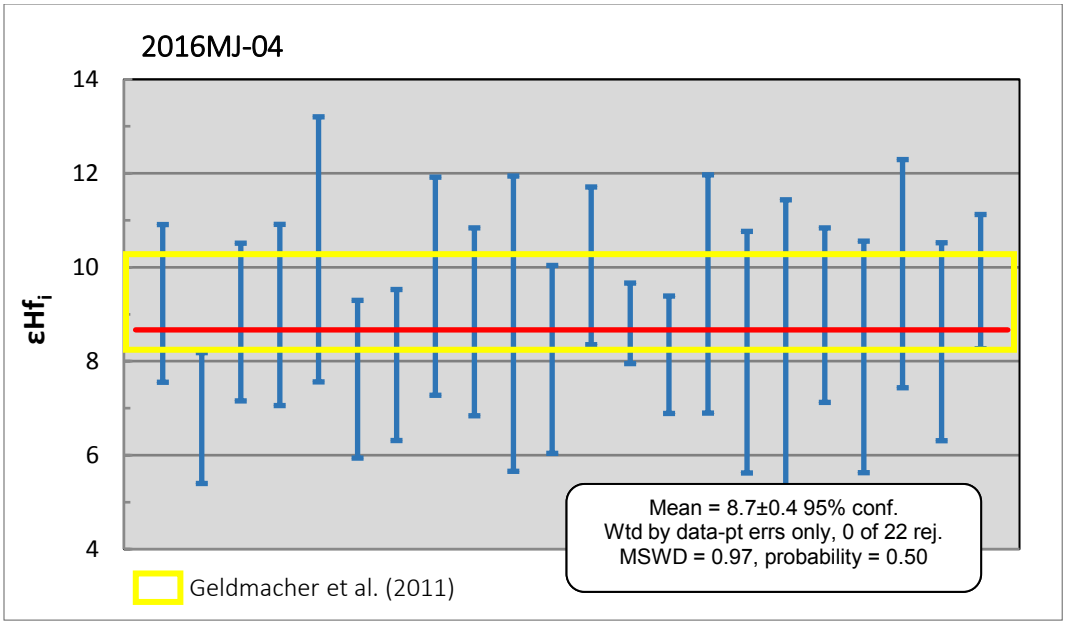

Figure. 4.3a. Playa del Águila (2016MJ-04) detrital zircon εHfi values. The yellow field represents whole rock εHf_i values from recent (<0.5 Ma) volcanics on Fuerteventura (Geldmacher et al., 2011).

The central sample from Playa de Garcey beach (2016MJ-38) contains the largest εHf_i variation detected in this study, ranging from -0.3 to +15.2 εHf_i units (Figure. 4.3b; Figure. 4.3c). A small population falls within the εHf_i range of young basalts previously reported by Geldmacher et al. (2011); however, there is a significant zircon population that plots directly below the young basalt field with a weighted mean of εHf_i= +8.4 ± 0.6 (2 SE) (MSWD= 2.8, n= 18) (Figure. 4.3b). The remaining data, which were obtained from zircon with crystallization ages of 20 to 4 Ma, show extreme variation in Hf isotope compositions. This variation can be subdivided into two trends: a depleted MORB-like signature and an enriched signature (Figure. 4.3f). The depleted signature is prevalent in 20 to 15 Ma grains and range from +11.0 to +15.2 εHf_i. The enriched signature (-0.3 to +6.2 εHf_i units) is observed in 20 to 4 Ma grains. The greatest enriched peaks are observed at ~16 Ma and ~4 Ma.

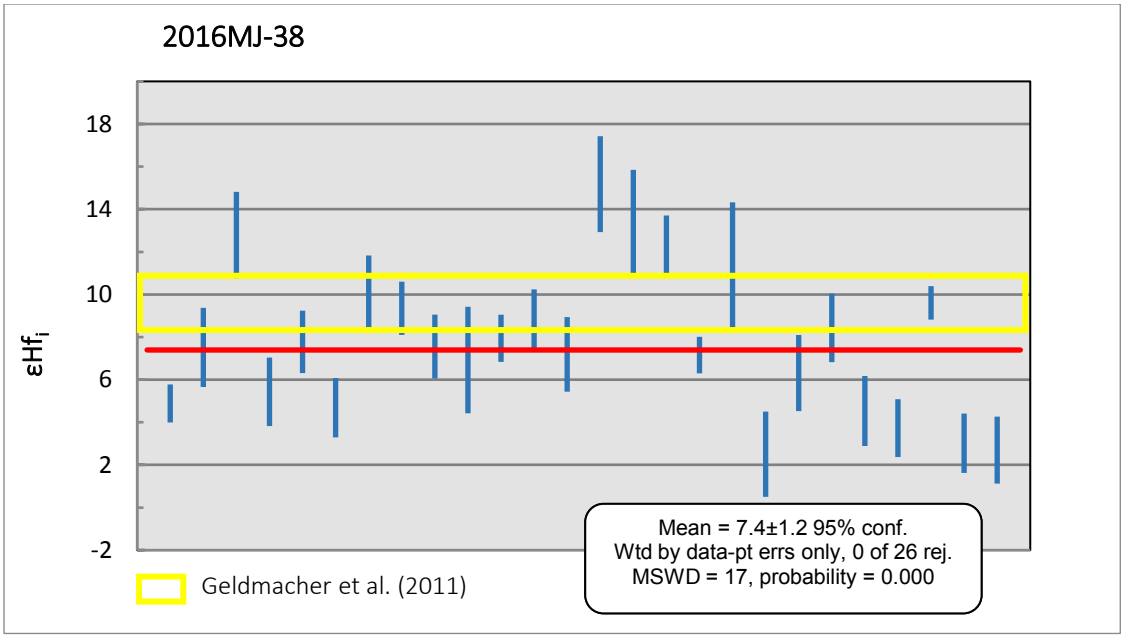

Figure. 4.3b. Playa de Garcey (2016MJ-38) εHfi values with Geldmacher et al. (2011) εHf_i values in the yellow field from the recent (<0.5 Ma) volcanics on Fuerteventura.

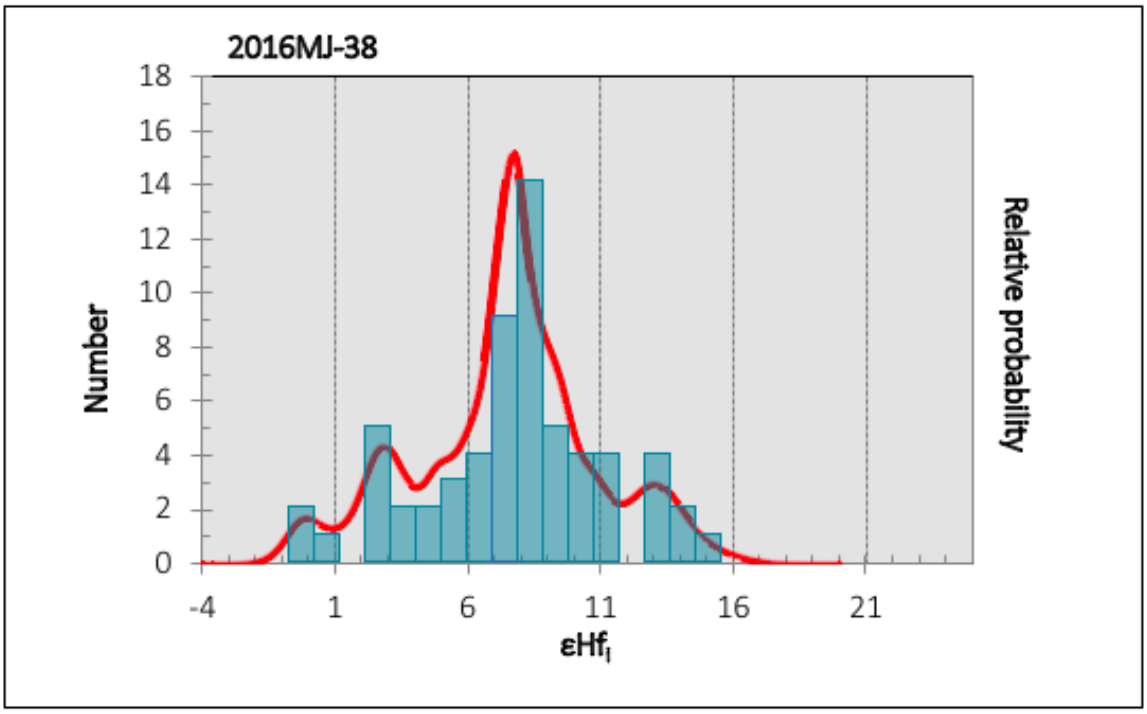

Figure. 4.3c. Playa de Garcey (2016MJ-38) εHfi histogram distribution to demonstrate the wide range of values.

The central sample from Barranco de la Solapa (2016MJ-39) records a similar εHf_i cluster observed in samples 2016MJ-04 and 2016MJ-38 with a εHf_i range from +7.5 to +8.8 (Figure. 4.3d.). The main cluster has a weighted mean of εHf_i= +8.3 ± 0.1 (2 SE) (MSWD= 1.4, n=46), a trend that is observed from 23-16 Ma (Figure. 4.3d). After an observed hiatus from 16.1 to 4.9 Ma, there is a shift to more enriched values, ranging from +4.9 to +5.8 εHf_i with a weighted mean of +5.3 ± 0.8 (2 SE) (MSWD=0.38, n=3) (Figure. 4.3e).

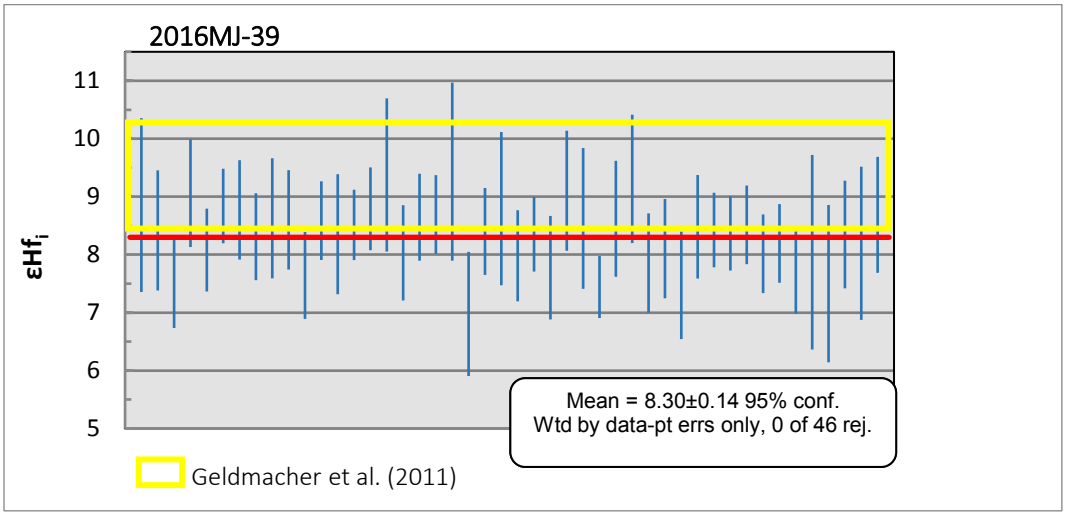

Figure. 4.3d. Barranco de la Solapa (2016MJ-39) εHfi values with Geldmacher et al. (2011) εHf_i values in the yellow field from the recent (<0.5 Ma) volcanics on Fuerteventura.

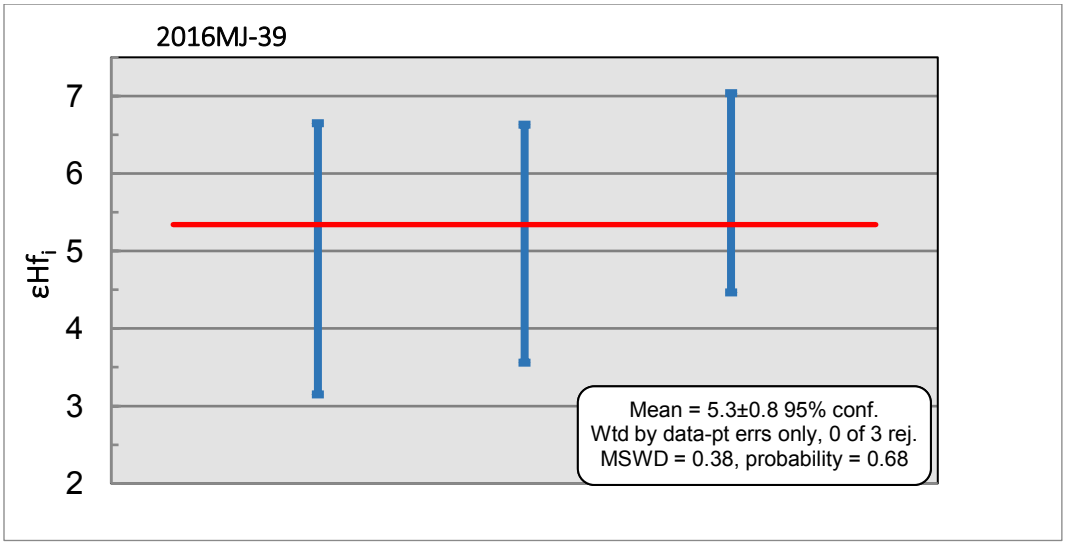

Figure. 4.3e. εHfi values of dated Miocene and Pliocene zircons from Barranco de la Solapa (2016MJ-39). Note the relatively enriched values compared to the other grains from this sample.

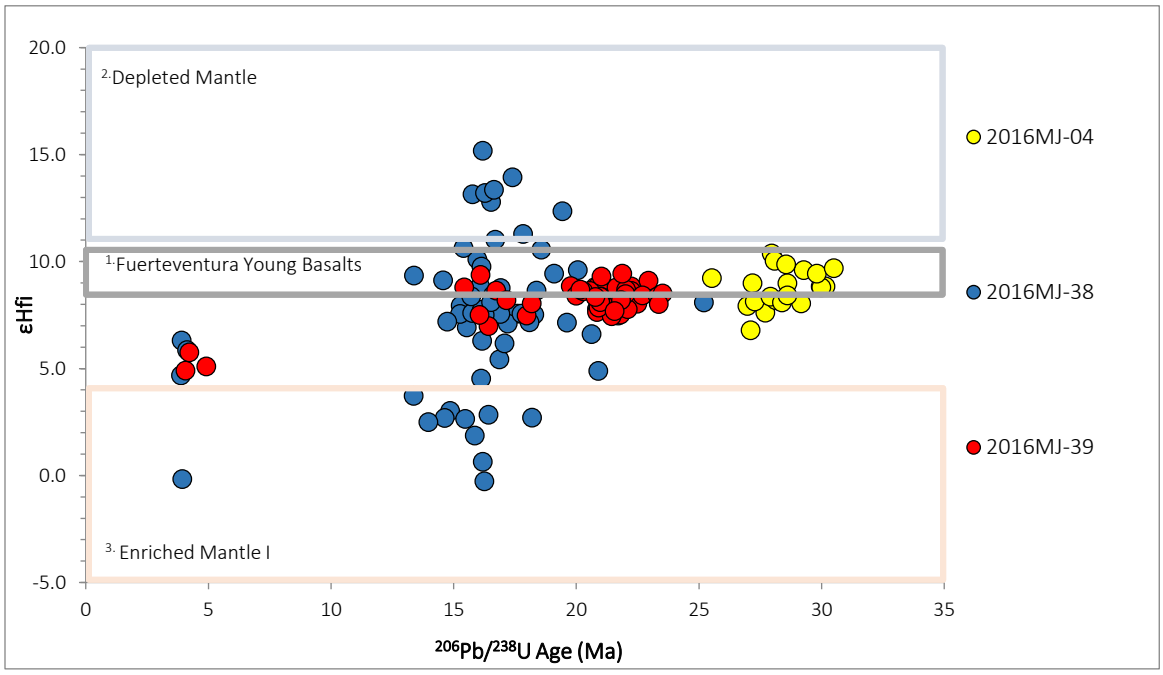

Figure. 4.3f. Hf isotope data for Fuerteventura detrital zircons. Reference fields shown for comparison are: (1) Mid-Atlantic MORB signature (Deballie et al., 2006); (2) Whole rock hafnium isotopic data from young (<0.1 Ma) basalts on Fuerteventura (Geldmacher et al., 2011); (3) Enriched mantle reservoir (EM1 of Barker et al., 2009).

4.4 Oxygen Isotope Compositions of Zircon

Zircon occurs in a wide variety of plutonic igneous rocks (e.g. granite, syenite, nepheline syenite, gabbro, carbonatite). Although many whole-rock samples from the basal complex in Fuerteventura have been modified by deformation and low-grade metamorphism (Féraud et al., 1985; Balogh et al. 1998), zircon is one of the most robust minerals in these rocks that can survive a range of crustal processes from low-temperature alteration to high-grade metamorphism. It has been shown in previous studies that the zircon oxygen isotope composition are generally well preserved relative to other minerals after a rock has experienced intense hydrothermal activity or high-grade metamorphism (Valley, 2003). This characteristic of zircon offers an opportunity to determine if the primary, igneous oxygen

isotope signature of plutonic rocks that comprise Fuerteventura's basal complex are directly derived from the mantle or have experienced a more complex history.

In this study, we determined 188 O-isotope spot analyses from 91 detrital zircon grains from three sand samples collected along the west side of Fuerteventura, near previously described basal complex outcrops (Coello et al., 1992; Ancochea et al., 1996; Muñoz et al., 2005; Allibon et al., 2011). The grains were selected based on various ages and morphologies to ensure no sampling bias. Multiple analyses were completed on each zircon grain to assess whether there is any correlation between the observed CL structure and oxygen isotope composition. The O-isotope analyses were remarkably homogeneous within grains despite CL complexity, with data from multiple spots on individual grains in agreement within the 2σ error (‰) (see Appendix. D1-D3B for CL images). A summary of the zircon oxygen isotope data can be found in Appendix G1-3. These grains were also analyzed for U-Pb geochronology and a subgroup of these were analyzed for trace-element and hafnium isotope compositions. The $\delta^{18}O$ values displayed in the plots below represent the O-isotope analyses acquired closest to the U-Pb analyses.

The oxygen isotope results for Fuerteventura detrital zircons can be subdivided into two populations. The first group lies within the mantle oxygen field (+5.3 ± 0.3‰) ranging from 5.00-5.48‰ with an average of 5.14‰; the other group lies below the mantle-like zircon $\delta^{18}O$ ranging from 3.27- 4.99‰, with an average of 4.31‰ (Valley et al., 1998).

The northern sample (2016MJ-04) collected at Playa de Águila (Figure. 4.4b.) contains the oldest known zircon population, with a majority of the zircon dates ranging from 33-25 Ma. The two detrital zircon grains 2016MJ-024 and 2016MJ-043 (27.1 ± 1.4 Ma; 16.1 ± 1.0 Ma) that lie within the zircon mantle-like range have a weighted average of $\delta^{18}O$ =+5.30 ±

0.15‰ (MSWD 2.5; n=2) (Valley et al. 1998). This represents 8.3% of the sample population. The weighted average of low-$\delta^{18}O$ zircon analyses is =+4.23 ± 0.17‰ (MSWD 13; n=22), representing 91.67% of the sample population.

The central samples, collected at Playa de Garcey beach and in Barranco de la Solapa, 2016MJ-38 and 2016MJ-39, respectively, yielded similar zircon ages, but have different O-isotope systematics (Figure 4.4c, Figure 4.4d.). The range of $\delta^{18}O$ values for 2016MJ-38 and 2016MJ-39 zircons is 3.27-5.11‰ and 3.77-5.31‰, respectively. The weighted average of $\delta^{18}O$ mantle-like values for 2016MJ-38 =+5.08 ± 0.12‰ (MSWD 0.22; n= 3), representing 10.7% of the sample population, while sample 2016MJ-39 =+5.11 ± 0.08‰ (MSWD 0.94; n= 7), representing 18.4% of the zircon population. The low-$\delta^{18}O$ zircon weighted average of 2016MJ-38 =+4.03 ± 0.22‰ (MSWD 21; n=25); however, there are two distinct groupings within this population (blue region, Figure. 4.4a). If the samples are further divided into more defined clusters, they have a weighted average at +3.64 ± 0.08‰ (MSWD 1.4; n=14) and +4.62 ± 0.17‰ (MSWD 4.3; n= 11). The low-$\delta^{18}O$ values from sample 2016MJ-39 = +4.61 ± 0.12‰ (MSWD 8.1; n= 28).

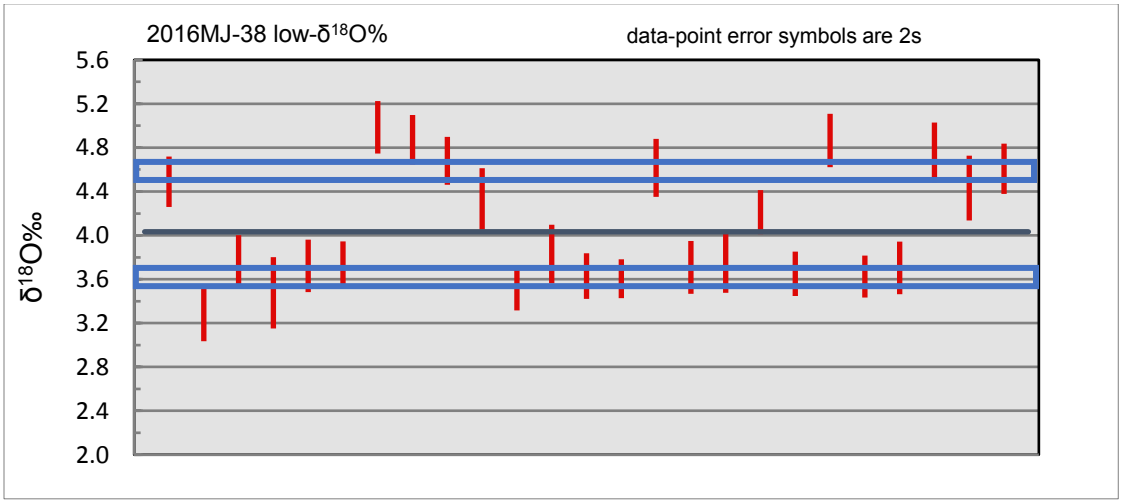

Figure. 4.4a. Detrital zircon from the Playa de Garcey beach sample demonstrating two different low- δ18O populations in the blue regions.

The detrital zircons with dates >20 Ma in sample 2016MJ-38 consistently fall below the mantle zircon field, with the lowest oxygen value of 3.27‰ observed in a 27.8 ± 2.8 Ma grain, the oldest reported date from the sample. Mantle-like oxygen isotope signatures are observed in a 17.1 ± 0.6 Ma grain and in the Pliocene zircon population ranging between 3.8 ± 0.2 - 4.4 ± 0.3 Ma. Sample 2016MJ-38 has two pronounced populations below the mantle-like field at +3.64 and +4.62 between 27-15 Ma.

The detrital zircon dates in sample 2016MJ-39 exhibit a diverse population containing both mantle-like zircon and low- $\delta^{18}O$ values. The values that lie within the mantle-like field are observed throughout all the analyzed grains, ranging from 25 to 4 Ma. The low-oxygen isotope values occur in grains that formed between 22-15 Ma, with $\delta^{18}O$ values ranging from 4.00-4.90‰. In contrast to sample 2016MJ-38, a ~3.6‰ population is not observed in sample 2016MJ-39. The younger dates from the Pliocene fall within the mantle-like oxygen range.

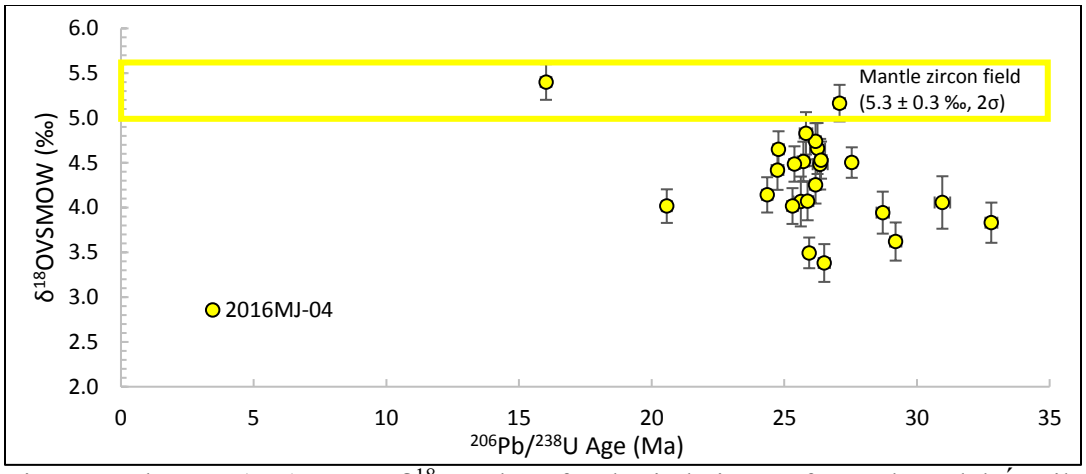

Figure. 4.4b. Age (Ma) versus $\delta^{18}O$ values for detrital zircons from Playa del Águila beach (2016MJ-04).

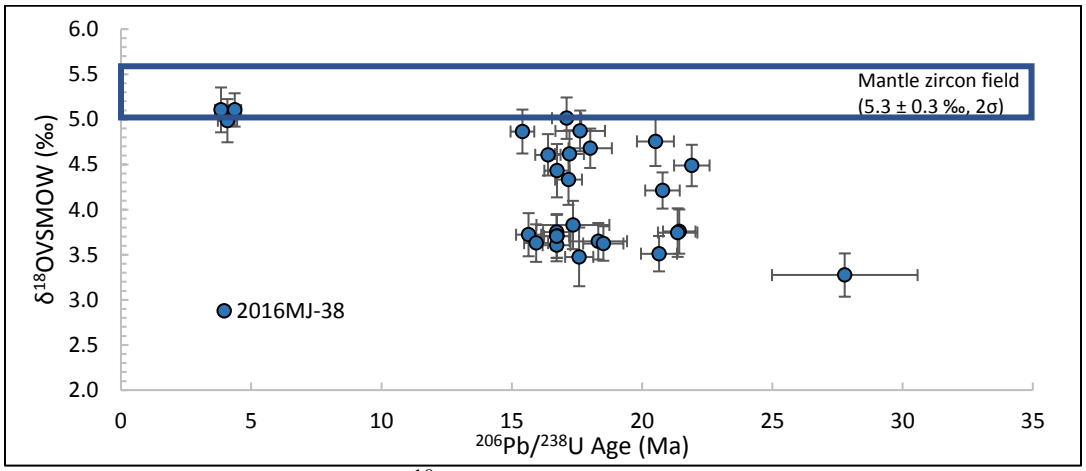

Figure. 4.4c. Age (Ma) versus $\delta^{18}O$ values for detrital zircon from Playa de Garcey beach (2016MJ-38).

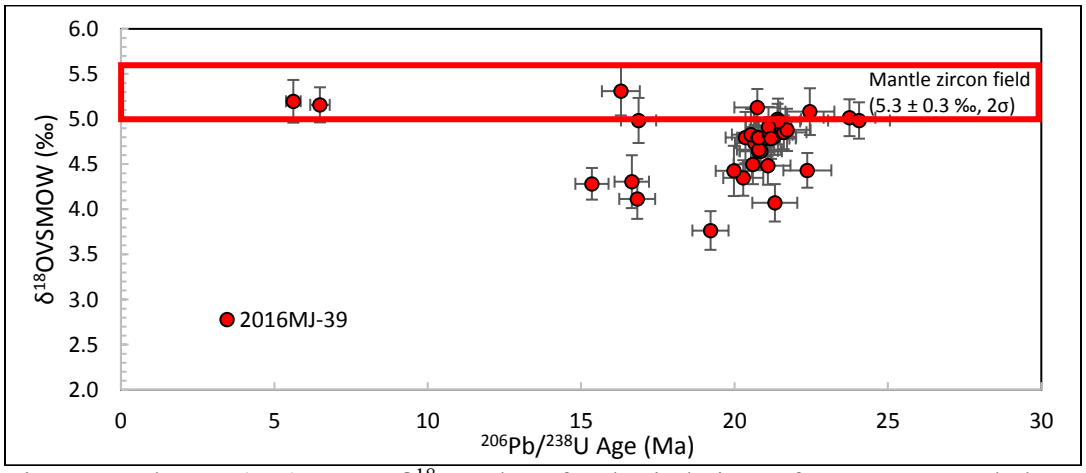

Figure. 4.4d. Age (Ma) versus $\delta^{18}O$ values for detrital zircon from Barranco de la Solapa (2016MJ-39).

Low- $\delta^{18}O$ signatures are frequently observed in plume or mid-ocean ridge settings because hot magma near the surface generates geothermal gradients that drive hydrothermal fluid circulation cells above the magma chamber or assimilation of high-temperature hydrothermal alteration from meteoric waters in sediments (Taylor & Sheppard, 1986; Demény et al., 1998). Hydrothermal alteration can alter the oxygen isotope signatures of the parental rock, high temperature fluid interaction can lower the oxygen isotopic signature in the altered rock. Ocean island basalts that exhibit lower than typical mantle oxygen isotope values ($\delta^{18}O$ <5.0‰) have been interpreted be associated with assimilation of altered oceanic crust during magma ascent, melting altered subducted oceanic crust at mantle depths, or assimilating high-temperature meteoric hydrothermally altered sediments (Ringwood et al., 1992; Eiler et al., 1997; Demény et al., 1998; Lassiter and Hauri, 1998). These signatures record evidence of a more complex magma evolution than simply a mantle-derived magma.

5. DISCUSSION

5.1 Duration and main periods of zircon-bearing alkaline magmatism

The age and duration of Fuerteventura's initial magmatic activity has been a contentious subject for several decades, hindering the understanding of the island's history and evolution (Fúster et al., 1968; Stillman & Robertson, 1979; Le Bas et al., 1986; Balogh et al., 1999; Coello et al., 1992; Cantagrel et al., 1993; Ancochea et al., 1996; Muñoz et al., 2005; Gutiérrez et al., 2006; Allibon et al., 2011). A majority of the published dates have been determined using conventional K-Ar and Ar/Ar radiogenic dating methods. The relatively old late-Cretaceous and early-Paleocene dates reported from syenites and nepheline-syenites in the central sector of the island by Caleta de la Cruz are mostly K-Ar whole rock dates (Le Bas et al., 1986; Balogh et al., 1999). However, the veracity of these dates has been questioned in more recent studies (e.g., Munoz et al., 2005). It has been demonstrated in previous studies that K-Ar mineral and whole rock analyses from the initial magmatic complex are commonly associated with excess argon or are thermally reset, which could be related to the pervasive hydrothermal greenschist metamorphism, extensive metasomatism, and shear-zone deformation in the region (Rona & Nalwalk, 1970; Abdel-Monen et al., 1971; Le Bas et al., 1986; Cantagrel et al., 1993; Muñoz et al., 1997; Balogh et al., 1999). Due to the uncertainty associated with these previously published argon dates, the detailed timing of the early magmatic activity on Fuerteventura remains largely unknown.

In the recent literature, there have been a few published U-Pb dates from zircon and baddeleyite using Laser Ablation Inductively Coupled Plasma Mass Spectrometry (LA-ICPMS) and Isotope Dilution Thermal Ionization Mass Spectrometry (ID-TIMS) methods. Although the previous U-Pb work is limited (n=4), these recent ages suggest a different intrusion history than

the K-Ar studies, with the initial plutonic activity starting around the Oligocene at 25 Ma (Canagrel et al., 1993; Muñoz et al. 2005; Allibon et al., 2011). At present, there is no confirmation from modern techniques (Ar/Ar or U-Pb) of purported Cretaceous magmatism from the northern or central sectors.

The comparison of K-Ar and U-Pb dates highlights the limitation of the K-Ar method in regions that have been affected by regional or local metamorphism, intense dyke swarm intrusion, tectonic activity, and metasomatism (Ancochea et al., 1996; Muñoz et al., 2003, Muñoz et al., 2005). The reported K-Ar method is more likely to experience a thermal resetting or disruption, obstructing the true age of the whole rock or mineral. One clear example of the discrepancies in the two dating methods was demonstrated in Muñoz et al. (2005) in their analysis of the oldest known intrusive complex in the Caleta de la Cruz region, commonly referred to as EM1 alkaline-carbonatite complex. They obtained a nepheline-syenite U-Pb zircon LA-ICPMS date of 25.4 ± 0.3 Ma, in contrast to Balogh et al.'s (1999) late Cretaceous (63-64 Ma) K-Ar and Ar/Ar dates for 'early-stage' syenites from the same region. Another notable age discrepancy is found in the PX1 gabbro-pyroxenite pluton (also referred to as the outermost part of the Pájara pluton). Le Bas et al. (1986) dated a cross-cutting dyke in the PX1 body (sample CR-S-4) and obtained a whole-rock K-Ar age of 48 Ma, suggesting the minimum age of the unit is 48 Ma. Allibon et al. (2011) report high-precision U-Pb ID-TIMS (zircon and baddeleyite) and Ar/Ar (amphibole) dates that constrain the life-span of the PX1 volcanic feeder system. The onset of magma crystallization of the feeder dyke is constrained by the zircon U-Pb date of 22.10 ± 0.07 Ma, with the magmatic activity lasting for a minimum of 0.52 Myr. The Ar/Ar age from the amphibole yielded ages from 21.9 ± 0.6 Ma to 21.8 ± 0.3 Ma, lower than the reported U-Pb dates. These dates contradict the former reported K-Ar age of 48 Ma for a cross cutting dyke in

the PX1 intrusion and is best explained by the presence of excess argon in the K-Ar dyke analysis (Le Bas et al., 1986).

The U-Pb detrital zircon data presented and discussed in this study provides an alternative approach to constraining the timing and duration of the intrusive bodies in the northern and central sectors of Fuerteventura for zircon-bearing rocks such as syenites, nepheline-syenites, anorthosites, gabbros, and carbonatites (Summary table of U-Pb, Hf, and O in Appendix. H.). A detrital zircon study as a first-order proxy to the timing of magmatism on Fuerteventura by contributing a large catchment of the basal complex in a relatively short period of time, and, unlike other surface dating approaches, recording the existence of intrusions that are no longer exposed. In addition, zircon is a robust mineral that has a high closure temperature to Pb-diffusion (>900ºC; Lee et al., 1997), therefore is not susceptible to disturbance by low-grade metamorphism and metasomatism, and high-precision U-Pb dates (±0.01%) can be obtained.

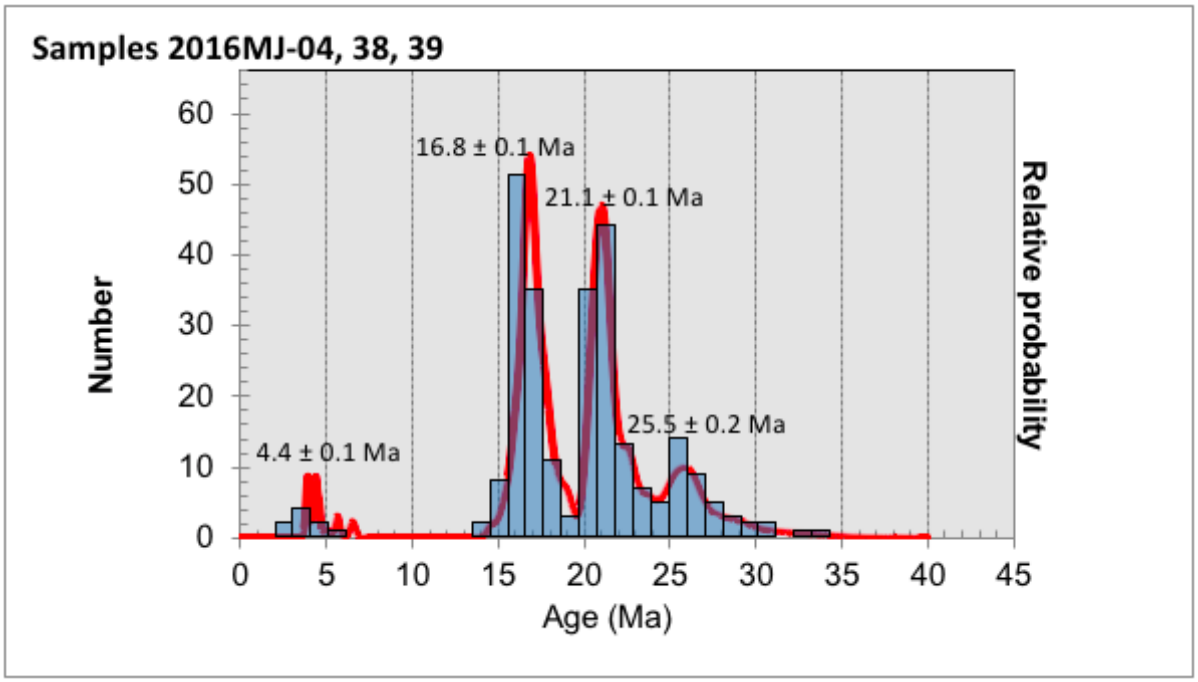

Figure. 5.1a. LA-MC-ICPMS probability density plot for detrital zircon U-Pb dates from Playa del Águila beach (2016MJ-04), Playa de Garcey beach (2016MJ-38), and Barranco de la Solapa river (2016MJ-39).

Based on mixture modelling results for detrital zircon from all three sand samples, there are four main zircon crystallization age peaks at 4.4, 16.8, 21.1, and 25.5 Ma (Figure. 5.1a). One of the key findings in this study is the identification of a significant number of Oligocene detrital zircons (n=25) that are older than the oldest published U-Pb zircon dates (~25 Ma) for exposed plutons. The prediction from this study is that older carbonatite and syenite intrusions must exist on the island, especially in the northern sector. The initial alkaline-carbonatite magmatic activity in the central sector has been dated using zircon U-Pb LA-ICPMS and correlates to the late Oilgocene at 25.4 Ma (Muñoz et al., 2005). This study extends the oldest known zircon date to 33.7 ± 2.9 Ma from the northern sector, recorded in detrital zircons isolated from Playa del Águila beach sand (see Results; Figure. 4.1.1a.). The peak observed at 25.5 ± 0.2 Ma lies within error of the initial intrusion (referred to as EM1) date, supporting the idea that zircon-bearing

plutonic bodies (alkaline-carbonatite suite) date around 25 Ma of Munoz et al. (2005). The second oldest peak at 21.1 ± 0.1 Ma is similar to that of the PX1 gabbro intrusion dated in the central volcanic sector. Allibon et al. (2011) dated a volcanic feeder dyke from the central region with ID-TIMS U-Pb zircon/baddeleyite ages of 21.6 ± 0.25 Ma to 22.1 ± 0.04 Ma. The difference in age is considered to be the duration of the volcanic feeder activity, lasting 0.48 ± 0.29 Myr years. These PX1 U-Pb zircon dates are similar to the 21.1 ± 0.1 Ma peak age observed in the detrital zircon population. Another potential source of 21.1 Ma detritus could be the Vega del Río Palmas syenite-nepheline syenite complex. This intrusive suite is considered to be the youngest phase of the basal complex and in previous literature have been dated from 21-18 Ma using conventional K-Ar methods (Rona & Nalwalk, 1970: Abel Monem et al., 1971; Grunau et al., 1975; Le Bas et al., 1986; Canagrel et al., 1993; Allibon et al., 2011).

The detrital zircon age peak at 16.8 ± 0.1 Ma is observed in all three of the samples (04, 38, 39). This age peak closely resembles the Betancuria Massif suite of plutonic intrusions (gabbros, pyroxenites, and syenites) located in the west-central region near Pájara and Mesquer. A recently acquired ID-TIMS U-Pb zircon age of 16.1 Ma from a syenite in the central sector by Betancuria Massif (Heaman, unpublished data) is comparable to this detrital zircon age peak. The northern sector of the island contains dates of basalts ranging from 18-13 Ma using the K-Ar method; however, no intrusive bodies around 16 Ma have been identified in the area.

It should also be noted that there is an apparent period of magmatic quiescence observed in the data set, from 14.5-6.5 Ma. These results are comparable with an apparent period of magmatic quiescence from 11.8-4.3 Ma in the K-Ar date of Abdel-Monem et al. (1971) or in the K-Ar date of 12.8-5.0 Ma Coello et al. (1992). The limitation of a zircon study is it only captures the magmatic history of zircon-bearing rocks and does not reflect mafic volcanic or ultramafic-

mafic plutonic activity; therefore, we cannot assess if this hiatus reflects an absence only of zircon-bearing plutonic rocks or a hiatus in all magmatic activity.

Another significant finding in this study is the discovery of young Miocene- Pliocene detrital zircon ages with a peak at 4.4 ± 0.1 Ma. Previous studies have identified Late Miocene, Pliocene, and Recent volcanics using K-Ar and Ar/Ar methods from olivine basalts or pillow basalts; however there have been no young intrusive bodies reported in this region (Coello et al., 1992; Meco et al., 2007; Meco et al., 2015). These young grains have only been observed in the central sector samples 2016MJ-38 and 2016MJ-39. The new 'young' zircon dates from this study significantly extend the duration of known intrusive activity on Fuerteventura, with several ages recording activity through the late Miocene and Pliocene (3.8-6.5 Ma, n=7). Summarizing these new detrital zircon dates, the duration of the zircon-bearing magmatism on the island ranges from 33.7 ± 2.9 to 3.8 ± 0.2 Ma, spanning across a majority of the island's magmatic activity.

5.2 Age progression of magmatism on Fuerteventura

There is a prominent age distinction between the west-northern sample (2016MJ-04) and west-central samples (2016MJ-38 and 2016MJ-39) (Figure. 5.2a; Figure. 5.2b.). The northern sector largely comprises ages >20 Ma (94.4%), with the exception of 2 analyses at the 16 Ma peak (Figure. 5.2a.). The dominant ages observed are around 26.4 Ma with the oldest grain at 33.7 ± 2.9 Ma (2σ). In contrast to this northern sector sample, the two central sector samples contain a small portion of grains ≥25 Ma (3.3%), with the prominent ages observed around 21 and 16 Ma (Figure. 5.2b). Furthermore, the late-Miocene and Pliocene populations observed in the central sector are absent in the northern sector. The apparent southward younging in magmatism from the northern to central sectors revealed in this detrital zircon study is consistent

with the proposed hotspot track moving in the southwest direction, with the northern portions of the island likely to form earlier than the central components (Geldmacher et al. 2011). Previous U-Pb zircon studies have not captured this age progression; the central sector of the island, including the EM1 and PX1 complexes are dated around 25-21 Ma (Muñoz et al., 2005; Allibon et al., 2011) and a single carbonatite zircon date from the northern sector around Barranco Esquinzo is reported at 23.2 ± 0.02 Ma (Cantagrel et al., 1993).

The ~30 Ma detrital zircon dates are significant because they could potentially alter the understanding of the Canary domain hotspot track progression. Geldmacher et al. (2005; 2011) analyzed the age versus distance relationship in the Canarian islands using dates summarized bySchmincke and Sumita (2010) to interpret if there was a single hot spot track system in the Canary domain. In this particular study, the oldest age of plume magmatism on Fuerteventura (22 Ma) is younger than predicted (~30 Ma) by the preferred hotspot track constructed by considering the earliest 'Shield Stage' volcanic activity on each Canary island (Figure. 5.2c). The 30 Ma date range is not included in the 'Shield Building' phase of the island; however, the plutonic rocks are considered to be a part of the transitional period between the seamount and shield building phase of the island (Coello et al., 1992; Ancochea et al., 1996; Muñoz et al., 2005). If the oldest detrital zircon dates obtained in this study reflect magmatism/volcanism occurring during the shield building stage of the islands growth, then the oldest intrusive activity on Fuerteventura would lie perfectly along the proposed Canary Island hotspot track (Figure. 5.2c.).

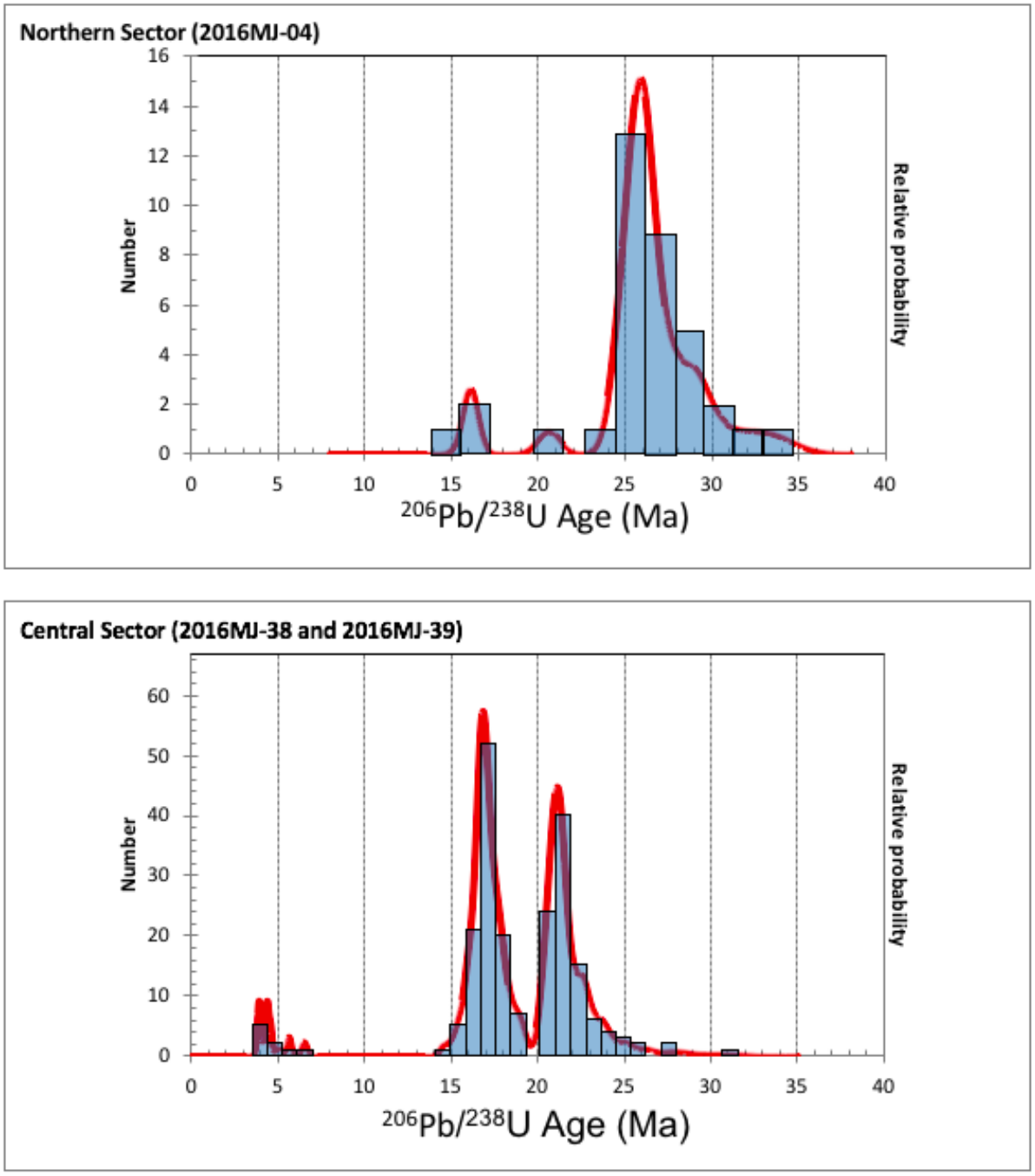

Figure. 5.2a. (top) and Figure. 5.2b. (bottom) demonstrates the U-Pb detrital zircon age variations between Fuerteventura's northern and central sectors. The most prominent feature is the dominance of an 'old' (>25 Ma) population from the northern sector, in comparison to the dominance of Miocene and Pliocene detrital zircons in the central sector.

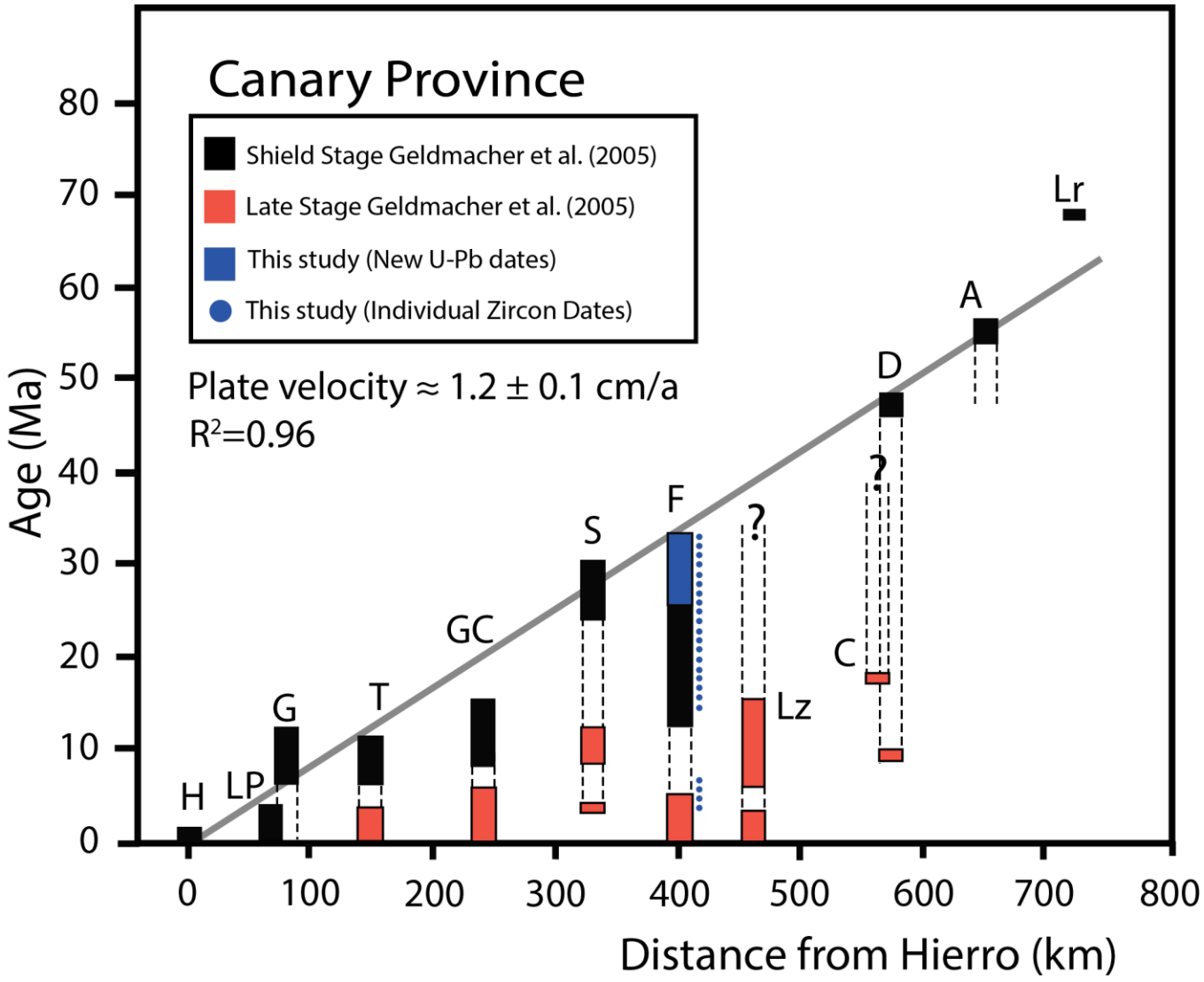

Figure. 5.2c. Distance versus Age plot for the Canary archipelago. This diagram has been modified from Geldmacher et al. (2005; 2011). This diagram represents the oldest radiometric ages of shield stage and late stage (rejuvenated stage) of the islands and seamounts in the Canary domain. The blue region represents the new U-Pb zircon ages on Fuerteventura from this study, lying within the proposed hotspot track. The blue dots beside the main Fuerteventura bar represent the range of individual detrital zircon dates, highlighting the hiatus observed from 14.5-6.5 Ma. Abbreviations of the islands and seamounts: H =Hierro, LP= La Palma, G= Gomera, T= Tenerife, GC= Gran Canaria, S= Selvagen Islands, F= Fuerteventura, Lz= Lanzarote, C= Conception Seamount, D= Dacia Seamount, A= Anika Seamount, and Lr= Lars Seamount.

5.3 Defining the magma provenance of zircon using minor and trace elements

In order to further understand the geological significance of these dates, we utilize a select number of minor and trace-elements contained in the detrital zircons to decipher their provenance. Previous zircon trace-element studies have established that zircon can record unique geochemical characteristics that reflect the magma composition from which they crystallized and offer potential to distinguish zircons that crystallize from syenites, nepheline-syenites, carbonatites, anorthosites, kimberlites, granites, and gabbros. We conclude that the Ti and Y contents in Fuerteventura detrital zircons and their Eu/Eu* are the most sensitive geochemical indicators to broadly identify zircon provenance. In particular, nepheline syenites and carbonatites have absent or negligible Eu/Eu* anomalies, and low Ti concentrations (<8 ppm) (Murali et al., 1983; Belousova et al., 2002; Schmitt et al., 2010; Dubyna et al., 2014). There is also a presence of bizarre wavy zoning and sponge-like textures associated with carbonatite zircons revealed in cathodoluminescence microscopy images (see Results 4.1, Figure. 4.1a). Yttrium concentrations in zircon are also useful to distinguish syenites and nepheline-syenites (>1000 ppm) from carbonatites (300-600 ppm) (Belousova et al., 2002). Syenite zircons generally have more geochemical variability, with typically more pronounced negative Eu/Eu* anomalies, and Ti concentrations ranging from several ppm to hundreds of ppm (Belousova et al., 2002).

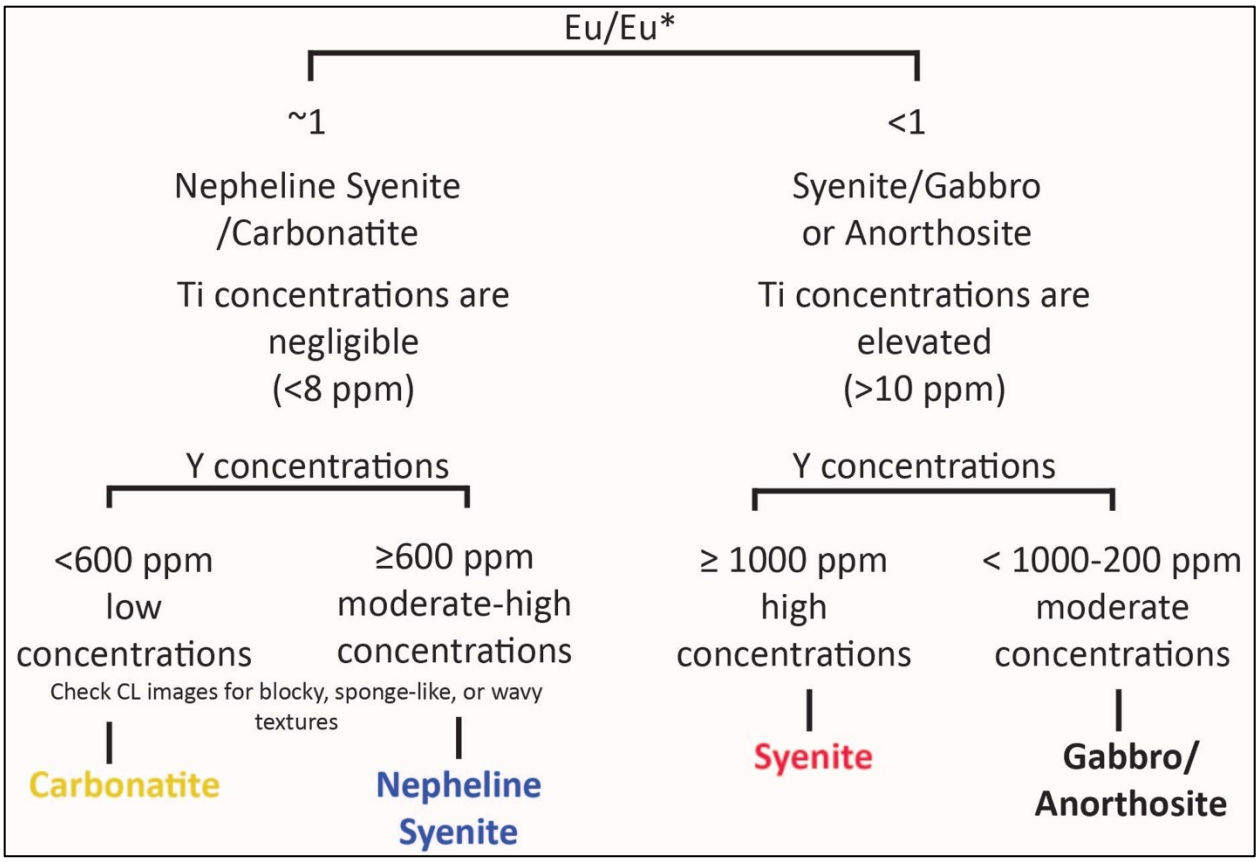

Figure. 5.3 CART classification utilized for geochemical discriminators in the alkaline suite to distinguish syenites, nepheline-syenites, gabbros/anorthosites, and carbonatites.

Applying these geochemical discriminators (Figure. 5.3), the Fuerteventura detrital zircons can be subdivided into 4 board categories: anorthosite/gabbro, carbonatite, nepheline-syenite, and syenite. For comparison, the geochemistry of zircons isolated from two Canary Island syenites 2016MJ-14 and 2016MJ-34 (Heaman, unpublished data) and an anorthosite (Allibon et al., 2011) are plotted in Figures 5.3h-j. Using these geochemical criteria, the detrital zircons analysed from this study indicate the following provenance: 51% syenite, 36% anorthosite/gabbro, 7% nepheline-syenite, and 5% carbonatite (Figure. 5.3a).

The detrital zircon provenance can be further subdivided based on geographic distribution (northern vs. central sector) (Figure. 5.3b-c) and crystallization age (Figure. 5.3d-g). The charts subdivided into northern and central sectors highlights that there is a change in

detrital zircon provenance based on geography. The northern sector consists of detrital zircons derived from nepheline-syenites, carbonatites, and syenites, with no occurrence of anorthosite/gabbro zircons (Figure. 5.3b). There is an approximately equal proportion of northern sector detrital zircons that are derived from these three rock types, with nepheline-syenite zircons slightly higher at 40%. In contrast to the northern sector, the central sector contains a very small portion of nepheline-syenite and carbonatite derived zircons (1-2%), with a majority of source rocks being identified as syenite (54%) or anorthosite or gabbro (42%) (Figure. 5.3c.).

We have also investigated whether there is any change in detrital zircon provenance and crystallization age. The oldest major detrital zircon population, which has an age peak at 25.5 ± 0.2 Ma was derived from nepheline-syenite (40%), syenite (32%), and carbonatite (28%) source rocks (Figure. 5.3d). These detrital zircons contain negligible Eu/Eu* anomalies (~1) and low Ti (<8 ppm) (Figure. 5.3h; Figure. 5.3j). The rock types were further subdivided based on Y concentrations, demonstrating a clear distinction between carbonatite and the nepheline-syenite/syenite populations (Figure. 5.3i.). These data are complementary with the known early magmatic activity of the alkaline-carbonatite intrusions (refs). The second peak at 21.1 ± 0.1 Ma contains 63% anorthosite/gabbro, 33% syenite, 2% nepheline-syenite, and, 2% carbonatite, corresponding with the temporal relationships of PX1(22.1 Ma) and Vega del Rio Palmas (21-18 Ma) regions (Figure. 5.3e) (Cantegrel et al., 1993; Ancochea et al., 1996; Allibon et al., 2011). The anorthosite/gabbro components have high Ti contents, with variable negative Eu/Eu* anomalies and moderate Y concentrations (>300 ppm; <1000 ppm) (Figure. 5.3h-j). The syenite population fall within a similar Ti and Eu/Eu* range, with higher Y concentrations (Figure. 5.3h-j). The 16.8 ± 0.1 Ma peak contains 81% syenite, 17% gabbro, and 2% undefined (Figure. 5.3f), containing the highest majority of syenite signatures. This is generally supported by sample

2016MJ-14 and 2016MJ-34; however, sample 2016MJ-14 demonstrates elevated Ti concentrations compared to the other syenite body (Figure. 5.3j). The youngest peak at 4.4 ± 0.1 Ma contains 57% anorthosite/gabbro and 43% syenite populations (Figure. 5.3g.). The occurrence of such young intrusive bodies on Fuerteventura has not been previously recognized but their existence is confirmed in this detrital zircon study. The Eu/Eu* anomalies closely resemble the Canary Islands syenite and anorthosite samples, the main distinction is between the Y contents of the samples (Figure. 5.3i.).

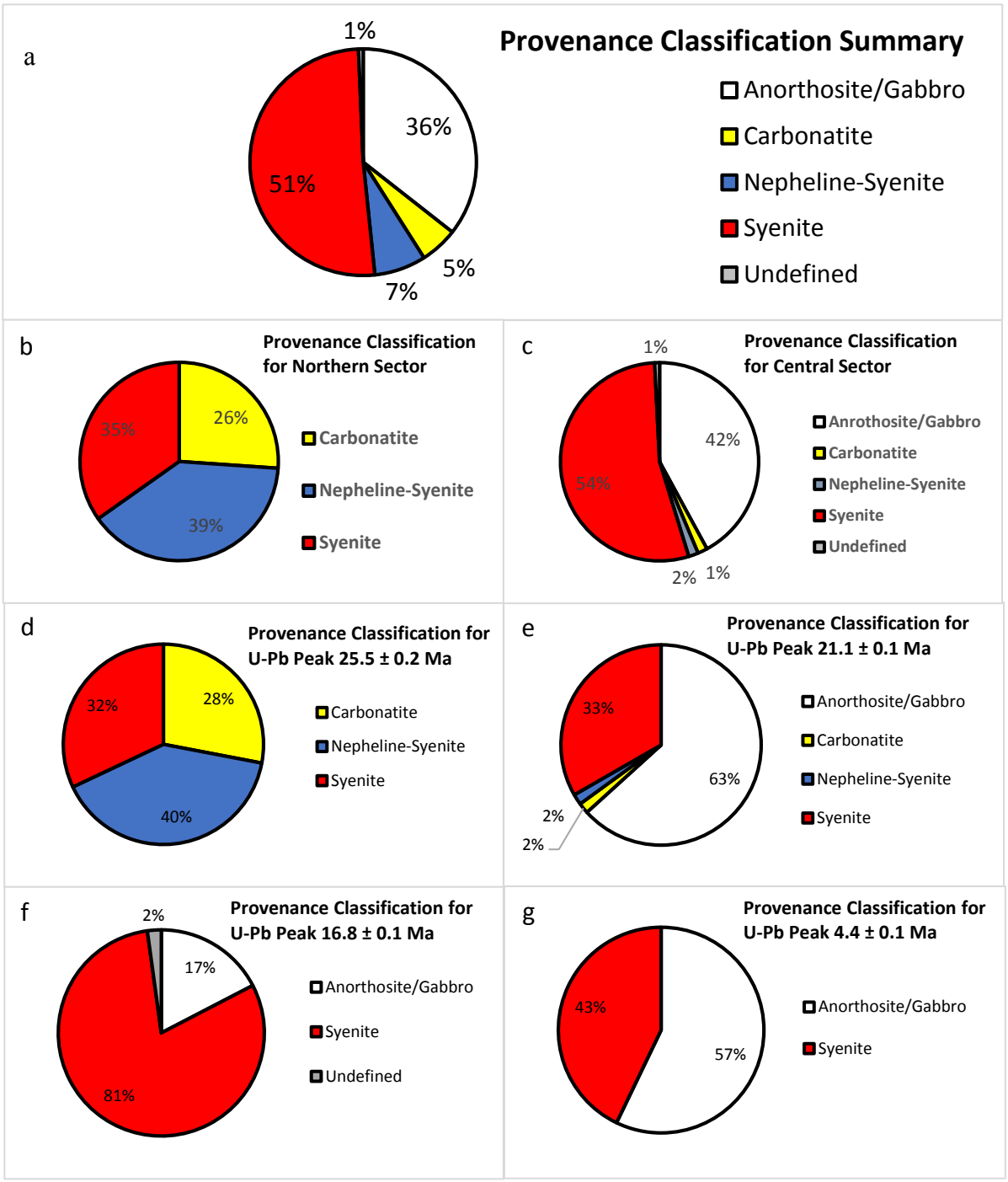

Figure. 5.3a-g. Provenance classification of detrital zircons from samples 2016MJ-04, 2016MJ-38, and 2016MJ-39 based on minor and trace element geochemistry. Figures b and c represent detrital zircons recovered from northern and central sector samples, respectively. Figures d-g present detrital zircon provenance based on their crystallization age.

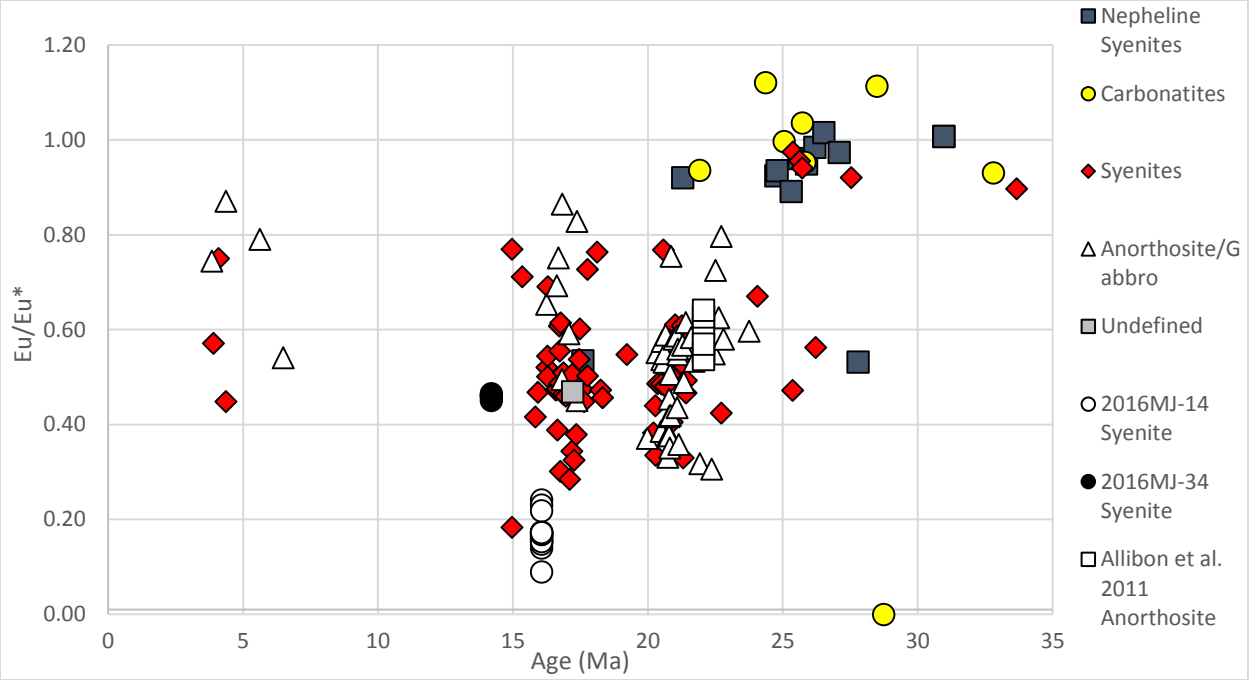

Figure. 5.3h. Age versus Eu/Eu* in Fuerteventura detrital zircons. Zircon isolated from two Fuerteventura syenites and an anorthosite are also shown for comparison.

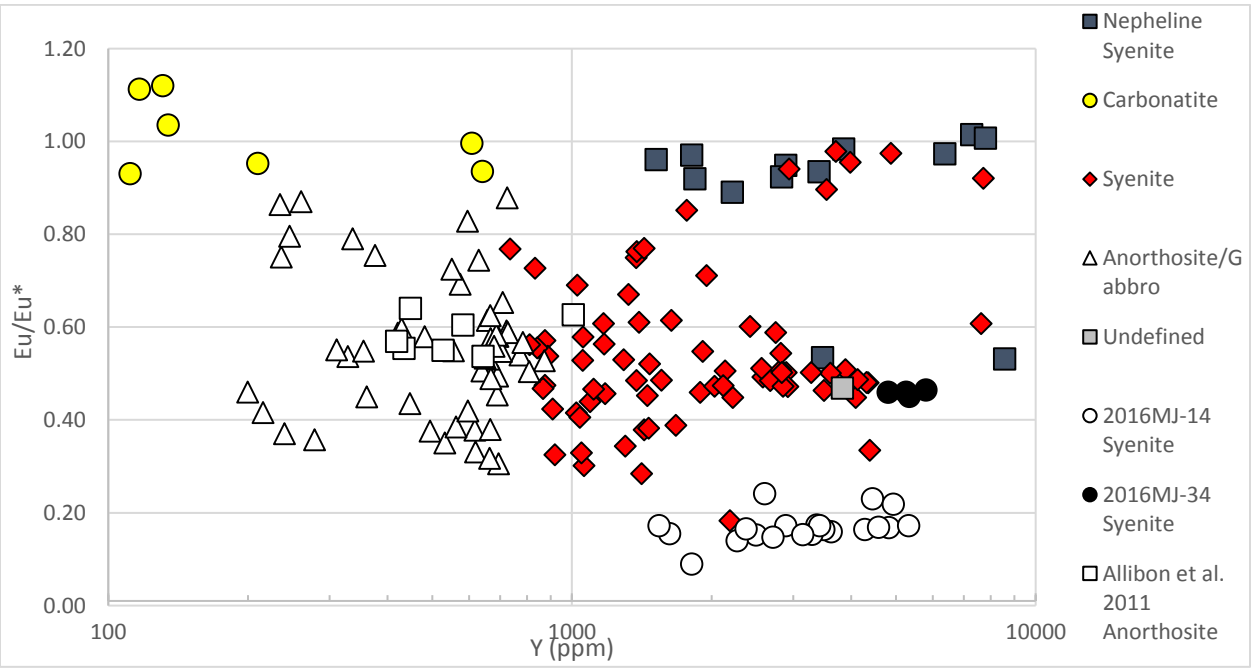

Figure. 5.3i. Yttrium (ppm) versus Eu/Eu* in Fuerteventura detrital zircons. Zircon isolated from two Fuerteventura syenites and an anorthosite are also shown for comparison.

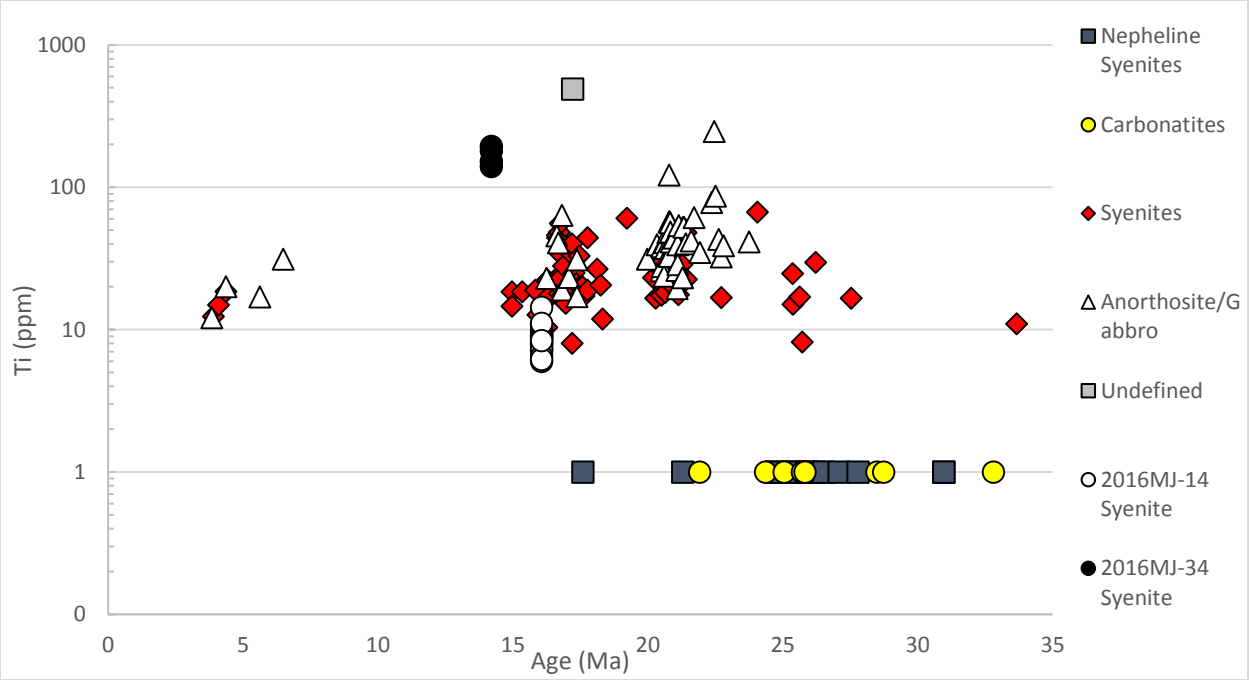

Figure. 5.3j. Fuerteventura magma provenance Age versus Ti (ppm) in Fuerteventura detrital zircons. Zircon isolated from two Fuerteventura syenites also shown for comparison.

5.4 Magma sources and the role of lithosphere contamination in the magma evolution

Although there have been several hypotheses proposed for the origin of the Canary Islands (Rothe et al., 1968; Demény et al., 1998; Widom et al., 1999; Hoernle et al., 2002; Demény et al., 2004; Geldmacher et al., 2005; de Ignacio et al., 2006; Demény et al., 2008; Gurenko et al., 2010; van den Bogaard et al., 2013), the prevailing view is that they are linked to the impingement of a relatively long-lived mantle plume responsible for the Canary hotspot track (e.g. Geldmacher et al., 2011). There is extensive literature on the role of mantle plumes in oceanic intraplate volcanic settings (Salters and Hart, 1991; Salters and White, 1998; Chauvel et al., 2007), however it remains challenging to deduce the nature and involvement of various mantle sources based on the compositions of ocean island volcanic rocks erupted at the surface. Radiogenic isotopes (e.g., Sr, Nd, Pb, Hf, and Os) are sensitive tools for understanding magma genesis and helping to define the involvement of discrete mantle sources and the mixing/entrainment of crust in ocean island studies. For example, many ocean islands require the involvement of several distinct mantle end-members, including sources with high long-term U/Pb ratios (HIMU), depleted mantle (DM), enriched mantle (EM1 and EM2), and asthenosphere. In addition, these mantle source end-members can be distinguished using minor- and trace-element geochemistry due to the fractionation behaviour of some elements in the mantle (Hofmann, 2003).

A fundamental challenge in all ocean island basalt isotopic studies is identifying the primeval plume signature because these mantle-derived magmas often experience modification during their ascent through the upper mantle and oceanic lithosphere. One suggestion is that the prevalent isotopic signature has been identified in both mid-ocean ridge basalts (MORB), denoted C-component by Hanan and Graham (1996), and in many ocean island basalts (OIB),

denoted focal zone (FOZO) by Hart et al. (1992), might be the best constraint for the nature of the plume source. This plume source is inferred to have the following isotopic composition; $^{206}Pb/^{204}Pb$=19.2 to 19.8; $^{207}Pb/^{204}Pb$=15.55 to 15.65, $^{208}Pb/^{204}Pb$=38.8 to 39.6, $^{87}Sr/^{86}Sr$=0.703 to 0.704, εNd=+4 to +6, εHf~+6 to +11 (Hanan and Graham, 1996; Hanan et al., 2000) and is generally viewed to have originated by incorporation of ancient recycled oceanic crust located in the Transition Zone (Hanan and Graham, 1996).

The mantle source and contamination history for Fuerteventura magmas remains a contentious topic. Previous geochemical/isotopic studies of typically young volcanic and some plutonic (mostly carbonatites) rocks on Fuerteventura have utilized Sr-Nd-Pb and O-C isotopic characteristics to define their mantle sources and the role of lithospheric contamination during magma ascent (Hoernle and Tilton, 1991; Demény et al., 1998; Demény et al., 2004; Hoernle et al., 2002; de Ignacio et al., 2006). A study by Hoernle et al. (2002) analyzed oceanic carbonatites from Fuerteventura and the Cape Verde Islands. Based on their geochemistry and Sr-Nd-Pb-O-C isotope compositions, the carbonatites on Fuerteventura are thought to have a HIMU-type ocean island basalt signature (Hoernle et al., 2002). It was interpreted that the carbonatites were derived from melting of recycled carbonated oceanic crust (eclogite) with an age of ~1.6 Ga, containing enriched components acquired through interaction with shallow, subcontinental-lithospheric mantle and deep lower mantle sources (Hoernle et al., 2002). The oxygen and carbon isotope compositions of calcite were thought to strictly reflect secondary processes (Hoernle et al., 2002).

The only hafnium isotope study of samples from the Canary Islands (Geldmacher et al., 2011) included four young (0.05 Ma) volcanic samples from Fuerteventura to understand the origin of intraplate volcanism in the Canary domain. The epsilon Hf values obtained in that study

ranged from +8.4 to +10.4, with the cluster lying between a low HIMU signature, a depleted member, and moderately enriched end of the Madeira domain trend (Figure 5.5a). This Hf isotope compositional range is comparable to the "C" component identified by Hanan et al. (2000), which in Hoernle et al. (2002) was interpreted to represent subducted, <1 Ga oceanic lithosphere (oceanic lithosphere with some possible sediment addition). The more enriched portion of the Canary Islands was interpreted to be associated with older (>1 Ga) recycled oceanic crust.

Previous studies have identified three potential endmember sources for the Fuerteventura magmas using the Sr-Nd-Pb tracer isotope studies (Widom et al., 1999; Hoernle et al., 2002; de Ignacio et al., 2006). These compositions resemble HIMU plume, N-MORB, and EM1 (de Ignacio et al., 2006). It is thought the magmatic source is mainly from a heterogeneous mantle plume with a deep-seated (FOZO or C-component) signature (Hart et al., 1992; Hanan et al., 2000). The previous Hf isotope results from Fuerteventura in the early volcanics have not captured this three-endmember mixing trend, only highlighting the DM and plume domains (Geldmacher et al., 2011). In this study, we would like to identify the endmember components in the magma source and develop an understanding of the potential lithospheric contamination on the island (EM) (Widom et al., 1999; Hoernle et al., 2002; de Ignacio et al., 2006).

The geochemical results from this detrital zircon study provide a large dataset of precise Hf and oxygen isotope analyses, representing a significant portion of the intrusive magmatic activity throughout the islands history. A study like this has not been completed previously and offers a new approach to clarify the potential mantle magma sources and role of lithosphere contamination over the life-time of the island's development. It also offers a unique opportunity to evaluate the nature of eroded material on the island that may no longer be exposed at surface.

5.5 Zircon Hafnium Isotope Signatures

Hafnium isotope data have been obtained for a total of 133 detrital zircons isolated from three Fuerteventura sands in this study (Appendix. F). These new data can be divided into three separate groups: the predominant zircon population with εHf_i values ranging from +7.5 to +10.4 (73% of the grains), a more 'depleted' population ranging from +10.6 to +15.2 (8% of the grains), and a more 'enriched' population ranging from -0.2 to +7.0 (19% of the grains) (Figure. 5.5a). The zircon εHfi values are relatively consistent (+7.5 to +10) in the early part of Fuerteventura's magmatic history from 34-20 Ma, but a substantial change occurs at ~20 Ma, where these younger zircons display great variation (Figure 5.5). Interestingly, this zircon εHf variation records both depleted and enriched isotopic signatures. Based on the current results, this abrupt change in Hf isotopic behaviour occurs only in detrital zircons sourced from the central sector of the island and is present in grains from both the Playa de Garcey beach sand sample (2016MJ-38) and Barranco de la Solapa river sand sample (2016MJ-39). After a hiatus in known magmatism (14.5 to 6.5 Ma) recognized in both this and previous studies, a suite of younger late-Miocene and Pliocene zircon grains (4.9 to 3.9 Ma) identified in this study record only enriched hafnium isotopic signatures with εHfi values that vary between -0.2 and +6.3.

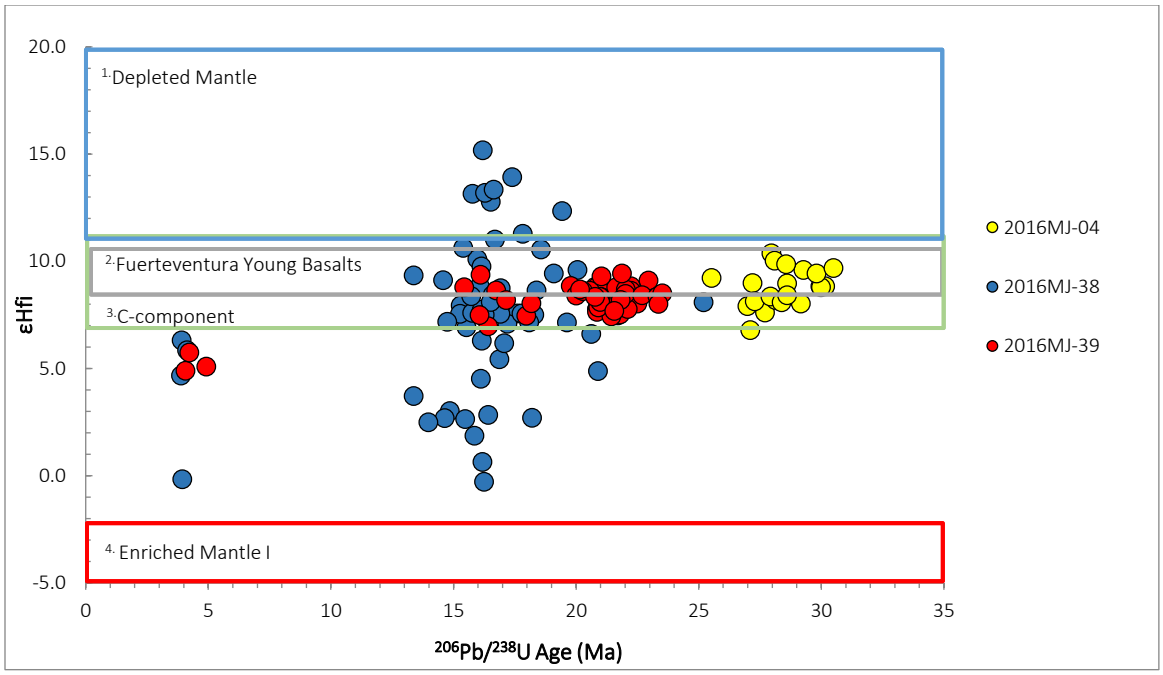

Figure. 5.5a. Epsilon Hf versus age of detrital zircons from Fuerteventura. Reference fields are: (1) Depleted mantle represented by Mid-Atlantic MORB data (Deballie et al., 2006); (2) whole rock data for Fuerteventura young (<0.1 Ma) basalts (Geldmacher et al., 2011); (3) C-component (Hanan et al., 2000); (4) Enriched mantle (EM1 of Barker et al. 2009).

It is noteworthy that the dominant Hf isotope signature (εHf_i=+7.5 to +10.4) observed for detrital zircons in this study are similar to values reported by Geldmacher et al. (2011) for recent (0.05 Ma) mafic volcanics on Fuerteventura (εHf_i=+8.4 to +10.4) (Figure. 5.5a). This is the most pervasive signature recorded throughout the island's ~34 Myr of development. We interpret this dominant Hf isotope signature to reflect the pristine Canary plume signature recorded in both the lavas and zircon-bearing alkaline plutonic rocks on Fuerteventura. This composition overlaps FOZO mantle signature (Stracke, 2005) and the C-component signature (+7 to +11) proposed by Hanan et al. (2000) as the pristine plume component identified in most OIB and MORB magmas. As noted by others, this C-component isotopic signature is best explained by derivation from ancient subducted oceanic lithosphere residing in the Transition Zone, either by initial mantle melting in this region or by substantial interaction with this material by lower mantle-derived

melts. This consistent detrital zircon Hf isotope signature, which we interpret to represent a characteristic of magma compositions on Fuerteventura could be acquired by melting of recycled older (~1 Ga) oceanic, representing a consistent plume composition.

During the Miocene shield-building stage initiated at ~20 Ma, there is a prominent divergence from the C-component Hf isotope signature into both depleted and enriched compositions (Figure. 5.5a). The shift to more depleted compositions is towards the Mid-Atlantic MORB signature, with the most depleted signature observed at ~16 Ma. Fuerteventura's depleted isotopic trend is thought to be a result of assimilating additional oceanic lithosphere during a period of high magma production rates on the island, increasing the εHf values (Hauri et al., 1994). This isotopic behaviour has been observed in post-shield volcanism (alkalic basalts) and has been attributed to interaction with the depleted mantle lithosphere; however, if the magma production rates are higher, they could be linked to higher entrainment rates of the oceanic lithosphere (Chen and Frey, 1985; Hauri et al., 1994). The enrichment trend could be a consequence of incorporation into the magmas of subducted sediments, continental crust, or possible existence of delaminated subcontinental lithospheric blocks in the oceanic mantle (White and Hofmann, 1982; Stracke et al., 2005). In previous studies, the Canary Islands have been considered to be derived by decompressional melting of a plume source carrying a HIMU and enriched component from recycled oceanic crust (Hoernle and Tilton, 1991; Hoenle et al., 1991; Gurenko et al., 2006). The more eastern islands, including Fuerteventura, show evidence of an enriched component (EM1), possibly representing continental lithosphere from either detached crustal blocks or subcontinental lithosphere in the upper mantle (Hoernle and Tilton, 1991; Hoenle et al., 1991, Widom et al., 1999).

This element and isotopic variation documented in Fuerteventura has also been observed in Cape Verde archipelago lavas from Hf, Sr, Nd, and Pb studies, indicating mixing trend between a HIMU plume, EM1 and DM type mantle components on Santiago (Martins et al., 2009). The EM1-like signature observed is considered to be derived from incorporation of SCLM with εHf_i values ranging from +2.5 to +7.2. Another comparable study was completed in the Réunion Islands from Piton des Neiges and Piton de la Fournaise. Bosch et al. (2008) describes these basaltic rocks to be sourced from a "pure" plume mantle-source similar to the C-component of Hanan and Graham (1996). There are minor components of depleted mantle observed in the geochemistry, closely resembling MORB in the Indian Ocean. The εHf_i range observed in the Réunion basaltic lavas average around +9, similar to the range we see in this εHf study and the young volcanics from Geldmacher et al. (2011).

5.6 Hf-O

As noted in the O isotope results section, there is significant variation in the Fuerteventura detrital zircon oxygen isotope compositions (+3.09 to +5.48‰). A striking feature of these data is that the majority of the zircon oxygen isotope compositions (88%) fall below the typical 'mantle' field defined as 5.3 ± 0.3‰ (Valley, 2003; Figure. 5.6a). Oxygen isotope heterogeneity (+4.6 to +6.1‰) was also reported for olivine from Canary mafic volcanic rocks (Wiechert et al., 1997; Gurenko et al., 2011). Unlike the olivine results, the Fuerteventura detrital zircon O-isotope data do not indicate compositions that are more ^{18}O enriched than asthenospheric mantle. The mantle-like oxygen isotope compositions are observed in a few detrital zircons that fall within the main Hf suite signature (εHf= 4.7-10.4; n=5) and a few that have minor enriched Hf isotope mantle signatures. Importantly, there are no depleted Hf

signatures containing mantle-like oxygen values (Figure. 5.6a). The low $\delta^{18}O$ detrital zircon values suggest a hydrothermally altered oceanic crust was assimilated, or hydrothermally altered sediments from high-temperature meteoric water was assimilated. The $\delta^{18}O$ depletion in plume-derived volcanic rocks is commonly interpreted to be associated with high-temperature water-rock interaction of oceanic lithosphere and/or high-temperature meteoric water-rock interaction with sediments can lower the $\delta^{18}O$ signature (Eiler et al., 1996; Eiler et al., 1997). This has been observed in Hawaiian basaltic olivines from several volcanos and is commonly referred to as the Kea trend (Eiler et al., 1996). The mantle-like zircon oxygen isotope values are recorded in grains that, based on trace element provenance tracing, indicate a variety of source rocks, including nepheline syenite, anorthosite/gabbro, and minor syenite (Figure. 5.6b). We interpret these results to indicate that some early magmas on Fuerteventura did not form from or interact with altered rock/sediments. The prevalent low-$\delta^{18}O$ signature in the Fuerteventura detrital zircons is present in all three mantle components identified from the Hf isotope results (enriched, depleted, and HIMU plume) and reflects variable involvement of high-temperature hydrothermal fluid altered oceanic lithosphere and sediment during magma upwelling on Fuerteventura.

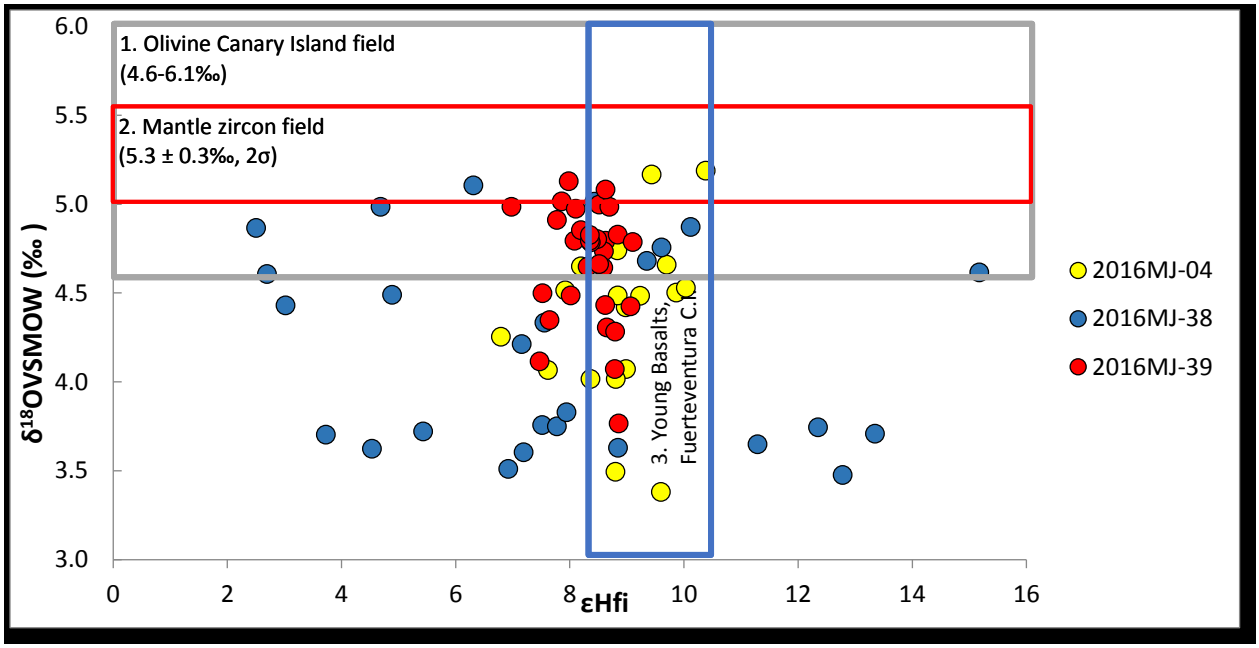

Figure. 5.6a. Fuerteventura detrital zircon εHfi versus $\delta^{18}O$ plot. Reference fields include: (1) Canary Island olivine oxygen isotope results (Wiechert et al., 1997; Gurenko et al., 2011); (2) Zircon Mantle-like oxygen isotope field (Valley, 2003); (3) whole rock Hf isotope data for young basalt volcanics (Geldmacher et al., 2011) – note there are no companion oxygen isotope data for these samples.

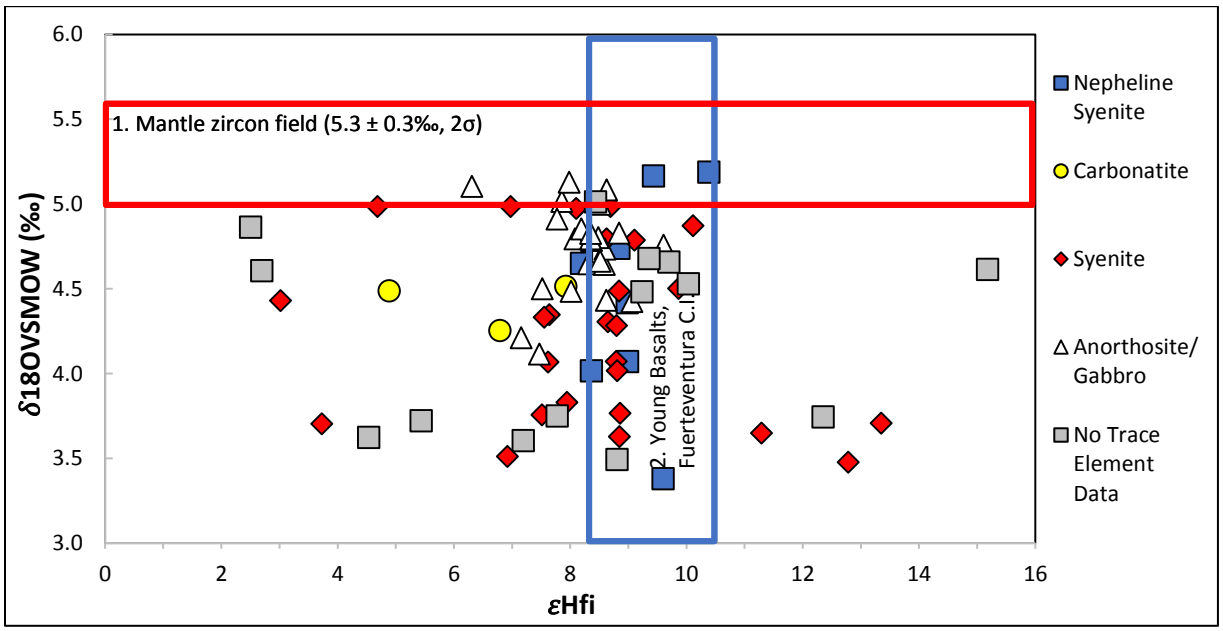

Figure. 5.6b. Fuerteventura detrital zircon εHfi versus $\delta^{18}O$ plot correlated to the rock type (1) Zircon mantle-like oxygen isotope field (Valley, 2003); (2) Hf isotope whole rock data from Fuerteventura young (0.05 Ma) basalts (Geldmacher et al., 2011).

Based on the detrital zircon Hf-O isotope results, the Fuerteventura magmas require the involvement of at least three different reservoirs in their genesis (Figure. 5.5c). The first reservoir (R1) is based on a HIMU-plume like source, produced by recycling of subducted oceanic crust with εHf ranging from +7.5 to +10 (Figure. 5.6c; Hanan et al., 2000; Stracke et al., 2005). This is considered to represent a C-component or FOZO signature and has been observed over the duration of the island's magmatic activity (Hanan et al., 2000; Stracke et al., 2005). The next reservoir (R2) is the depleted source (DM), which is considered to be from the Mid-Atlantic Jurassic MORB component. This old oceanic crust has εHf values that range from +10 to + 20, significantly higher than the HIMU plume component, and is incorporated during either decompressional melting or assimilated during upwelling of the plume source. The oceanic crust has experienced high-temperature rock-water alteration, creating the low-$\delta^{18}O$ signatures observed in the zircons. The more enriched $\delta^{18}O$ signatures (3.00-3.50‰) could be explained by the assimilation of sediments that have high-temperature meteoric rock-water alteration. The zircon grains that contain mantle-like values (5.3 ± 0.3‰) are generally observed during the shield-building stage of the island from 20-16 Ma. We suggest that the volcanic pipes have created a corridor to avoid hydrothermally altered crust or sediments in the oxygen isotope signature, allowing minor amounts of mantle-like zircon signatures to form. The last reservoir (R3) represents the enriched component (EM1). This signature is only observed in the central sector of the island, possibly mapping an enriched source residing under the center of the island. The R3 reservoir could represent a detached continental block, subcontinental lithospheric mantle, or oceanic sediments (Hoernle and Tilton, 1991; Hoernle et al., 1991, Widom et al., 1999). The enriched Hf signatures have assimilated portions of this continental source, creating an array of lower εHf values.

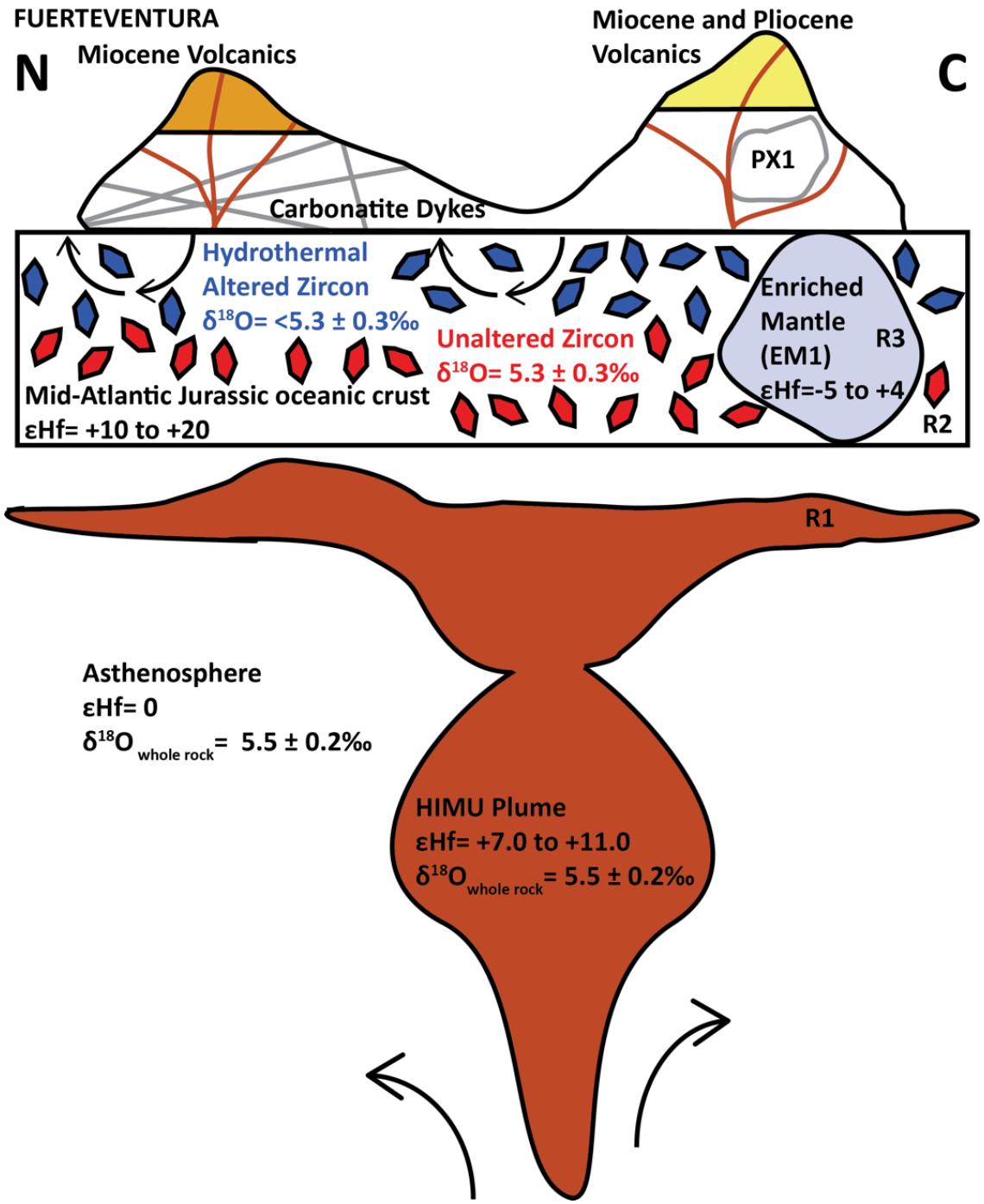

Figure. 5.6c. Schematic representation of the various mantle reservoirs involved in generating Fuerteventura's magmatic activity based on detrital zircon Hf-O isotopic compositions. Mantle reservoirs include a HIMU-plume source (R1), ancient (Jurassic) depleted Mid-Atlantic oceanic crust (R2), and an enriched mantle source (R3). Hf isotope reservoirs used in this study are as follows: R1 (Hanan et al., 2000); R2 (Deballie et al., 2006); and R3 (Barker et al. 2009). The mantle-like zircon values (5.3 ± 0.3‰; Valley, 2003) represented in red and the low- $\delta^{18}O$ values in blue (<5.3 ± 0.3‰) and asthenosphere/ plume whole rock values 5.5 ± 0.2‰ (Kyser et al., 1981).

CONCLUSIONS

Fuerteventura (Spain) is one of seven islands in the Canary archipelago, ~100 km west of southern Morocco. Despite numerous previous studies, the origin and magmatic history of the island remains poorly understood. We have conducted an integrated geochemical, U-Pb geochronology, and Hf and O isotope tracer study of detrital zircon grains from beach and river deposits located in the western half of Fuerteventura. These new findings have implications for the timing, duration and origin of Fuerteventura's magmatic history and lead to the following conclusions:

1. The LA-ICPMS U-Pb detrital zircon study identified a population of early Oligocene (~34-28 Ma) grains, largely derived from the northern sector of the island, that constrain the onset of the earliest shield-building stage of Fuerteventura. The oldest detrital zircon in this study is 33.7±2.9 Ma and, based on its geochemistry (higher Ti and Y content), is likely derived from a syenite. The recognition of early Oligocene magmatism in the earliest history of Fuerteventura provides a better fit to the Canary hotspot track age progression proposed by Geldmacher et al. (2005; 2011).

2. This study did not identify any Cretaceous or Jurassic ages in the detrital zircon populations analyzed from both the northern and central sectors of the island. The absence of these ages supports previous suggestions (e.g. Munoz et al., 2005) that many published K-Ar and Ar/Ar dates for intrusive rocks on Fuerteventura are erroneous, likely due to excess argon in the samples.

3. The LA-ICPMS U-Pb geochronology study identified a number of 'young' late Miocene to Pliocene (6.5-3.8 Ma, n=7) detrital zircons, which extends the duration of known intrusive activity on Fuerteventura. These intrusive bodies have not been previously identified or described on the island. Based on zircon trace-element geochemistry, the provenance of these detrital zircon indicate the existence of 'young' syenite and anorthosite/gabbro intrusive bodies on Fuerteventura.

4. An evaluation of the geographic distribution of detrital zircon dates indicates that there is a previously unrecognized age progression in magmatism with an apparent younging southward from the northern (16.0 ± 1.0 - 33.7 ± 2.9 Ma) with a peak age of ~26 Ma to central (3.8 ± 0.2 - 30.8 ± 2.9 Ma) sectors of the island with peak ages of 21 and 16 Ma. This is consistent with the Canary mantle plume hotspot track hypothesis.

5. The combined zircon U-Pb geochronology and trace-element geochemistry identifies the dominance of relatively old zircon-bearing carbonatite intrusions in the northern sector of the island.

6. Fuerteventura detrital zircons record a large range in Hf isotope compositions (εHfi=+15.2 to -0.3), much larger than recorded in recent (0.05 Ma) volcanics on Fuerteventura (+10.4 to +8.4; Geldmacher et al., 2011). This range in detrital zircon Hf isotope compositions can be explained by the involvement of at least three mantle reservoirs that contribute to the origin of magmas during island development including: HIMU-plume, depleted mantle (DM), and enriched mantle (EM1) sources. The prevalent

detrital zircon Hf isotopic composition (+7.5 to +10.5) overlaps with the young volcanic signature and is considered to reflect the composition of the Canary plume. The DM and EM1 signatures are only preserved in zircons younger than ~21 Ma. The DM component diverge in the early Miocene (~21 Ma) and lasts until 16 Ma, while the EM1 mixing is observed from the early Miocene (~21 Ma) to the late Pliocene (~3 Ma). The enriched mantle component is only associated with the central sector samples, possibly mapping the existence at depth of a SCLM or continental component in this region (Widom et al., 1999).

7. The detrital zircon oxygen isotope compositions also record a significant range in $\delta^{18}O$ from +3.09 to +5.48‰. The detrital zircons reveal both mantle-like $\delta^{18}O$ (n=23; 12%) and low-$\delta^{18}O$ values (n=168; 88%). The low oxygen values reflect magma interaction with hydrothermally altered oceanic crust or assimilation of hydrothermally altered sediment prior to zircon crystallization. The timing of hydrothermal alteration is unknown; however, it could be related to the original oceanic crust formation in the Jurassic.

FUTURE RESEARCH

The research completed in this thesis has improved our understanding of the duration and source of the initial magmatism on Fuerteventura; however, it is limited to zircon-bearing rocks such as carbonatite, anorthosite, grabbro, granite, syenite, and nepheline-syenite. In order to develop a complete understanding of the initial magmatic activity of Fuerteventura's alkaline-complex, an ultra-mafic and mafic alkaline rock study on ijolite-melteigite and clinopyroxenite rocks should be completed. These particular rocks have been reported to contain perovskite, a viable option for further U-Pb geochronology (Muñoz et al., 2003). It is imperative to see if the ultramafic and mafic components formed during the same time as the more felsic components, to offer insight on alkaline-complex evolution.

Additionally, I believe this thesis has demonstrated the importance of a detrital study to assess the initial magmatic activity in this particular region. It would be beneficial to complete large-scaled zircon study to further develop our understanding of the island from north to south. The limited analyses from the northern sector of the island should be further analyzed in conjunction with barrancos to further distinguish the differences between the north and central complex components. It would also be beneficial to study the southern complex, which does not contain any basal complex intrusions and should hypothetically contain the youngest zircon ages.

Another beneficial assessment would incorporate both Hf and Nd isotope zircon analyses to assess the mantle array of the samples analyzed. This is a powerful tool for identification of components (HIMU, EM1, and DM) contributing to the origin of mafic magmas to further understand the mantle dynamic observed on Fuerteventura and offer some insight to the source of the enriched signature.

REFERENCES

Abdel-Monem, Watkins, N.D., and Gast, P.W. 1971. Potassium-argon ages, volcanic stratigraphy, and geomagnetic polarity history of the Canary Islands: Lanzarote, Fuerteventura, Gran Canada and La Gomera. *Amer. J. of Sci.,* **271,** 490-521.

Allibon, J., Ovtcharova, M., Bussy, F., Cosca, M., Schaltegger, U., Bussien, D., & Lewin, É. 2011. Lifetime of an ocean island volcano feeder zone: constraints from U-Pb dating on coexisting zircon and baddeleyite, and $^{40}Ar/^{39}Ar$ age determinations, Fuerteventura, Canary Islands. *Can. J. Earth Sci.*, **48**, 567-592.

Amelin, Y. and Zaitsev, A.N. 2002. Precise geochronology of phoscorites and carbonatites: the critical role of U-series disequilibrium in age interpretations, *Geochim Cosmochim Acta,* **66**, 2399-2419.

Ancochea, E., Fúster, J.M., Ibarrola, E., Cendrero, A., Coello, J., Hernan, F., Cantagrel, J.M., and Jamond, C. 1990. Volcanic evolution of the island of Tenerife (Canary Islands) in the light of new K-Ar data. *J. Volcanol. Geotherm. Res*., **44**, 231-249.

Ancochea, E., Brändle, J. L., Cubas, C. R., Hernán, F. & Huertas, M. J. 1996. Volcanic complexes in the eastern ridge of the Canary Islands: the Miocene activity of the island of Fuerteventura. *J. Volcanol. Geotherm. Res.,* **70**, 183–204.

Anguita, F. & Hernán, F. 1975. A propagating fracture model versus a hotspot origin for the Canary Islands. *Earth Planet. Sci. Lett,* **27**, 11–19.

Araña, V. and Oritz, R. 1991. The Canary Islands. Tectonics, Magmatism and Geodynmaic framework. A.B. Kampunzu, R.T. Lubala (Eds.), Magmatism in Extensional Structural Settings. The Phanerozoic African Plate, Springer, New York, 209-249.

Balogh, K., Ahijado, A., Casillas, R., and Fernàndez, C. 1999. Contributions to the chronology of the Basal Complex of Fuerteventura, Canary Islands. *J. Volcanol. Geotherm. Res*., **90**, 81–101.

Barker, A.K., Holm, P.M., Peate, D.W., Baker, J.A. 2009. Geochemical stratigraphy of submarine lavas (3-5 Ma) from the Flamengos Valley, Santiago, Cape Verde. *J. Petrol.*, **50**, 169-193.

Belousova, E.A., Griffin, W.L., O'Reilly, S.Y., and Fisher, N.I. 2002. Igneous zircon: trace element composition as an indicator of source rock type. *Contrib Mineral Petrol*, **143**, 602-622.

Bindeman, I.N., Valley, J.W., 2001. Low-δ18O Rhyolites from Yellowstone: Magmatic Evolution Based on Analyses of Zircons and Individual Phenocrysts. *J. Petrol.,* **42**, 1491–1517.

Black, L. P., Kamo, S. L., Allen,C. M., Davis, D., Aleinikoff, J. N., Valley, J. W., Mundil, R., Campbell, I. H., Korsch, R. J., Williams, I. S., and Foudoulis, C., 2004. Improved $^{206}Pb/^{238}U$ microprobe geochronology by the monitoring of a trace-element-related matrix effect; SHRIMP, ID-TIMS, ELA-ICP-MS and oxygen isotope documentation for a series of zircon standards. *Chem. Geol,.* **205**, 115-140.

Bosch, D., Blichert-Toft, J., Moynier, F., Nelson, B.K., Telouk, P., Gillot, P.Y., Albaréde, F. 2008. Pb, Hf, and Nd isotope composiyions of the two Réunion volcanoes (Indian Ocean): A tale of two small-scale mantle "blobs". *Earth Planet. Sci. Lett.*, **265**, 748-765.

Bouvier, A., Vervoort, J. D., and Patchett, P. J., 2008. The Lu-Hf and Sm-Nd isotopic composition CHUR: Constraints from unequilibrated chondrites and implications for the bulk composition of terrestrial planets. *Earth Planet. Sci. Lett*, **273**, 48–57.

Cantagrel, J.M., Fúster, J.M., Pin, C., Renaud, U., and Ibarrola, E. 1993. Age Miocene inférieur des carbonatites de Fuerteventura (23 Ma U–Pb zircon) et le magmatisme précoce dúne ile océanique (Iles Canaries). *Compte Rendu de l'Acade´mie des Sciences*, Paris, **316**, 1147–1153.

Carracedeo, J.C., Day, S., Guillou, H., Rodríguez Badiolaś, E., Canas, J.A., and Pérez Torrado, F.J. 1998. Hotspot volcanism close to a passive continental margin: the Canary Islands. *Geol. Mag* **135**, 591-604.

Chauvel, C., Lewin, E., Carpentier, M., Arndt, N.T., and Marini, J.C. 2007. Role of recycled oceanic basalt and sediment in generating the Hf-Nd mantle array. *Nature*, **1**, 64-67.

Chen, C. and Frey, F.A. 1985. Trace element and isotopic geochemistry of lavas from haleakala volcano, East Maui, Hawaii: Implications for the origin of Hawaiian Basalts. *J. Geophys. Res.*, **90**, 9743-8768.

Coello, J., Cantagrel, J.M., Hernán, F., Fústerm J.M., Ibarrola, E., Anocochea, E., Casquet, C., Jamond, C., Teran, J.R., and, Cendrero, A. 1992. Evolution of the eastern volcanic ridge of the Canary Islands based on new K-Ar data. *J. Volcanol. Geotherm. Res.*, **53**, 251-274.

de Ignacio, C., Muñoz, M., Sagredo, J., Barbero, L., 2002b. Preliminary apatite-fission track geochronology of the Montaña Blanca-Milocho alkaline pluton (NW Fuerteventura, Canary Islands, Spain). *Geotemas,* **4**, 55–59.

de Ignacio, C., Muñoz, M., Sagredo, J., Fernández-Santín, S., Johansson, Å. 2006. Isotope geochemistry and FOZO mantle component of the alkaline-carbonatite association of Fuerteventura, Canary Islands, Spain. *Chem. Geol.*, **232**, 99-113.

Deballie, V., Blichert-Toft, J., Agranier, A., Doucelance, R., Schiano, P., and Albarede, F. 2006. Geochemical component relationships in MORB from the Mid-Atlantic Ridge, 22-35°N. *Earth Planet. Sci. Lett.*, **241**, 844-862.

Demény, A., Ahijado, A., Casillas, R., Vennemann, T.W. 1998. Crustal contamination and fluid/rock interaction in the carbonatites of Fuerteventura (Canary Islands, Spain): C, O, H isotope study. *Lithos,* **44**, 101-115.

Demény, A., Vennemann, T.W., Ahijado, A., and Casillas, R. 2004. Oxygen isotope thermometry in carbonatites, Fuerteventura, Canary Islands, Spain. *Mineral and Petrology*, **80**, 155-172.

Demény, A., Vennemann, T.W., Hegner, E., Ahijado, A., Casillas, R., Hagy, G., Homonnay, Z., Gutierrez, M., and Szabo, C. 2004. H, O, Sr, Nd, and Pb isotopic evidence for recycled oceanic crust in the Transitional Volcanic Group of Fuerteventura, Canary Islands, Space *Chem. Geol.*, **205**, 37-54.

Demény, A., Casillas, R., Vennemann, T.W., Hegner, E., Nagy, G., Ahijado, A., De La Nuez, J., Sipos, P., Pilet, S., and Milton, J. 2008. Plume-related stable isotope compositions and fluid-rock interaction processes in the Basal Complex of La Palma, Canary Islands, Spain. In Metasomatism in Oceanic and Continental Lithospheric Mantle, vo. 293 (eds M. Coltorti and M. Greogoire). Geological Society, London, Special Publications, 155-175.

Dubyna, A.V., Kryvdi, S.G., and Sharygin, V.V. 2014. Geochemistry of alkali and nepheline syenites of the Ukrainian Shield: ICP-MS data. *Geochemistry International*, **52**, 842-856.

Eiler, J.M., Farley, K.A., Valley, J.W., Hofmann, A.W., and Stolper, E.M. 1996. Oxygen isotope constraints on the sources of Hawaiian volcanism. *Earth and Planet. Sci. Lett.*, **144**, 453-468.

Eiler, J.M., 2001. Oxygen isotope variations of basaltic lavas and upper mantle rocks. *Reviews in Mineralogy and Geochemistry,* **43**, 319–364.

Feraud, G., Giannerini, G., Campredon, R., Stillman, C.J., 1985. Geochronology of some canarian dyke swarms: contribution to the tectonic evolution of the archipelago. *J. Volcanol. Geotherm. Res.,* **25**, 29–52.

Fisher, C. M., Hanchar, J. M., Samson, S. D., Dhuime, B., Blichert-Toft, J., Vervoort, J. D., and Lam, R., 2011. Synthetic zircon doped with hafnium and rare earth elements: A reference material for in situ hafnium isotope analysis. *Chem. Geol.*, **286**, 32–47.

Fisher, C.M., Vervoort, J.D., and DuFrane, S.A., 2014. Accurate Hf isotope determinations of complex zircons using the "laser ablation split stream" method. *Geochem., Geophys., Geosys.*, **15**, 121-139.

Fu, B., Page, F., Cavosie, A., Fournelle, J., Kita, N., Lackey, J., Wilde, S., Valley, J. 2008. Ti-in-zircon thermometry: applications and limitations. *Contrib Mineral Petrol,* **156**, 197-215.

Fuster, J.M., Aguilar Tomás, M.J., 1965. Nota previa sobre la geología del macizo de Betancuria, Fuerteventura (Islas Canarias). *Estud. Geol.*, **21**, 181–197.

Geldmacher, J., Hoernle, K., Bogaard, P.V.D., Duggen, S., and Werner, R. 2005, New 40Ar/39Ar age and geochemical data from seamounts in the Canary and Madeira Volcanic Provinces: A contribution to the "Great Plume Debate". *Earth and Planet. Sci. Lett.*, **237**, 85–101.

Geldmacher, J., Hoernle, K., Hanan, B.B., Blichert-Toft, J., Hauff, F., Gill, J.B. and Schmincke, H.U. 2011. Hafnium isotopic variations in East Atlantic intraplate volcanism. *Mineral Petrol*, **162**, 21–36.

Grunau, H.R., Lehner, P., Cleintaur, M.R., Allenback, P., and Bakkar, G. 1975. New radiometric ages and seismic data from Fuerteventura (Canary Islands), Maio (Cape Verde Islands), and São Tomé (Gulf of Guinea). Progress in Geodynamics. Royal Society of the Netherlands Academy of Arts and Sciences, Amsterdam, 90–108.

Gurenko, A.A., Hoernle, K.A., Hauff, F., Schminke, H.U., Han, D., Miura, Y.N., and Kaneoka, I. 2006. Major, trace element and Nd-Sr-Pb-O-He-Ar isotope sigantures of shield stage lavas from the central and western Canary Islands: insights into mantle and crustal processes. *Chem. Geol*., **233**, 75-112.

Gurenko, A.A., Sobolev, A.V., Hoernle, K.A., Hauff, F., and Schmincke, H.U. 2009. Enriched, HIMU-type peridotite and depleted recycled pyroxenite in the Canary plume: a mixed-up mantle. *Earth Planet. Sci. Lett.,* **277**, 514-524.

Gurenko, A.A., Bindeman, I.N., and, Chaussidon, M. 2011. Oxygen isotope heterogeneity of the mantle beneath the Canary Islands: insights from olivine phenocrysts. *Contrib Mineral Petrol*., **162**, 349-363.

Gutierrez, M., Casillas, R., Fernandez, C., Balogh, K., Ahijado, A., Castillo, C., Colmenero, J. R. & Garcia-Navarro, E. 2006. The submarine volcanic succession of the basal complex of Fuerteventura, Canary Islands: A model of submarine growth and emergence of tectonic volcanic islands. *Geological Society of America Bulletin,* **118**, 785–804.

Hanan, B.B. and Graham, D.W. 1996. Lead and helium isotope evidence from oceanic basalts for a common deep source of mantle plumes. *Science*, **272**, 991-995.

Hanan, B.D., Blichert-Toft, J., Kingsley, R., Schilling, J.G. 2000. Depleted Iceland mantle plume geochemical signature: artifact of multi-component mixing? *Geochem. Geophys. Geosyst 1*.

Hart, S.R., Hauri, E.H., Oschmann, L.A., and Whitehead, J.A. 1992. Mantle plumes and entrainment- Isotopic evidence. *Science*, **256**, 517-520.

Hauri, E.H., Whitehead, J.A., and Hart, S.R. 1994. Fluid dynamic and geochemical aspects of entrainment in mantle plumes. *J. Geophys*., **99**, 24,275-24,300.

Heaman, L.M., Bowins, R., and Crocket, J. 1990. The chemical composition of igneous zircon suites: implications for geochemical tracer studies. *Geochim Cosmochim Acta,* **54**, 1597–1607.

Hoernle, K.A. and Tilton, G.R. 1991. Sr-Nd-Pb isotope data for Fuerteventura (Canary Islands) basal complex and subaerial volcanics: applications to magma genesis and evolution. *Mineral. Petrogr. Mitt*, **71**, 3-18.

Hoernle, K.A., Tilton, G.R., Le Bas, M.J., Duggen, S., and, Garbe-Schönberg, C.D. 2002. Geochemistry of oceanic carbonatites compared with continental carbonatites: mantle recycling of oceanic crustal carbonatite. *Contrib Mineral Petrol*., **142**, 520-542.

Hoffman, A.W. and White, W.M. 1982. Mantle plumes from ancient ocean crust. *Earth Planet. Sci. Lett.*, **57**, 421-436.

Hofmann, A.W. 2003. Sampling mantle heterogeneity through oceanic basalts: Isotopes and trace elements, in *Treatise on Geochemistry: The Mantle and Core*, edited by R.W. Carlson, H.D. Holland, and K.K. Turekian, 61-101, Elsevier, New York.

Hoskin, P.W.O. 2005. Trace-element composition of hydrothermal zircon and the alteration of Hadean zircon from the Jack Hills, Australia. *Geochim Cosmochim Acta,* **69**, 637-648.

Hoskin, P.W.O. and Schaltegger, U. 2003. The composition of zircon and igneous and metamorphic petrogenesis. *Reviews in Mineralogy and Geochemistry*, **53**, 27-62.

Jackson, S. E., Pearson, N. J., Griffin, W. L., and Belousova, E. A., 2004. The application of laser ablation-inductively coupled plasma-mass spectrometry to in situ U–Pb zircon geochronology, *Chem. Geol.*, **211**, 47–69.

Jaffey, A. H., Flynn, K. F., Glendenin, L. E., Bentley, W. C., and Essling, A. M. (1971). Precision measurement of half-lives and specific activities of ^{235}U and ^{238}U. *Physical Review*, **C4**, 1889–1906.

Jochum K.P., Weis U., Stoll B., Kuzmin D., Yang Qichao, Raczek I., Jacob D.E., Stracke A., Birbaum K., Frick D.A., Günther D., Enzweiler J., 2011. Determination of Reference Values for NIST SRM 610-617 Glasses Following ISO Guidelines *Geostandards and Geoanalytical Research,* **35**, 397-429.

Kirkland, C.L., Smithies, R.H., Taylor, R.J.M., Evans, N., and McDonald, B. 2015. Zircon Th/U ratios in magmatic environs. *Lithos*, **212-215**, 397-414.

Klepeisa, K.A., Crawford, M.L., and Gehrel., G., 1998. Structural history of the crustal- scale Coast sheer zone north of Portland Canal, southeast Alaska and British Columbia. *Journal of Structural Geology*, **20**, 883-904.

Kyser, T.K., O'Neil, J.R., Carmichael, I.S.E. 1981. Oxygen isotope thermometry of basic lavas and mantle nodules. *Contrib Mineral Petrol,* **77**, 11-23.

Lassiter, J. C., E. H. Hauri, P. W. Reiners, and M. O. Garcia (2000), Generation of Hawaiian post-erosional lavas by melting of a mixed lherzolite/pyroxenite source. *Earth Planet. Sci. Lett.,* **178**, 269–284.

Le Bas, M.J., Rex, D.C., and Stillman, C.J. 1986. The early magmatic chronology of Fuerteventura, Canary Islands. *Geol. Mag*., **123(3)**, 287-298.

Lee, J.K.W., Williams, I.S., and Ellis, D.J. 1997. Pb, U, and Th diffusion in natural zircon. *Nature,* **390**, 159-161.

Liebsch, H. 1996. Die Genese der Laacher See-Karbonatite. PhD thesis. Georg-August Universitt, Gottingen, 1-111.

Ludwig, K.R., 2008, Manual for Isoplot 3.7: Berkeley Geochronology Center, Special Publication No. 4. rev. August 26, 2008, 77 pp.

Martins, M., Mata, J., Munhá, J., Mendes, M.H., Maerschalk, C., Caldeira, R., and Mattielli, N. 2009. Chemical and mineralogical evidence of the occurrence of mantle metasomatism by carbonate-rich melts in an oceanic environment (Santiago Island, Cape Verde). *Mineral Petrol.,* **99**, 43-65.

Meco, J., Stearns, C.E., 1981. Emergent littoral deposits in the Eastern Canary Islands. *Quat. Res.,* **15**, 199–208.

Meco, J., Scaillet, S., Guillou, H., Lomoschitz, A., Carracedo, J.C., Ballester, J., Betancort, J.F., Cilleros, A., 2007. Evidence for long-term uplift on the Canary Islands from emergent Mio–Pliocene littoral deposits. *Global Planet. Chang*., **57**, 222–234.

Meco, J., Koppers, A.A.P., Miggins, D.P., Lomoschitz, A., and Betancort, J.F., 2015. The Canary Record of the Evolution of the North Atlantic Pliocene: New 40Ar/39Ar Ages and Some Notable Palaeontological Evidence. *Palaeogeo. Palaeoclim. Palaeoeco*., **435**, 53-69.

Muñoz, M., de Ignacio, C. and Sagredo, J. 2003. Fieldtrip guide: Fuerteventura. IV EuroCarb Workshop, Canary Islands, Spain. 35-64.

Muñoz, M., Sagredo, J., de Ignacio, C., Fernàndez-Suàrez, J., and Jeffries, T.E. 2005. New data (U–Pb, K–Ar) on the geochronology of the alkaline–carbonatitic association of Fuerteventura, Canary Islands, Spain. *Lithos*, **85(1-4)**, 140–153.

Murali, A.V., Parthasarathy, R., Mahadevan, T.M., Sankar Das, M. 1983. Trace element characteristics, REE patterns and partition coefficients of zircons from different geological environments – a case study on Indian zircons. *Geochim Cosmochim Acta,* **47**, 2047–2052.

Ringwood A. E. and Lovering J. F. (1970) Significance of pyroxene-ilmenite intergrowths among kimberlite xenoliths. *Earth Planet. Sci. Lett*., **7**, 371-375.

Robertson, A.H.F. and Stillman, C.J. 1979a. Submarine volcanic and associated sedimentary rocks of the Fuerteventura Basal Complex, Canary Islands. *Geol. Mag*., **116**, 203-214.

Rothe, P. and Schminke, H.U. 1968. Contrasting Origins of the Eatern and Western Islands of the Canarian Archipelgo. *Nature*, **218**, 1152-1154.

Rona, P.A. and Nalwalk, A.J. 1970. Post-early Pliocene unconformity on Fuerteventura, Canary Islands. *Geological Society of America Bulletin,* **81,** 2117-2122.

Sagredo, J., Muñoz, M., and Galindo, C. 1996. Caracteristicas petrologicas y edad K–Ar de las sienitas nephelinicas del Morro del Recogedero (Fuerteventura, Islas Canarias). *Geogaceta*, **20**, 506– 509.

Salters, V.J.M. and Hart, S.R. 1991. The mantle sources of ocean islands and arc basalts: The Hf isotope connection. *Earth Planet. Sci. Lett.*, **104**, 364-380.

Salters, V.J.M. and W.M. White. 1998. Hf isotope constraints on mantle evolution. *Chem. Geol.*, **145**, 447-460.

Schmitt, A.K., Wetzel, F., Cooper, K.M., Zou, H., and Wörner, G. 2010. Magmatic Longevity of Laacher See Volcano (Eifel, Germany) Indicated by U-Th Dating of Intrusive Carbonatites. *J. of Petrol*, **51**, 1053-1085.

Schoene, B., Crowley, J. L., Condon, D. J., Schmitz, M. D., and Bowring, S.A., 2006. Reassessing the uranium decay constants for geochronology using ID-TIMS U-Pb data. *Geochimica et Cosmochimica Acta*, **70**, 426–445.

Simonetti, A., Heaman, L.M., Hartlaub, R.P., Creaser, R.A., MacHattie, T.G., & Bohm, C., 2005. U–Pb zircon dating by laser ablation-MC-ICP-MS using a new multiple ion counting Faraday collector array. *J. of Analytical Atomic Spectrometry*, **20**, 677-686.

Simonetti, A., Heaman, L.M., and Chacko, T., 2008. Use of discrete-dynode secondary electron multipliers with Faradays- a 'reduced volume' approach for in-situ U-Pb dating of accessory minerals within petrographic thin sections by LA-MC-ICP-MS. Mineralogical Association of Canada Short Course Series, **40**, 241-261.

Sláma, J., Košler, J., Condon, D.J., Crowley, J.L., Gerdes, A., Hanchar, M.H., Horstwood, M.S.A., Morris, G.A., Nasdala, L., Norberg, N., Schaltegger, U., Schoene, B., Tubrett, M.N., and Whitehouse, M.J., 2008. Plešovice zircon—A new natural reference material for U–Pb and Hf isotopic microanalysis. *Chem. Geol.*, **249**, 1–35.

Smyth, D.J. and Brenan, J.M. 2016. Magmatic oxygen fugacity estimated using zircon melt partitioning of cerium. *Earth Planet. Sci. Lett.*, **453**, 260-266.

Söderlund, U., Patchett, P. J., Vervoort, J. D., and Isachsen, C. E., 2004. The ^{176}Lu decay constant determined by Lu-Hf and U-Pb isotope systematics of Perecambrian mafic intrusions. *Earth Planet. Sci. Lett.*, **219**, 311–324.

Stillman, C.J., Fuster, J.M., Bennell-Baker, M.J., Muñoz, M., Smewing, J.D., Sagredo, J. 1975. Basal complex of Fuerteventura (Canary Islands) is an oceanic intrusive complex with rift-system affinities. *Nature,* **257,** 469-71.

Stracke, A., Hofmann, A.W., and Hart, S.R. 2005. FOZO, HIMU, and the rest of the mantle zoo. *Geochem. Geophys. Geosyst*., **6**,1-20.

Sun, S.S. and McDonough, W.F. 1989. Chemical and isotopic systematic of oceanic basalts: implications for mantle composition and processes. *Geol. Society*, **42**, 313-345.

Taylor, H.P., Sheppard, S.M.F., 1986. Igneous rocks; I Processes of isotopic fractionation and isotope systematics. *Reviews in Mineralogy and Geochemistry* **16**, 227–271.

Valley, J.W., Kinny, P.D., Schulze, D.J., and Spicuzza, M.J., 1998, Zircon megacrysts from kimberlite; oxygen isotope variability among mantle melts. *Contrib Mineral Petrol.,* **133**, 1–11.

Valley, J.A., 2003. Oxygen isotopes in zircon. In: Hanchar, J.M., Hoskin, P.W.O. (Eds.), Zircon. Reviews in Mineralogy and Geochemistry. *Mineralogical Society of America, Washington, DC*, **53**, 1 – 40.

van den Bogaard, P. The origin of the Canary Island Seamount Province- New ages of old seamounts 3, Scientific Reports, 1-7.

Watson, E. and Thomas, J. 2006. Crystallization thermometers for zircon and rutile. *Contrib Mineral Petrol,* **151**, 413-433.

Widom, E., Hoernle, K.A., Shirey, S.B., and Schminke, H.U. 1999. Os isotope systematics in the Canary Islands and Maderia: lithospheric contaminations and mantle plume signatures. *J. Petrol*., **40**, 279-296.

Wiechert, U., Hoernle, K., Graham, D. 1997. Oxygen isotope evidence for high temperature altered oceanic crust in the Canary plume, EOS Transactions, American Geophysical Union Fall Meeting, 825-826.

Wiedenbeck M., Hanchar J.M., Peck W.H., Sylvester P., Valley J.W., Whitehouse M.J., Kronz A., Morishita Y., Nasdala L., Fiebig J., Franchi I.A., Girard J.-P., Greenwood R.C., Hinton R.W., Kita N.T., Mason P.R.D., Norman M.D., Ogasawara M., Piccoli P.M., Rhede D., Satoh H., Schulz-Dobrick B., Skår Ø., Spicuzza M.J., Terada K., Tindle A.G., Togashi S., Vennemann T.W., Xie Qianli, Zheng Yong-Fei., 2004. Further characteristics of the 91500 Zircon crystals. *Geostandards and Geoanalytical Research* 28 (1) 9-39.

Xie, L. W., Zhang, Y. B., Zhang, H. H., Sun, J. F., and Wu, F. Y., 2008. In situ simultaneous determination of trace elements, U\Pb and Lu\Hf isotopes in zircon and baddeleyite. *Chin. Sci. Bull.*, **53**, 1565–1573.

Yuan H.L., Gao S., Liu Xiaoming, Li Huiming, Günther D., Wu F, 2004. Accurate U-Pb age and trace element determinations of zircon by laser ablation-inductively coupled plasma-mass spectrometry. *Geostandards and Geoanalytical Research,* **28(3)**, 353-370.

Yuan, H.L., Gao, S., Dai, M.N, Zong, C.L., Günther, D., Fontaine, G.H., Liu, X.M., and Diwu, C., 2008. Simultaneous determinations of U-Pb age, Hf isotopes and trace element compositions of zircon by excimer laser-ablation quadrupole and multiple-collector ICP-MS. *Chem. Geol,* **247**, 100-11.

APPENDIX A: FUERTEVENTURA GEOCHRONOLOGY SUMMARY

Basal Complex				Dating				
Sample ID	Code	Rock type	Locality	Material	Method	Age	Error	Reference
FV-19	B	Metavolcanic	Molinas Canyon, 23 m below cap basalt flow, 100 m NW of the dam	Whole rock	K-Ar	35.3	0.9	Abdel-Monem et al. 1971
FV-14	S	Alkali syenite	Montana Tejeda, west side of road, north from Pajara at 29 km post	Aegirine-augite	K-Ar	38.6	3.8	Abdel-Monem et al. 1971
FV-16	G	Gabbro	South side of road south from Vega de Rio de Palmas at 32 km post	Hornblende	K-Ar	20.8	0.5	Abdel-Monem et al. 1971
FV-16	G	Gabbro	South side of road south from Vega de Rio de Palmas at 32 km post	Biotite	K-Ar	18.4	0.3	Abdel-Monem et al. 1971
FT-17	B	Meta-dolerite dyke	Tulneje-Puerte Pena-Fayagua	Whole rock	K-Ar	20.3	0.6	Feraud et al. 1985
FT-17	B	Meta-dolerite dyke	Tulneje-Puerte Pena-Fayagua	Whole rock	Ar/Ar	24.0	2	Feraud et al. 1985
FT-12	B	Meta-dolerite dyke	Pta Guadalupe-Puerto Nuevo	Whole rock	K-Ar	19.9	0.4	Feraud et al. 1985
FT-3	B	Meta-dolerite dyke	Fuentita-Monte Agudo-SE coast SE area: near Casas Violente	Whole rock	K-Ar	17.3	0.3	Feraud et al. 1985
FT-5	B	Meta-dolerite dyke	Fuentita-Monte Agudo-SE coast SE area: near Casas Violente	Whole rock	K-Ar	18.7	0.5	Feraud et al. 1985
FT-5	B	Meta-dolerite dyke	Fuentita-Monte Agudo-SE coast SE area: near Casas Violente	Whole rock	Ar/Ar	21.1	1	Feraud et al. 1985
FT-2	B	Meta-dolerite dyke	Fuentita-Monte Agudo-SE coast SE area: near Casas Violente	Whole rock	K-Ar	19.9	0.4	Feraud et al. 1985
FT-4	B	Meta-dolerite dyke	Fuentita-Monte Agudo-SE coast SE area: near Casas Violente	Whole rock	K-Ar	20.0	0.5	Feraud et al. 1985
FT-8	B	Meta-dolerite dyke	Jandia Peninsula	Whole rock	K-Ar	20.7	0.4	Feraud et al. 1985
FT-10	B	Meta-dolerite dyke	Jandia Peninsula	Whole rock	K-Ar	15.4	0.3	Feraud et al. 1985
FT-11	B	Meta-dolerite dyke	Jandia Peninsula	Whole rock	K-Ar	14.9	0.3	Feraud et al. 1985
FT-7	B	Meta-dolerite dyke	Jandia Peninsula	Whole rock	K-Ar	14.45	0.25	Feraud et al. 1985
FT-6	B	Meta-dolerite dyke	Jandia Peninsula	Whole rock	K-Ar	14.2	0.4	Feraud et al. 1985
FT-9	B	Meta-dolerite dyke	Jandia Peninsula	Whole rock	K-Ar	12.0	0.3	Feraud et al. 1985
FT-19	B	Meta-dolerite dyke	Tulneje-Puerte Pena-Fayagua	Whole rock	Ar/Ar	24.0	1	Feraud et al. 1985
FT-21	B	Meta-dolerite dyke	Tulneje-Puerte Pena-Fayagua	Whole rock	Ar/Ar	22.5	1	Feraud et al. 1985
FT-14	B	Meta-dolerite dyke	Pta Guadalupe-Puerto Nuevo	Amphibole	Ar/Ar	19.0	1	Feraud et al. 1985
F779	I	Bio-rich xenolith in ijolite	Punta de Caleta Mansa, west of Pajara	Biotite	K-Ar	20	1	Le Bas et al. 1986
75/199	P	Pyroxenite	Caleta de la Cruz, coast west of Pajara	Phlogopite	K-Ar	22	1	Le Bas et al. 1986
2754	S	Syenite ring dyke	Barranco las Penitas, Vega de Rio de Palmas	Whole Rock	K-Ar	21	1	Le Bas et al. 1986
68-SC-71	P	Ijolitic pyroxenite	Barranco del Agua Salada Esquinzo, Tindaya	Biotite	K-Ar	25	1	Le Bas et al. 1986
F824	P	Submarine basaltic agglomerate	Barranco de los Mozos	Phlogopite	K-Ar	29	1	Le Bas et al. 1986

2770	B	N-trending 1-m-wide metabasalt dyke	Barranco de Ajui, near Pajara	Whole Rock	K-Ar	35	2	Le Bas et al. 1986
2746	B	NE-trending 0.4-m-wide metabasalt dyke	Majada Negras, 2 km NW of Pajara	Whole Rock	K-Ar	39	2	Le Bas et al. 1986
2751	B	NNE-trending 0.35-m-wide basalt dyke	Majada Negras, 2 km NW of Pajara	Whole Rock	K-Ar	48	2	Le Bas et al. 1986
X52	C	Carbonatite	Las Montanetas	Zircon	U-Pb	23.2	0.2	Cantagrel et al. 1993
B9586	I	Ijolite	Ajui	Whole Rock	K-Ar	19.2	0.9	Cantagrel et al. 1993
B9587	C	Carbonatite	Penon Blanco	Whole Rock	K-Ar	25.0	0.9	Cantagrel et al. 1993
B9588	S	Syenite	Penon Blanco	Whole Rock	K-Ar	21.6	0.9	Cantagrel et al. 1993
H9095	S	Syenite	Vega Rio Palmas	Hornblende	K-Ar	18.7	0.8	Cantagrel et al. 1993
R9818	S	Syenite	Castillo Lara	Whole Rock	K-Ar	13.0	0.9	Cantagrel et al. 1993
R9907	T	Trachyte	La Platilla	Whole Rock	K-Ar	14.6	0.9	Cantagrel et al. 1993
MR-431	S	Syenite	Morro del Recogedero	Whole rock	K-Ar	21.6	0.9	Sagredo et al. 1996
MR-363	S	Syenite	Morro del Recogedero	Whole rock	K-Ar	25.2	1.0	Sagredo et al. 1996
3119	Am	Amphibolite	La Matanza	Whole rock	K-Ar	31.4	1.4	Balogh et al. 1999
3120	P	Pyroxenite	La Matanza	Whole rock	K-Ar	64.7	3.2	Balogh et al. 1999
80-40-39	Am	Amphibolite	Caleta de la Cruz	Whole rock	K-Ar	23.5	1.0	Balogh et al. 1999
CR-S-1	S	Syenite	Caleta de la Cruz	Whole rock	K-Ar	38.5	1.5	Balogh et al. 1999
CR-S-2	S	Syenite	Caleta de la Cruz	Whole rock	K-Ar	45.7	1.9	Balogh et al. 1999
CR-S-3	S	Syenite	Caleta de la Cruz	Whole rock	K-Ar	60.0	2.3	Balogh et al. 1999
CR-S-3	S	Syenite	Caleta de la Cruz	Biotite	K-Ar	50.6	4.2	Balogh et al. 1999
CR-S-4	S	Syenite	Caleta de la Cruz	Whole rock	K-Ar	47.6	1.8	Balogh et al. 1999
80-40-36	S	Syenite	Caleta de la Cruz	Whole rock	K-Ar	70.6	3.9	Balogh et al. 1999
80-40-38	S	Syenite	Caleta de la Cruz	Whole rock	K-Ar	45.2	1.7	Balogh et al. 1999
Es-C-1	C	Carbonatite	Las Montañetas	Feldspar	K-Ar	109	4.1	Balogh et al. 1999
Es-C-2	C	Carbonatite	Las Montañetas	Feldspar	K-Ar	211	9	Balogh et al. 1999
Es-C-4	C	Carbonatite	Las Montañetas	Feldspar	K-Ar	27.7	1.2	Balogh et al. 1999
ES-CII-1	S	Syenite	Los Jablitos	Feldspar	K-Ar	30.9	1.2	Balogh et al. 1999
Salada-1	C	Carbonatite	Barranco del Aqua Salada	Phlogopite	K-Ar	26.9	1.0	Balogh et al. 1999
Jablitos	C	Carbonatite	Los Jablitos	Phlogopite	K-Ar	28.1	4.3	Balogh et al. 1999
Es-Si-1	S	Syenite	Barranco de Esquinzo	Feldspar	K-Ar	36.3	1.7	Balogh et al. 1999

NAO-1	C	Carbonatite	Punta La Nao, Ajui-Solapa complex	Feldspar	K-Ar	38.0	1.4	Balogh et al. 1999
NAO-1	C	Carbonatite	Punta La Nao, Ajui-Solapa complex	Magnetic minerals	K-Ar	56.7	2.2	Balogh et al. 1999
CR-S-5	S	Syenite	Caleta de la Cruz, Ajui-Solapa complex	Whole rock	K-Ar	26.7	1.1	Balogh et al. 1999
CR-C-1	C	Carbonatite	Caleta de la Cruz, Ajui-Solapa complex	Biotite	K-Ar	23.8	1.0	Balogh et al. 1999
R-17	S	Syenite	Punta del Penon Blanco Complex	Whole rock	K-Ar	22.1	1.3	Balogh et al. 1999
3125	C	Carbonatite	Punta del Penon Blanco Complex	Biotite	K-Ar	22.7	0.9	Balogh et al. 1999
3126	C	Carbonatite	Punta del Penon Blanco Complex	Feldspar	K-Ar	24.0	0.9	Balogh et al. 1999
UL-1	P	Perovskite clinopyroxenite	Los Jablitos	Phlogopite	K-Ar	26.2	3.0	de Ignacio et al. 2002
BM-3	G	Amph, neph-bearing gabbro	Montana Tarabates	Whole Rock	K-Ar	26.7	1.2	de Ignacio et al. 2003
BM-1	P	Amph, apatite clinopyroxenite	Montana Tarabates	Apatite	Fission Tracks	25.4	3.6	de Ignacio et al. 2004
BM-2	G	Amph, neph-bearing gabbro	Montana Milocho	Apatite	Fission Tracks	29.3	3.5	de Ignacio et al. 2005
5 basanites	Bs	Piedra de Fuera (unit G3)	Piedra de Fuera	Phlogopite/Amphibole	Rb-Sr	22.5	0.2	Demeny et al. 2004
086	S	Syenite	Caleta de la Cruz	Zircon	U-Pb	25.4	0.4	Munoz et al. 2005
505	P	Glimmerite pyroxenite	Caleta de la Cruz	Whole rock	K-Ar	26.7	3.2	Munoz et al. 2005
744	S	Nepheline syenite	Caleta de la Cruz	Whole rock	K-Ar	26.6	1	Munoz et al. 2005
622	P	Mica pyroxenite	Caleta de la Cruz	Phlogopite	K-Ar	23.4	0.6	Munoz et al. 2005
CPV-2	B	Barranco del Tarajalito (unit A)	Caleta de la Peña Vieja	Biotite	K-Ar	26.4	1.1	Gutiérrez et al. 2006
CPV-3	B	Barranco del Tarajalito (unit A)	Caleta de la Peña Vieja	Biotite	K-Ar	29.7	1.2	Gutiérrez et al. 2006
CPV-3	B	Barranco del Tarajalito (unit A)	Caleta de la Peña Vieja	Biotite	Ar/Ar	25.1	0.4	Gutiérrez et al. 2006
ANA-34	B	La Gatera (unit D)	Barranco de Los Negros	Amphibole	K-Ar	31.2	2.2	Gutiérrez et al. 2006
80–50–310	B	La Gatera (unit D)	Barranco de Los Negros	Phlogopite	K-Ar	28.4	1.1	Gutiérrez et al. 2006
80–50–309	B	El Valle (unit F)	Barranco de Los Negros	Amphibole	K-Ar	23.2	0.9	Gutiérrez et al. 2006
ANA-29	B	Piedra de Fuera (unit G3)	Piedra de Fuera	Phlogopite	K-Ar	25.3	1.0	Gutiérrez et al. 2006
80–55–90	B	Piedra de Fuera (unit G3)	Bajas de la Bonancilla	Phlogopite	K-Ar	23.4	0.9	Gutiérrez et al. 2006

JA 15	P	Olivine clinopyronxenite	Barranco de la Palmita	Amphibole	Ar/Ar	21.8	0.3	Allibon et al. 2011
JA 57	G	Poikilitic gabbro	SW Morro de Pedregullo 28 R 584279 3136681	Amphibole	Ar/Ar	21.9	0.6	Allibon et al. 2011
JA 89	G	Isotropic leucocratic gabbro	Barranco de Ayamas 28 R 584819 3137391	Amphibole	Ar/Ar	21.8	0.5	Allibon et al. 2011
JA 222	An	Anorthosite	SW Morro de Pedregullo 28 R 584058 3136543	Zircon	U-Pb	22.06	0.04	Allibon et al. 2011
JA 250	G	Isotropic leucocratic gabbro	Punta del Viento 28 R 582112 3139303	Zircon/Baddeleyite	U-Pb	21.94	0.02	Allibon et al. 2011

Miocene and Pliocene

Sample ID	Code	Rock type	Locality	Material	Method	Age	Error	Reference
KA-69-84	B	Biotite hornblende andesite	Barranco de los Molinos, mouth	Whole rock	K-Ar	18.0	0.22	Rona and Nalwalk 1970
KA-69-85	B	Olivine basalt	Barranco de los Molinos, mouth	Whole rock	K-Ar	22.3	0.4	Rona and Nalwalk 1970
KA-69-86	B	Basalt	Barranco de los Molinos, mouth	Whole rock	K-Ar	14.4	0.2	Rona and Nalwalk 1970
KA-69-87	G	Gabbro	Barranco de los Molinos, mouth	Whole rock	K-Ar	12.1	0.5	Rona and Nalwalk 1970
KA-69-88	B	Basalt	Barranco de los Molinos, mouth	Whole rock	K-Ar	22.3	0.6	Rona and Nalwalk 1970
FV-23	B	Plag basalt	Tostin Cotillo on sea cliff below round tower	Whole rock	K-Ar	20.6	0.94	Abdel-Monem et al. 1971
FV-2	B	Augite basalt	Jandia del-Risco Punta	Whole rock	K-Ar	16.55	0.61	Abdel-Monem et al. 1971
FV-4	B	Augite basalt	Roque del Morro	Whole rock	K-Ar	15.88	1.68	Abdel-Monem et al. 1971
FV-5	B	Augite basalt	Roque del Mara	Whole rock	K-Ar	14.3	0.52	Abdel-Monem et al. 1971
FV-30	B	Olivine basalt	Montana Tindaya, road from Casilla del Angel to Puerto del Rosario	Whole rock	K-Ar	11.8	0.33	Abdel-Monem et al. 1971
FV-18	B	Olivine basalt	Molinas Canyon	Whole rock	K-Ar	4.25	0.44	Abdel-Monem et al. 1971
FV-24	B	Olivine basalt	Barranco Esquinzo 900 m SE of Taca, N side of road	Whole rock	K-Ar	1.83	0.24	Abdel-Monem et al. 1971
KSEPL-1	D	Diorite	Vega de Rio de Palmas	Whole rock	K-Ar	19	9	Grunau et al., 1975
KSEPL-2	S	Syenite	Vega de Rio de Palmas	Whole rock	K-Ar	18	10	Grunau et al., 1975
KSEPL-3	B	Altered olgoclase-bearing dyke	Vega de Rio de Palmas	Whole rock	K-Ar	16.8	4.1	Grunau et al., 1975
KSEPL-5	B	Meta-dolerite dyke	Puerto de la Peña, NW of Pajara	Whole rock	K-Ar	22.4	3.3	Grunau et al., 1975
FUE-76-1	B	Basalt	Ajui	Whole rock	K-Ar	5.8	0.5	Meco and Stearns 1981
FUE-76-20	B	Olivine basalt	Las Cruz - Los Molinas	Whole rock	K-Ar	2.7	0.2	Meco and Stearns 1981

Volcanic rocks from Series I from Fuerteventura

		Southern edifice						
F-16-C	B	Aug-oliv basalt	Barranco de los Escobones	Whole rock	K-Ar	15.8	0.3	Coello et al. 1992
F-19-C	B	Aug-oliv basalt	Punta de Jandia-Faro	Whole rock	K-Ar	15.4	0.4	Coello et al. 1992
F-50-AC	T	Trachyte	S of Casa del Mosquito (dyke)	Whole rock	K-Ar	15.2	0.3	Coello et al. 1992
F-76-AC	B	Basalt	Pico de la Zarza 380m, south side	Whole rock	K-Ar	15.0	0.3	Coello et al. 1992
F-73-AC	A	Ankaramite	Pico de la Zarza, south side	Whole rock	K-Ar	14.9	0.3	Coello et al. 1992
F-17-C	T	Trachyte	Montana Azufra	Whole rock	K-Ar	14.3	0.3	Coello et al. 1992
		Central edifice						
F-24-C	A	Ankaramite	Montana de Gran Tarajal	Whole rock	K-Ar	20.4	0.4	Coello et al. 1992
FV-33-F	B	Basalt	Tablero de las Estancias	Whole rock	K-Ar	19.0	0.5	Coello et al. 1992
F-27-C	B	Olivine basalt	Faro de la Entallada	Whole rock	K-Ar	18.3	0.3	Coello et al. 1992
F-58-AC	B	Basalt	S of Morro de los Tarajales	Whole rock	K-Ar	15.6	0.3	Coello et al. 1992
F-59-AC	B	Trachybasalt	Atalaya Pozo Negro	Whole rock	K-Ar	15.4	0.3	Coello et al. 1992
F-25-C	B	Aug-oliv basalt	Huertas de Chilegua	Whole rock	K-Ar	14.5	0.4	Coello et al. 1992
F-60-AC	B	Picritic basalt	Tablero del Saladillo	Whole rock	K-Ar	13.2	0.3	Coello et al. 1992
		Northern edifice						
F-1-C	T	Trachyte	Tindaya	Whole rock	K-Ar	18.7	0.3	Coello et al. 1992
F-69-AC	B	Plagioclase basalt	Toston-Cotillo	Whole rock	K-Ar	16.1	0.3	Coello et al. 1992
F-9-C	B	Trachybasalt	Punta de la Atalaya	Whole rock	K-Ar	14.3	0.3	Coello et al. 1992
F-71-AC	B	Aug-oliv basalt	SE of Morro Carnero	Whole rock	K-Ar	13.9	0.3	Coello et al. 1992
FV-49-F	B	Plagioclase basalt	Toston-Cotilla	Whole rock	K-Ar	13.7	0.8	Coello et al. 1992
F-20-C	B	Plagioclase basalt	Montana de Enmedio	Whole rock	K-Ar	13.6	0.3	Coello et al. 1992
F-30-C	B	Trachybasalt	Montana de Campo	Whole rock	K-Ar	13.0	0.3	Coello et al. 1992
F-52-AC	B	Plagioclase-Aug basalt	Pico de la Muda	Whole rock	K-Ar	13.0	0.2	Coello et al. 1992
F-21-C	B	Basalt	Morro de la Galera	Whole rock	K-Ar	12.8	0.3	Coello et al. 1992
Post-Miocene volcanic series, Fuerteventura								
488-4	B	Olivine basalt	Barranco de Ajui	Whole rock	K-Ar	5.0	0.3	Coello et al. 1992
F-11-C	B	Olivine basalt	Barranco de Los Molinas	Whole rock	K-Ar	2.9	0.2	Coello et al. 1992
491-5	B	Olivine basalt	Puerto de Los Molinas	Whole rock	K-Ar	2.7	0.2	Coello et al. 1992
F-67-AC	N	Olivine nephelinite	Tablero de Golfete	Whole rock	K-Ar	2.9	0.3	Coello et al. 1992

F-8-C	Bs	Basanite	Barranco de Antigua	Whole rock	K-Ar	2.6	0.2	Coello et al. 1992
492-6	B	Basalt	Aljibe de la Cueva, Tost6n-Cotillo	Whole rock	K-Ar	2.4	0.3	Coello et al. 1992
487-3	Bs	Basanite	Barranco de la Herradura	Whole rock	K-Ar	1.8	0.5	Coello et al. 1992
485-1	B	Olivine basalt	El Veril de Santiago	Whole rock	K-Ar	1.7	0.3	Coello et al. 1992
F-68-AC	B	Olivine basalt	Barranco de Jarubio	Whole rock	K-Ar	0.83	0.09	Coello et al. 1992
486-2	B	Olivine basalt	La Salina	Whole rock	K-Ar	0.4	0.1	Coello et al. 1992
FV-38	B	Basalt	Ajui	Whole rock	K-Ar	4.8	0.1	Meco et al. 2007

** Rock Type Code: A=Ankaramite, Am=Amphibolite, An=Anorthosite, B=Basalt, C=Carbonatite, G=Gabbro, I=Ijolite, P=Pyroxenite, S=Syenite, T=Trachyte*

APPENDIX B1: LA-ICPMS U-Pb SUMMARY (SESSION 1-9435)

2016MJ-04

sample name	^{206}Pb (cps)	^{204}Pb (cps)	$^{206}Pb/^{238}U$	2 s	$^{206}Pb^*/^{238}U$ age (Ma)	2 s error (Ma)
9435-1-S1	13626	17	0.0088005	0.0004184	56.5	2.7
9435-2-S1	6385	40	0.0089249	0.0004243	57.3	2.7
9435-3-S1	11854	12	0.0089120	0.0004204	57.2	2.7
9435-4-S1	5509	14	0.0089116	0.0004251	57.2	2.7
9435-5-S1	8207	9	0.0087181	0.0004174	56.0	2.7
9435-6-S1	7275	0	0.0085370	0.0004038	54.8	2.6
9435-7-S1	13464	85	0.0084813	0.0004130	54.4	2.6
9435-8-S1	8759	8	0.0085826	0.0004027	55.1	2.6
9435-9-S1	8705	15	0.0085418	0.0003970	54.8	2.5
9435-10-S1	7395	45	0.0083359	0.0003971	53.5	2.5

APPENDIX B2: LA-ICPMS U-Pb SUMMARY (SESSION 2-9435)

2016MJ-38 sample name	^{206}Pb (cps)	^{204}Pb (cps)	$^{206}Pb/^{238}U$	2 s	$^{206}Pb^*/^{238}U$ age (Ma)	2 s error (Ma)
9435-1-S2	7476	94	0.0088513	0.0002848	56.8	1.8
9435-2-S2	6964	31	0.0088795	0.0002507	57.0	1.6
9435-3-S2	7307	37	0.0088453	0.0002916	56.8	1.9
9435-4-S2	6838	45	0.0089547	0.0002693	57.5	1.7
9435-5-S2	6345	51	0.0089998	0.0002625	57.8	1.7
9435-6-S2	7123	59	0.0091964	0.0002689	59.0	1.7
9435-7-S2	6106	35	0.0088759	0.0002597	57.0	1.7
9435-8-S2	5148	83	0.008902	0.0002505	57.1	1.6
9435-9-S2	5007	147	0.0089561	0.0002748	57.5	1.8
9435-10-S2	4278	143	0.0096299	0.0002949	61.8	1.9
9435-11-S2	3937	57	0.0088737	0.0002812	57.0	1.8
9435-12-S2	4570	28	0.009137	0.0003819	58.6	2.4

APPENDIX B3: LA-ICPMS U-Pb SUMMARY (SESSION 3-9435)

2016MJ-39 sample name	^{206}Pb (cps)	^{204}Pb (cps)	$^{206}Pb/^{238}U$	2 s	$^{206}Pb^*/^{238}U$ age (Ma)	2 s error (Ma)
9435-1-S3	6320	66	0.0089816	0.0003012	57.6	1.9
9435-2-S3	17610	33	0.0085393	0.0002882	54.8	1.8
9435-3-S3	12882	12	0.0087434	0.0002835	56.1	1.8
9435-4-S3	19645	20	0.0085908	0.0002856	55.1	1.8
9435-5-S3	19659	0	0.0083913	0.0002693	53.9	1.7
9435-6-S3	21521	0	0.0082428	0.000268	52.9	1.7
9435-7-S3	11349	92	0.0088356	0.0002861	56.7	1.8
9435-8-S3	5368	97	0.0090609	0.0003047	58.2	2.0
9435-9-S3	14024	74	0.0090082	0.0002877	57.8	1.8
9435-10-S3	3695	14	0.0091303	0.0002903	58.6	1.9
9435-11-S3	9795	14	0.0088486	0.0002767	56.8	1.8
9435-12-S3	6498	18	0.0089613	0.0002806	57.5	1.8
9435-13-S3	5534	23	0.0085678	0.0002844	55.0	1.8

APPENDIX C1: LA-ICPMS U-Pb SUMMARY (Sample 2016MJ-04)

2016MJ-04 Sample name	^{206}Pb (cps)	^{204}Pb (cps)	^{206}Pb/^{238}U	2 s	^{206}Pb*/^{238}U age (Ma)	2 s error (Ma)
04-003	3298	26	0.0044	0.0002	28.5	1.6
04-014	23893	61	0.0043	0.0002	27.5	1.3
04-016	676	37	0.0045	0.0003	28.7	1.6
04-023	59660	26	0.0040	0.0002	25.7	1.3
04-024	4793	27	0.0042	0.0002	27.1	1.4
04-026	307	8	0.0048	0.0003	31.0	2.2
04-032	1425	2	0.0025	0.0001	16.1	0.8
04-039	57004	2	0.0041	0.0002	26.4	1.3
04-047	722	4	0.0045	0.0003	28.7	1.9
04-049	1968	42	0.0032	0.0002	20.6	1.3
04-054	9800	0	0.0041	0.0002	26.2	1.3
04-058	45785	1	0.0042	0.0002	26.8	1.3
04-062	15382	0	0.0045	0.0002	29.2	1.4
04-063	9766	16	0.0041	0.0002	26.4	1.3
04-067	37441	0	0.0040	0.0002	25.6	1.2
04-070	123275	0	0.0040	0.0002	25.9	1.2
04-076	1146	0	0.0038	0.0002	24.4	1.2
04-078	3667	83	0.0052	0.0004	33.7	2.9
04-079	28684	71	0.0040	0.0002	25.9	1.3
04-080	5274	83	0.0040	0.0002	25.7	1.4
04-081	39510	50	0.0040	0.0002	25.6	1.3
04-082	42993	77	0.0040	0.0002	26.0	1.3
04-083	813	41	0.0025	0.0002	16.0	1.0
04-084	21918	31	0.0040	0.0002	25.5	1.2
04-086	16724	35	0.0041	0.0002	26.2	1.3
04-093	7205	6	0.0038	0.0002	24.7	1.2
04-098	55150	4	0.0039	0.0002	25.3	1.3
04-103	40916	3	0.0040	0.0002	25.8	1.3
04-109	645	2	0.0051	0.0004	32.8	2.7
04-111	31888	3	0.0039	0.0002	24.8	1.2
04-115	8051	8	0.0041	0.0002	26.5	1.3
04-116	2810	7	0.0039	0.0002	25.4	1.3
04-119	4310	11	0.0043	0.0002	27.6	1.4
04-127	5499	73	0.0046	0.0003	29.8	1.9
04-133	56873	50	0.0039	0.0002	25.1	1.2
04-138	3787	38	0.0041	0.0002	26.3	1.3

Notes:

Uranium decay contant, $^{238}U=1.55125\times10^{-10}$ year^{-1} (Jaffey et al., 1971)

APPENDIX C2: LA-ICPMS U-Pb SUMMARY (Sample 2016MJ-38)

2016MJ-38 Sample name	^{206}Pb (cps)	^{204}Pb (cps)	^{206}Pb/^{238}U	2 s	^{206}Pb*/^{238}U age (Ma)	2 s error (Ma)
38-001	3638	31	0.0027	0.0001	17.1	0.5
38-002	1064	26	0.0026	0.0001	16.7	0.6
38-003	2746	14	0.0034	0.0001	21.9	0.7
38-004	2777	18	0.0028	0.0001	17.8	0.6
38-005	5049	26	0.0027	0.0001	17.2	0.5
38-006	1445	39	0.0043	0.0004	27.8	2.8
38-007	1362	34	0.0028	0.0001	18.1	0.6
38-008	20451	15	0.0033	0.0001	20.9	0.6
38-009	1911	24	0.0027	0.0001	17.5	0.6
38-011	3523	15	0.0025	0.0001	15.8	0.5
38-012	21885	19	0.0033	0.0001	21.4	0.6
38-013	4665	15	0.0027	0.0001	17.6	0.5
38-014	13801	23	0.0039	0.0001	25.0	0.7
38-015	1261	31	0.0027	0.0001	17.3	0.5
38-016	745	32	0.0026	0.0001	17.0	0.6
38-017	760	38	0.0029	0.0001	19.0	0.6
38-018	6614	34	0.0026	0.0001	17.0	0.5
38-019	9364	29	0.0028	0.0001	17.7	0.5
38-020	4171	28	0.0026	0.0001	16.7	0.5
38-021	1036	38	0.0006	0.000021	3.9	0.1
38-022	2861	27	0.0025	0.0001	16.3	0.5
38-023	1415	40	0.0025	0.0001	16.3	0.6
38-025	2342	36	0.0026	0.0001	16.6	0.6
38-026	5738	47	0.0026	0.0001	16.7	0.5
38-028	2952	40	0.0025	0.0001	16.4	0.5
38-029	1688	21	0.0024	0.0001	15.6	0.5
38-030	1575	40	0.0025	0.0001	16.1	0.5
38-031	1061	34	0.0026	0.0001	16.7	0.7
38-032	3272	32	0.0025	0.0001	16.3	0.5
38-033	3013	27	0.0026	0.0001	16.9	0.5
38-034	5297	10	0.0035	0.0001	22.7	0.7
38-035	10969	32	0.0023	0.0001	15.0	0.4
38-036	1798	20	0.0027	0.0001	17.4	0.6
38-037	2643	30	0.0032	0.0001	20.5	0.7
38-038	2678	32	0.0026	0.0001	16.7	0.5
38-039	6119	34	0.0039	0.0001	25.4	0.8
38-040	5258	25	0.0026	0.0001	16.8	0.5
38-041	2973	4	0.0033	0.0001	21.3	0.7
38-042	7860	6	0.0041	0.0001	26.2	0.8
38-043	2592	22	0.0033	0.0001	21.1	0.6
38-044	1650	23	0.0007	0.00002	4.4	0.1
38-045	2994	40	0.0028	0.0001	17.8	0.6
38-046	6711	35	0.0025	0.0001	15.9	0.5
38-047	3495	19	0.0026	0.0001	16.8	0.5
38-048	538	15	0.0026	0.0001	16.8	0.7
38-050	1975	60	0.0028	0.0003	17.8	1.6
38-052	2284	23	0.0027	0.0001	17.4	0.6

38-053	1413	29	0.0026	0.0001	16.7	0.5
38-054	1915	40	0.0028	0.0001	18.0	0.8
38-055	737	33	0.0029	0.0001	18.7	0.8
38-056	3319	23	0.0027	0.0001	17.6	0.5
38-057	1911	22	0.0024	0.0001	15.4	0.5
38-058	1414	15	0.0027	0.0001	17.2	0.5
38-059	2370	5	0.0026	0.0001	17.0	0.5
38-060	1248	11	0.0026	0.0001	17.0	0.6
38-061	2346	15	0.0032	0.0001	20.7	0.7
38-062	6000	30	0.0026	0.0001	16.5	0.5
38-063	2308	12	0.0025	0.0001	16.3	0.5
38-064	497	29	0.0006	0.0000	3.8	0.2
38-065	6317	17	0.0026	0.0001	16.8	0.5
38-066	3158	20	0.0025	0.0001	15.9	0.5
38-067	1107	21	0.0027	0.0002	17.3	1.4
38-068	2078	66	0.0026	0.0001	16.9	0.5
38-069	2481	59	0.0026	0.0001	17.0	0.6
38-070	12974	64	0.0032	0.0001	20.8	0.7
38-071	2163	53	0.0026	0.0001	16.6	0.5
38-072	3410	42	0.0033	0.0001	21.0	0.7
38-073	5797	81	0.0026	0.0001	16.5	0.5
38-074	5976	114	0.0027	0.0001	17.1	0.5
38-075	2710	100	0.0027	0.0001	17.3	0.6
38-076	14837	97	0.0026	0.0001	16.6	0.5
38-077	1936	119	0.0028	0.0002	18.3	1.1
38-078	2273	132	0.0033	0.0004	21.3	2.4
38-079	1203	150	0.0027	0.0001	17.6	1.0
38-080	1419	106	0.0026	0.0001	16.6	0.6
38-081	3083	120	0.0027	0.0001	17.2	0.5
38-082	1769	127	0.0026	0.0001	16.8	0.6
38-083	5688	166	0.0026	0.0001	17.0	0.5
38-084	2063	156	0.0026	0.0001	16.8	0.5
38-085	1437	143	0.0025	0.0001	16.0	0.5
38-086	4667	147	0.0027	0.0001	17.1	0.6
38-087	2074	142	0.0029	0.0001	18.5	0.8
38-088	17884	151	0.0024	0.0001	15.4	0.5
38-089	6151	161	0.0025	0.0001	15.9	0.5
38-090	12522	314	0.0048	0.0003	30.8	2.2
38-091	19312	193	0.0025	0.0001	16.1	0.7
38-092	3444	148	0.0027	0.0001	17.6	0.6
38-093	3702	139	0.0027	0.0001	17.4	0.5
38-094	1537	112	0.0026	0.0001	16.7	0.5
38-095	1793	97	0.0027	0.0001	17.2	0.6
38-096	1055	106	0.0029	0.0001	18.9	0.7
38-097	2041	99	0.0033	0.0001	21.4	0.8
38-099	8271	123	0.0026	0.0001	16.9	0.5
38-102	1373	73	0.0028	0.0001	17.9	0.6
38-103	1089	75	0.0026	0.0001	16.7	0.5
38-105	3294	61	0.0023	0.0001	14.5	0.4
38-106	6236	74	0.0026	0.0001	16.6	0.5

38-107	3184	66	0.0026	0.0001	16.7	0.5
38-108	1797	81	0.0033	0.0001	21.1	0.6
38-109	13890	70	0.0032	0.0001	20.4	0.6
38-110	1045	61	0.0027	0.0001	17.7	0.8

Notes:

Uranium decay contant, $^{238}U=1.55125\times10^{-10}$ $year^{-1}$ (Jaffey et al., 1971)

APPENDIX C3: LA-ICPMS U-Pb SUMMARY (Sample 2016MJ-39)

2016MJ-39 Sample name	^{206}Pb (cps)	^{204}Pb (cps)	$^{206}Pb/^{238}U$	2 s	$^{206}Pb^*/^{238}U$ age (Ma)	2 s error (Ma)
39-001	9262	13	0.0029853	0.0000917	19.2	0.6
39-002	24692	9	0.0031854	0.0000962	20.5	0.6
39-003	13890	23	0.0032007	0.0000979	20.6	0.6
39-004	17562	4	0.0031036	0.0000919	20.0	0.6
39-005	45875	13	0.0032260	0.0000958	20.8	0.6
39-006	9490	9	0.0031904	0.0000964	20.5	0.6
39-007	7264	6	0.0032576	0.0001047	21.0	0.7
39-008	81562	6	0.0032299	0.0000972	20.8	0.6
39-009	64343	10	0.0031627	0.0001007	20.4	0.6
39-010	3072	5	0.0032093	0.0000995	20.7	0.6
39-011	14166	5	0.0031516	0.0001014	20.3	0.7
39-012	3993	10	0.0032407	0.0001069	20.9	0.7
39-013	19856	38	0.0032852	0.0001163	21.1	0.7
39-014	3435	39	0.0033255	0.0001190	21.4	0.8
39-015	8762	49	0.0033117	0.0001141	21.3	0.7
39-016	4631	40	0.0033734	0.0001198	21.7	0.8
39-017	19453	173	0.0025974	0.0000880	16.7	0.6
39-018	23979	33	0.0033028	0.0001179	21.3	0.8
39-019	4969	27	0.0025863	0.0000874	16.7	0.6
39-021	2357	38	0.0037388	0.0001568	24.1	1.0
39-022	8605	40	0.0031529	0.0001091	20.3	0.7
39-023	5573	40	0.0026207	0.0000890	16.9	0.6
39-024	2689	40	0.0027155	0.0000967	17.5	0.6
39-025	18256	15	0.0032290	0.0001085	20.8	0.7
39-026	23868	24	0.0032565	0.0001081	21.0	0.7
39-028	2840	49	0.0032927	0.0001253	21.2	0.8
39-029	1745	85	0.0040208	0.0006609	25.9	4.2
39-030	11380	33	0.0034224	0.0001247	22.0	0.8
39-031	6271	47	0.0032803	0.0001157	21.1	0.7
39-033	12870	33	0.0031967	0.0001077	20.6	0.7
39-035	7119	7	0.0033572	0.0001151	21.6	0.7
39-036	1528	13	0.0028166	0.0000989	18.1	0.6
39-037	47579	13	0.0032798	0.0001152	21.1	0.7
39-038	5051	15	0.0032745	0.0001116	21.1	0.7
39-039	4792	12	0.0026397	0.0000887	17.0	0.6
39-040	21439	7	0.0032227	0.0001091	20.7	0.7
39-041	1484	11	0.0032914	0.0001089	21.2	0.7
39-042	2597	10	0.0032925	0.0001227	21.2	0.8
39-043	2643	11	0.0032343	0.0001100	20.8	0.7
39-045	2003	10	0.0035435	0.0001281	22.8	0.8
39-046	1042	6	0.0025240	0.0000970	16.3	0.6
39-047	2069	3	0.0032305	0.0001109	20.8	0.7
39-049	3476	6	0.0026616	0.0000911	17.1	0.6
39-050	3692	19	0.0026565	0.0000985	17.1	0.6
39-051	1690	8	0.0032034	0.0001089	20.6	0.7
39-052	4785	6	0.0032650	0.0001098	21.0	0.7
39-053	1878	2	0.0031600	0.0001127	20.3	0.7

39-054	13890	2	0.0032492	0.0001101	20.9	0.7
39-056	8945	1	0.0032339	0.0001122	20.8	0.7
39-057	8261	2	0.0032855	0.0001145	21.1	0.7
39-058	2091	3	0.0032763	0.0001149	21.1	0.7
39-059	1592	0	0.0032797	0.0001187	21.1	0.8
39-060	3629	2	0.0026045	0.0000881	16.8	0.6
39-061	4045	0	0.0026348	0.0000915	17.0	0.6
39-062	1805	0	0.0023844	0.0000841	15.4	0.5
39-063	5278	0	0.0032229	0.0001164	20.7	0.7
39-064	7078	1	0.0032163	0.0001095	20.7	0.7
39-065	2505	35	0.0025308	0.0000961	16.3	0.6
39-067	1653	54	0.0034897	0.0001242	22.5	0.8
39-068	2117	60	0.0034104	0.0001315	21.9	0.8
39-069	3491	74	0.0033504	0.0001113	21.6	0.7
39-070	28482	104	0.0031910	0.0001127	20.5	0.7
39-071	2927	47	0.0035117	0.0001236	22.6	0.8
39-072	1617	49	0.0036905	0.0001312	23.7	0.8
39-073	14923	55	0.0033277	0.0001124	21.4	0.7
39-074	5827	86	0.0031497	0.0001289	20.3	0.8
39-075	4840	66	0.0026139	0.0000910	16.8	0.6
39-076	5674	68	0.0033078	0.0001122	21.3	0.7
39-078	2308	98	0.0027685	0.0000915	17.8	0.6
39-079	531	88	0.0008722	0.0000370	5.6	0.2
39-080	19952	114	0.0031834	0.0001104	20.5	0.7
39-081	1831	84	0.0028352	0.0001017	18.3	0.7
39-082	2378	76	0.0034975	0.0001190	22.5	0.8
39-083	2420	79	0.0027313	0.0000910	17.6	0.6
39-084	44652	78	0.0032105	0.0001074	20.7	0.7
39-086	2282	91	0.0029530	0.0000958	19.0	0.6
39-087	4439	99	0.0034903	0.0001187	22.5	0.8
39-088	4084	91	0.0035410	0.0001189	22.8	0.8
39-089	2543	104	0.0036470	0.0001258	23.5	0.8
39-091	2105	84	0.0038226	0.0001320	24.6	0.8
39-092	3031	85	0.0036743	0.0001268	23.6	0.8
39-093	3666	87	0.0035261	0.0001194	22.7	0.8
39-094	13858	72	0.0033749	0.0001147	21.7	0.7
39-095	1815	51	0.0037258	0.0001381	24.0	0.9
39-096	804	75	0.0010069	0.0000492	6.5	0.3
39-097	2259	95	0.0043370	0.0002360	27.9	1.5
39-100	3274	49	0.0034768	0.0001218	22.4	0.8
39-101	12028	124	0.0029258	0.0001969	18.8	1.3
39-102	2303	50	0.0036230	0.0001279	23.3	0.8
39-103	6717	24	0.0032364	0.0001102	20.8	0.7
39-104	4847	15	0.0034077	0.0001124	21.9	0.7
39-105	3217	26	0.0033009	0.0001172	21.2	0.8
39-106	14471	2	0.0031398	0.0000969	20.2	0.6
39-107	11332	9	0.0026491	0.0000907	17.1	0.6
39-109	4923	14	0.0035009	0.0001088	22.5	0.7
39-110	2490	14	0.0033138	0.0001183	21.3	0.8
39-111	13927	33	0.0026040	0.0000846	16.8	0.5

39-112	901	35	0.0007055	0.0000271	4.5	0.2
39-113	8370	20	0.0033062	0.0001039	21.3	0.7
39-114	2404	25	0.0034849	0.0001187	22.4	0.8
39-116	20129	17	0.0033557	0.0001125	21.6	0.7
39-117	10702	21	0.0033120	0.0001062	21.3	0.7
39-118	8544	12	0.0035009	0.0001122	22.5	0.7
39-119	11943	17	0.0025079	0.0000823	16.1	0.5
39-121	32606	25	0.0032844	0.0001136	21.1	0.7
39-123	3421	7	0.0033141	0.0001123	21.3	0.7
39-124	4887	7	0.0033101	0.0001155	21.3	0.7
39-125	8191	24	0.0032783	0.0001114	21.1	0.7
39-126	1386	16	0.0027738	0.0001040	17.9	0.7
39-127	1304	8	0.0034164	0.0001153	22.0	0.7
39-128	79239	15	0.0025934	0.0000848	16.7	0.5
39-130	2266	10	0.0035898	0.0001797	23.1	1.2
39-131	3465	17	0.0033507	0.0001133	21.6	0.7
39-132	3179	15	0.0028791	0.0001109	18.5	0.7
39-133	1633	26	0.0036610	0.0001290	23.6	0.8
39-134	5202	19	0.0033020	0.0001077	21.3	0.7
39-135	8206	15	0.0032981	0.0001106	21.2	0.7

Notes:

Uranium decay contant, $^{238}U=1.55125\times10^{-10}$ year^{-1} (Jaffey et al., 1971)

APPENDIX D1: CATHODOLUMINSCENCE IMAGES (2016MJ-04)

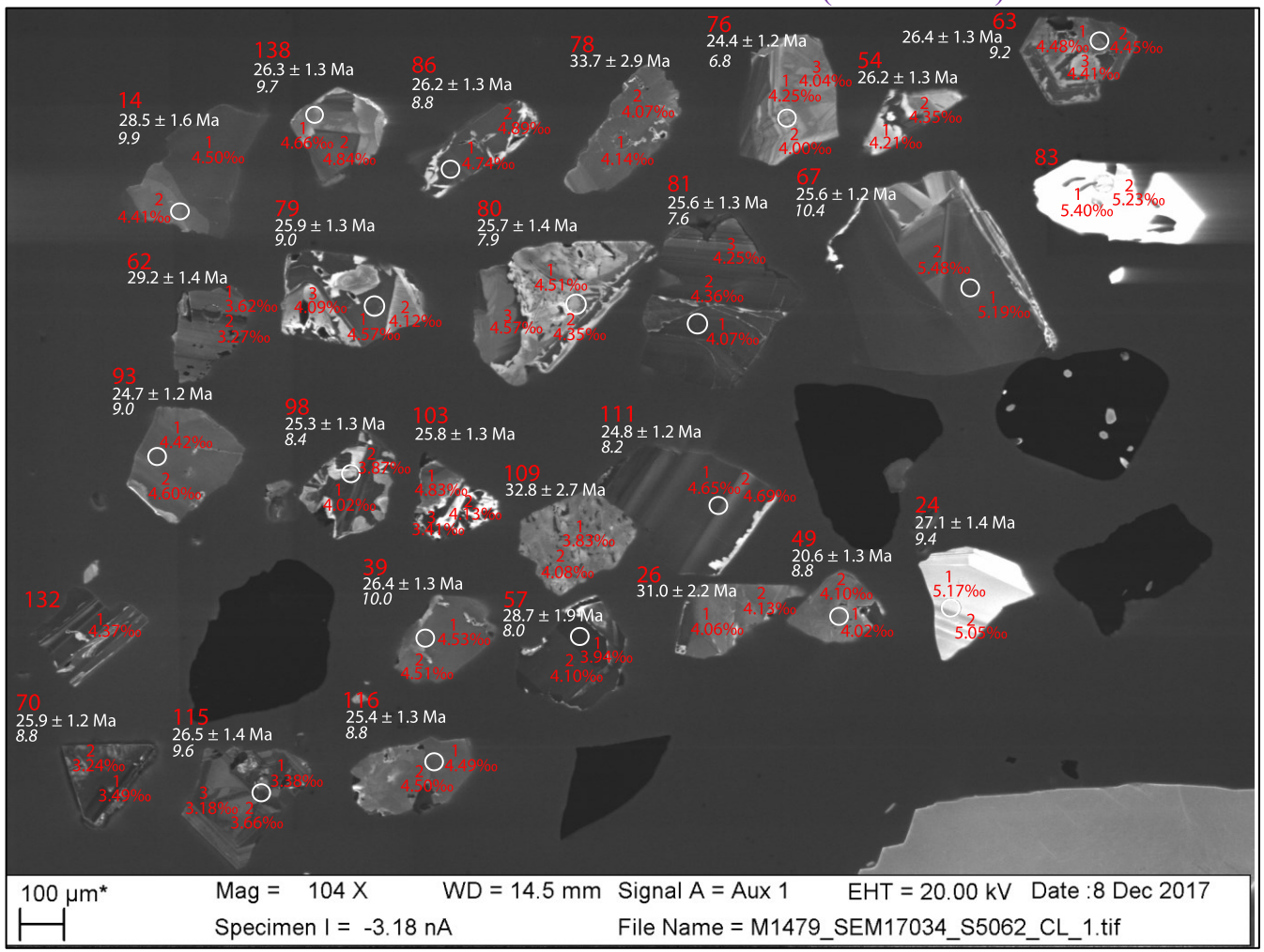

Appendix D1: Cathodoluminscence images with grain identification number in red, $^{206}Pb/^{238}U$ Age in white (2σ error), εHf_i values reported in white italics with 40 µm spot in white, and $\delta^{18}O$ spots in red with corresponding numbers.

APPENDIX D2: CATHODOLUMINSCENCE IMAGES (2016MJ-38)

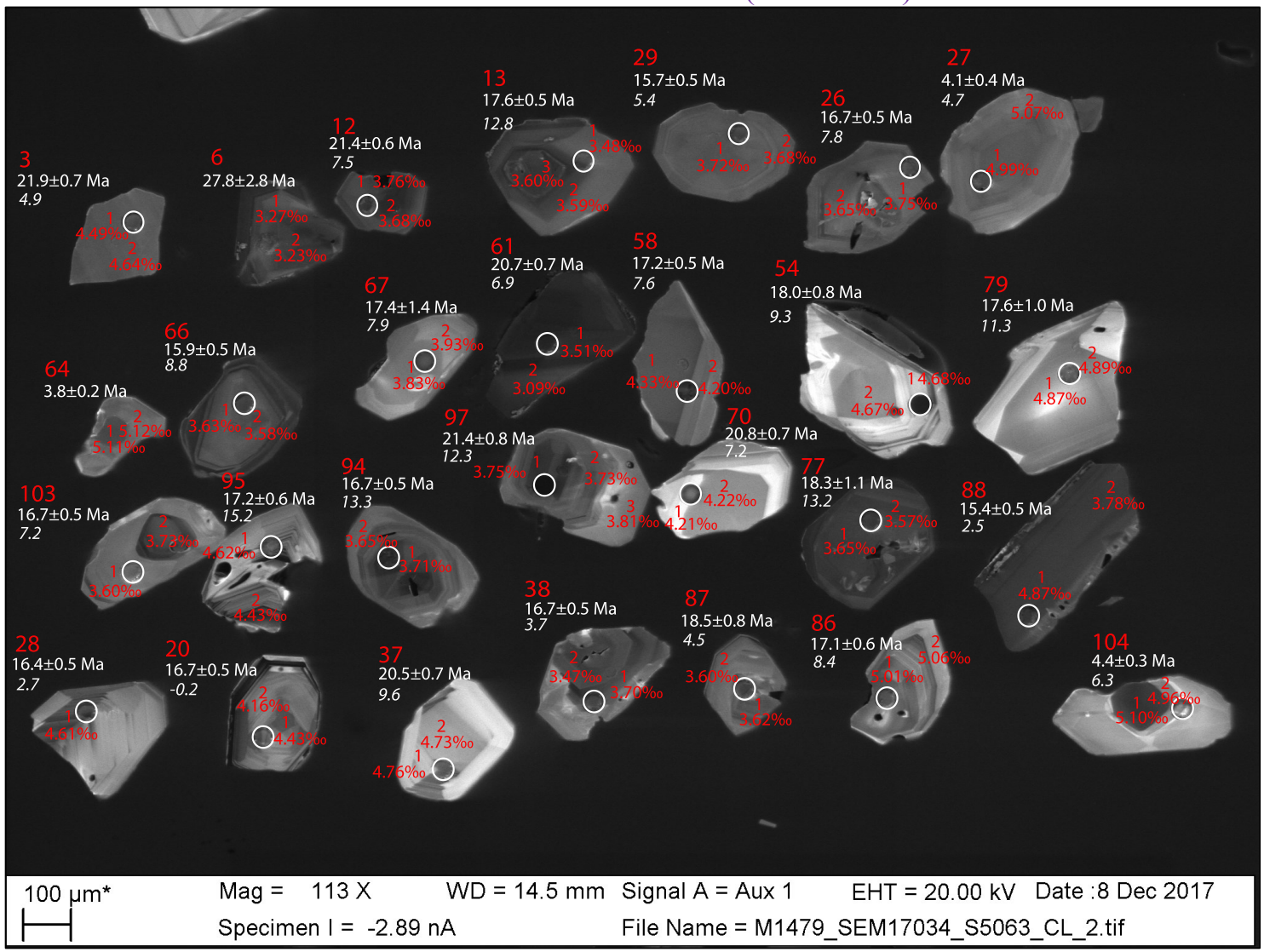

Appendix D2: Cathodoluminscence images with grain identification number in red, $^{206}Pb/^{238}U$ Age in white (2σ error), εHf_i values reported in white italics with 40 µm spot in white, and $\delta^{18}O$ spots in red with corresponding numbers.

APPENDIX D3A: CATHODOLUMINSCENCE IMAGES (2016MJ-39)

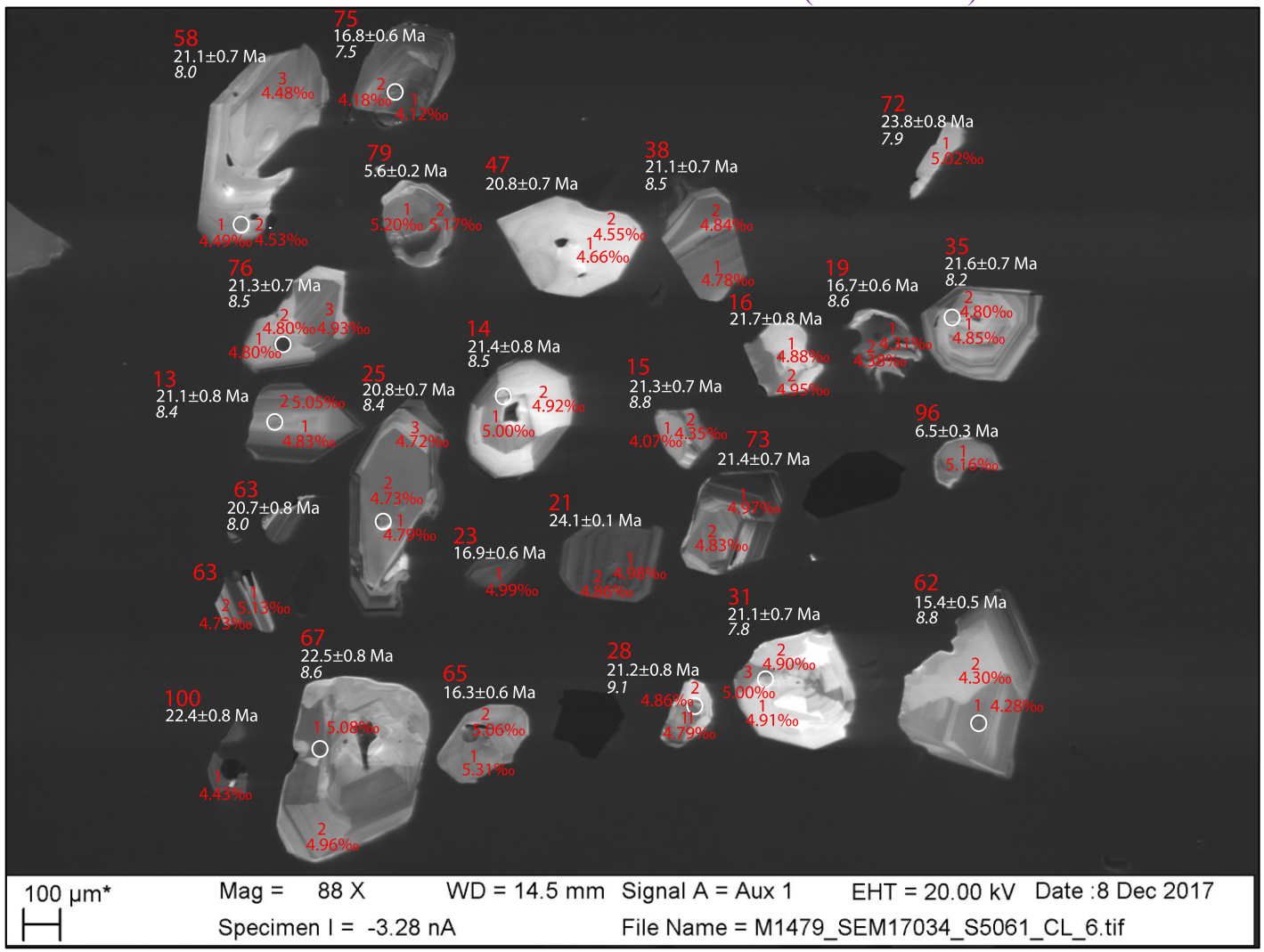

Appendix D3A: Cathodoluminscence images with grain identification number in red, $^{206}Pb/^{238}U$ Age in white (2σ error), εHf_i values reported in white italics with 40 µm spot in white, and $\delta^{18}O$ spots in red with corresponding numbers.

APPENDIX D3B: CATHODOLUMINSCENCE IMAGES (2016MJ-39)

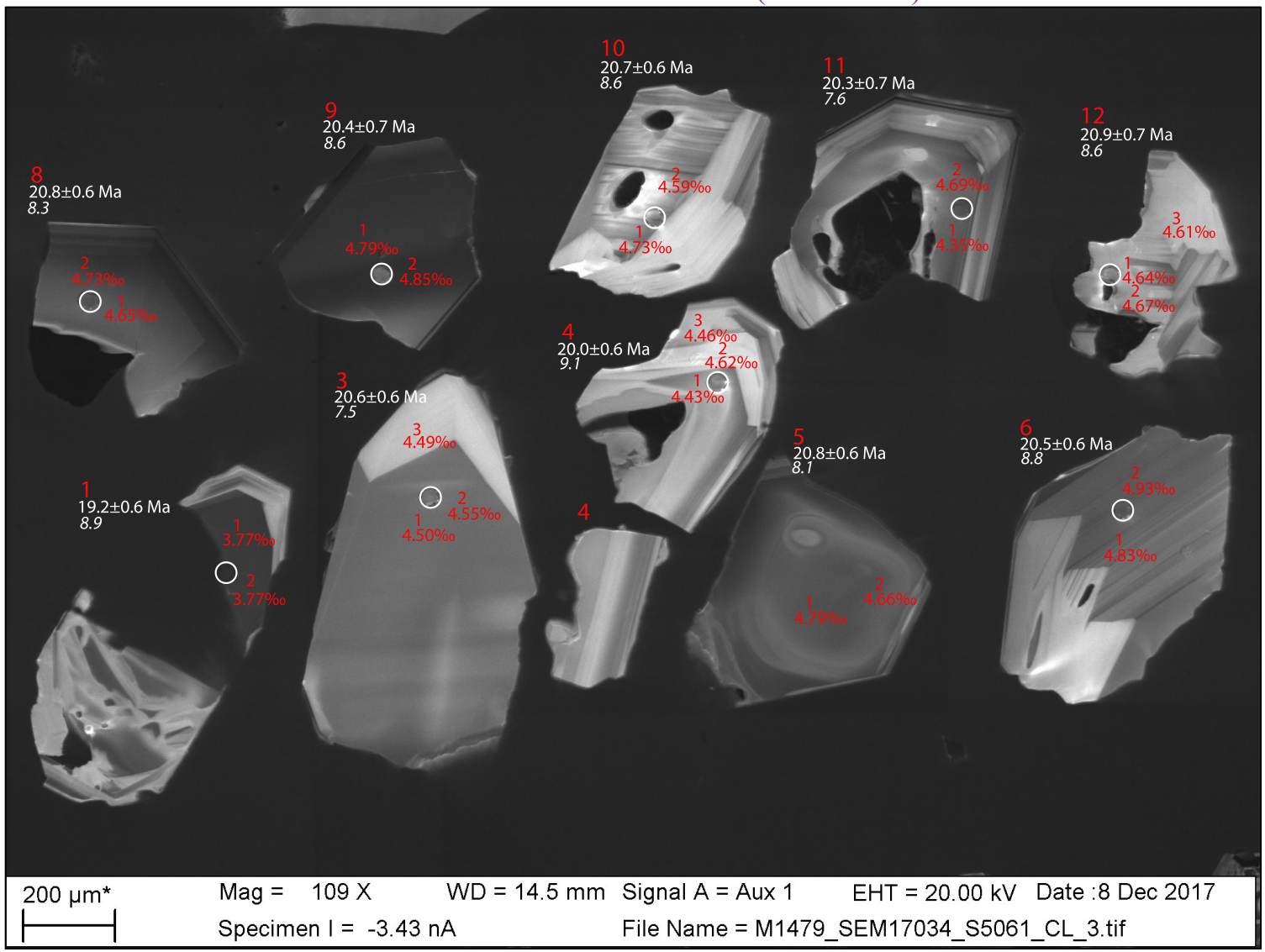

Appendix D3B: Cathodoluminscence images with grain identification number in red, $^{206}Pb/^{238}U$ Age in white (2σ error), εHf_i values reported in white italics with 40 µm spot in white, and $\delta^{18}O$ spots in red with corresponding numbers.

APPENDIX E: GEOCHEMISTRY SUMMARY

	04-003	04-014	04-016	04-023	04-024	04-026	04-049	04-067	04-076	04-078	04-079	04-080	04-081	04-086	04-093
U-Pb (Ma)	28.48	27.54	28.73	25.72	27.08	30.96	20.57	25.60	24.36	33.67	25.88	25.72	25.62	26.18	24.74
Error (2se)	1.60	1.34	1.63	1.27	1.39	2.19	1.27	1.24	1.16	2.87	1.26	1.40	1.26	1.26	1.21
P 31	BDL	BDL	29	BDL	BDL	34	93	23	34	35	40	34	BDL	51.2	59
Sc 45	266.8	271	275.9	271	268	341	373	337.5	287.7	278	295.8	300	309	278	341.4
Ti 49	1	16.6	1	8.2	1	1	23.4	1	1	11	1	1	17	1	1
Y 89	116.6	7710	87.2	2940	6360	7780	735	1517	131	3540	2887	134.6	3980	3850	2830
Nb 93	1.85	25.56	2.05	31.9	24.2	31.1	2.38	1.08	0.93	51	10.72	0.942	80.7	19.64	8.91
La 139	BDL	22.67	0.028	0.402	1.25	0.848	0.056	0.022	BDL	0.164	0.654	0.03	4.71	0.93	0.19
Ce 140	0.162	519	1.74	118	109	72	9.3	20.4	0.162	31.9	13.55	1.09	49.7	61.7	57.8
Pr 141	BDL	41.2	BDL	2.78	5.05	3.7	0.5	0.283	BDL	1.24	1.65	0.068	7.99	3.31	1.236
Nd 146	0.135	364	BDL	38.1	50.4	46.3	5.9	3.95	BDL	14.69	17.6	0.58	68.9	41.4	16.8
Sm 147	0.154	218.6	BDL	42.9	55.9	55.6	6.73	6.6	0.22	17	22.1	0.46	47.7	49.5	23.6
Eu 153	0.175	104.9	0.16	25.8	35	34.4	3.26	4.86	0.177	10.69	13.52	0.356	24.8	29.5	14.17
Gd 157	1.5	555	1.62	163.8	216	196	25	36.2	1.06	78.1	85.8	2.4	132	169.6	93.1
Tb 159	0.636	120.2	0.77	43	66.4	58	7.19	9.95	0.544	28.4	26.06	0.798	36.9	45.9	28.24
Dy 163	10.67	1132	10.6	425	910	697	82.9	116.7	8.95	396	323.9	12.19	427	509	339.6
Ho 165	4.64	290	4.25	115	290	231	24	41.4	4.62	157.7	106.4	4.16	130.4	155.1	105
Er 166	30	1119	22.7	453	1420	1001	100	191	29.1	877	496	23.7	593	688	444
Tm 169	8.08	219.9	5.11	81.1	279	211	18.8	41.5	8.01	204.7	103.6	5.45	120.2	141.8	84.3
Yb 172	85.6	1834	51.3	555	2220	1575	170	344	82.7	1705	833	48.8	953	1107	647
Lu 175	18.76	318.9	11.85	89.4	335	233	35.1	61.5	15.84	262.3	146.2	9.49	144.2	170.4	116.1
Hf 177	7450	10500	20750	10100	9050	5070	7270	3310	6170	9030	7200	3720	3160	11580	4490
Ta 181	0.21	0.96	0.9	0.85	1.31	1.63	1.14	0.139	0.169	0.95	0.369	0.09	0.326	1.27	0.347
Th 232	4.31	2566	9.64	3880	3630	3280	60.4	1122	5.26	6800	915	44.2	1909	1486	777
U 238	21	1606	27.3	2620	415	1290	55.4	383	48.3	127.2	1021	63.6	1055	1154	243.3
Nb/Ta	8.8	26.6	2.3	37.5	18.5	19.1	2.1	7.8	5.5	53.7	29.1	10.5	247.5	15.5	25.7
Th/U	0.2	1.6	0.4	1.5	8.7	2.5	1.1	2.9	0.1	53.5	0.9	0.7	1.8	1.3	3.2
Eu/Eu*	1.11	0.92	-	0.94	0.97	1.01	0.77	0.96	1.12	0.90	0.95	1.04	0.96	0.98	0.92
Ce/Ce*	-	4.2	-	27.4	10.6	10.0	13.6	63.4	-	17.3	3.2	5.9	2.0	8.6	29.2

APPENDIX E: GEOCHEMISTRY SUMMARY CONTINUED

	04-098	04-103	04-109	04-111	04-115	04-116	04-300	04-301	38-001	38-002	38-003	38-004	38-005	38-006	38-007
U-Pb (Ma)	25.31	25.82	32.80	24.78	26.51	25.38	N/A	N/A	17.08	16.68	21.91	17.77	17.20	27.78	18.12
Error (2se)	1.26	1.28	2.66	1.19	1.35	1.27	N/A	N/A	0.52	0.57	0.68	0.61	0.51	2.79	0.62
P 31	45	155	37	33.8	28	BDL	BDL	55	81.7	37.6	57.7	115	37.9	168	65.8
Sc 45	352.7	358.7	363.5	342.8	377	357	273.9	348	361	344	358	354	343	327	348
Ti 49	1	1	1	1	1	15.1	9.3	1	23.3	40.8	1	18.9	8	1	26.6
Y 89	2215	210	111.4	3410	7270	4870	3707	1810	723	236	640	2898	2140	8560	1380
Nb 93	9.39	11.79	7	35.7	20.1	56.1	19.09	125.1	5.29	0.98	3.37	21.99	21.3	98.8	7.14
La 139	0.066	16.6	0.082	1.68	0.032	2.07	1.22	20.8	0.023	0.0104	0.0087	0.127	0.12	0.169	0.059
Ce 140	9.41	93.1	0.459	286	13.7	96.3	87.8	155	52.4	6.71	6.52	192.2	206	446	45.6
Pr 141	0.359	9.66	BDL	9.22	0.192	6.44	3.06	22.7	0.165	0.067	BDL	0.574	0.731	2.6	0.35
Nd 146	4.07	61.2	0.34	117.1	2.74	62.6	39.1	147	2.37	0.95	0.51	9.1	9.68	48.9	4.01
Sm 147	6.43	15.7	0.19	94.6	12.4	58.3	45.3	67.7	3.59	1.47	1.69	15.7	12.3	94.6	4.07
Eu 153	4.43	5.44	0.146	46.5	11.4	33.4	29.9	29.1	1.56	0.73	1.35	5.54	4.17	32.7	2.28
Gd 157	35.9	19.4	1.21	244.1	95	188.3	192.6	124	18.1	6	11.5	72.4	51.7	373	20.5
Tb 159	13.48	3.42	0.432	54	36.8	47.4	55.6	28.5	5.69	1.7	4.43	24.7	16.7	114.5	7.23
Dy 163	193.5	23.9	7.2	467	532	464	623	274	69.3	20.5	61.1	303	200	1235	106
Ho 165	77.6	5.08	3.16	118.6	199	121.7	187.1	64.6	24.8	7.5	22.2	103.2	72.1	361	44.3
Er 166	423	15.9	18.3	413	1060	464	751	240	108	35	112.3	448	340	1368	230
Tm 169	94.3	2.48	5.05	71.1	254	83	145.5	44.9	21.4	7.67	26.4	81	68.2	224	49.9
Yb 172	793	17	51.9	506	2300	610	1119	313	180.7	69.1	249	627	599	1463	437
Lu 175	125	2.47	9.73	75.6	423	89.9	198.9	45.7	35.7	15.2	53.6	116.3	112.1	214	96
Hf 177	4000	6640	5300	3066	6750	3650	11260	5770	7140	7960	7990	6360	5960	5130	6060
Ta 181	0.207	0.393	0.124	0.519	0.79	0.92	1.04	2.94	2.26	0.489	0.459	5.22	3.36	14.3	1.55
Th 232	876	58	8.31	3700	643	1027	2053	2760	85.1	19.4	62.5	226.5	456	809	133
U 238	1409	261	10.57	730	338	239	690	33.6	49.1	11.85	106.3	110.2	223	439	78.6
Nb/Ta	45.4	30.0	56.5	68.8	25.4	61.0	18.4	42.6	2.3	2.0	7.3	4.2	6.3	6.9	4.6
Th/U	0.6	0.2	0.8	5.1	1.9	4.3	3.0	82.1	1.7	1.6	0.6	2.1	2.0	1.8	1.7
Eu/Eu*	0.89	0.95	0.93	0.94	1.02	0.97	0.98	0.97	0.59	0.75	0.94	0.50	0.51	0.53	0.76
Ce/Ce*	15.0	1.8	-	17.8	42.9	6.5	11.1	1.7	208.5	62.3	-	174.5	170.5	165.0	77.8

APPENDIX E: GEOCHEMISTRY SUMMARY CONTINUED

	38-008	38-009	38-011	38-012	38-013	38-014	38-015	38-020	38-021	38-022	38-023	38-027-1	38-027-2	38-031	38-032
U-Pb (Ma)	20.93	17.46	15.83	21.43	17.59	25.04	17.27	16.73	3.90	16.28	16.26	4.09	N/A	16.65	16.28
Error (2se)	0.64	0.58	0.47	0.62	0.54	0.74	0.54	0.48	0.14	0.53	0.59	0.37	N/A	0.67	0.51
P 31	111	55.7	117.6	131.2	72.3	53.4	163.6	99	81	175	72.5	63.3	37.6	190	107
Sc 45	344	336	345	335.5	338.5	349.1	369.9	360	340	342.8	341.9	177.9	172.7	368	343.7
Ti 49	20.2	32.9	18.9	22.6	1	1	25	41.8	12.4	22.3	10.4	14.9	10.6	44.2	16.4
Y 89	2820	887	1021	2580	3470	608	919	842	874	3610	1470	1375	1335	874	2820
Nb 93	4.74	4.54	11.02	28.2	38.2	3.11	4.59	4.16	6.26	42.9	27.2	5.37	3.42	5.25	13.9
La 139	0.086	0.027	0.016	0.054	0.028	0.0119	0.068	BDL	3.9	0.084	0.271	0.102	0.136	0.0074	0.121
Ce 140	52.9	25.6	75.3	323	232	9.35	22.07	18.5	115.8	448	151.8	69	64	23.58	164
Pr 141	0.78	0.111	0.246	0.78	0.56	0.091	0.456	0.176	0.64	0.975	0.208	0.553	0.663	0.164	0.98
Nd 146	13.8	1.37	3.29	13.6	9.7	1.12	5.82	2.33	4.27	19.56	3	7.14	9.53	2.23	17.3
Sm 147	24.9	2.13	5.6	22.6	18.5	2.81	6.64	4.08	2.95	32.3	5.58	6.32	8.24	4.16	27.9
Eu 153	8.12	0.9	1.65	7.19	7.6	2.22	1.45	1.53	1.17	10.6	2.02	3.18	4.04	1.45	9.86
Gd 157	96	12.3	26.3	88.1	102	16.5	28	17.4	13.3	129.4	25.2	26.6	31.2	20.95	110.1
Tb 159	27.1	4.82	8.54	26.5	35.4	5.11	8.41	6.08	4.28	36.47	9.09	8.11	8.87	6.66	31.6
Dy 163	302	67	106	300	415	63.6	95.9	77.9	57.2	404.2	124	102.1	106.2	83.1	349
Ho 165	95	28.5	37.3	94.9	133	22.9	31.2	29.1	23.9	130.2	46.8	40.9	40.2	29.1	110.5
Er 166	413	146.8	173	391	561	97.7	138.9	136	124.2	546	230.5	206.5	199.3	135.4	451
Tm 169	74.3	32.2	33.2	72.7	99.8	18.73	26.8	27.7	30.3	97.7	48.3	45.5	43.78	27.09	80.2
Yb 172	518	289	275	538	709	157.1	219.1	230	295	730	398	412.3	390.8	234	611
Lu 175	83	61.6	53.1	99.4	115	28.6	41.9	47.1	62.1	132.2	74.5	86.2	83	46.2	105.1
Hf 177	7910	6420	8670	6160	6040	2729	10430	7920	6160	5780	8620	5050	4990	8160	5990
Ta 181	1.97	1.16	4.21	8.31	6.81	0.232	3.6	1.98	0.675	10.49	4.94	0.774	0.632	2.48	4.04
Th 232	1760	138	126.6	1495	307	101.1	373	74.2	1045	1563	502	163.4	147.7	68	169.5
U 238	571	69.6	93.1	381	242	128.6	250.8	57.2	334	386	158	80.9	73.7	58.6	87.3
Nb/Ta	2.4	3.9	2.6	3.4	5.6	13.4	1.3	2.1	9.3	4.1	5.5	6.9	5.4	2.1	3.4
Th/U	3.1	2.0	1.4	3.9	1.3	0.8	1.5	1.3	3.1	4.0	3.2	2.0	2.0	1.2	1.9
Eu/Eu*	0.51	0.54	0.42	0.49	0.53	1.00	0.33	0.56	0.57	0.50	0.52	0.75	0.77	0.47	0.54
Ce/Ce*	50.1	114.7	294.3	385.9	454.3	69.7	30.7	-	18.0	383.8	156.8	71.2	52.3	166.0	116.8

APPENDIX E: GEOCHEMISTRY SUMMARY CONTINUED

	38-033	38-034	38-035	38-036	38-037	38-038	38-039	38-041	38-042	38-043	38-044	38-045	38-052	38-058	38-061
U-Pb (Ma)	16.87	22.72	14.96	17.37	20.51	16.72	25.36	16.81	21.29	26.22	21.13	4.36	17.77	17.18	20.65
Error (2se)	0.53	0.73	0.44	0.58	0.71	0.48	0.80	0.49	0.72	0.81	0.62	0.14	0.59	0.51	0.69
P 31	120	56.2	43.5	60.7	109.7	117.5	335	179	28.8	118	58.1	107.4	109.4	79.5	92
Sc 45	348	323	329	340.5	354	343.1	340	380.2	347	359	348	347	348	341	347
Ti 49	17.7	16.8	14.6	30.9	38.2	18	24.8	63.6	1	29.7	17.6	18.5	44.2	40.1	18.2
Y 89	3890	908	1430	361	328.8	2678	2922	691	1840	810	2750	4090	832	1304	4320
Nb 93	15.7	6.67	4.79	1.46	1.22	13.15	23.61	2.38	17.29	5.06	15.9	32.6	1.67	6.22	55.5
La 139	0.23	0.021	0.132	0.012	BDL	0.128	0.126	0.021	0.053	BDL	0.492	0.077	BDL	0.033	0.077
Ce 140	187	68	70	4.1	6.23	142.8	259	9.87	89.3	18.5	275	334	11.32	28.5	530
Pr 141	1.38	0.177	0.652	0.059	0.069	0.96	0.977	0.201	0.759	0.099	2.16	0.707	0.284	0.286	1.08
Nd 146	21.7	2.13	10.1	0.76	1.05	15.01	14.6	2.66	11.18	1.88	23.3	11	4.65	4.06	19.7
Sm 147	39.8	3.29	9.8	1.63	1.79	22.1	24.3	4.42	19.7	3.31	18.7	18.1	6.49	7.88	26.6
Eu 153	12.9	0.99	4.52	0.564	0.681	6.95	7.62	1.46	11.48	1.3	6.52	6.32	3.34	2	8.2
Gd 157	151	15.5	32.9	9	8.4	86.7	100.2	18.4	73.8	15.1	61.3	102.6	30.4	40.2	102.2
Tb 159	41.4	5.16	10.24	2.57	2.66	25.53	29.02	6.27	20	5.41	17.6	33.5	8.02	11.88	32.2
Dy 163	460	75	128.7	33.7	31.2	288.8	332.2	72.2	201.9	65.7	200	404	92.5	135.5	414
Ho 165	147	27.9	47.4	12.05	10.31	94	108.2	25	62.5	24.7	79.1	141.4	29.25	45	139
Er 166	579	136	232	54.7	47.6	401.8	451.4	112	258	118	382	610	123.2	190.5	657
Tm 169	106.3	28.8	50.1	12.15	9.39	72.1	82.7	21.62	46.5	25.5	82.6	115	23	35.6	123
Yb 172	806	242	460	104.7	78.1	545	628	176.9	339	220	718	859	191.8	286	967
Lu 175	148.1	46.9	97.9	20.9	14.86	100.5	119.3	35.2	59.7	44.3	143	145.4	37.4	52.3	173
Hf 177	6340	7040	5860	7650	8970	6020	6350	9240	4480	8220	5010	5690	7570	8040	5310
Ta 181	4.6	2.08	0.93	0.98	0.96	3.53	6.65	1.24	1.36	2.3	1.37	5.3	1.07	3.27	8.9
Th 232	259	83.7	169	163.2	224	158.7	321	109.2	1257	112	1890	432	73.7	1691	1400
U 238	110.6	60.3	79	119.9	240	80.3	152.3	82.5	520	90.4	422	158	43.3	641	463
Nb/Ta	3.4	3.2	5.2	1.5	1.3	3.7	3.6	1.9	12.7	2.2	11.6	6.2	1.6	1.9	6.2
Th/U	2.3	1.4	2.1	1.4	0.9	2.0	2.1	1.3	2.4	1.2	4.5	2.7	1.7	2.6	3.0
Eu/Eu*	0.51	0.42	0.77	0.45	0.54	0.49	0.47	0.49	0.92	0.56	0.59	0.45	0.73	0.34	0.48
Ce/Ce*	81.4	273.5	58.5	37.8	-	99.9	181.0	37.2	109.2	-	65.4	351.0	-	71.9	450.6

APPENDIX E: GEOCHEMISTRY SUMMARY CONTINUED

	38-064-1	38-064-2	38-066	38-067	38-070	38-071	38-077	38-079	38-080	38-094	38-095	38-104-1	38-104-2	38-302	38-303
U-Pb (Ma)	3.84	N/A	15.93	17.35	20.79	16.59	18.32	17.63	16.62	16.74	17.21	4.36	N/A	N/A	N/A
Error (2se)	0.23	N/A	0.46	1.40	0.66	0.51	1.10	0.95	0.55	0.51	0.56	0.25	N/A	N/A	N/A
P 31	30	43.8	55.5	82.4	97.7	118.7	76.9	101.5	105.4	157.8	170.6	56	45.1	55.4	124.2
Sc 45	176.2	175.7	341.5	345	331	341.8	353.5	348	360.5	344.9	338.2	177.9	173.8	339.1	349.9
Ti 49	12.1	10.4	12.7	21.1	122	22.7	11.9	17.2	45.6	22.9	490	20	14.9	10.8	48.2
Y 89	629	395.7	866	1430	494	2850	1179	2222	573.9	4127	3826	260.7	213	1057	871
Nb 93	1.77	2.5	6.81	3.84	4.9	35.4	9.67	17.64	1.39	36.4	65	1.36	1.13	5.89	5.34
La 139	0.066	0.0131	0.021	0.048	0.78	0.13	0.04	0.068	0.044	0.141	9.9	0.024	0.0062	0.053	0.021
Ce 140	26.36	24.49	51	57	13.55	340	104.5	144.8	6.04	408	553	12.94	13.38	61.5	35.5
Pr 141	0.323	0.067	0.13	0.792	0.22	1.04	0.208	0.381	0.209	1.5	6.2	0.063	0.052	0.276	0.147
Nd 146	3.11	0.75	2.47	10.52	1.91	14.1	3.54	5.41	3.24	24.8	46	0.81	0.46	2.85	2.77
Sm 147	2.57	0.84	4.43	13.4	1.84	20.2	5.34	7.16	4.14	37.4	44.3	1.11	0.65	2.13	5.11
Eu 153	1.35	0.301	1.43	3.18	0.57	6.24	1.75	2.42	2.04	11.51	12.66	0.655	0.443	0.95	1.88
Gd 157	11.96	4.12	19.7	49.2	11.66	80.7	25.7	38	19.58	139.5	153.7	4.77	3.24	11.82	23.2
Tb 159	3.72	1.49	6.27	15.6	3.73	25	8.32	13.81	5.53	41.6	42	1.475	1.041	4.3	7.38
Dy 163	47.8	21.49	80.7	169	47.5	300	106.7	184.4	63.3	464	448	18.28	14.25	60.6	88.6
Ho 165	18.17	10.27	28.7	52.7	17	95.9	38.3	70.8	20.39	146.8	141.1	8.06	5.78	27.9	30.14
Er 166	95.4	63.3	135.7	221	81	441	180.7	341.8	87.7	612	556	41.7	34.25	160.2	132.2
Tm 169	21.58	16.34	27.81	38.7	17.1	83.7	37.7	73.5	17.37	111.2	98.7	9.84	8.15	39.4	24.7
Yb 172	206.4	169.7	228.7	293	142.8	643	294.1	614	146.3	862	744	97.6	85.2	380	203.7
Lu 175	44.6	39.63	46.1	54.2	28.6	121	58.2	120.6	29.33	156.4	133.2	22.05	19.77	85.9	37.8
Hf 177	5540	5510	6560	7220	11830	6830	6580	7210	8360	6060	5890	5330	5470	6360	8340
Ta 181	0.31	0.39	2.71	2.86	2.1	7.61	3.31	3.42	0.855	8.71	14.7	0.377	0.243	0.623	2.66
Th 232	90	78.9	38.5	59.9	218	1160	174	255	111.3	857	2403	19.62	26.89	228	378
U 238	54.26	63.2	36.5	32.8	244	331	110.4	128.4	73.9	263.7	503	19.1	23.2	140	136.8
Nb/Ta	5.7	6.4	2.5	1.3	2.3	4.7	2.9	5.2	1.6	4.2	4.4	3.6	4.7	9.5	2.0
Th/U	1.7	1.2	1.1	1.8	0.9	3.5	1.6	2.0	1.5	3.2	4.8	1.0	1.2	1.6	2.8
Eu/Eu*	0.74	0.49	0.47	0.38	0.38	0.47	0.46	0.45	0.69	0.49	0.47	0.87	0.93	0.58	0.53
Ce/Ce*	44.3	202.7	239.3	71.7	8.0	226.7	280.9	220.6	15.4	217.5	17.3	81.6	182.7	124.7	156.7

APPENDIX E: GEOCHEMISTRY SUMMARY CONTINUED

	38-304	38-305	38-306	38-307	38-308	38-309	38-310	38-311	39-001	39-002	39-003	39-004	39-005	39-006	39-007
U-Pb (Ma)	N/A	N/A	N/A	N/A	N/A	N/A	N/A	N/A	19.22	20.50	20.60	19.98	20.76	20.53	20.97
Error (2se)	N/A	N/A	N/A	N/A	N/A	N/A	N/A	N/A	0.59	0.62	0.63	0.59	0.62	0.62	0.67
P 31	129.6	172.2	85	100	66	159.6	161	74.3	141.2	137	101.7	112.5	107	134	145
Sc 45	339.1	362.9	345.4	340.4	326.7	353.3	338	356.7	357.6	360.3	369.6	360.1	371.1	379.3	355.7
Ti 49	23.4	27.3	11.5	18.6	28	30.6	13.2	17.3	60.6	17.4	23.8	31.2	34.4	27.8	44
Y 89	2834	2562	809	1768	199.9	1455	3280	725	1914	1377	662	240	617	667	481
Nb 93	21.91	6.31	6.31	15.25	6.86	5.8	79.9	1.64	7.81	2.59	1.6	1.95	1.93	2.42	37.54
La 139	0.075	0.152	0.0071	0.087	0.2	0.038	0.23	0.077	0.095	0.055	0.0082	0.025	0.055	0.047	0.204
Ce 140	203	24.28	49.1	202.3	24.8	19.03	243.3	12.02	34.2	14.58	9.42	7.18	14.25	7.16	18.06
Pr 141	0.711	1.033	0.16	0.591	0.065	0.298	1.09	0.253	0.935	0.469	0.132	0.074	0.311	0.295	0.149
Nd 146	11.45	14.78	2.09	10.1	0.37	4.55	14.1	2.58	14.16	5.68	3.15	0.59	5.44	3.68	1.82
Sm 147	19.8	23.4	3.29	14	0.38	8.39	18.8	2.66	19.7	7.27	5.97	1.19	6.25	5.4	2.12
Eu 153	6.76	7.95	1.1	7.41	0.141	2.83	6.43	1.56	6.74	2.67	2.09	0.306	1.48	1.96	0.92
Gd 157	85.5	96.5	13.5	50.5	2.31	43.5	81.5	11.07	71.9	38.9	24.2	5.35	22.9	20.1	11.11
Tb 159	27.24	27.84	5	14.11	0.906	13.35	26.9	3.37	20.41	12.15	6.99	1.8	6.24	6.06	3.49
Dy 163	310.2	303.1	63.8	157.1	13	152.5	324	46.3	218	143.9	77.9	22.8	68.3	73.1	40.8
Ho 165	102.7	95	25.5	55.1	5.85	51.2	112	19.31	64.7	46.9	22.66	7.53	20.33	22.64	14.98
Er 166	432.6	384	129.6	249.4	33.6	209.8	491	114.1	273.3	195.6	93.3	35.5	85.7	94.6	72.5
Tm 169	79.9	68.5	27.6	49.6	8.46	39.1	97.3	29.74	54.7	38.7	16.94	7.51	16.08	17.98	15.73
Yb 172	620	538	243.6	397.5	79.9	298.8	798	306	436	308	137.8	66.3	133.1	142.5	145.3
Lu 175	115.8	96.8	48.9	78.2	17.16	54.2	143.3	72.4	85.2	59.3	26.16	13.68	26	27.37	29.5
Hf 177	6380	8130	6980	5730	8880	7110	7990	6960	7200	8710	8600	10520	8750	8150	7110
Ta 181	5.58	2.95	1.95	2.59	1.91	2.4	14.2	0.347	3.09	1.65	0.98	1.29	1.5	1.89	34.4
Th 232	246	230.9	63.8	1665	36	647	688	111.7	509	1163	277.2	70	899	358.6	2748
U 238	116.2	171.5	52.7	397	42.1	304.2	396	75.4	362.2	650	193.9	83.1	507	252	439.6
Nb/Ta	3.9	2.1	3.2	5.9	3.6	2.4	5.6	4.7	2.5	1.6	1.6	1.5	1.3	1.3	1.1
Th/U	2.1	1.3	1.2	4.2	0.9	2.1	1.7	1.5	1.4	1.8	1.4	0.8	1.8	1.4	6.3
Eu/Eu*	0.50	0.51	0.50	0.85	0.46	0.45	0.50	0.88	0.55	0.49	0.53	0.37	0.38	0.58	0.58
Ce/Ce*	215.5	15.0	357.2	218.7	53.3	43.8	119.1	21.1	28.1	22.3	70.2	40.9	26.7	14.9	25.4

APPENDIX E: GEOCHEMISTRY SUMMARY CONTINUED

	39-008	39-009	39-010	39-011	39-012	39-013	39-014	39-015	39-016	39-017	39-018	39-019	39-021	39-022	39-023
U-Pb (Ma)	20.79	20.36	20.66	20.28	20.86	21.14	21.40	21.31	21.71	16.72	21.26	16.65	24.06	20.29	16.87
Error (2se)	0.62	0.65	0.64	0.65	0.69	0.75	0.76	0.73	0.77	0.57	0.76	0.56	1.01	0.70	0.57
P 31	177	158	140	122.2	142	96.4	108	166.1	167.9	397	174	124.2	217	87.9	156.3
Sc 45	360.4	356	367.7	367	374.6	358	373	364.9	359	344.5	373	353.9	389	340.3	339.4
Ti 49	32.7	27.7	37.2	32.3	41.3	53.9	40.1	52.1	61.4	48.3	28.6	46.1	67	16.6	28.1
Y 89	690	1560	727	1094	375.8	278.6	657	1048	650	7630	1170	1675	1323	4385	3496
Nb 93	3.55	12.4	2.15	3.35	1.69	5.06	1.54	5.41	2.02	349.2	5.37	9.07	3.55	26.03	37
La 139	0.018	0.114	0.057	0.085	BDL	BDL	0.024	0.09	0.026	8.9	0.04	0.06	0.222	0.93	0.136
Ce 140	19.6	20.3	9.52	22.4	5.84	10.94	7.79	14.45	9.78	934	25.3	45.5	18.4	109.4	388
Pr 141	0.231	0.519	0.348	0.53	0.107	BDL	0.273	0.435	0.209	5.8	0.201	0.322	0.424	2.49	1.31
Nd 146	2.54	6.14	3.87	7.55	1.12	1.1	3.88	5.59	2.41	64.2	2.75	5.14	7.64	33.8	21.1
Sm 147	3.33	7.56	5.93	7.63	1.55	2.05	5.1	6.4	4.26	87.7	8.3	10.6	11	45.9	32.7
Eu 153	1.13	2.43	2.4	2.33	0.94	0.45	2.13	1.44	1.51	33.4	4.08	2.89	4.95	9.6	9.68
Gd 157	17.4	30.9	26.2	34.4	9.36	7.21	22	27.9	17.6	322	50.7	48.8	46.3	167.2	124.4
Tb 159	5.63	9.88	6.8	9.95	2.76	2.35	6.01	8.36	5.59	93	15.4	15.76	12.8	49.6	36
Dy 163	67.3	132.7	78.1	111.7	35.5	27.2	70.1	98.2	62.7	1010	170	180.2	148	549.8	409
Ho 165	22.41	51.1	23.9	36.2	12.43	9.04	23.45	33.8	21.23	286	44.7	57.4	45.9	166.2	123.8
Er 166	104.5	253	102.9	157	58.6	41.1	97.2	157.2	102.4	1090	159	249.9	196	664	521
Tm 169	21.3	49.3	19.3	30.4	12.02	8.35	19.34	31.6	20.36	190.1	27.9	48.5	36.6	119.4	96.6
Yb 172	181.9	417	159	256	109.5	68.6	161.9	269	181.1	1405	206	399	308	884	740
Lu 175	34.9	83	31.9	49.7	23.85	13.57	34	53.1	38.1	237.8	30.9	76.3	63	153.9	134.7
Hf 177	9040	10090	7620	9200	8450	6360	8580	9540	7840	8630	8170	8160	8200	6530	6020
Ta 181	2.14	10.9	1.25	1.94	0.815	3.39	0.81	2.81	1.2	54.8	2.83	4.11	1.24	6.51	9.21
Th 232	3300	2400	187	757	120.8	601	154.3	548	111.5	2648	1910	724	370	342.8	1020
U 238	1365	1600	115.2	435	125	317	95.4	428	93.4	1032	1160	352	159	303.1	293
Nb/Ta	1.7	1.1	1.7	1.7	2.1	1.5	1.9	1.9	1.7	6.4	1.9	2.2	2.9	4.0	4.0
Th/U	2.4	1.5	1.6	1.7	1.0	1.9	1.6	1.3	1.2	2.6	1.6	2.1	2.3	1.1	3.5
Eu/Eu*	0.45	0.49	0.59	0.44	0.75	0.36	0.61	0.33	0.53	0.61	0.61	0.39	0.67	0.34	0.46
Ce/Ce*	74.5	20.5	16.6	25.9	-	-	23.6	17.9	32.5	31.9	69.2	80.3	14.7	17.6	225.4

APPENDIX E: GEOCHEMISTRY SUMMARY CONTINUED

	39-024	39-025	39-028	39-031	39-035	39-038	39-043	39-045	39-046	39-047	39-050	39-051	39-052	39-053	39-054
U-Pb (Ma)	17.48	20.78	21.19	21.11	21.61	21.07	20.82	22.80	16.25	20.79	17.10	20.62	21.01	20.34	20.91
Error (2se)	0.62	0.70	0.80	0.74	0.74	0.72	0.71	0.82	0.62	0.71	0.63	0.70	0.71	0.72	0.71
P 31	90.5	115.3	143.9	211	175.8	111.2	111	112	119	121	65.2	127.8	213	155.9	170.6
Sc 45	352.4	346.6	365.3	384	385	368.2	360.7	366	350.2	356.5	339.3	366	375	379.5	368.1
Ti 49	20	32.9	49.6	39.5	42	26.1	56.3	38.9	22.9	57.2	35	40.9	44.1	39.4	30.6
Y 89	2420	666	1055	705	687	420.7	639	692	709	215.5	1412	555	1395	311	1039
Nb 93	19.5	2.4	2.59	3.96	3.18	2.29	2.04	1.76	4.73	1.82	2.43	2.11	3.08	1.5	3.1
La 139	0.103	BDL	0.056	0.018	0.013	BDL	0.118	0.03	0.028	0.0078	0.098	0.101	0.084	BDL	0.024
Ce 140	255	11.17	16.21	9.59	8.92	6.59	12.05	10.04	37.5	7.07	15.53	9.74	13.53	6.25	15.11
Pr 141	1.119	0.083	0.395	0.105	0.138	0.091	0.547	0.269	0.173	0.063	0.69	0.255	0.5	0.059	0.364
Nd 146	15.02	1.6	5.04	1.63	2.28	1.09	6.15	3.25	2.16	0.6	9.74	3.7	7.28	0.82	5.3
Sm 147	14.63	3.09	7.78	2.48	3.56	2.1	6.74	4.89	3.86	1.47	13.84	4.16	10.26	1.56	9.12
Eu 153	5.49	0.89	2.75	0.99	1.5	0.91	2.09	1.89	1.85	0.422	2.37	1.52	4.29	0.602	2.41
Gd 157	53.2	16.6	32.5	12.32	17.37	10.7	23.7	20.3	19.4	6.53	46.8	17.2	45	7.14	36.2
Tb 159	15.58	5.36	9.39	4.44	5.76	3.23	6.09	6.5	5.84	2	13.69	5.21	12.45	2.37	10.22
Dy 163	198	65.2	106.9	60.3	67.7	39.7	69.7	72.1	72.3	22.3	154.4	53.1	144.2	28.6	110.6
Ho 165	73	21.91	36.01	23.04	22.69	14.14	22.1	23.6	24.07	7.1	50.1	18.5	47.1	10.04	35.67
Er 166	355	102.1	159.7	111.1	104.5	64.4	93	104.7	113.2	31.6	214.8	82.7	202.5	46.5	143.5
Tm 169	79.2	21.53	32.15	21.73	21.28	13.25	18.2	21.16	22.4	6.3	40.4	15.5	39.1	9.9	26.65
Yb 172	713	189	271.3	193.4	185.5	114.7	147.5	188.5	191.4	52.7	312	127	321	87.4	200.1
Lu 175	154.7	36.03	54.6	41	37.55	23.65	29.1	35.5	40.4	10.45	56.1	24.5	62.6	17.6	34.7
Hf 177	6520	11290	8240	7390	10530	9270	8050	8710	7640	8740	7250	8410	6890	7730	9620
Ta 181	2.39	1.55	1.43	2.01	1.98	1.09	1.11	1.09	2.2	0.85	1.57	0.992	1.53	0.85	2.75
Th 232	1820	242.8	206.5	294	259.5	123.2	117.8	118.3	48.8	91.5	200.9	107	383	44.7	772
U 238	370	197.6	112.7	199.8	234.6	136.7	79.5	76	38	69.2	136.1	69.2	178.6	40.8	394.9
Nb/Ta	8.2	1.5	1.8	2.0	1.6	2.1	1.8	1.6	2.2	2.1	1.5	2.1	2.0	1.8	1.1
Th/U	4.9	1.2	1.8	1.5	1.1	0.9	1.5	1.6	1.3	1.3	1.5	1.5	2.1	1.1	2.0
Eu/Eu*	0.60	0.38	0.53	0.55	0.58	0.59	0.51	0.58	0.65	0.42	0.28	0.55	0.61	0.55	0.41
Ce/Ce*	184.2	-	26.7	54.1	51.6	-	11.6	27.4	132.1	78.2	14.6	14.9	16.2	-	39.6

APPENDIX E: GEOCHEMISTRY SUMMARY CONTINUED

	39-056	39-058	39-059	39-060	39-061	39-062	39-063	39-065	39-067	39-072	39-073	39-075	39-076	39-079-1	39-079-2
U-Pb (Ma)	20.81	21.09	21.11	16.77	16.96	15.35	20.74	16.29	22.46	23.75	21.42	16.83	21.29	5.62	N/A
Error (2se)	0.72	0.74	0.76	0.57	0.59	0.54	0.75	0.62	0.80	0.84	0.72	0.58	0.72	0.24	N/A
P 31	117.3	120.8	137	139.3	108.8	307	114.3	56	85.9	152	292	47.4	125.5	67	57
Sc 45	344.6	369	371.2	363.7	347	362.8	345.2	351.1	327.9	365.3	390	342	366.5	173.4	172.4
Ti 49	57.1	19.4	28.6	34	15.3	20.5	48.1	16.9	246	41.4	48	19	23.2	17	15.6
Y 89	532	447	679	1638	1891	4240	619	1027	355	429	1113	234.4	784	336.6	167.6
Nb 93	1.374	3.93	1.56	4.38	20.6	20.22	2.22	3.1	18.4	2.63	4.47	0.809	1.74	1.72	1.181
La 139	BDL	BDL	BDL	0.06	0.035	0.266	0.02	0.122	5.5	0.013	0.07	BDL	0.012	BDL	BDL
Ce 140	9.69	18.06	10.25	22.64	208.5	72.3	16.48	44.3	23.4	8.55	26.1	2.41	7.32	26.98	15.05
Pr 141	0.199	0.052	0.101	0.409	0.464	2.84	0.233	0.466	0.73	0.123	0.375	0.016	0.208	0.094	0.041
Nd 146	2.88	0.67	2.03	7.89	6.13	41.9	3.76	6.13	3.12	1.26	4.74	0.21	3.32	1.09	0.47
Sm 147	4.83	1.56	4.22	15.3	8.58	50.1	5.62	5.09	2.41	2.28	6.41	0.54	5.81	1.15	0.67
Eu 153	1.19	0.519	1.75	6.18	2.72	20.15	1.21	2.4	0.86	0.91	2.07	0.417	2.24	0.691	0.287
Gd 157	22.3	8.5	21.7	61.8	38.1	165.1	22.2	22.2	9.53	9.54	28.7	4.03	25.1	6.21	2.81
Tb 159	5.82	3.13	6.12	17.12	12.37	45.4	6.16	5.96	2.78	2.88	9.05	1.22	7.66	1.74	0.985
Dy 163	62	39.1	68.6	184.3	152	468	66.9	78.6	35.8	36.7	104.9	16.99	87	24.47	12.65
Ho 165	18.78	14.08	23.06	58.6	57.2	147.2	20.88	29.25	11.56	13.43	36	6.96	27.5	9.33	4.69
Er 166	75.3	69.5	97.8	238.2	284.4	599	85.4	152.8	53.3	67.7	164.6	38	111.4	48.8	25.4
Tm 169	13.89	15.28	18.67	44.9	56.9	116.1	16.38	36.9	11.22	13.76	32.6	9.75	21.77	11.28	5.77
Yb 172	107.3	140.9	153.1	348	483	922	130	340	92.5	121.8	267.5	102.9	178.2	109.8	56.3
Lu 175	20.45	29.5	29.8	64.8	95.1	168.5	23.68	76.7	18.77	25.79	53	25.1	34.6	23.68	12.53
Hf 177	9390	10370	7980	8010	6410	6550	9280	6680	6590	7790	10000	6330	10900	5280	5880
Ta 181	0.78	2.36	0.81	2.21	4.58	4.4	1.41	0.422	1.95	1.42	4.32	0.209	1.26	0.338	0.248
Th 232	330.3	62.7	86.2	354.1	1091	760	385	184.5	70.9	111.7	1675	38.6	226.8	154.3	46.4
U 238	188.1	58.2	57.7	179.1	312.3	356	248.9	94.2	55.5	103.9	724	52.8	194.4	78.4	27.11
Nb/Ta	1.8	1.7	1.9	2.0	4.5	4.6	1.6	7.3	9.4	1.9	1.0	3.9	1.4	5.1	4.8
Th/U	1.8	1.1	1.5	2.0	3.5	2.1	1.5	2.0	1.3	1.1	2.3	0.7	1.2	2.0	1.7
Eu/Eu*	0.35	0.44	0.56	0.61	0.46	0.68	0.33	0.69	0.55	0.60	0.47	0.86	0.57	0.79	0.64
Ce/Ce*	-	-	-	35.4	401.1	20.4	59.2	45.6	2.9	52.4	39.5	-	35.9	-	-

APPENDIX E: GEOCHEMISTRY SUMMARY CONTINUED

	39-080	39-081	39-082	39-083	39-084	39-096-1	39-096-2	39-098	39-100	39-103	39-104	39-105	39-106	39-111	39-123
U-Pb (Ma)	20.49	18.25	22.51	17.58	20.66	6.49	N/A	22.62	22.37	20.83	21.93	21.24	20.21	16.76	21.33
Error (2se)	0.71	0.65	0.76	0.59	0.69	0.32	N/A	0.77	0.78	0.71	0.72	0.75	0.62	0.54	0.72
P 31	135	107.3	95.2	127	124	73	77	119	131	231.8	180	195	177.9	226	110.1
Sc 45	361.6	352.1	348.8	350.8	376	179.7	182.7	372.9	368	379	365.4	383	366.5	372.1	365.1
Ti 49	26	20.5	86.8	20	28	31.3	26.8	43	78.2	48.5	34.8	48.8	23.2	55.8	52.5
Y 89	562	2030	551	2119	1174	773	425	666	695	596	664	1292	1463	1062	668
Nb 93	1.82	18.16	3.45	17.93	1.26	2.6	2.19	1.71	2.07	2.58	2.17	3.51	3.53	5.92	1.46
La 139	BDL	0.06	0.075	0.049	0.184	0.115	0.0102	0.09	0.089	0.023	0.029	0.152	0.073	0.065	0.086
Ce 140	9.24	131.5	19.98	178.3	18.76	19.65	13.6	7.89	14.19	12.08	10.87	18.64	23.4	21.4	11.94
Pr 141	0.061	0.285	0.507	0.396	0.552	0.407	0.109	0.422	0.522	0.19	0.291	0.715	0.475	0.249	0.458
Nd 146	0.96	5.44	6.14	6.22	7.09	4.31	1.72	4.6	6.74	2.37	3.04	9.67	6.83	3.69	6.36
Sm 147	2.31	10.11	6.39	10.35	8.54	5.52	1.98	4.98	7.95	4.56	4.31	13.03	10.5	4.71	7.22
Eu 153	0.674	3.39	2.7	3.78	3.25	2.06	0.83	2.07	1.51	1.28	0.91	4.19	2.64	0.95	2.2
Gd 157	12.37	47.5	20.3	57.4	36.4	24.6	8.44	20.6	28.6	19.1	17.8	44.9	42.4	19.7	26.2
Tb 159	4.35	16.16	6.08	17.6	10.77	6.77	2.56	6.29	7.57	5.92	5.31	12.91	12.34	6.86	6.91
Dy 163	53.8	201.4	60.3	201.7	120.5	76.3	33.5	71.1	78.5	61	60.2	138.4	139.8	87.3	72.6
Ho 165	19.14	70.5	18.96	71	39.9	25.51	12.95	23.24	23.77	20.52	20.93	44.1	47.2	33.5	22.54
Er 166	85.3	311	78.4	314	169.4	112.4	65.7	101	99.5	86.2	94.4	186.3	211.4	157.9	95.2
Tm 169	16.76	58.2	15.11	57.5	32	22.93	14.43	19.2	18.26	15.86	18.58	35.24	41.6	31.6	17.71
Yb 172	136	444	119.3	444	254.4	194	129	161.6	147.7	123.6	153.8	283.3	334	260.5	136.4
Lu 175	25.38	80.9	21.6	82.9	46.5	37.1	27.38	33.6	27.95	22.6	30	54.8	64.3	50.3	25.28
Hf 177	9210	6290	6470	6060	8090	5380	5280	7900	8810	8550	9240	7450	8260	7430	7540
Ta 181	1.32	5.02	2.09	5.06	0.84	1.149	1.347	1.09	1.25	1.81	1.79	1.78	1.85	2.43	0.73
Th 232	815	117.7	172	307	3426	201.7	88.1	147.1	276.2	255.1	177.5	252.1	338	254	123
U 238	381	70.4	81.7	131.2	1379	106.7	82.1	100.8	152.8	193.7	163.2	138.6	209.2	161.7	76.2
Nb/Ta	1.4	3.6	1.7	3.5	1.5	2.3	1.6	1.6	1.7	1.4	1.2	2.0	1.9	2.4	2.0
Th/U	2.1	1.7	2.1	2.3	2.5	1.9	1.1	1.5	1.8	1.3	1.1	1.8	1.6	1.6	1.6
Eu/Eu*	0.39	0.47	0.72	0.47	0.56	0.54	0.62	0.62	0.31	0.42	0.32	0.53	0.38	0.30	0.49
Ce/Ce*	-	246.6	25.1	313.8	14.4	22.3	100.0	9.9	16.1	44.8	29.0	13.9	30.8	41.2	14.8

APPENDIX F: SUPPLEMENTARY DATA FROM HF LASS ANALYSIS

Sample 2016MJ-04	$^{206}Pb/^{238}U$ Age (Ma)	2σ	$^{176}Lu/^{177}Hf$	2σ	$^{176}Yb/^{177}Hf$	2σ	$^{178}Hf/^{177}Hf$	2σ	$^{180}Hf/^{177}Hf$	2σ	$^{176}Hf/^{177}Hf_m$	2σ	εHf_i	2σ
04-003	28.4	0.7	0.002990	0.000038	0.1136	0.0029	1.46725	0.00006	1.88669	0.00011	0.28300	0.00007	**8.1**	**2.5**
04-014	28.6	0.6	0.004840	0.000017	0.1878	0.0020	1.46732	0.00005	1.88674	0.00012	0.28305	0.00007	**9.9**	**2.4**
04-023	27.3	0.6	0.001277	0.000033	0.0556	0.0011	1.46724	0.00005	1.88664	0.00010	0.28300	0.00004	**8.1**	**1.3**
04-024	29.8	1.3	0.005152	0.000082	0.2046	0.0022	1.46727	0.00005	1.88665	0.00012	0.28303	0.00007	**9.4**	**2.5**
04-039	28.1	0.6	0.002751	0.000020	0.1107	0.0008	1.46728	0.00006	1.88665	0.00009	0.28305	0.00005	**10.0**	**1.7**
04-049	20.8	0.8	0.000572	0.000003	0.0182	0.0003	1.46726	0.00004	1.88663	0.00005	0.28302	0.00002	**8.8**	**0.9**
04-057	29.2	0.6	0.002979	0.000037	0.1268	0.0014	1.46725	0.00004	1.88671	0.00009	0.28299	0.00006	**8.0**	**2.0**
04-063	25.5	0.7	0.001205	0.000039	0.0410	0.0015	1.46731	0.00007	1.88673	0.00018	0.28303	0.00005	**9.2**	**1.7**
04-067	28.0	0.6	0.004020	0.000200	0.1560	0.0100	1.46728	0.00006	1.88668	0.00010	0.28306	0.00008	**10.4**	**2.8**
04-070	30.0	0.8	0.002692	0.000093	0.1244	0.0075	1.46724	0.00014	1.88665	0.00015	0.28302	0.00009	**8.8**	**3.1**
04-076	27.1	0.9	0.000591	0.000019	0.0215	0.0008	1.46728	0.00006	1.88680	0.00011	0.28296	0.00004	**6.8**	**1.4**
04-079	27.2	0.6	0.003429	0.000006	0.1280	0.0009	1.46725	0.00005	1.88667	0.00010	0.28302	0.00005	**9.0**	**1.9**
04-080	27.0	0.7	0.000879	0.000028	0.0328	0.0015	1.46726	0.00004	1.88676	0.00011	0.28299	0.00005	**7.9**	**1.6**
04-081	27.7	0.6	0.002944	0.000004	0.1277	0.0008	1.46723	0.00005	1.88665	0.00010	0.28298	0.00005	**7.6**	**1.7**
04-086	30.0	0.8	0.001660	0.000041	0.0714	0.0026	1.46726	0.00005	1.88671	0.00009	0.28302	0.00005	**8.8**	**1.7**
04-093	28.6	0.7	0.003241	0.000096	0.1161	0.0030	1.46731	0.00004	1.88663	0.00009	0.28302	0.00005	**9.0**	**1.9**
04-098	27.9	0.7	0.002819	0.000059	0.1157	0.0028	1.46718	0.00008	1.88654	0.00015	0.28300	0.00009	**8.4**	**3.1**
04-111	28.1	0.6	0.003334	0.000044	0.1455	0.0035	1.46724	0.00005	1.88667	0.00014	0.28300	0.00007	**8.2**	**2.6**
04-115	29.3	0.7	0.006160	0.000190	0.2187	0.0072	1.46726	0.00006	1.88665	0.00009	0.28304	0.00007	**9.6**	**2.3**
04-116	30.2	1.1	0.001620	0.000130	0.0679	0.0060	1.46729	0.00005	1.88671	0.00010	0.28302	0.00006	**8.8**	**2.0**
04-132	28.6	0.6	0.004004	0.000021	0.1691	0.0023	1.46726	0.00006	1.88668	0.00010	0.28301	0.00006	**8.4**	**2.1**
04-138	30.5	1.2	0.000556	0.000052	0.0187	0.0021	1.46726	0.00005	1.88661	0.00011	0.28304	0.00004	**9.7**	**1.4**

Notes:

$^{176}Hf/^{177}Hf_m$=measured ratio, corrected for isobaric interferences (Fisher et al., 2014)

$\lambda^{176}Lu=1.867\pm0.008 \times 10^{-11}$ Yr^{-1} (Soderlund et al., 2004)

Present-Day CHUR Values: $^{176}Hf/^{177}Hf=0.282785\pm11$, $^{176}Lu/^{177}Hf=0.0336\pm0.0001$ (Bouvier et al., 2008)

$\varepsilon Hf_i = (^{176}Hf/^{176}Hf)_{probe}/(^{176}Hf/^{177}Hf)_{Chondrite}$

Sample 2016MJ-38	$^{206}Pb/^{238}U$ Age (Ma)	2σ	$^{176}Lu/^{177}Hf$	2σ	$^{176}Yb/^{177}Hf$	2σ	$^{178}Hf/^{177}Hf$	2σ	$^{180}Hf/^{177}Hf$	2σ	$^{176}Hf/^{177}Hf_m$	2σ	EHf_i	2σ
38-003	20.9	1.2	0.002010	0.000130	0.0575	0.0033	1.46770	0.00005	1.88776	0.00011	0.28291	0.00003	**4.9**	**0.9**
38-006	25.2	1.2	0.005570	0.000160	0.2453	0.0053	1.46724	0.00006	1.88660	0.00013	0.28300	0.00006	**8.1**	**2.2**
38-012	18.3	0.5	0.003170	0.000150	0.1069	0.0044	1.46727	0.00004	1.88658	0.00010	0.28299	0.00005	**7.5**	**1.9**
38-013	16.5	0.9	0.000865	0.000063	0.0270	0.0019	1.46747	0.00007	1.88713	0.00021	0.28314	0.00006	**12.8**	**2.0**
38-019	14.9	0.8	0.001295	0.000097	0.0460	0.0024	1.46783	0.00012	1.88825	0.00029	0.28286	0.00004	**3.0**	**1.4**
38-020	3.9	0.3	0.001121	0.000068	0.0347	0.0018	1.46785	0.00014	1.88826	0.00036	0.28278	0.00005	**-0.2**	**1.9**
38-025	15.8	0.9	0.003991	0.000092	0.1492	0.0079	1.46695	0.00010	1.88625	0.00021	0.28315	0.00005	**13.2**	**1.4**
38-026	15.7	0.9	0.000734	0.000006	0.0247	0.0003	1.46722	0.00010	1.88696	0.00023	0.28300	0.00004	**7.8**	**1.5**
38-027	3.9	0.3	0.002909	0.000044	0.0984	0.0018	1.46753	0.00005	1.88752	0.00011	0.28292	0.00004	**4.7**	**1.4**
38-028	14.6	0.7	0.001337	0.000022	0.0408	0.0003	1.46779	0.00011	1.88822	0.00028	0.28285	0.00004	**2.7**	**1.6**
38-029	16.9	1.2	0.002040	0.000220	0.0656	0.0074	1.46754	0.00006	1.88750	0.00017	0.28293	0.00005	**5.4**	**1.6**
38-037	20.1	0.6	0.000419	0.000025	0.0137	0.0009	1.46724	0.00003	1.88664	0.00007	0.28304	0.00002	**9.6**	**0.8**
38-038	13.4	1.0	0.001101	0.000023	0.0340	0.0007	1.46758	0.00007	1.88782	0.00022	0.28288	0.00004	**3.7**	**1.4**
38-054	13.4	0.8	0.001513	0.000034	0.0496	0.0011	1.46707	0.00012	1.88663	0.00031	0.28304	0.00004	**9.3**	**1.3**
38-058	15.3	0.7	0.001520	0.000140	0.0495	0.0041	1.46715	0.00012	1.88674	0.00031	0.28299	0.00004	**7.6**	**1.5**
38-061	15.5	0.8	0.002536	0.000016	0.0775	0.0003	1.46737	0.00011	1.88736	0.00031	0.28297	0.00007	**6.9**	**2.5**
38-066	16.1	0.9	0.000610	0.000080	0.0201	0.0032	1.46721	0.00010	1.88688	0.00021	0.28303	0.00004	**8.8**	**1.4**
38-067	15.3	1.1	0.000355	0.000015	0.0112	0.0004	1.46724	0.00007	1.88693	0.00020	0.28300	0.00003	**7.9**	**1.1**
38-070	19.6	0.5	0.000686	0.000011	0.0232	0.0005	1.46726	0.00005	1.88668	0.00008	0.28298	0.00002	**7.2**	**0.9**
38-071	16.2	0.8	0.002190	0.000120	0.0704	0.0036	1.46725	0.00008	1.88719	0.00023	0.28295	0.00003	**6.3**	**1.1**
38-077	16.3	1.0	0.002026	0.000054	0.0764	0.0028	1.46682	0.00006	1.88575	0.00010	0.28315	0.00004	**13.2**	**1.7**
38-079	17.8	1.2	0.004350	0.000200	0.1493	0.0061	1.46673	0.00020	1.88574	0.00055	0.28309	0.00009	**11.3**	**3.0**
38-080	16.0	1.0	0.002730	0.000260	0.0964	0.0092	1.46691	0.00011	1.88624	0.00032	0.28306	0.00005	**10.1**	**1.7**
38-086	16.6	1.4	0.000620	0.000110	0.0181	0.0031	1.46719	0.00011	1.88687	0.00030	0.28301	0.00005	**8.4**	**1.6**
38-087	16.1	1.0	0.000529	0.000013	0.0176	0.0006	1.46727	0.00011	1.88724	0.00042	0.28290	0.00005	**4.5**	**1.6**
38-088	14.0	0.7	0.000950	0.000002	0.0296	0.0001	1.46750	0.00012	1.88821	0.00044	0.28285	0.00006	**2.5**	**2.0**
38-094	16.6	0.8	0.000675	0.000019	0.0173	0.0006	1.46660	0.00013	1.88531	0.00033	0.28315	0.00007	**13.3**	**2.5**
38-095	16.2	0.9	0.000723	0.000058	0.0190	0.0017	1.46661	0.00012	1.88537	0.00035	0.28320	0.00006	**15.2**	**2.3**
38-097	19.4	1.2	0.003910	0.000260	0.1343	0.0083	1.46682	0.00010	1.88582	0.00033	0.28312	0.00004	**12.3**	**1.4**
38-103	14.7	1.0	0.002817	0.000077	0.0939	0.0024	1.46723	0.00010	1.88712	0.00036	0.28298	0.00005	**7.2**	**1.8**
38-104	3.9	0.6	0.000397	0.000006	0.0088	0.0002	1.46706	0.00013	1.88661	0.00037	0.28296	0.00005	**6.3**	**1.8**
38-300	18.2	1.5	0.001725	0.000073	0.0564	0.0024	1.46740	0.00008	1.88794	0.00021	0.28285	0.00004	**2.7**	**1.4**
38-301	17.6	1.0	0.001117	0.000014	0.0381	0.0011	1.46718	0.00007	1.88695	0.00022	0.28299	0.00003	**7.6**	**1.1**
38-302	15.5	0.9	0.001880	0.000120	0.0527	0.0034	1.46721	0.00010	1.88702	0.00033	0.28285	0.00003	**2.6**	**1.2**

38-303	15.8	0.8	0.001131	0.000050	0.0337	0.0015	1.46684	0.00014	1.88597	0.00040	0.28299	0.00006	**7.6**	**2.3**
38-304	16.7	0.9	0.001710	0.000110	0.0613	0.0036	1.46675	0.00005	1.88552	0.00018	0.28309	0.00004	**11.0**	**1.4**
38-305	15.4	1.4	0.004970	0.000270	0.1695	0.0093	1.46691	0.00007	1.88597	0.00011	0.28308	0.00004	**10.6**	**1.5**
38-306	16.4	1.0	0.000875	0.000084	0.0249	0.0024	1.46735	0.00004	1.88770	0.00022	0.28286	0.00004	**2.8**	**1.5**
38-307	16.2	1.0	0.000555	0.000018	0.0141	0.0004	1.46759	0.00012	1.88863	0.00052	0.28279	0.00005	**0.6**	**1.9**
38-308	16.1	0.9	0.000915	0.000052	0.0303	0.0020	1.46686	0.00013	1.88589	0.00040	0.28305	0.00005	**9.8**	**1.8**
38-309	15.9	0.7	0.002560	0.000170	0.0944	0.0062	1.46707	0.00008	1.88638	0.00019	0.28283	0.00006	**1.9**	**2.2**
38-310	17.2	1.4	0.000878	0.000054	0.0250	0.0015	1.46722	0.00009	1.88695	0.00033	0.28298	0.00005	**7.1**	**1.6**
38-311	16.3	1.2	0.000555	0.000011	0.0141	0.0002	1.46751	0.00006	1.88880	0.00032	0.28277	0.00003	**-0.3**	**1.1**
38-312	17.4	1.3	0.000913	0.000033	0.0303	0.0013	1.46662	0.00011	1.88485	0.00032	0.28317	0.00005	**13.9**	**1.6**
38-313	20.6	1.0	0.002540	0.000110	0.0936	0.0040	1.46710	0.00010	1.88628	0.00038	0.28296	0.00006	**6.6**	**2.1**
38-314	4.1	0.4	0.001582	0.000037	0.0436	0.0009	1.46727	0.00004	1.88666	0.00007	0.28295	0.00003	**5.9**	**1.1**
38-315	18.6	0.7	0.001147	0.000019	0.0377	0.0007	1.46727	0.00005	1.88664	0.00010	0.28307	0.00004	**10.6**	**1.3**
38-316	16.9	0.8	0.001655	0.000041	0.0544	0.0016	1.46727	0.00004	1.88664	0.00009	0.28302	0.00004	**8.8**	**1.4**
38-317	14.6	0.7	0.000994	0.000007	0.0304	0.0004	1.46726	0.00004	1.88661	0.00007	0.28303	0.00002	**9.1**	**0.8**
38-318	17.1	0.7	0.004420	0.000280	0.1504	0.0090	1.46727	0.00005	1.88667	0.00010	0.28295	0.00007	**6.2**	**2.3**
38-319	17.8	0.7	0.003490	0.000160	0.1128	0.0050	1.46727	0.00005	1.88664	0.00008	0.28299	0.00004	**7.6**	**1.5**
38-320	20.9	0.5	0.000234	0.000003	0.0076	0.0001	1.46725	0.00003	1.88664	0.00007	0.28299	0.00002	**7.8**	**0.6**
38-321	16.2	0.9	0.000633	0.000022	0.0194	0.0006	1.46730	0.00004	1.88663	0.00008	0.28299	0.00002	**7.7**	**0.9**
38-322	15.7	1.0	0.000655	0.000029	0.0209	0.0010	1.46728	0.00005	1.88659	0.00009	0.28301	0.00003	**8.4**	**1.2**
38-323	16.9	0.5	0.004044	0.000056	0.1431	0.0030	1.46724	0.00004	1.88667	0.00008	0.28299	0.00005	**7.6**	**1.8**
38-324	18.1	0.7	0.000972	0.000023	0.0332	0.0007	1.46721	0.00003	1.88657	0.00007	0.28298	0.00003	**7.2**	**0.9**
38-325	16.3	0.5	0.002266	0.000033	0.0782	0.0016	1.46726	0.00004	1.88669	0.00008	0.28299	0.00004	**7.5**	**1.3**
38-326	16.5	0.7	0.001503	0.000025	0.0439	0.0010	1.46724	0.00004	1.88662	0.00007	0.28300	0.00003	**8.1**	**1.0**
38-327	21.7	1.3	0.000476	0.000031	0.0147	0.0010	1.46730	0.00006	1.88666	0.00011	0.28298	0.00003	**7.5**	**0.9**
38-328	20.9	0.8	0.001010	0.000052	0.0331	0.0017	1.46728	0.00005	1.88659	0.00008	0.28299	0.00003	**7.8**	**1.1**
38-329	19.1	0.6	0.002971	0.000016	0.0941	0.0011	1.46725	0.00005	1.88667	0.00008	0.28304	0.00005	**9.4**	**1.6**
38-330	18.4	0.8	0.001580	0.000150	0.0470	0.0050	1.46731	0.00004	1.88672	0.00008	0.28302	0.00003	**8.6**	**1.1**

Notes:

$^{176}Hf/^{177}Hf_m$=measured ratio, corrected for isobaric interferences (Fisher et al., 2014)

$\lambda^{176}Lu=1.867\pm0.008 \times 10^{-11}$ Yr^{-1} (Soderlund et al., 2004)

Present-Day CHUR Values: $^{176}Hf/^{177}Hf=0.282785\pm11$, $^{176}Lu/^{177}Hf=0.0336\pm0.0001$ (Bouvier et al., 2008)

$\varepsilon Hf_i = (^{176}Hf/^{176}Hf)_{probe}/(^{176}Hf/^{177}Hf)_{Chondrite}$

Sample 2016MJ-39	$^{206}Pb/^{238}U$ Age (Ma)	2σ	$^{176}Lu/^{177}Hf$	2σ	$^{176}Yb/^{177}Hf$	2σ	$^{178}Hf/^{177}Hf$	2σ	$^{180}Hf/^{177}Hf$	2σ	$^{176}Hf/^{177}Hf_m$	2σ	EHf_i	2σ
39-001	19.8	0.4	0.001888	0.000003	0.0653	0.0005	1.46722	0.00005	1.88672	0.00008	0.28302	0.00004	**8.9**	**1.5**
39-002	22.4	0.3	0.001127	0.000030	0.0386	0.0012	1.46727	0.00004	1.88665	0.00008	0.28301	0.00003	**8.4**	**1.0**
39-003	21.8	0.4	0.000463	0.000006	0.0162	0.0001	1.46729	0.00003	1.88663	0.00007	0.28298	0.00002	**7.5**	**0.8**
39-004	21.0	0.5	0.000571	0.000019	0.0198	0.0007	1.46724	0.00005	1.88658	0.00007	0.28303	0.00003	**9.1**	**0.9**
39-005	21.5	0.4	0.000420	0.000006	0.0143	0.0001	1.46725	0.00004	1.88665	0.00007	0.28300	0.00002	**8.1**	**0.7**
39-006	22.2	0.3	0.000554	0.000004	0.0184	0.0004	1.46725	0.00003	1.88665	0.00005	0.28302	0.00002	**8.8**	**0.6**
39-007	20.8	0.5	0.000467	0.000005	0.0158	0.0001	1.46730	0.00003	1.88671	0.00007	0.28302	0.00002	**8.8**	**0.9**
39-008	22.3	0.3	0.000460	0.000005	0.0151	0.0001	1.46729	0.00003	1.88664	0.00007	0.28301	0.00002	**8.3**	**0.8**
39-009	22.2	0.4	0.001000	0.000180	0.0334	0.0060	1.46729	0.00003	1.88668	0.00006	0.28302	0.00003	**8.6**	**1.0**
39-010	21.0	0.6	0.000553	0.000057	0.0168	0.0016	1.46729	0.00003	1.88664	0.00006	0.28302	0.00002	**8.6**	**0.9**
39-011	20.9	0.4	0.000621	0.000030	0.0218	0.0009	1.46726	0.00003	1.88667	0.00006	0.28299	0.00002	**7.6**	**0.8**
39-012	22.0	1.1	0.000206	0.000004	0.0067	0.0003	1.46723	0.00004	1.88665	0.00008	0.28301	0.00002	**8.6**	**0.7**
39-013	21.0	0.3	0.000288	0.000006	0.0097	0.0002	1.46723	0.00004	1.88669	0.00012	0.28301	0.00003	**8.4**	**1.0**
39-014	21.9	0.6	0.000526	0.000018	0.0168	0.0008	1.46727	0.00003	1.88662	0.00006	0.28301	0.00002	**8.5**	**0.6**
39-015	21.6	0.5	0.000583	0.000013	0.0194	0.0004	1.46725	0.00003	1.88665	0.00006	0.28302	0.00002	**8.8**	**0.7**
39-017	16.1	0.3	0.004791	0.000017	0.1787	0.0010	1.46726	0.00005	1.88661	0.00008	0.28304	0.00004	**9.4**	**1.3**
39-018	22.5	0.3	0.000599	0.000031	0.0246	0.0014	1.46727	0.00003	1.88670	0.00007	0.28300	0.00002	**8.0**	**0.8**
39-019	16.7	0.6	0.000494	0.000009	0.0169	0.0002	1.46725	0.00004	1.88667	0.00007	0.28302	0.00002	**8.6**	**0.8**
39-021	22.0	0.7	0.000636	0.000011	0.0194	0.0005	1.46727	0.00003	1.88667	0.00007	0.28302	0.00002	**8.7**	**0.7**
39-022	21.9	0.5	0.003400	0.000160	0.1248	0.0054	1.46727	0.00003	1.88670	0.00007	0.28304	0.00004	**9.4**	**1.5**
39-023	16.4	0.6	0.000890	0.000006	0.0302	0.0007	1.46727	0.00004	1.88669	0.00009	0.28297	0.00003	**7.0**	**1.1**
39-025	21.0	0.4	0.000596	0.000037	0.0198	0.0015	1.46727	0.00003	1.88668	0.00006	0.28301	0.00002	**8.4**	**0.6**
39-028	23.0	0.8	0.000993	0.000031	0.0314	0.0014	1.46731	0.00004	1.88672	0.00006	0.28303	0.00003	**9.1**	**1.0**
39-031	22.1	0.6	0.000428	0.000012	0.0129	0.0003	1.46729	0.00004	1.88670	0.00008	0.28299	0.00003	**7.8**	**0.9**
39-032	20.0	0.3	0.000338	0.000001	0.0100	0.0001	1.46727	0.00004	1.88662	0.00006	0.28301	0.00002	**8.4**	**0.8**
39-035	21.8	0.5	0.000502	0.000006	0.0159	0.0002	1.46727	0.00004	1.88663	0.00006	0.28300	0.00002	**8.2**	**0.7**
39-037	23.3	0.3	0.000228	0.000015	0.0074	0.0005	1.46727	0.00003	1.88669	0.00005	0.28301	0.00002	**8.4**	**0.6**
39-038	23.5	0.6	0.000387	0.000023	0.0126	0.0010	1.46727	0.00003	1.88666	0.00008	0.28301	0.00002	**8.5**	**0.7**
39-056	22.7	0.4	0.000349	0.000009	0.0120	0.0004	1.46732	0.00003	1.88675	0.00007	0.28301	0.00002	**8.4**	**0.6**
39-058	23.4	0.5	0.000567	0.000004	0.0179	0.0002	1.46726	0.00004	1.88668	0.00006	0.28300	0.00002	**8.0**	**0.7**
39-062	15.4	0.5	0.001303	0.000093	0.0422	0.0028	1.46722	0.00005	1.88662	0.00008	0.28302	0.00004	**8.8**	**1.3**
39-063	21.8	0.4	0.000409	0.000004	0.0142	0.0003	1.46724	0.00004	1.88665	0.00007	0.28300	0.00002	**8.0**	**0.8**
39-067	20.6	0.6	0.000617	0.000004	0.0210	0.0003	1.46724	0.00004	1.88655	0.00009	0.28302	0.00003	**8.6**	**1.2**
39-068	4.1	0.4	0.001477	0.000009	0.0437	0.0015	1.46726	0.00006	1.88669	0.00013	0.28292	0.00005	**4.9**	**1.8**
39-070	21.4	0.3	0.000337	0.000007	0.0108	0.0004	1.46726	0.00003	1.88670	0.00006	0.28298	0.00002	**7.4**	**0.5**
39-072	20.9	0.6	0.000391	0.000003	0.0117	0.0002	1.46726	0.00003	1.88664	0.00007	0.28299	0.00002	**7.9**	**0.9**

39-073	21.0	0.3	0.000946	0.000022	0.0308	0.0011	1.46729	0.00003	1.88667	0.00008	0.28300	0.00002	**8.1**	**0.9**
39-075	18.0	0.6	0.000836	0.000027	0.0226	0.0006	1.46729	0.00004	1.88672	0.00009	0.28299	0.00003	**7.5**	**0.9**
39-076	22.0	0.7	0.000363	0.000009	0.0123	0.0008	1.46727	0.00004	1.88664	0.00009	0.28301	0.00003	**8.5**	**0.9**
39-097	21.0	0.8	0.000515	0.000007	0.0157	0.0005	1.46741	0.00007	1.88673	0.00009	0.28304	0.00003	**9.3**	**1.1**
39-099	20.3	0.5	0.000433	0.000035	0.0146	0.0011	1.46728	0.00003	1.88668	0.00008	0.28302	0.00003	**8.6**	**1.0**
39-300	21.6	0.5	0.000163	0.000005	0.0053	0.0002	1.46729	0.00004	1.88665	0.00007	0.28299	0.00002	**7.7**	**0.7**
39-301	18.2	0.4	0.003420	0.000062	0.1022	0.0010	1.46728	0.00004	1.88671	0.00009	0.28300	0.00005	**8.0**	**1.7**
39-302	16.1	0.4	0.001847	0.000015	0.0582	0.0004	1.46726	0.00004	1.88661	0.00008	0.28299	0.00004	**7.5**	**1.4**
39-303	20.8	0.6	0.000412	0.000027	0.0130	0.0008	1.46729	0.00003	1.88666	0.00007	0.28301	0.00003	**8.3**	**0.9**
39-304	4.9	0.3	0.002080	0.000046	0.0614	0.0021	1.46728	0.00005	1.88668	0.00009	0.28293	0.00004	**5.1**	**1.5**
39-305	4.2	0.2	0.001854	0.000016	0.0532	0.0002	1.46727	0.00004	1.88668	0.00009	0.28295	0.00004	**5.8**	**1.3**
39-306	17.2	0.4	0.002500	0.000260	0.0764	0.0079	1.46730	0.00003	1.88677	0.00008	0.28301	0.00004	**8.2**	**1.3**
39-307	20.2	0.8	0.000893	0.000024	0.0293	0.0013	1.46725	0.00003	1.88673	0.00007	0.28302	0.00003	**8.7**	**1.0**

Notes:

$^{176}Hf/^{177}Hf_m$=measured ratio, corrected for isobaric interferences (Fisher et al., 2014)

$\lambda^{176}Lu=1.867\pm0.008 \times 10^{-11}$ Yr^{-1} (Soderlund et al., 2004)

Present-Day CHUR Values: $^{176}Hf/^{177}Hf=0.282785\pm11$, $^{176}Lu/^{177}Hf=0.0336\pm0.0001$ (Bouvier et al., 2008)

$\varepsilon Hf_i = (^{176}Hf/^{176}Hf)_{probe}/(^{176}Hf/^{177}Hf)_{Chondrite}$

APPENDIX G1: $\delta^{18}O$ SIMS ANALYSIS (2016MJ-04)

2016MJ-04 Sample Name	Session	$^{18}O/^{16}O$	1σ (%) inter-session	$\delta^{18}O$ (VSMOW)	2σ (‰)
04-007-2	IP17056A	0.002014124	0.016	4.45	0.31
04-007-3	IP17056A	0.002014035	0.013	4.41	0.26
04-014-1	IP17056A	0.002014228	0.009	4.50	0.18
04-014-2	IP17056A	0.002014049	0.014	4.41	0.27
04-024-1	IP17056A	0.002015559	0.010	5.17	0.19
04-024-2	IP17056A	0.002015324	0.008	5.05	0.17
04-026-1	IP17056A	0.002013334	0.009	4.06	0.18
04-026-2	IP17056A	0.002013476	0.011	4.13	0.22
04-039-1	IP17056A	0.002014283	0.010	4.53	0.21
04-039-2	IP17056A	0.002014240	0.009	4.51	0.17
04-047-1	IP17056A	0.002013108	0.009	3.94	0.17
04-047-2	IP17056A	0.002013423	0.016	4.10	0.31
04-049-1	IP17056A	0.002013253	0.010	4.02	0.20
04-049-2	IP17056A	0.002013417	0.012	4.10	0.24
04-054-1	IP17056A	0.002013633	0.012	4.21	0.24
04-062-1	IP17056A	0.002012460	0.013	3.62	0.25
04-062-2	IP17056A	0.002011762	0.014	3.27	0.27
04-063-1	IP17056A	0.002014191	0.009	4.48	0.18
04-063-2	IP17056A	0.002013917	0.010	4.35	0.19
04-064-2	IP17056A	0.002016197	0.010	5.48	0.20
04-067-1	IP17056A	0.002015604	0.011	5.19	0.22
04-070-1	IP17056A	0.002012207	0.011	3.49	0.23
04-070-2	IP17056A	0.002011699	0.010	3.24	0.20
04-076-1	IP17056A	0.002013732	0.011	4.25	0.22
04-078-1	IP17056A	0.002013505	0.011	4.14	0.23
04-079-1	IP17056A	0.002013366	0.012	4.07	0.25
04-079-2	IP17056A	0.002013464	0.010	4.12	0.20
04-079-3	IP17056A	0.002013394	0.011	4.09	0.23
04-080-1	IP17056A	0.002014253	0.012	4.51	0.23
04-080-2	IP17056A	0.002013931	0.010	4.35	0.19
04-080-3	IP17056A	0.002014373	0.013	4.57	0.27
04-081-1	IP17056A	0.002013356	0.013	4.07	0.25
04-081-2	IP17056A	0.002013938	0.013	4.36	0.26
04-081-3	IP17056A	0.002013725	0.014	4.25	0.27
04-083-1	IP17056A	0.002016032	0.012	5.40	0.23
04-083-2	IP17056A	0.002015692	0.010	5.23	0.21
04-086-1	IP17056A	0.002014705	0.012	4.74	0.23
04-086-2	IP17056A	0.002014998	0.012	4.89	0.25
04-093-1	IP17056A	0.002014061	0.010	4.42	0.21
04-093-2	IP17056A	0.002014417	0.011	4.60	0.23
04-098-1	IP17056A	0.002013255	0.012	4.02	0.25
04-098-2	IP17056A	0.002012959	0.014	3.87	0.29
04-103-2	IP17056A	0.002014883	0.013	4.83	0.26
04-103-3	IP17056A	0.002014084	0.011	4.43	0.21
04-103-4	IP17056A	0.002012043	0.016	3.41	0.31
04-109-1	IP17056A	0.002012882	0.011	3.83	0.21
04-109-2	IP17056A	0.002013372	0.011	4.08	0.21
04-111-1	IP17056A	0.002014526	0.010	4.65	0.19
04-111-2	IP17056A	0.002014605	0.009	4.69	0.19
04-115-1	IP17056A	0.002011980	0.013	3.38	0.25
04-115-2	IP17056A	0.002012544	0.010	3.66	0.20
04-115-3	IP17056A	0.002011570	0.012	3.18	0.24
04-116-1	IP17056A	0.002014196	0.011	4.49	0.23
04-116-2	IP17056A	0.002014214	0.014	4.50	0.27
04-132-1	IP17056A	0.002013969	0.014	4.37	0.27
04-138-1	IP17056A	0.002014543	0.011	4.66	0.22
04-138-2	IP17056A	0.002014896	0.013	4.84	0.26

APPENDIX G2: $\delta^{18}O$ SIMS ANALYSIS (2016MJ-38)

2016MJ-38 Sample Name	Session	$^{18}O/^{16}O$	1σ (%) inter-session	$\delta^{18}O$ (VSMOW)	2σ (‰)
38-003-1	IP17056A	0.002014201	0.011	4.49	0.23
38-003-2	IP17056A	0.002014509	0.014	4.64	0.28
38-006-1	IP17056B	0.002011767	0.012	3.27	0.24
38-006-2	IP17056B	0.002011683	0.012	3.23	0.23
38-012-1	IP17056B	0.002012733	0.012	3.76	0.25
38-012-2	IP17056B	0.002012579	0.012	3.68	0.25
38-013-1	IP17056B	0.002012171	0.016	3.48	0.33
38-013-2	IP17056B	0.002012389	0.009	3.59	0.19
38-013-3	IP17056B	0.002012410	0.010	3.60	0.20
38-020-1	IP17056B	0.002014086	0.015	4.43	0.30
38-020-2	IP17056B	0.002013583	0.011	4.18	0.21
38-026-1	IP17056B	0.002012719	0.010	3.75	0.20
38-026-2	IP17056B	0.002012523	0.011	3.65	0.22
38-027-1	IP17056B	0.002015197	0.012	4.99	0.24
38-027-2	IP17056B	0.002015369	0.012	5.07	0.24
38-028-1	IP17056B	0.002014438	0.011	4.61	0.23
38-029-1	IP17056B	0.002012663	0.012	3.72	0.24
38-029-2	IP17056B	0.002012583	0.010	3.68	0.19
38-037-1	IP17056B	0.002014737	0.014	4.76	0.27
38-037-2	IP17056B	0.002014676	0.012	4.73	0.24
38-038-1	IP17056B	0.002012626	0.012	3.70	0.24
38-038-2	IP17056B	0.002012149	0.013	3.47	0.25
38-054-1	IP17056B	0.002014584	0.011	4.68	0.22
38-054-2	IP17056B	0.002014562	0.015	4.67	0.30
38-058-1	IP17056B	0.002013888	0.014	4.33	0.28
38-058-2	IP17056B	0.002013620	0.013	4.20	0.25
38-061-1	IP17056B	0.002012242	0.010	3.51	0.20
38-061-2	IP17056B	0.002011399	0.015	3.09	0.29
38-064-1	IP17056B	0.002015437	0.012	5.11	0.25
38-064-2	IP17056B	0.002015465	0.010	5.12	0.19
38-066-1	IP17056B	0.002012477	0.010	3.63	0.21
38-066-2	IP17056B	0.002012376	0.009	3.58	0.18
38-067-1	IP17056B	0.002012879	0.013	3.83	0.27
38-067-2	IP17056B	0.002013077	0.011	3.93	0.21
38-070-1	IP17056B	0.002013646	0.010	4.21	0.20
38-070-2	IP17056B	0.002013656	0.010	4.22	0.20
38-077-1	IP17056B	0.002012518	0.010	3.65	0.20
38-077-2	IP17056B	0.002012351	0.013	3.57	0.26
38-079-1	IP17056B	0.002014969	0.011	4.87	0.23
38-079-2	IP17056B	0.002015007	0.012	4.89	0.24
38-086-1	IP17056B	0.002015253	0.011	5.01	0.23
38-086-2	IP17056B	0.002015353	0.010	5.06	0.20
38-087-1	IP17056B	0.002012468	0.010	3.62	0.19
38-087-2	IP17056B	0.002012411	0.013	3.60	0.26
38-088-1	IP17056B	0.002014956	0.012	4.87	0.24
38-088-2	IP17056B	0.002014782	0.013	4.78	0.27
38-094-1	IP17056B	0.002012635	0.012	3.71	0.24
38-094-2	IP17056B	0.002012517	0.013	3.65	0.26
38-095-1	IP17056B	0.002014455	0.013	4.62	0.26
38-095-2	IP17056B	0.002014074	0.009	4.43	0.18
38-097-1	IP17056B	0.002012711	0.013	3.75	0.27
38-097-2	IP17056B	0.002012673	0.012	3.73	0.23
38-097-3	IP17056B	0.002012844	0.010	3.81	0.19
38-103-1	IP17056B	0.002012428	0.009	3.60	0.18
38-103-2	IP17056B	0.002012673	0.013	3.73	0.26
38-104-1	IP17056B	0.002015435	0.009	5.10	0.18
38-104-2	IP17056B	0.002015141	0.012	4.96	0.23

APPENDIX G3: $\delta^{18}O$ SIMS ANALYSIS (2016MJ-39)

2016MJ-39 Sample Name	Session	$^{18}O/^{16}O$	1σ (%) inter-session	$\delta^{18}O$ (VSMOW)	2σ (‰)
39-001-1	IP17056A	0.002012751	0.011	3.77	0.21
39-001-2	IP17056A	0.002012754	0.013	3.77	0.26
39-003-1	IP17056A	0.002014222	0.011	4.50	0.22
39-003-2	IP17056A	0.002014326	0.009	4.55	0.18
39-003-3	IP17056A	0.002014202	0.012	4.49	0.23
39-004-1	IP17056A	0.002014074	0.014	4.43	0.28
39-004-2	IP17056A	0.002014460	0.011	4.62	0.23
39-004-3	IP17056A	0.002014136	0.011	4.46	0.22
39-005-1	IP17056A	0.002014814	0.010	4.79	0.20
39-005-2	IP17056A	0.002014552	0.015	4.66	0.29
39-006-1	IP17056A	0.002014883	0.014	4.83	0.28
39-006-2	IP17056A	0.002015077	0.011	4.93	0.22
39-008-1	IP17056A	0.002014520	0.009	4.65	0.17
39-008-2	IP17056A	0.002014678	0.011	4.73	0.23
39-009-1	IP17056A	0.002014815	0.014	4.79	0.28
39-009-2	IP17056A	0.002014934	0.010	4.85	0.19
39-010-1	IP17056A	0.002014693	0.010	4.73	0.20
39-010-2	IP17056A	0.002014597	0.014	4.69	0.27
39-011-1	IP17056A	0.002013918	0.010	4.35	0.20
39-011-2	IP17056A	0.002014611	0.008	4.69	0.16
39-012-1	IP17056A	0.002014511	0.010	4.64	0.21
39-012-2	IP17056A	0.002014555	0.011	4.67	0.22
39-012-3	IP17056A	0.002014438	0.011	4.61	0.23
39-013-1	IP17056A	0.002014878	0.010	4.83	0.20
39-013-2	IP17056A	0.002015326	0.011	5.05	0.22
39-014-1	IP17056A	0.002015222	0.009	5.00	0.17
39-014-2	IP17056A	0.002015069	0.010	4.92	0.19
39-015-1	IP17056A	0.002013366	0.010	4.07	0.21
39-015-2	IP17056A	0.002013927	0.012	4.35	0.23
39-016-1	IP17056A	0.002014986	0.012	4.88	0.23
39-016-2	IP17056A	0.002015092	0.013	4.93	0.26
39-019-1	IP17056A	0.002013836	0.015	4.31	0.29
39-019-2	IP17056A	0.002013987	0.009	4.38	0.18
39-021-1	IP17056A	0.002015195	0.010	4.98	0.20
39-021-2	IP17056A	0.002014944	0.010	4.86	0.20
39-023-1	IP17056A	0.002015196	0.012	4.99	0.25
39-025-1	IP17056A	0.002014813	0.011	4.79	0.21
39-025-2	IP17056A	0.002014675	0.010	4.73	0.20
39-025-3	IP17056A	0.002014674	0.011	4.72	0.22
39-028-1	IP17056A	0.002014798	0.011	4.79	0.23
39-028-2	IP17056A	0.002014917	0.012	4.85	0.24
39-028-3	IP17056A	0.002015101	0.013	4.94	0.25
39-031-1	IP17056A	0.002015048	0.011	4.91	0.22
39-031-2	IP17056A	0.002015021	0.013	4.90	0.27
39-031-3	IP17056A	0.002015217	0.015	5.00	0.30
39-035-1	IP17056A	0.002014933	0.009	4.85	0.19
39-035-2	IP17056A	0.002014827	0.013	4.80	0.26
39-038-1	IP17056A	0.002014795	0.010	4.78	0.20
39-038-2	IP17056A	0.002014913	0.010	4.84	0.20
39-047-1	IP17056A	0.002014548	0.011	4.66	0.22
39-047-2	IP17056A	0.002014318	0.009	4.55	0.17
39-058-1	IP17056A	0.002014194	0.011	4.49	0.21
39-058-2	IP17056A	0.002014286	0.009	4.53	0.19
39-058-3	IP17056A	0.002014188	0.009	4.48	0.19
39-062-1	IP17056A	0.002013789	0.009	4.28	0.18
39-062-2	IP17056A	0.002013830	0.010	4.30	0.20
39-063-1	IP17056A	0.002015486	0.010	5.13	0.20
39-063-2	IP17056A	0.002014675	0.012	4.73	0.23

39-065-1	IP17056A	0.002015845	0.013	5.31	0.27
39-065-2	IP17056A	0.002015354	0.009	5.06	0.19
39-067-1	IP17056A	0.002015392	0.013	5.08	0.26
39-067-2	IP17056A	0.002015139	0.011	4.96	0.21
39-072-1	IP17056A	0.002015257	0.010	5.02	0.20
39-073-1	IP17056A	0.002015174	0.013	4.97	0.25
39-073-2	IP17056A	0.002014889	0.008	4.83	0.16
39-075-1	IP17056A	0.002013453	0.011	4.12	0.22
39-075-2	IP17056A	0.002013585	0.008	4.18	0.16
39-076-1	IP17056A	0.002014831	0.010	4.80	0.20
39-076-2	IP17056A	0.002014833	0.011	4.80	0.23
39-076-3	IP17056A	0.002015092	0.015	4.93	0.30
39-079-1	IP17056A	0.002015622	0.012	5.20	0.24
39-079-2	IP17056A	0.002015558	0.011	5.17	0.22
39-096-1	IP17056A	0.002015543	0.010	5.16	0.19
39-100-1	IP17056A	0.002014087	0.010	4.43	0.19

APPENDIX H: SUMMARY OF U-Pb, Hf, and O ISOTOPIC DATA, FUERTEVENTURA, DETRITAL ZIRCONS

Sample	P*	$^{206}Pb/^{238}U$ Age	2σ	$^{176}Hf/^{177}Hf_i$	2σ	εHf_i	2σ	$\delta^{18}O$ (VSMOW)	2σ (‰)	n
2016MJ-04										
04-003	**C**	28.4	0.7	0.28300	0.00007	8.1	2.5	-	-	-
04-014	**C**	28.6	0.6	0.28305	0.00007	9.9	2.4	4.47	0.15	2
04-023	**S**	27.3	0.6	0.28300	0.00004	8.1	1.3	-	-	-
04-024	**N**	29.8	1.3	0.28303	0.00007	9.4	2.5	5.10	0.12	2
04-039	-	28.1	0.6	0.28305	0.00005	10.0	1.7	4.52	0.13	2
04-049	-	20.8	0.8	0.28302	0.00002	8.8	0.9	4.05	0.15	2
04-057	-	29.2	0.6	0.28299	0.00006	8.0	2.0	-	-	-
04-063	-	25.5	0.7	0.28303	0.00005	9.2	1.7	4.42	0.13	2
04-067	**N**	28.0	0.6	0.28306	0.00008	10.4	2.8	5.19	0.22	1
04-070	-	30.0	0.8	0.28302	0.00009	8.8	3.1	3.35	0.15	2
04-076	**C**	27.1	0.9	0.28296	0.00004	6.8	1.4	4.25	0.22	1
04-079	**N**	27.2	0.6	0.28302	0.00005	9.0	1.9	4.10	0.13	3
04-080	**C**	27.0	0.7	0.28299	0.00005	7.9	1.6	4.45	0.13	3
04-081	**S**	27.7	0.6	0.28298	0.00005	7.6	1.7	4.22	0.13	3
04-086	-	30.0	0.8	0.28302	0.00005	8.8	1.7	4.81	0.17	2
04-093	**N**	28.6	0.7	0.28302	0.00005	9.0	1.9	4.50	0.16	2
04-098	**N**	27.9	0.7	0.28300	0.00009	8.4	3.1	3.96	0.19	2
04-111	**N**	28.1	0.6	0.28300	0.00007	8.2	2.6	4.67	0.13	2
04-115	**N**	29.3	0.7	0.28304	0.00007	9.6	2.3	3.34	0.13	3
04-116	**S**	30.2	1.1	0.28302	0.00006	8.8	2.0	4.49	0.17	2
04-132	-	28.6	0.6	0.28301	0.00006	8.4	2.1	4.37	0.27	1
04-138	-	30.5	1.2	0.28304	0.00004	9.7	1.4	4.74	0.17	2
2016MJ-38										
38-003	**C**	20.9	1.2	0.28291	0.00003	4.9	0.9	4.55	0.17	2
38-006	**N**	25.2	1.2	0.28300	0.00006	8.1	2.2	3.25	0.16	2
38-012	**S**	18.3	0.5	0.28299	0.00005	7.5	1.9	3.72	0.17	2
38-013	**N**	16.5	0.9	0.28314	0.00006	12.8	2.0	3.59	0.13	2
38-019	-	14.9	0.8	0.28286	0.00004	3.0	1.4	-	-	-
38-020	**S**	3.9	0.3	0.28278	0.00005	-0.2	1.9	4.26	0.17	2
38-025	-	15.8	0.9	0.28315	0.00004	13.2	1.4	-	-	-
38-026	-	15.7	0.9	0.28300	0.00004	7.8	1.5	3.70	0.15	2
38-027	**S**	3.9	0.3	0.28292	0.00004	4.7	1.4	5.03	0.17	2
38-028	-	14.6	0.7	0.28285	0.00004	2.7	1.6	4.61	0.23	1
38-029	-	16.9	1.2	0.28293	0.00005	5.4	1.6	3.70	0.15	2
38-037	**GA**	20.1	0.6	0.28304	0.00002	9.6	0.8	4.74	0.18	2
38-038	**S**	13.4	1.0	0.28288	0.00004	3.7	1.4	3.59	0.17	2
38-054	-	13.4	0.8	0.28304	0.00004	9.3	1.3	4.68	0.17	2
38-058	**S**	15.3	0.7	0.28299	0.00004	7.6	1.5	4.26	0.18	2
38-061	**S**	15.5	0.8	0.28297	0.00007	6.9	2.5	3.37	0.16	2
38-066	**S**	16.1	0.9	0.28303	0.00004	8.8	1.4	3.60	0.13	2
38-067	**S**	15.3	1.1	0.28300	0.00003	7.9	1.1	3.89	0.16	2
38-070	**GA**	19.6	0.5	0.28298	0.00002	7.2	0.9	4.22	0.14	2
38-071	**S**	16.2	0.8	0.28295	0.00003	6.3	1.1	-	-	-
38-077	**S**	16.3	1.0	0.28315	0.00005	13.2	1.7	3.62	0.16	2
38-079	**S**	17.8	1.2	0.28309	0.00009	11.3	3.0	4.88	0.16	2
38-080	**GA**	16.0	1.0	0.28306	0.00005	10.1	1.7	-	-	-
38-086	-	16.6	1.4	0.28301	0.00005	8.4	1.6	5.04	0.15	2
38-087	-	16.1	1.0	0.28290	0.00005	4.5	1.6	3.61	0.15	2
38-088	-	14.0	0.7	0.28285	0.00006	2.5	2.0	4.83	0.18	2
38-094	**S**	16.6	0.8	0.28315	0.00007	13.3	2.5	3.68	0.17	2

38-095	**-**	16.2	0.9	0.28320	0.00006	15.2	2.3	4.49	0.15	2
38-097	**-**	19.4	1.2	0.28312	0.00004	12.3	1.4	3.74	0.17	2
38-103	**-**	14.7	1.0	0.28298	0.00005	7.2	1.8	3.64	0.15	2
38-104	**GA**	3.9	0.6	0.28296	0.00005	6.3	1.8	5.05	0.14	2
38-300	**-**	18.2	1.5	0.28285	0.00004	2.7	1.4	-	**-**	**-**
38-301	**N**	17.6	1.0	0.28299	0.00003	7.6	1.1	-	**-**	**-**
38-302	**S**	15.5	0.9	0.28285	0.00003	2.6	1.2	-	**-**	**-**
38-303	**GA**	15.8	0.8	0.28299	0.00006	7.6	2.3	-	**-**	**-**
38-304	**S**	16.7	0.9	0.28309	0.00004	11.0	1.4	-	**-**	**-**
38-305	**S**	15.4	1.4	0.28308	0.00004	10.6	1.5	-	**-**	**-**
38-306	**GA**	16.4	1.0	0.28286	0.00004	2.8	1.5	-	**-**	**-**
38-307	**S**	16.2	1.0	0.28279	0.00005	0.6	1.9	-	**-**	**-**
38-308	**GA**	16.1	0.9	0.28305	0.00005	9.8	1.8	-	**-**	**-**
38-309	**S**	15.9	0.7	0.28283	0.00006	1.9	2.2	-	**-**	**-**
38-310	**S**	17.2	1.4	0.28298	0.00005	7.1	1.6	-	**-**	**-**
38-311	**GA**	16.3	1.2	0.28277	0.00003	-0.3	1.1	-	**-**	**-**
38-312	**-**	17.4	1.3	0.28317	0.00005	13.9	1.6	-	**-**	**-**
38-313	**-**	20.6	1.0	0.28296	0.00006	6.6	2.1	-	**-**	**-**
38-314	**-**	4.1	0.4	0.28295	0.00003	5.9	1.1	-	**-**	**-**
38-315	**-**	18.6	0.7	0.28307	0.00004	10.6	1.3	-	**-**	**-**
38-316	**-**	16.9	0.8	0.28302	0.00004	8.8	1.4	-	**-**	**-**
38-317	**-**	14.6	0.7	0.28303	0.00002	9.1	0.8	-	**-**	**-**
38-318	**-**	17.1	0.7	0.28295	0.00007	6.2	2.3	-	**-**	**-**
38-319	**-**	17.8	0.7	0.28299	0.00004	7.6	1.5	-	**-**	**-**
38-320	**-**	20.9	0.5	0.28299	0.00002	7.8	0.6	-	**-**	**-**
38-321	**-**	16.2	0.9	0.28299	0.00002	7.7	0.9	-	**-**	**-**
38-322	**-**	15.7	1.0	0.28301	0.00003	8.4	1.2	-	**-**	**-**
38-323	**-**	16.9	0.5	0.28299	0.00005	7.6	1.8	-	**-**	**-**
38-324	**-**	18.1	0.7	0.28298	0.00003	7.2	0.9	-	**-**	**-**
38-325	**-**	16.3	0.5	0.28299	0.00004	7.5	1.3	-	**-**	**-**
38-326	**-**	16.5	0.7	0.28300	0.00003	8.1	1.0	-	**-**	**-**
38-327	**-**	21.7	1.3	0.28298	0.00003	7.5	0.9	-	**-**	**-**
38-328	**-**	20.9	0.8	0.28299	0.00003	7.8	1.1	-	**-**	**-**
38-329	**-**	19.1	0.6	0.28304	0.00005	9.4	1.6	-	**-**	**-**
38-330	**-**	18.4	0.8	0.28302	0.00003	8.6	1.1	-	-	-
2016MJ-39										
39-001	**S**	19.8	0.4	0.28302	0.00004	8.9	1.5	3.37	0.16	2
39-002	**S**	22.4	0.3	0.28301	0.00003	8.4	1.0	-	**-**	**-**
39-003	**GA**	21.8	0.4	0.28298	0.00002	7.5	0.8	4.52	0.12	3
39-004	**GA**	21.0	0.5	0.28303	0.00003	9.1	0.9	4.51	0.14	3
39-005	**GA**	21.5	0.4	0.28300	0.00002	8.1	0.7	4.75	0.16	2
39-006	**GA**	22.2	0.3	0.28302	0.00002	8.8	0.6	4.89	0.17	2
39-007	**GA**	20.8	0.5	0.28302	0.00002	8.8	0.9	-	**-**	**-**
39-008	**GA**	22.3	0.3	0.28301	0.00002	8.3	0.8	4.68	0.13	2
39-009	**S**	22.2	0.4	0.28302	0.00003	8.6	1.0	4.83	0.15	2
39-010	**GA**	21.0	0.6	0.28302	0.00002	8.6	0.9	4.72	0.16	2
39-011	**S**	20.9	0.4	0.28299	0.00002	7.6	0.8	4.56	0.12	2
39-012	**GA**	22.0	1.1	0.28301	0.00002	8.6	0.7	4.64	0.12	3
39-013	**GA**	21.0	0.3	0.28301	0.00003	8.4	1.0	4.93	0.15	2
39-014	**GA**	21.9	0.6	0.28301	0.00002	8.5	0.6	4.96	0.12	2
39-015	**S**	21.6	0.5	0.28302	0.00002	8.8	0.7	4.20	0.16	2
39-017	**S**	16.1	0.3	0.28304	0.00004	9.4	1.3	-	**-**	**-**
39-018	**S**	22.5	0.3	0.28300	0.00002	8.0	0.8	-	**-**	**-**
39-019	**S**	16.7	0.6	0.28302	0.00002	8.6	0.8	4.36	0.15	2
39-021	**S**	22.0	0.7	0.28302	0.00002	8.7	0.7	4.92	0.14	2
39-022	**S**	21.9	0.5	0.28304	0.00004	9.4	1.5	-	**-**	**-**
39-023	**S**	16.4	0.6	0.28297	0.00003	7.0	1.1	4.99	0.25	1

39-025	**GA**	21.0	0.4	0.28301	0.00002	8.4	0.6	4.75	0.12	3
39-028	**S**	23.0	0.8	0.28303	0.00003	9.1	1.0	4.86	0.14	3
39-031	**GA**	22.1	0.6	0.28299	0.00003	7.8	0.9	4.93	0.15	3
39-032	**-**	20.0	0.3	0.28301	0.00002	8.4	0.8	-	**-**	**-**
39-035	**GA**	21.8	0.5	0.28300	0.00002	8.2	0.7	4.83	0.15	2
39-037	**-**	23.3	0.3	0.28301	0.00002	8.4	0.6	-	**-**	**-**
39-038	**GA**	23.5	0.6	0.28301	0.00002	8.5	0.7	4.81	0.14	2
39-056	**GA**	22.7	0.4	0.28301	0.00002	8.4	0.6	-	**-**	**-**
39-058	**GA**	23.4	0.5	0.28300	0.00002	8.0	0.7	4.50	0.11	3
39-062	**S**	15.4	0.5	0.28302	0.00004	8.8	1.3	4.29	0.13	2
39-063	**GA**	21.8	0.4	0.28300	0.00002	8.0	0.8	4.96	0.15	2
39-067	**GA**	20.6	0.6	0.28302	0.00003	8.6	1.2	5.01	0.16	2
39-068	**-**	4.1	0.4	0.28292	0.00005	4.9	1.8	-	**-**	**-**
39-070	**-**	21.4	0.3	0.28298	0.00002	7.4	0.5	-	**-**	**-**
39-072	**GA**	20.9	0.6	0.28299	0.00002	7.9	0.9	5.02	0.20	1
39-073	**S**	21.0	0.3	0.28300	0.00002	8.1	0.9	4.87	0.13	2
39-075	**GA**	18.0	0.6	0.28299	0.00003	7.5	0.9	4.16	0.13	2
39-076	**GA**	22.0	0.7	0.28301	0.00003	8.5	0.9	4.83	0.13	3
39-097	**-**	21.0	0.8	0.28304	0.00003	9.3	1.1	-	**-**	**-**
39-099	**-**	20.3	0.5	0.28302	0.00003	8.6	1.0	-	**-**	**-**
39-300	**-**	21.6	0.5	0.28299	0.00002	7.7	0.7	-	**-**	**-**
39-301	**-**	18.2	0.4	0.28300	0.00005	8.0	1.7	-	**-**	**-**
39-302	**-**	16.1	0.4	0.28299	0.00004	7.5	1.4	-	**-**	**-**
39-303	**-**	20.8	0.6	0.28301	0.00003	8.3	0.9	-	**-**	**-**
39-304	**-**	4.9	0.3	0.28293	0.00004	5.1	1.5	-	**-**	**-**
39-305	**-**	4.2	0.2	0.28295	0.00004	5.8	1.3	-	**-**	**-**
39-306	**-**	17.2	0.4	0.28301	0.00004	8.2	1.3	-	**-**	**-**
39-307	**-**	20.2	0.8	0.28302	0.00003	8.7	1.0	-	-	-

Notes: zircon grain provenance - C=carbonatite, GA=gabbro/anorthosite, N=nepheline syenite, S=syenite
(-) indicates the grain has not been analyzed for minor and trace elements